Aus der Klinik für Plastische, Ästhetische und Handchirurgie
der Medizinischen Fakultät
der Otto-von-Guericke-Universität Magdeburg
Arbeitsgruppe Gravitationsbiologie und translationale regenerative Medizin

The Effects of Real and Simulated Microgravity on Human Cancer Cells

Dissertation

zur Erlangung des Doktorgrades

Dr. rer. medic.

(doctor rerum medicarum)

an der Medizinischen Fakultät
der Otto-von-Guericke-Universität Magdeburg

vorgelegt von **M. Sc. Sascha Kopp**
aus **Troisdorf, Deutschland**
Magdeburg 2018

Angefertigt von **April 2015 bis Januar 2018** in der Klinik für Plastische, Ästhetische und Handchirurgie, Arbeitsgruppe Gravitationsbiologie und translationale regenerative Medizin von Frau Professor Daniela Grimm.

Klinikdirektor: **Herr Professor Dr. med. Manfred Infanger**

Betreuer: **Frau Professor Dr. med. Daniela Grimm**
                            Herr Professor Dr. med. Manfred Infanger

Bibliographical Description:

Abstract

Since NASA announced their plans to take mankind deeper into space, the need to understand the basic reaction of human cells to the altered gravity environment has increased. Generally, it is hypothesized that human cells sense gravity changes via the cytoskeleton. However, live cell imaging was not possible until now. In addition, various cell types cultured under microgravity conditions grew in the form of multicellular spheroids (MCS). These MCS often closely resemble the *in vivo* tissue from which they originate. This thesis includes four publications highlighting cytoskeletal alterations in cancer cells under altered gravity conditions, as well as, the formation and the mechanisms of MCS growth in thyroid- and breast cancer cells.

The first paper focused on the development of a compact fluorescence microscope (FLUMIAS) for fast live-cell imaging in real microgravity. For the first time, the F-actin cytoskeleton was visualized in living Lifeact-GFP expressing follicular thyroid cancer cells (FTC-133) in response to microgravity.

The second paper investigated the early changes in gene expression of follicular thyroid cancer cells exposed to the RPM. The genes were regulated in a pro-angiogenic manner in MCS compared to controls.

Driven by the hypothesis that cells form tissue-specific MCS under microgravity conditions, MCF-7 breast cancer cells were exposed to the RPM. After a five-day RPM-exposure, the majority of MCS presented a cell-free lumen resembling ducts formed *in vivo* by human epithelial breast cells. Pathway analyses revealed involvement in the organization and regulation of cell shape, cell tip formation and membrane-to-membrane docking (Paper 3).

Paper number 4 demonstrated the importance of NF-κB for MCS formation in RPM-exposed MCF-7 cells. An interaction analysis of 47 investigated genes suggested that *HMOX-1*, *ICAM1* and NF-κB variants are activated when multicellular spheroids are formed. In addition, the application of NF-κB inhibitors resulted in a decrease in MCS formation.

Schlüsselwörter:

Schilddrüsenzellen; Schilddrüsenkarzinom; Brustzellen, Mammakarzinom, Tissue-Engineering, Höhenforschungsrakete; reale Mikrogravitation; Simulation der Mikrogravitation; Random Positioning Machine; Transkriptom; Zytoskelett

Keywords:

Thyroid cells; thyroid cancer; mammary cells; breast cancer; tissue engineering; Sounding Rocket; real microgravity; simulation of microgravity; Random Positioning Machine; transcriptome; cytoskeleton;

This thesis is based on the following chronologically ordered papers:

1. Corydon TJ, **Kopp S**, Wehland M, Braun M, Schütte A, Mayer T, Hülsing T, Oltmann H, Schmitz B, Hemmersbach R, Grimm D. Alterations of the cytoskeleton in human cells in space proved by life-cell imaging. Sci Rep. 2016 Jan 28;6:20043. doi: 10.1038/srep20043.

2. Riwaldt S, Bauer J, Wehland M, Slumstrup L, **Kopp S**, Warnke E, Dittrich A, Magnusson NE, Pietsch J, Corydon TJ, Infanger M, Grimm D. Pathways regulating spheroid formation of human follicular thyroid cancer cells under simulated microgravity conditions: a genetic approach. Int J Mol Sci. 2016 Apr 8;17(4):528. doi: 10.3390/ijms17040528.

3. **Kopp S**, Slumstrup L, Corydon TJ, Sahana J, Aleshcheva G, Islam T, Magnusson NE, Wehland M, Bauer J, Infanger M, Grimm D. Identifications of novel mechanisms in breast cancer cells involving duct-like multicellular spheroid formation after exposure to the Random Positioning Machine. Sci Rep. 2016 May 27;6:26887. doi: 10.1038/srep26887.

4. **Kopp S**, Sahana J, Islam T, Bauer J, Corydon TJ, Schulz H, Saar K, Hübner N, Slumstrup L, Riwaldt S, Wehland M, Infanger M, Lützenberg R, Grimm D. The role of NF-κB in spheroid formation of human breast cancer cells cultured on the Random Positioning Machine. Sci Rep. 2018 Jan 17;8:921. doi: 10.1038/s41598-017-18556-8

The publication texts can be found in the appendix of this dissertation.

Table of Contents

Abbreviations:

μ*g*	microgravity		IκB (*IKBKG*)	NF-kappa-B essential modulator (gene)
2D	Two-dimensional		*IL8*	Interleukin-8 gene
3D	Three-dimensional		ISS	International space station
ACTA2	Actin, aortic smooth muscle gene		*ITGB1*	Integrin beta-1 gene
ACTB	Beta-actin gene		km	Kilometre
AD	Adherently growing cells after μg		*KRT8*	Keratin, type II cytoskeletal 8 gene
ADM	Adrenomedullin gene		*LAMA3*	Laminin subunit alpha-3 gene
ALDOC	Fructose-bisphosphate aldolase C gene		LEO	Low earth orbit
ANGPTL4	Angiopoietin-related protein 4 gene		MCF-7	Breast cancer cell line
ANKRED37	Ankyrin repeat domain-containing protein 37 gene		MCS	Multicellular spheroid
ANXA1	Annexin A1 gene		min	minutes
ANXA2	Annexin A2 gene		mm	Millimetre
BAX	Apoptosis regulator BAX gene		*MMP3*	Matrix metalloproteinase-3 gene
BCL2	Apoptosis regulator Bcl-2 gene		*MMP9*	Matrix metalloproteinase-9 gene
BNIP3	BCL2/adenovirus E1B 19 kDa protein-interacting protein 3 gene		NASA	National astronautics and space administration
CASP3	Caspase-3 gene		*NDRG1*	Differentiation-related gene 1 protein gene
CASP9	Caspase-9 gene		*NFKB1*	Nuclear factor NF-kappa-B p105 gene
CAV1	Caveolin-1 gene		*NFKB2*	Nuclear factor NF-kappa-B p100 gene
CAV2	Caveolin-2 gene		*NFKB3*	Nuclear factor NF-kappa-B p65 gene
COL4A5	Collagen alpha-5(IV) chain gene		*NFKBIA*	NF-kappa-B inhibitor alpha gene
CSS	Chinese space station		*NFKBIB*	NF-kappa-B inhibitor beta gene gene
CTGF	Connective tissue growth factor gene		*NFKBIE*	NF-kappa-B inhibitor epsilon gene
CYC1	Cytochrome c1 gene		NF-κB	Nuclear factor NF-kappa-B
d	Days		*P53*	Tumour suppressor p53 gene
DLR	Deutsches Zentrum für Luft-und Raumfahrt		*PAI1*	Plasminogen activator inhibitor 1 gene
ECM	Extracellular matrix		*PARD3*	Partitioning defective 3 homolog gene
ESR1	Oestrogen receptor gene		*PARD6*	Partitioning defective 6 homolog gene
EZR	Ezrin gene		*PARP1*	Poly [ADP-ribose] polymerase 1 gene
F-actin	Filamentous actin		PCR	Polymerase chain reaction
FAS	Tumour necrosis factor receptor superfamily member 6 gene		*PGR1*	Progesterone receptor gene
FLK1	Vascular endothelial growth factor receptor 2 gene		*PKC*	Protein kinase C gene
FLUMIAS	Compact fluorescence microscope for fast live-cell imaging under real microgravity		pLAGICT	Lifeact-GFP-IRES-mCherry-Tubulin
FN	Fibronectin gene		*PRKCA*	Protein kinase C alpha gene
FTC-133	Follicular thyroid cancer cell line		*PRKCI*	Protein kinase C iota gene
g	Gravity force		r-μ*g*	Real microgravity
GFP	Green fluorescent protein		*RDX*	Radixin gene gene
h	Hours		*RHOA*	Transforming protein RhoA gene
Her2	Human epidermal growth factor 2		RPM	Random positioning machine
HMOX1	Heme oxygenase 1 gene		rpm	Revolutions per minute
ICAM1	Intercellular adhesion molecule 1 gene		s	Seconds

s-µ*g*	Simulated microgravity	*VEGFA*	Vascular endothelial growth factor A gene
TUBB	Tubulin beta chain gene	*VEGFD*	Vascular endothelial growth factor D gene
UCLA RO-82-W-1	Thyroid cancer cell line	ZARM	Zentrum für Angewandte Raumfahrttechnologie und Mikrogravitation

1 Preface

This doctoral thesis includes experiments conducted and analysed between April 2015 and December 2017 at the University Clinic (Clinic for Plastic, Aesthetic and Hand Surgery, working group of Professor Dr. med. Daniela Grimm) of the Otto-von-Guericke-University Magdeburg in Germany. Experiments using the Random Positioning Machine (RPM), enzyme-linked immunosorbent assays (ELISAs) and confocal laser scanning microscopy (CLSM) were performed at Aarhus University, Department of Biomedicine (Aarhus, Denmark), in the laboratories of Professor Dr. med. Daniela Grimm.

Live-cell imaging analyses of human cells were performed during the 24th DLR parabolic flight campaign (PFC) in February 2014 at NOVESPACE, Bordeaux-Merignac, France and during the TEXUS 52 Mission in April 2015 at Esrange, launch centre, Kiruna, Sweden. In addition, the group attended the 25th DLR PFC. These missions were possible due to the cooperation of the German Aerospace Agency with the Swedish Space Agency and the companies Airbus Defence & Space (ADS), FEI Munich GmbH, DLR MORABA, OHB-System AG and Novespace (Bordeaux, France).

(24th and 25th parabolic flight campaigns: http://www.dlr.de/rd/desktopdefault.aspx/tabid-9288/15996_read-39383/; http://www.dlr.de/rd/desktopdefault.aspx/tabid-9964/17036_read-41225; and sounding rocket flight campaign TEXUS-52: http://www.dlr.de/rd/desktopdefault.aspx/tabid-9288/15996_read-39383/).

Supervisors:

Professor Dr. med. Daniela Grimm
Institute for Biomedicine, Pharmacology, Aarhus University,
Aarhus, Denmark
and
Guest Professor for Gravitational Biology and Translational Regenerative Medicine
Otto-von-Guericke-University, Magdeburg, Germany

Professor Dr. med. Manfred Infanger
Director of the Clinic for Plastic, Aesthetic and Hand Surgery
University Hospital, Otto-von-Guericke-University Magdeburg,
Magdeburg, Germany

Mentor:
Professor Thomas Corydon
Professor for Experimental Ocular Gene Therapy
Department of Biomedicine and Department of Clinical Medicine, Aarhus University,
Aarhus, Denmark

2 Hypotheses

The hypotheses for this thesis are: 1) Microgravity alters the cytoskeleton in different cell types. 2) Exposure to the RPM induces scaffold-free 3D multicellular spheroid (MCS) formation. These spheroids might be a valuable tool for the identification of new drug targets as they resemble the *in vivo* tissue much closer than conventional cell culture. 3) Several signalling pathways influence 3D growth of thyroid cancer cells and breast cancer cells. 4) These cancer cells synthesize different proteins in microgravity, showing an altered gene expression pattern of genes involved in angiogenesis and 5) the NF-κB signalling pathway is involved in the formation of MCS.

3 Aims

The principal aims of this doctoral thesis were:

a. to verify whether and how the cytoskeleton changes in microgravity using live-cell imaging with a newly engineered microscope, suitable for operation during parabolic flights and sounding rocket flights.
b. to investigate the mechanisms of 3D growth after cell exposure to the RPM by focusing on factors playing a key role in angiogenesis and metastasis in cancer.
c. to evaluate the gene expression in 3D spheroids and adherent cancer cells via microarray and qPCR techniques. This was performed by evaluating gene and protein data using pathway analysis programs

4 Introduction

Long-term stays of astronauts on space stations like the International Space Station (ISS), as well as recent plans for human deep space exploration, have boosted interest in microgravity-related changes occurring in the human body (1). In addition, a stay in real microgravity in space was found to be an interesting environment for the investigation of cell growth behaviour and 3D tissue engineering (2-4). To study the effects of real microgravity (r-μg) on human cells, a variety of platforms are available, ranging from drop-towers to space stations. However, there are also some devices aiming to simulate microgravity (s-μg), which are easily accessible to perform control and pilot studies on Earth (see below).

4.1 Humans in Space

The desire to explore the unknown is an innate trait of humanity, which has also driven mankind to conquer space. However, humans have to face different kinds of challenges when they live in space for a longer time period, for example severe health problems (5). Despite the psychological aspects of being confined to a restricted area and being exposed to a variety of cosmic radiation, the condition of weightlessness is a challenge that has an immediate effect on the astronauts (5). As life on Earth evolved under a constant gravitational force, it is imaginable that microgravity conditions can induce in massive changes. Especially the weight-bearing structures like bones, muscles and cartilage are exposed to different sets of stresses (5).

The most prominent weight-bearing system affected by microgravity is the skeleton, which develops osteoporosis-like lesions when exposed to microgravity (4, 6). The bone mass is decreased, and its microarchitecture is altered due to disuse, especially in the lower limbs (6).

Comparable effects can be observed when investigating the muscle mass and strength of astronauts. As smaller forces are necessary for the movement and handling of objects or their own bodies, astronauts' muscles degenerate in a comparable fashion to muscle atrophy on Earth (7).

In addition, cartilage needs a moderate but continuous load to stay healthy. As the tissue is not directly blood supplied, nutrient exchange is mainly achieved by a sponge effect when it is loaded and released. Due to unloading in microgravity, cartilage tissue is not sufficiently supplied and, as a result, degenerates (8).

Furthermore, microgravity induces a fluid shift in the body, leading to fluid accumulation in the upper part, a condition called "Puffy Face Birds Leg Syndrome" (5). While blood is not flowing with the gravity vector into the lower body, the heart does not need to pump blood against gravity into the upper body.

Additional systems that undergo dysregulation during and after long-term residence in microgravity are the immune system (1), the cardiovascular system (9) and the ocular system (10).

4.2 Microgravity Research Platforms

The following paragraphs will explain the different possibilities to investigate biological samples in real and simulated microgravity. They will give an overview about the duration of microgravity and how it is possible to simulate microgravity on Earth.

4.2.1 Real Microgravity

The platforms for research in real microgravity can be arranged by the duration of achieved microgravity, ranging from a couple of seconds up to weeks (Fig. 1).

Drop towers, such as the one operated by the Zentrum für Angewandte Raumfahrttechnologie und Mikrogravitation (ZARM) in Bremen, can provide up to 9 s of high-quality, perturbation-free microgravity of about 10^{-6} g. A vacuum is generated inside the tower. A capsule, carrying the experiments, is shot upright with the help of a catapult, following a ballistic flight path, during which the samples on board the capsule experience weightlessness (11).

The next platform to obtain real microgravity is a parabolic flight. A specially equipped aircraft conducts a parabolic flight manoeuvre up to 31 times. Each parabola starts with a 20-s hyper-g phase of ~1.8 g, followed by 22 s of microgravity and ends with a second 20-s hyper-g phase. In total, one flight day results in a cumulative time of about 12 min of microgravity. On this unique platform, scientists can perform their own experiments while in weightlessness (12).

Another platform for studies in microgravity are sounding rockets. They carry payloads equipped with experiments on a very steep parabola up to a height of 705 km depending on the motor system used. In Europe, the rocket launch centre is ESRANGE, located near Kiruna, Sweden, in a sparsely inhabited area. This is necessary, as during the flight, the motors of the rocket are ejected and fall back uncontrolled to Earth. In addition, the payload will land on Earth, speed-controlled by a parachute. The most famous cargo rockets are MASER/TEXUS, which reach an apogee of about 260 km and maximum microgravity duration of 6 min, and MAXUS, which reaches 705 km and microgravity duration of 15 min. During the flight, most of the experiments can be checked and controlled via telemetry (13).

An unmanned spacecraft can increase the duration the time in orbit up to weeks. These are usually satellites equipped with a variety of experiments, which are automatically executed. Brought into lower Earth orbit (LEO), they accomplish their tasks and return to Earth. An example is the SIMBOX/Shenzhou-8 mission flown in 2011, where thyroid cancer cells, among other cell types, were carried into space by a Shenzhou rocket. During the 2-week stay in space, the cells were automatically fed and fixed before the capsule returned to Earth (14).

In addition, the most famous laboratory in space is the ISS. It was built in space piece by piece starting in 1998 with the Russian module Zarya. From 2000 until now, it was continuously used and experiments from various disciplines have been executed (http://www.space.com/16748-international-space-station.html) in its facilities. Moreover, the PR China is currently constructing a Chinese Space Station (CSS), Tiangong, which will consist of multiple modules and is supposed to be in operative condition by 2020 (http://www.space.com/27320-tiangong-1.html).
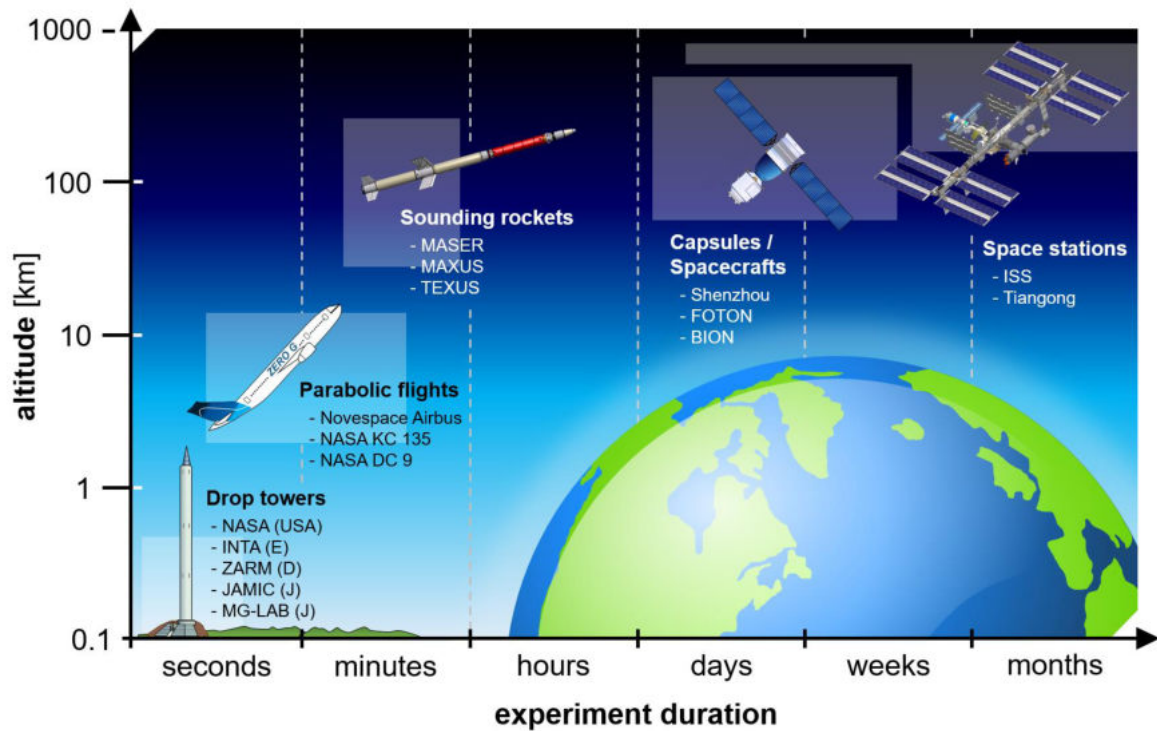
Figure 1 Schematic representation of real microgravity research platforms arranged by experiment duration and altitude. Highlighted boxes indicate the range of flight altitudes achieved by the various platforms.

4.2.2 Simulated Microgravity

Bringing a sample into space and to the ISS is a financial and logistical challenge and only a few scientists have the opportunity to carry out a space experiment (15). In addition, the replications of the experiments and the number of samples are also severely limited (16). Therefore, simulations prior to the actual r-µg experiments are the method of choice to optimize the experimental setup and minimize failure. Furthermore, performing s-µg experiments, exposing biological samples to this special culture environment can increase our knowledge of cell behaviour. For that purpose, a variety of devices were invented to cancel particle sedimentation. In theory, that should simulate microgravity and is called clinorotation (17); however, each approach has its own inherent drawbacks.

The classical 2-dimensional (2D) clinostat rotates a sample around an axis perpendicular to the gravity vector (18). Details of the device are published in Herranz *et al.* 2013 (19). Calculations revealed that samples should not exceed a radius of 1.5 mm around the rotation axis, and rotation speed should be restricted to less than 60 rpm, which results in a theoretical g-force of 6×10^{-3} g (18). While the fluid disturbance and the shear forces are rather low using the 2D clinostat, the sample size itself is clearly limited (18).

The RPM, uses a comparable principle but can add two additional dimensions (Fig. 2A). Two cardanic frames are rotated independently, enabling random motion and increasing the sample

diameter (20). While the sample is rotated, it follows a spherical path of movement (Fig. 2 B) Calculations revealed that at a radius of 7 cm around the rotation point and at 12.5 rpm, the residual acceleration is between 10^{-4} and 10^{-3} g (21). Even though the sample size is larger compared to that in the 2D clinostat, depending on the cell culture flasks used, shear forces arise, especially on the walls of the flasks, which need to be taken into account when discussing experimental results (22, 23).
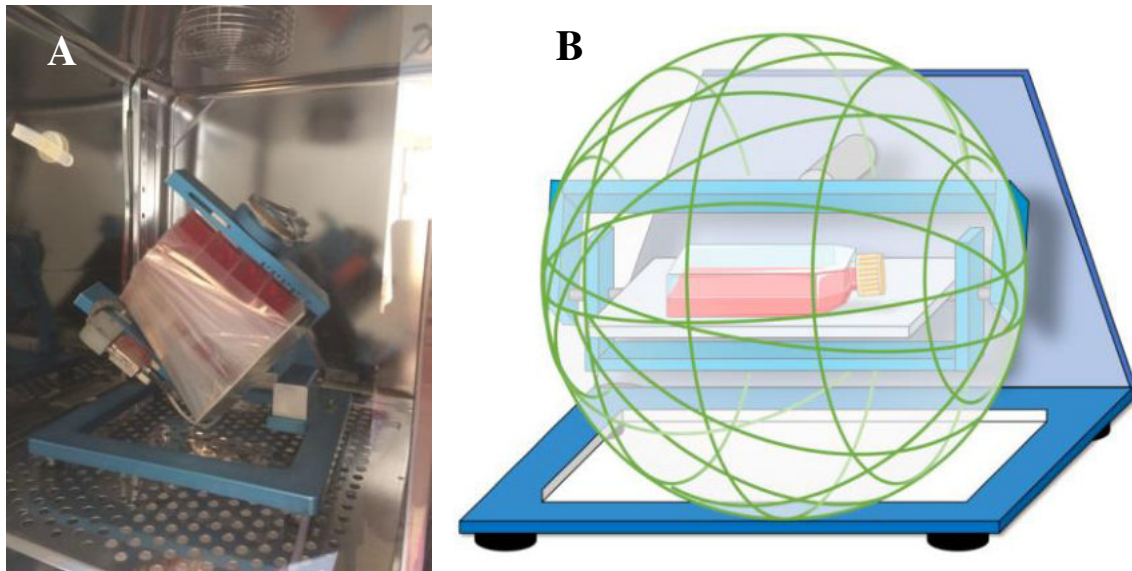

Figure 2 The Random Positioning Machine. Operating RPM (A) and the principle of annulling particle sedimentation on the RPM (B).

4.3 The Cytoskeleton as a "Gravireceptor"?

The cytoskeleton is a composite of microfilaments, microtubules and intermediate filaments, which, in concert, contribute to cell shape and maintenance. In addition, it connects the cell environment with the cytoplasm by transmitting chemical and physical signals (24).

Usually, higher organisms use gravity-specific organs to perceive gravity and to orientate themselves in the 3D environment on Earth. While plants use statocytes in their roots, in which statoliths fall on receptors and provide the plant information in up and down directions (25), mammals have comparable mechanisms in the inner ear. The vestibular organ, especially the ortholitic organ, is responsible for sensing changes in linear acceleration and for the initiation of related reactions (25).

Interestingly, single cells without a specific gravity-sensing organ are also reacting to changes in g-forces. Human immune cells exposed to r- and s-µg presented various alterations. T-lymphocytes, for example, lost their mitogenic activation during weightlessness in space (26). In addition, experiments in r-µg revealed gene expression changes in monocytes associated with differentiation into macrophages (27, 28). Differentiated macrophages in turn presented a reduced activity of reactive oxygen species immediately in response to microgravity during a parabolic flight (29).

However, in addition to highly reactive immune cells, cells of lower turnover tissues like bone and cartilage also showed changes upon exposure to weightlessness. Osteoblasts flown on a space shuttle mission presented a reduced growth rate even though cell viability was normal (30). In addition, chondrocytes cultured on the RPM changed their extracellular matrix (ECM) expression leading to enhanced ECM secretion (31). Further cell types that altered their usual 1-*g* behaviour were endothelial cells (32) and glial cells (33), which exhibited an increased apoptosis rate in adherent cells, among other changes, when cultured under gravitational unloading conditions.

How can we explain the sometimes-massive changes of the different cell types, assuming they are not specialized gravity-sensing? How is the physical signal of gravity perceived by the cell and translated into a chemical signal? All cell types mentioned above, among others, showed a similar phenomenon. Irrespective of r- or s-µ*g*, cytoskeletal changes developed upon various durations of exposure (34). Even though there are cell-type-specific differences, especially in the speed of the rearrangement and the re-adaptation to its previous state, the highly dynamic major cytoskeletal parts are postulated to be the "gravireceptor" of non-specialized cells (34). Having a deeper insight into the properties and functions of the cytoskeleton makes this suggestion even more plausible, as its major roles are spatial organization of cell contents, physical and chemical connection of the cell's interior and environment and coordinated movement (24). While it is still unclear how cells can transduce mechanical stress, including gravity changes, into a chemical signal, a model was postulated that relies on the cells having a tension-dependent architecture to organize and stabilize the cytoskeleton. In short, this "tensegrity model" is based on a pre-existing tension in cells (Fig. 3). When mechanical stress is applied, cells are forced to change their morphology. This change is transmitted via focal adhesion complexes in the cell membrane to the anchored cytoskeleton. As a result, the cytoskeleton rearranges, cell organelles are newly organized and gene expression is changed (35).
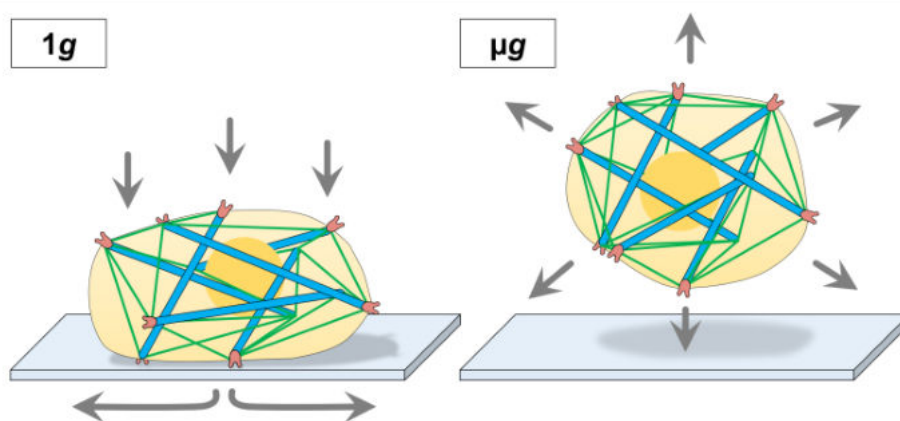

Figure 3 The tensegrity model. The tensegrity model describes the cell under pressure during 1 *g* and the released form during microgravity. Arrows indicate physical pressure. Red applications present focal adhesions, while green and blue show actin filaments and microtubules.

4.4 Tissue Engineering in Microgravity

Tissue engineering is the combination of the disciplines cell culture, engineering and biomaterials to replace or improve biological tissues. For a long time, the increased interest and its manifold applications made tissue engineering a stand-alone discipline (36). In addition to its definition, engineered tissue can also be used for testing new drugs or even as a food source (37).

Despite the fundamental reactions of cells to microgravity conditions and the importance for future space adventures, one important change is the formation of living 3D cell aggregates, also called multicellular spheroids (38). During long-term cultivation of adherent cell monolayers, either in space or on ground-based s-µg devices, some cells start to detach from the substrate and form aggregates (Fig. 4). These MCS, depending on the origin of the cells, resemble their tissue-specific morphologies and properties (15).
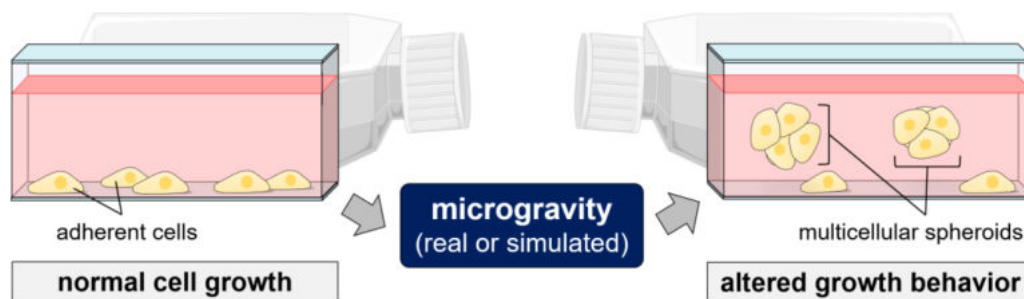

Figure 4 Formation of multicellular spheroids. During cultivation of adherent cells under altered gravity conditions a part of the cells detach from the substrate and form viable 3D-aggregates which float in the supernatant.

Recent space experiments for 7 d revealed a scaffold-free development of tube-like MCS using the human endothelial cell line EA.hy926 (39). Comparable results were found when EA.hy926 cells were cultured under s-µg conditions for various time spans (32, 40, 41). Tubes that resembled an intima-like structure were found after 3 d of culturing EA.hy926 cells on the RPM, accompanied by an increased rate of apoptosis (32). Furthermore, cultivation on the RPM for a longer time period elicited an elongation of the tubular structures of up to 12 mm (15).

Human chondrocytes cultured on the RPM formed 3D aggregates after 5 d (42). This process was accompanied by a changed production of extracellular matrix proteins (ECM) enhancing the functionality of the tissue (42). Human adult retinal pigment epithelial cells exposed to the RPM for 5 and 10 d formed MCS. As observed in chondrocytes, this was accompanied by changes in the production of ECM proteins (10).

Different studies of thyroid cells were conducted in r- and s-µg using different devices. Experiments on an unmanned spacecraft (Fig. 1) during the SIMBOX/Shenzhou-8 mission showed MCS formation of the thyroid cancer cell line FTC-133 after 10 d in space. Gene array analyses revealed over 2880 differentially expressed genes in the space samples, of which most were classified as involved in the stress response and proliferation, with the majority of them regulated in an anti-

proliferative direction (43). Of note, after an exposure to the RPM for 7 or 14 d, healthy thyroid cells of the cell line Nthy-ori 3-1 form 3D multicellular structures resembling the metastasis-like MCS produced by thyroid cancer cells (44). Even though MCS produced by the normal cell line were smaller than the ones produced by cancer cells, major factors like the actin (*ACTB*) and tubulin (*TUBB*) genes were similarly differentially expressed (44).

4.5   Cancer

Cancer is a major cause of mortality worldwide with approximately 14 million new cases in 2012, a figure that is expected to increase by 70% in the next two decades (45). In 2015, cancer was responsible for 8.8 million deaths, making it the second leading cause of death globally (46). Cancer is a general term for a collection of diseases that can affect the whole body and is caused by abnormally growing cells (neoplasm or malignant tumour), which can grow beyond their normal boarders, invade neighbouring tissue and spread into far away body parts (metastases) (46). In this thesis, the focus is on the investigation of breast cancer, which was the second most common type of cancer in 2012 (45), and thyroid cancer, which is a frequent malignant neoplasm of the endocrine organs.

4.5.1   Thyroid Cancer

Thyroid cancer is classified histopathologically into five subtypes. Depending on the status of differentiation, mortality ranges from a very mild outcome with 97% and 93% 5- and 10-year survival rates, respectively, up to a very poor outcome of a 10% 1-year survival rate (47). The most common treatment for thyroid cancer is surgical removal accompanied by radioiodine therapy. While differentiated thyroid cancer cells are still capable of incorporating iodide, de-differentiated thyroid cancer cells lose this ability. For this reason, papillary and follicular thyroid carcinomas have a mild outcome in most cases, whereas de-differentiated thyroid cancer cells are difficult to treat (47).

To find new molecular targets for future treatment of de-differentiated thyroid carcinoma cells, low-differentiated FTC-133 follicular thyroid cancer cells are investigated when forming multicellular tumour spheroids on the RPM.

4.5.2   Breast Cancer

Breast cancer is the most frequent neoplasm in females and is divided into different subtypes on the basis of classical immunohistochemical markers like estrogen receptor and progesterone receptor, together with traditional clinico-pathological variables like tumour size and grade (48). Depending on the expression of these receptors in combination with the human epidermal growth factor 2 (Her2), the subtypes are ranked from 1, good outcome, to 3, poor outcome. However, as high-

throughput applications evolve and get easily accessible, the heterogeneity of these diverse neoplasms is found to be higher than expected (48). While early prognosis and good therapeutic treatment reduces the mortality of breast neoplasms, heterogeneity often results in resistance to pharmaceuticals (49).

This thesis focused on breast cancer cell behaviour when metastasis-like 3D structures formed on the RPM. Using the human breast cancer cells MCF-7, which are highly differentiated and express the estrogen and progesterone receptor, it focused on the driving factors of MCS. These factors might be interesting candidates in the search for future drug targets.

5 Discussion of the Publications

In the following sections, four selected publications are summarized and discussed.

5.1 Alterations of the Cytoskeleton in Human Cells in Space Proved by Live-Cell Imaging

A variety of experiments conducted on different cell types revealed cytoskeletal changes after short-term exposure to r-µg, however, investigations were only possible after fixation and post-flight analyses (12, 50). Ultimately, it remained unclear how fast the cytoskeleton rearranges itself, how it adapts to microgravity and if fixation in microgravity produces artefacts of cytoskeletal rearrangements. Therefore, the compact fluorescent confocal laser scanning microscope FLUMIAS was developed and was first tested during parabolic flights, successfully showing very-short-term reactions to r-µg in living cells, and finally used during a sounding rocket mission.

A major task for this study was to produce living cells that were stably transfected to visualize the F-actin cytoskeleton. We used the FTC-133 cell line, because these cells had been successfully used for space experiments (14, 51) and had proven to be relatively resistant to changes in temperature and lack of CO_2. They were stably transfected with a pcDNA3.1 (+)-based vector, entitled pLAGICT, simultaneously expressing the F-actin binding Lifeact-GFP hybrid protein as well as mCherry-tubulin (13). After cell transfection and G418 selection, resistant FTC-133 clones were isolated as those that showed bright GFP fluorescence (Ref. 13 Figure 3).

The key component of the FLUMIAS apparatus is a spinning disc confocal laser scanning fluorescence microscope, which was developed by FEI Munich GmbH. This microscope is capable of scanning thousands of sample points in parallel, resulting in rapid image creation. In addition, by using this setup, one has the advantage of eliminating out-of-focus light in each image plane, resulting in thin image slices with a high level of contrast and an improved signal-to-noise ratio (13)(Ref. 13 Figure. 1 and 2). Due to space requirements, the acceleration and vibration of the rocket during launch

14

and the restricted space, the alignment of the microscope components was adapted, and movable parts were limited to a minimum (Fig. 5D).

Prior to the experiments, human follicular thyroid cancer cells were seeded onto IBIDI µSlides (Fig. 5B), which hold medium chambers. Slides were then installed within the late access unit (developed and built by ADS), which was heated to 37 °C and kept until the very last moment before integration into the rocket.

To verify whether the microscope was working under microgravity conditions, and to obtain initial results of living cells in microgravity, the setup was tested during the 24th DLR parabolic flight campaign on board the A300 Zero G, operated by Novespace, Bordeaux, France. During the first parabola and as an immediate reaction to microgravity, actin bundles were disturbed and "holes" appeared in the cytoplasm, which were not visible in ground control samples. Furthermore, it seemed that the observed cytoskeletal changes developed during the following parabolas. In addition, the analysis indicated the disappearance of microvilli or filopodia- and lamellipodia-like structures during parabolic flights. These findings show that cytoskeletal changes are happening predominantly in the microgravity phase rather than in the hyper-g phases. To exclude the possibility of cytoskeletal changes due to vibration and hyper-g during the parabolic flights, cells were centrifuged at 1.8 g for 2 h, exposed to a parabolic flight vibration profile for 2 h and analysed with the FLUMIAS microscope. We found microvilli in 1 g ground control samples, which disappeared after 2 h of 1.8 g while prominent stress fibres arose. The vibration experiment, however, resulted in cells bearing cytoskeletal holes as seen during the parabolic flights.

To determine whether visible changes were in accordance with transcriptional changes, an experiment executed in parallel used fixed cells of the same batch after the last parabola for qPCR analysis. *ACTB* gene expression was highly upregulated in transfected cells after parabola 31, while vibration and hyper-g showed no influence on cytoskeleton-related genes, which supported the hypothesis that changes occur due to microgravity.

To minimize the effect of vibration and acceleration and to increase the duration of microgravity, FLUMIAS was flown on the TEXUS 52 sounding rocket mission. Cells were prepared as prior to the parabolic flight mission and kept at 37 °C until launch (Fig. 5C, E). Pictures were taken pre-launch to be compared with pictures from microgravity. Immediately after entering microgravity, the cell morphology changed markedly. Where prominent actin bundles were visible in the pre-flight picture, they were annihilated and noticeable cell attachments with microvilli arose (Fig. 5F).

In summary, live-cell imaging revealed that both cell morphology and the actin cytoskeleton are strikingly changed as a result of microgravity exposure. Finally, FLUMIAS proved to be a powerful tool to explore live translocations within biological systems upon µg influence.

Figure 5 Different stages of the FLUMIAS preparatory and experimental workflow. Clean bench work (A) and filling the IBIDI μSlides (B; Paper 1 Fig. 3 D). Further, the implementation of the slides into the late access unit (C) and incorporation of the late access unit into the microscope (D) (shown here is a test prior to installation in the rocket body). The rocket launch (E) and the results obtained from 1 *g* pre-flight followed by image stacks during microgravity in space (F). All work was performed at Esrange, Kiruna, Sweden.

5.2 Pathways Regulating Spheroid Formation of Human Follicular Thyroid Cancer Cells under Simulated Microgravity Conditions: A Genetic Approach.

Altered gravity conditions offer new possibilities to investigate cellular behaviour and can be a valuable tool for tissue engineering (15). A variety of cell types are known to form 3D cell aggregates when cultured under r-μ*g* (14, 39) and s-μ*g* (10, 32, 42, 44). However, the underlying mechanisms have yet to be studied. In most cases, the MCS are very similar to the *in vivo* tissue from which they originate, which makes cancer-related MCS an especially valuable tool to investigate new drug targets. The aim of this study was to identify pathways involved in MCS formation of the human thyroid cancer cell line UCLA RO82-W-1 after 24 h of RPM exposure by applying molecular biological as well as *in silico* methods. Semi-confluent UCLA RO82-W-1 cells exposed to the RPM separated into two cell populations. One continued to grow adherently (AD), while the other formed 3D cell aggregates (MCS).

To investigate the process of spheroid formation, 24 genes, which were implicated in the formation and inhibition of MCS in previous studies, were selected for further analysis. These could be classified as follows: establishing and regulating cell structure, extracellular proteins regulating cell behaviour and proteins involved in angiogenesis and signalling processes. A pathway studio analysis

revealed that the expression of these genes was mutually controlled within the frame of a network (Fig. 6) which spanned the cell exterior, the membrane, the cytoplasm and the nucleus.

Examining the gene expression of cytoskeleton and cytoskeleton-associated proteins revealed a significant downregulation in most MCS samples for *ACTB*, *KRT8*, *EZR*, *RDX*, *ACTA2* and *TUBB*. Factors involved in angiogenesis, like *VEGFA* and *VEGFD*, were upregulated in MCS samples in addition to an increased VEGFA protein concentration in the cell culture supernatant, while associated *VEGFR2* receptor was only slightly downregulated. A member of the protein kinase C (PKC) pathway, *PRKCA*, which is involved in proliferation, showed a clear downregulation in RPM samples, which was also the case for connective tissue growth factor (*CTGF*).

As previously described, the amount of ECM in concert with increased caveolin-1 (*CAV1*) can cause a firm anchoring of the cells and thus an inhibition of MCS formation (51). To complement these results, gene expression profiles of ECM proteins and ECM-degrading proteins were investigated. Matrix metalloproteinase-3 (*MMP3*) was significantly upregulated in AD and MCS samples, while *MMP9* was upregulated in AD but downregulated in MCS samples. In addition, *CAV1* and *CAV2* were downregulated in AD and MCS samples.
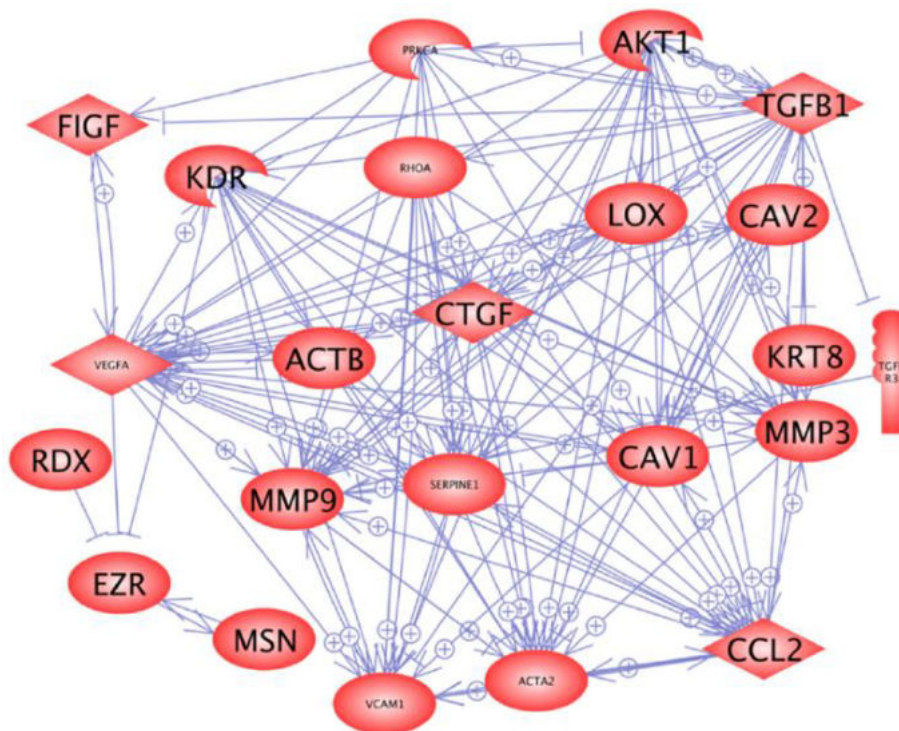

Figure 6 (Paper 2 Fig. 6) Mutual interaction of selected genes involved in spheroid formation. Arrows with a (+) indicate positive regulation, stand-alone arrows indicate interaction and connections with flat arrowhead indicate negative regulation.

An *in silico* search for mutual gene regulation between the selected genes revealed all genes to be in a network with *CTGF* representing the core. Furthermore, results from recent studies using the thyroid cancer cell line FTC-133 (52) indicated that plasminogen might inhibit proper spheroid formation. In this study on UCLA RO82-W1 thyroid cancer cells, the plasminogen activator inhibitor-1 (*PAI1*) was significantly downregulated.

qPCR indicated that in cells remaining adherent during the first 24 h of RPM exposure, 16 of the 24 genes investigated remained unaltered, while 7 were downregulated and 1 was upregulated. In contrast, MCS showed 10 non-regulated, 11 downregulated and 3 upregulated genes. To explain the different gene expression patterns of AD and MCS and how they might contribute to the formation of spheroids, qPCR results and pathway analyses results were matched. Most interestingly, *VEGFA* and *VEGFD* showed pronounced and simultaneous upregulation in MCS and were simultaneously upregulated earlier (53). In addition, RPM samples presented an elevated VEGFA protein content in the supernatant, suggesting the cells to be grown at higher levels of VEGFA. This proposes that only cells with a combined upregulation of *VEGFA* and *VEGFD* build spheroids. As presented in figure 5, VEGF affects the regulation of a variety of genes. Among other targets, it is known to downregulate α/β-actin gene expression (54) and to upregulate *MMP-3/9* expression (55, 56). In addition, we found in earlier experiments a downregulation of *PAI1,* which was associated with enhanced VEGF protein expression (57).

Taken together, the gene expression pattern of ECM-involved molecules and the regulatory features and resulting gene expression changes of VEGF point in the direction of an environment conducive to spheroid formation and might help the cells to switch from 2D to 3D growth.

5.3 Identifications of Novel Mechanisms in Breast Cancer Cells Involving Duct-Like Multicellular Spheroid Formation after Exposure to the Random Positioning Machine

In most cases, MCS of different cell types exhibit tissue-specific properties. Therefore, studies on MCS formed under altered gravity conditions are of high interest for tissue engineering and pharmaceutical development (58).

Breast cancer is the second most common cancer worldwide, and the probability of a complete cure is enhanced by the availability of a wide variety of effective treatments. However, tumours can either respond poorly to chemotherapeutics or can develop resistance to drugs, which increases the need to find new targets in this cancer type, in addition to easy-to-study tools.

In this publication, we investigated the formation of MCS of the human breast cancer cell line MCF-7. A time series of 2 h, 4 h, 16 h, 24 h and 5 d of exposure to the RPM was used to provide initial insight into the nature and course of changes in breast cancer cells transitioning from 2D growth to 3D-tissue-specific cell aggregate formation.

We detected that after a 16-h RPM exposure the cells started to form solid MCS being suspended in the supernatant along AD cells. After a 5-d exposure, these solid MCS were mostly replaced by MCS exhibiting a cell-free lumen. Histological examinations revealed that these structures consisted of a cavity lined by a single layer of cells comparable to ducts in breast tissue. In addition, the cells presented a visible polarization.

Polarization of cells is mandatory for the production of milk. To investigate changes in cell polarization, we examined the gene expression of the involved Par3(Bazooka)-Par6-aPKC protein complex, which localizes at the apical membrane and promotes the apical membrane identity. While *PRKCI* gene expression was downregulated in 5d-MCS, *PARD3*, *PARD6* and *RHOA,* mRNAs were unregulated, suggesting that the cells were not fully polarized.

This hypothesis was supported by investigation of the morphological changes revealed by F-actin and 4',6-diamidino-2-phenylindole (DAPI) nuclear staining of cells after RPM exposure. While short-term RPM exposure resulted in membrane blebbing after 2 h, stress fibres after 4 h and cytoskeletal holes after 24 h, these effects were all present in 5d-RPM-AD cells. An accumulation of F-actin was visible at the cell boundaries, and some cells showed pronounced cytoskeletal holes and stress fibres. Cells included in the MCS presented an accumulation of actin at the cell boundaries but no distinct polymerization direction was visible.

In order to identify the underlying mechanisms of the transition from 2D to 3D growth, we selected 29 genes, which came into focus during earlier studies. They consisted of 6 extracellular matrix proteins, 6 membrane proteins, 15 cytoplasmic proteins, and 2 nuclear proteins. Gene products are categorized as follows: regulation and maintenance of cell structure, apoptosis or specific to female epithelial cells. Pathway analysis revealed that the gene expression of 28 genes is mutually controlled within the frame of a network and its gene products are localized in the cell environment, the membrane and the nucleus (Fig. 7).
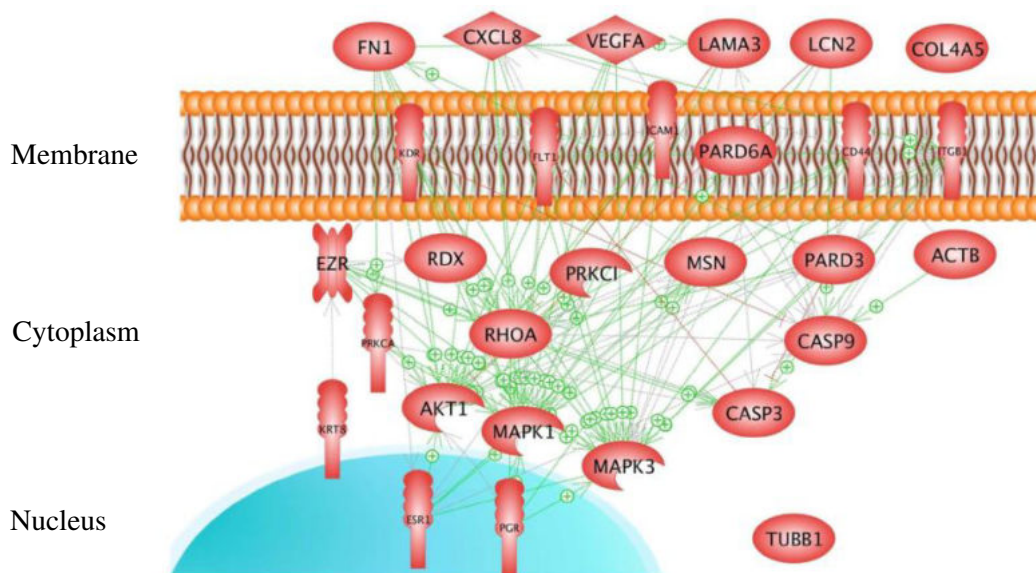

Figure 7 (Paper 3 Fig. 5) Network of mutually controlled gene products spanning from outside the cell, across the plasma membrane to the nucleus. (+) indicates positive regulation, while blunt arrowhead indicates negative interaction

First, we investigated the gene expression of cytoskeletal and associated proteins. While after short-term RPM exposure, no significant regulation of these genes was visible, remarkable downregulation of gene expression was found in 5-d-MCS, suggesting dramatic rearrangements.

Because the composition of the extracellular matrix is crucial for tissues, the gene expression of laminin (*LAMA3*), fibronectin (*FN*) and collagen IV (*COL4A5*) was analysed in concert with that of anchoring proteins like integrin-β-1 (*ITGB1*) and intercellular adhesion molecule 1 (*ICAM1*). While most genes were unregulated from 2 h to 16 h of RPM exposure, *FN* presented a downregulation in RPM-AD cells after 2 h and *ITGB1* an upregulation after 4 h. Notably, in the time course, anchoring gene products and most ECM gene products revealed a significant regulation in MCS after 24 h and 5 d of exposure to the RPM.

As a major factor in angiogenesis and a proven target for cancer therapy, the vascular endothelial growth factor signalling pathway is of high interest for tissue formation. We investigated the gene expression of involved genes and found vascular endothelial growth factor A (*VEGFA*) significantly upregulated after 2 h and 4 h in RPM-AD cells, while from 16 h to 5 d, it was massively downregulated in RPM-exposed cells. In contrast, the VEGF receptors were only marginally regulated after short-term exposure, and only vascular endothelial growth factor receptor 2 (*FLK1*) was noticeably downregulated after a 5-d exposure. In addition, downstream signalling pathway molecules were predominantly downregulated compared with the corresponding controls.

Finally, we investigated the expression of the signalling molecule interleukin 8 (*IL8*) and the female epithelial-associated oestrogen (*ESR1*) and progesterone (*PGR1*) receptors. *IL8* was highly upregulated in RPM-AD cells after 2 h and 4 h and in 24h-MCS. The estrogen receptor gene expression was only significantly upregulated in 5d-RPM-AD, while the progesterone receptor gene expression was significantly upregulated in 5d-RPM-AD and MCS cells.

As demonstrated in this thesis, cytoskeletal changes occurring as soon as 2 h after RPM exposure might mark the point of 3D growth initiation. By altering the cytoskeleton, signalling pathways, gene expression and protein synthesis are influenced. After 5 d of RPM culture, the cells had split into adherently growing cells and 3D-aggregates with a cell-free lumen. These cells presented an apical-basal polarity, which can only be established when cells interact with the surrounding medium, neighbouring cells and the ECM. Initiation of lumen building might be possible due to the interaction of integrin in the membrane and laminin, as both were upregulated in MCS.

While we, so far, could only present non-malignant cells to form tissue-like structures, such as chondrocytes form cartilage and endothelial cells form the intima of blood vessels, malignant cells usually had built up round metastases. The reason that MCF-7 breast cancer cells form gland-like structures to be found in mammary gland tissue might be due to the high grade of differentiation, also shown by the expression of estrogen and especially the highly upregulated progesterone receptors in MCS. In addition, other studies suggest that simulated microgravity initiates the reversion of the neoplastic phenotype of lung cancer stem cells (59) giving another hint as to why breast cancer cells form gland-like structures.

VEGF pathway molecules are involved in promoting angiogenesis and linked to increased malignancy of cancer cells (60). Therefore, targeting this molecular group to fight cancer is of high

interest (60). We found *VEGFA* to be highly upregulated in cells exposed to the RPM for 2 h and 4 h, which indicates that the cells were preparing the process of angiogenesis. In addition, after 16 h, 24 h and 5 d, a downregulation of *VEGFA* was detected, which was also shown for thyroid cells exposed to the RPM for 7 d (44) and in space (43). This suggests decreased malignancy of the breast cancer cells in the direction of a healthy cell phenotype, which may explain the formation of tissue look-alike spheroids and agrees with the results previously obtained for lung cancer cells, which exhibited a less aggressive phenotype after being exposed to simulated microgravity (59).

In summary, we could produce MCS from breast cancer cells by exposing them to the RPM. These 3D structures exhibit the morphology of healthy glands *in vivo*. In addition, we showed a decrease of angiogenesis initiation, suggesting differentiation of MCF-7 cells grown in 3D spheroids towards a less aggressive cancer type. If the spheroids resemble real ducts with comparable functions as *in vivo* has to be determined in future studies.

5.4 The role of NF-κB in Spheroid Formation of Human Breast Cancer Cells Cultured on the Random Positioning Machine.

Studies on low-differentiated follicular thyroid cancer cells of the FTC-133 cell line exposed to the RPM for 24 h suggested that NF-κB is involved in the process of spheroid formation (61). When this result can be confirmed for other cancer cell types, it might show new possibilities for therapeutic treatments. To investigate this option, we cultured MCF-7 breast cancer cells on the RPM for 24 h and analysed the changes of NF-κB and associated proteins in controls, adherently growing cells and MCS.

Seeding MCS into slideflasks and re-cultivation of the spheroids under static culture conditions revealed an early migration of the cells from the 3D aggregates and showed their vitality. In addition, acridine orange/ethidium bromide staining proved the viability of the cells in MCS.

To compare the results obtained for FTC-133 and MCF-7, we performed NF-κB p65 (RelA) immunofluorescence staining to evaluate its cellular distribution. While in control cells, NF-κB p65 was equally distributed in the cytoplasm and nucleus, RPM-exposed MCS presented a more intense staining of the cytoplasm and nucleus than RPM-exposed adherent cells. This suggests an increased amount of NF-κB p65 in MCS cells compared with RPM-AD cells.

In addition, NF-κB signalling factors were investigated. NF-κB p50, p52 and p65 are encoded by the gene loci *NFKB1, 2* and *3*, while the variations of its inhibitor IκB are encoded by *NFKBIA*, *NFKBIB*, *NFKBIE* and *NFKBG*. While *NFKB2*, *NFKB3* and *NFKBIB* showed a non-significant upregulation in RPM-AD and MCS cells, *NFKB1*, *NFKBIA*, *NFKBIE* and *IKBKG* presented a significant upregulation compared with control cells. RPM-AD cells only presented *IKBKG* to be significantly enhanced in comparison with control cells. Western blot analyses performed on unphosphorylated and phosphorylated NF-κB family analyses pointed in a similar direction as the

qPCR results. Interestingly, phosphorylated variants of the proteins are markedly enhanced in MCS samples, which suggest that phosphorylation of NF-κB family members is of importance during early MCS formation.

As we found similarities between the expression of *NFKB3* and the NF-κB p65 protein accumulation and growth behaviour to those of FTC-133 cells, we investigated additional genes, which had been the focus of our earlier studies. Of the selected genes (*ANXA1*, *ANXA2*, *CAV2*, *ICAM1*, *CTGF*), all were upregulated in MCS, while only *CTGF* was also upregulated in RPM-AD cells.

In addition, genes involved in intrinsic and extrinsic apoptosis pathways were investigated, as programmed cell death was found repeatedly to accompany cell responses to altered gravity conditions. While *CASP3* and *CASP9* mRNAs were not changed, *CASP8* was significantly upregulated in MCS versus control. *P53*, *CYC1*, *PARP1* and *FAS* were equally upregulated, while *BCL2* remained unaltered. The only expression change found in RPM-AD and MCS cells was an upregulation of *BAX*.

To detect additional genes that were differentially expressed in MCF-7 cells exposed to the RPM, we performed a microarray analysis. We found 319 genes and open reading frames to be differentially expressed, while 140 presented significant regulation of at least 1.4-fold. As a minimum two-fold differential gene expression is usually considered to indicate biological relevance, and this was found for only 23 genes, which were investigated further. Ten of these genes are linked to oxygen levels or hypoxia and were downregulated to an equal degree in RPM-AD and MCS cells. In addition, four genes were significantly (>2-fold) upregulated only in MCS, which coded for proteins suppressing apoptosis and regulating the heme concentration. A pathway analyses of the 23 genes revealed a network cross-linking 7 of the 23 genes, with hemoxygenase (*HMOX1*) being the most networked. To determine whether the genes determined by qPCR as upregulated in MCS cells interact with differentially expressed genes in the microarray, we subjected the results to a pathway analyses and found them to fit very well into the network.

CTGF and *BAX* as well as *ADM*, *ALDOC*, *ANGPTL4*, *ANKRD37*, *BNIP3* and *NDRG1* were comparably regulated in RPM-AD and MCS cells. Hence, an increase of oxygen in vented cell culture flasks due to rotation might induce expression changes. However, as spheroids also form in unvented flasks and in space, the increased oxygen availability might not be responsible for the transformation (14, 43).

In addition, we focused on gene expression changes between RPM-AD and MCS cells. Genes involved in apoptosis were markedly upregulated in MCS compared with RPM-AD cells. This was accompanied by upregulated genes whose products favour cell survival. One of these anti-apoptotic genes is *HMOX1*, whose product can be inhibited by caveolin-1, which in turn was postulated to inhibit spheroid formation. While *HMOX1* and *NFKB3* were found to be mutually downregulated, in

our experimental setup, *HMOX1* was upregulated while *NFKB3* remained unaltered. The upregulation could be due to the positive influence of *ADM* and *PARP-1*.

Despite the upregulation of *NFKB3*, an enhanced translocation of NF-κB p65 into the nucleus of MCS cells was noticed, regulated by the gene products of *NFKBIA* and *NFKBIB*, which were upregulated. Translocation initiates gene expression of various products, among them *ICAM1*, which was also upregulated in MCS. The effect of NF-κB p65 is also directed towards ICAM1 by *PARP1* and *S1PR3*. In concert, *CTGF*, *FAS* and *p53* have a positive influence on the gene expression of *ICAM1*. All genes were upregulated in MCS. ICAM-1 is a surface protein contributing to the cell-cell interaction, which is strongly required for spheroid formation. It either binds directly to integrin beta-2 or changes the structure of the cell adhesion complex.

To further investigate the involvement of NF-κB, PARP1 and PDE4 we treated the MCF-7 cells with specific chemical inhibitors during 24h RPM exposure. While various concentrations of olaparib (PARP1/2 inhibitor) and rolipram (PDE4 inhibitor) had no remarkable effect on MCS formation, increasing concentrations of dexamethasone (NF-κB inhibitor) markedly decreased the number of MCS.

In summary, it was demonstrated that cells within spheroids are viable and migrate out of the MCS when cultured at static condition, returning to their initial monolayer appearance. This shows that RPM exposure is of utmost importance to keep the 3D aggregate form and the two phenotypes (AD cells and MCS). In addition, a positive side effect of RPM exposure is an increased mixing of the nutrient medium, which was also demonstrated on the gene expression level.

And finally, *in silico* analyses suggested that NF-κB family members, HMOX-1 and ICAM1 interact when MCF-7 breast cancer cells transition from adherently growing cells to spheroids on the RPM. That was also underlined by the fact, that application of NF-κB inhibitors reduced the number of MCS. These preliminary findings, in concert with results obtained from studies with FTC-133 cells, suggest the NF-κB signalling pathway to be a potential new target for cancer treatment. This research topic will be in our focus in future investigations.

5.5   Conclusions

Early cytoskeletal and morphological changes were demonstrated in thyroid cancer cells (FTC-133) in r-µ*g* by live-cell imaging using the FLUMIAS device, in addition to expression changes of cytoskeletal and associated proteins. This thesis presents for the first time live-cell changes in space and proves that thyroid cancer cells are sensitive to microgravity.

These results were also detected when thyroid cancer cells (UCLA-RO-82-W1) and breast cancer cells (MCF-7) were exposed to a RPM, as all these cells presented changes in the cytoskeleton and associated proteins in concert with the formation of multicellular spheroids. The data confirm results achieved in previous studies under real and simulated microgravity on chondrocytes, endothelial cells and retina cells (10, 12, 31, 40). These results in concert with earlier findings, in addition to applying the tensegrity model, strongly suggest that cytoskeletal and morphological alterations are an initial trigger for cell behavioural changes under altered gravity conditions.

VEGF family member molecules were investigated for thyroid as well as breast cancer cells as they are strikingly involved in angiogenesis and cancer growth (60) and may be a key player in MCS formation. We measured an upregulation of *VEGFA* in MCF-7 breast cancer cells after short-term RPM exposure. Later, during the continuous development of the MCS, *VEGFA* gene expression was downregulated in RPM-exposed samples. In contrast, UCLA-RO-82-W1 thyroid cancer cells presented upregulation in 24-h-RPM-exposed samples. These results are comparable with previously obtained results. Long-term RPM-exposure (7–14 d) of the thyroid cells FTC-133 and Nthy-ori 3-1 presented a downregulation of *VEGFA* (44). A similar result was found in space, when FTC-133 cells were flown on a 5–10-d space mission (43). That suggests that *VEGFA* overexpression is mandatory for 3D aggregate initiation, independently of the cell type. However, in the following phase of MCS outgrowth, it is no longer needed. Though, deeper analysis is required to prove this point.

In addition to the initiation phase, the formation of tissue-specific MCS needs a favourable extracellular matrix composition. An increased expression of extracellular matrix proteins because of a launch delay was associated with the loss of the ability of the FTC-133 cells to form spheroids (51, 62). We found that the *MMP3* gene was upregulated and *CAV1*, *CAV2*, *PAI1* and *CTGF* were downregulated in 24-h-RPM-exposed UCLA-RO-82-W1 thyroid cancer cells, suggesting that proteinases degrade the ECM in concert with a reduced expression of ECM proteins. In contrast, MCF-7 cells presented an opposing result after cultivation on the RPM for 24 h as *CAV2*, *CTGF* and *PAI1* were upregulated. These results suggest that the composition of extracellular matrix proteins depends on the cell type and the state of differentiation of cancer cells. While the low-differentiated thyroid cancer cells enable migration through tissues by downregulating ECM proteins and upregulating proteases, the highly differentiated MCF-7 breast cancer cells produce spheroids, which resemble the tissue they originate from, which is why ECM protein expression could be upregulated and proteases are downregulated in MCS.

Finally, in previous studies, the formation of spheroids was in concert with an increased production of molecules involved in apoptosis while NF-κB p65 was translocated into the nucleus, which was interpreted as FTC-133 cells escaping late apoptosis initiation and forming spheroids (61). In this thesis, it was shown that pro-apoptotic molecules were downregulated in MCS, while NF-κB p65 immunostaining suggested translocation into the nucleus. These results confirm previous results and underline the assumption that cells escape apoptosis prior to forming spheroids. In addition, the rotation of the RPM is necessary to keep the 3D form, while it enabled increased gas and nutrition exchange, which was also evident at the gene expression level.

Future studies will be performed to clarify the exact mechanisms involved in the process of spheroid formation and tumour growth, such as genetic knockouts or knockins in cell lines.

5.6   Summary

Multicellular spheroids are formed in real and simulated microgravity irrespective of the cell type, and they mostly resemble their corresponding *in vivo* tissue. They are highly interesting for tissue engineering and drug testing; however, the mechanisms of 3D cell aggregation are still under investigation.

This cumulative thesis encompasses four publications, starting with live cell imaging of FTC-133 cells to examine cytoskeletal changes in real microgravity during a parabolic flight campaign and the TEXUS 52 sounding rocket mission. We were for the first time able to see live changes of the cytoskeletal in space.

The second paper reports the studies on the formation of MCS of the thyroid cancer cell line UCLA-RO-82-W1 after a 24-h-RPM-exposure. We found data in support of previous findings, suggesting an early involvement of VEGF in MCS formation.

The third publication reports data on differentiated MCF-7 breast cancer cells exposed to the RPM for a period of 2 h up to 5 d. While a short-term exposure resulted in solid MCS after 24 h, after 5 d, the MCS revealed a cell-free lumen resembling ducts within *in vivo* breast tissue. Their functionality must be more closely examined in the future.

The fourth manuscript showed investigations on the early MCS formation of MCF-7 cells in more detail. We found comparable results to the early spheroid formation of thyroid cancer cells, as the MCS cells presented reduced apoptosis activity in concert with NF-κB p65 translocation into the nucleus.

5.7   Zusammenfassung

Seitdem sich Raumfahrer regelmäßig über mehrere Monate am Stück im All aufhalten und besonders auch angesichts der Pläne der National Aeronautics and Space Administration (NASA), Menschen noch tiefer in den Weltraum zum Mars und möglicherweise darüber hinaus vordringen zu lassen, hat die Frage wie sich humane Zellen unter Schwerelosigkeit verhalten stark an Bedeutung gewonnen. Im Allgemeinen wird vermutet, dass humane Zellen Veränderungen der Gravitation über das Zytoskelett detektieren. Bislang jedoch konnten zytoskelettale Veränderungen nur nach der Fixierung in Schwerelosigkeit untersucht werden, was eine Darstellung der dynamischen Prozesse unmöglich machte. Eine Beobachtung war die Bildung von 3D-Zellaggregaten, den multizellulären Sphäroiden (multicelluar Spheroids, MCS) in Schwerelosigkeit. Diese MCS glichen häufig dem differenzierten *in-vivo* Gewebe aus dem die Zellen ursprünglich stammten.

Diese Dissertationsschrift besteht aus vier Publikationen, welche die dynamischen zytoskelettalen Veränderungen und die Mechanismen der MCS Bildung in Schilddrüsen- (FTC-133, UCLA RO82-W-1) - und Brustkrebszellen (MCF-7) näher beleuchten.

In der ersten Publikation wird die Entwicklung eines "compact fluorescence microscope (FLUMIAS) for fast live-cell imaging in real microgravity" dargestellt. Unter Verwendung dieses Mikroskops war es möglich, die zytoskelettalen Veränderungen in realer Schwerelosigkeit zu verfolgen. Um dies zu erreichen, wurden FTC-133 Zellen stabil mit Lifeact-GFP transfiziert und deren Aktin-Zytoskelett mittels des neuartigen Mikroskops während eines Parabelfluges und auf einer Höhenforschungsrakete untersucht.

Im zweiten Paper wurden die frühen genetischen Regulationen der Schilddrüsenkarzinomzelllinie UCLA RO82-W-1 während der MCS-Bildung näher studiert. Die Zellen wurden 24 Stunden lang auf der Random Positioning Machine (RPM), welche Schwerelosigkeit simulieren soll, kultiviert und danach analysiert. Die Ergebnisse wiesen auf eine pro-angiogene Regulation in MCS hin.

Der Hypothese folgend, dass humane Zellen unter Mikrogravitation gewebeähnliche Strukturen bilden, wurden MCF-7 Brustkrebszellen auf der RPM kultiviert. Nach fünf Tagen bildeten sich MCS mit einem zellfreien Lumen, die starke Ähnlichkeiten zu gesundem *in-vivo* Brustdrüsengewebe aufwiesen. Eine Pathway-Analyse verwies auf die Beteiligung von biologischen Prozessen wie der Organisation der Zellform, Zellpolarisation und Zell-Zell Kommunikation während der MCS-Bildung (Publikation 3).

In der vierten Publikation wird die Beteiligung von NF-κB bei der MCS Bildung von auf der RPM kultivierten MCF-7 Zellen untersucht. Eine Analyse der Interaktion von 47 untersuchten Genen lässt vermuten, dass *HMOX-1*, *ICAM1* und NF-κB Varianten bei der MCS Bildung aktiviert werden. Zudem wurde nach Applikation von NF-κB Inhibitoren eine verringerte MCS Bildung erreicht.

6 References

1. Frippiat, J. P., Crucian, B. E., de Quervain, D. J. F., Grimm, D., Montano, N., Praun, S., Roozendaal, B., Schelling, G., Thiel, M., Ullrich, O., and Chouker, A. (2016) Towards human exploration of space: The THESEUS review series on immunology research priorities. *Npj Microgravity* **2**

2. Pietsch, J., Bauer, J., Egli, M., Infanger, M., Wise, P., Ulbrich, C., and Grimm, D. (2011) The effects of weightlessness on the human organism and mammalian cells. *Curr Mol Med* **11**, 350-364

3. Grimm, D., Wise, P., Lebert, M., Richter, P., and Baatout, S. (2011) How and why does the proteome respond to microgravity? *Expert Rev Proteomics* **8**, 13-27

4. Grimm, D., Grosse, J., Wehland, M., Mann, V., Reseland, J. E., Sundaresan, A., and Corydon, T. J. (2016) The impact of microgravity on bone in humans. *Bone* **87**, 44-56

5. White, R. J., and Averner, M. (2001) Humans in space. *Nature* **409**, 1115-1118

6. Nagaraja, M. P., and Risin, D. (2013) The current state of bone loss research: data from spaceflight and microgravity simulators. *J Cell Biochem* **114**, 1001-1008

7. Vandenburgh, H., Chromiak, J., Shansky, J., Del Tatto, M., and Lemaire, J. (1999) Space travel directly induces skeletal muscle atrophy. *FASEB J* **13**, 1031-1038

8. Lang, T., van Loon, J., Bloomfield, S., Vico, L., Chopard, A., Rittweger, J., Kyparos, A., Blottner, D., Vuori, I., Gerzer, R., and Cavanagh, P. R. (2017) Towards human exploration of space: the THESEUS review series on muscle and bone research priorities. *Npj Microgravity* **3**, 1-10

9. Watenpaugh, D. E., and Hargens, A. R. (2010) The Cardiovascular System in Microgravity. In *Comprehensive Physiology*, John Wiley & Sons, Inc.

10. Corydon, T. J., Mann, V., Slumstrup, L., Kopp, S., Sahana, J., Askou, A. L., Magnusson, N. E., Echegoyen, D., Bek, T., Sundaresan, A., Riwaldt, S., Bauer, J., Infanger, M., and Grimm, D. (2016) Reduced Expression of Cytoskeletal and Extracellular Matrix Genes in Human Adult Retinal Pigment Epithelium Cells Exposed to Simulated Microgravity. *Cell Physiol Biochem* **40**, 1-17

11. von Kampen, P., Kaczmarczik, U., and Rath, H. J. (2006) The new drop tower catapult system. *Acta Astronaut* **59**, 278-283

12. Aleshcheva, G., Wehland, M., Sahana, J., Bauer, J., Corydon, T. J., Hemmersbach, R., Frett, T., Egli, M., Infanger, M., Grosse, J., and Grimm, D. (2015) Moderate alterations of the cytoskeleton in human chondrocytes after short-term microgravity produced by parabolic flight maneuvers could be prevented by up-regulation of BMP-2 and SOX-9. *FASEB J* **29**, 2303-2314

13. Corydon, T. J., Kopp, S., Wehland, M., Braun, M., Schutte, A., Mayer, T., Hulsing, T., Oltmann, H., Schmitz, B., Hemmersbach, R., and Grimm, D. (2016) Alterations of the cytoskeleton in human cells in space proved by life-cell imaging. *Sci Rep* **6**, 20043

14. Pietsch, J., Ma, X., Wehland, M., Aleshcheva, G., Schwarzwalder, A., Segerer, J., Birlem, M., Horn, A., Bauer, J., Infanger, M., and Grimm, D. (2013) Spheroid formation of human thyroid cancer cells in an automated culturing system during the Shenzhou-8 Space mission. *Biomaterials* **34**, 7694-7705

15.   Grimm, D., Wehland, M., Pietsch, J., Aleshcheva, G., Wise, P., van Loon, J., Ulbrich, C., Magnusson, N. E., Infanger, M., and Bauer, J. (2014) Growing tissues in real and simulated microgravity: new methods for tissue engineering. *Tissue Eng Part B Rev* **20**, 555-566

16.   Brungs, S., Egli, M., Wuest, S. L., M. Christianen, P. C., W. A. van Loon, J. J., Ngo Anh, T. J., and Hemmersbach, R. (2016) Facilities for Simulation of Microgravity in the ESA Ground-Based Facility Programme. *Microgravity Sci Tec* **28**, 191-203

17.   Anken, R. (2013) Simulation of Microgravity for Studies in Gravitational Biology: Principles, Devices and Applications. *Curr Biotechnol* **2**, 192-200

18.   Hemmersbach, R., von der Wiesche, M., and Seibt, D. (2006) Ground-based experimental platforms in gravitational biology and human physiology. *Signal Transduct* **6**, 381-387

19.   Herranz, R., Anken, R., Boonstra, J., Braun, M., Christianen, P. C., de Geest, M., Hauslage, J., Hilbig, R., Hill, R. J., Lebert, M., Medina, F. J., Vagt, N., Ullrich, O., van Loon, J. J., and Hemmersbach, R. (2013) Ground-based facilities for simulation of microgravity: organism-specific recommendations for their use, and recommended terminology. *Astrobiology* **13**, 1-17

20.   Borst, A. G., and van Loon, J. J. W. A. (2008) Technology and Developments for the Random Positioning Machine, RPM. *Microgravity Sci Tec* **21**, 287

21.   van Loon, J. J. W. A. (2007) Some history and use of the random positioning machine, RPM, in gravity related research. *Adv Space Res* **39**, 1161-1165

22.   Wuest, S. L., Richard, S., Kopp, S., Grimm, D., and Egli, M. (2015) Simulated microgravity: critical review on the use of random positioning machines for mammalian cell culture. *Biomed Res Int* **2015**, 971474

23.   Wuest, S. L., Stern, P., Casartelli, E., and Egli, M. (2017) Fluid Dynamics Appearing during Simulated Microgravity Using Random Positioning Machines. *Plos one* **12**, e0170826

24.   Fletcher, D. A., and Mullins, R. D. (2010) Cell mechanics and the cytoskeleton. *Nature* **463**, 485-492

25.   Morey-Holton, E. R. (2003) The impact of gravity on life. *Evolution on planet earth: the impact of the physical environment*, 143-159

26.   Schwarzenberg, M., Pippia, P., Meloni, M. A., Cossu, G., Cogoli-Greuter, M., and Cogoli, A. (1999) Signal transduction in T lymphocytes--a comparison of the data from space, the free fall machine and the random positioning machine. *Adv Space Res* **24**, 793-800

27.   Meloni, M. A., Galleri, G., Pani, G., Saba, A., Pippia, P., and Cogoli-Greuter, M. (2011) Space flight affects motility and cytoskeletal structures in human monocyte cell line J-111. *Cytoskeleton* **68**, 125-137

28.   Armstrong, J. W., Gerren, R. A., and Chapes, S. K. (1995) The effect of space and parabolic flight on macrophage hematopoiesis and function. *Exp Cell Res* **216**, 160-168

29.   Adrian, A., Schoppmann, K., Sromicki, J., Brungs, S., von der Wiesche, M., Hock, B., Kolanus, W., Hemmersbach, R., and Ullrich, O. (2013) The oxidative burst reaction in mammalian cells depends on gravity. *Cell Commun Signal* **11**, 98

30.   Hughes-Fulford, M., and Lewis, M. L. (1996) Effects of microgravity on osteoblast growth activation. *Exp Cell Res* **224**, 103-109

31.   Aleshcheva, G., Sahana, J., Ma, X., Hauslage, J., Hemmersbach, R., Egli, M., Infanger, M., Bauer, J., and Grimm, D. (2013) Changes in morphology, gene expression and protein content in chondrocytes cultured on a random positioning machine. *Plos one* **8**, e79057

32.   Infanger, M., Kossmehl, P., Shakibaei, M., Baatout, S., Witzing, A., Grosse, J., Bauer, J., Cogoli, A., Faramarzi, S., Derradji, H., Neefs, M., Paul, M., and Grimm, D. (2006) Induction of three-dimensional assembly and increase in apoptosis of human endothelial cells by simulated microgravity: impact of vascular endothelial growth factor. *Apoptosis* **11**, 749-764

33.   Uva, B. M., Masini, M. A., Sturla, M., Bruzzone, F., Giuliani, M., Tagliafierro, G., and Strollo, F. (2002) Microgravity-induced apoptosis in cultured glial cells. *Eur J Histochem* **46**, 209-214

34.   Vorselen, D., Roos, W. H., MacKintosh, F. C., Wuite, G. J., and van Loon, J. J. (2014) The role of the cytoskeleton in sensing changes in gravity by nonspecialized cells. *FASEB J* **28**, 536-547

35.   Ingber, D. (1999) How cells (might) sense microgravity. *FASEB J* **13 Suppl**, S3-15

36.   Griffith, L. G., and Naughton, G. (2002) Tissue engineering--current challenges and expanding opportunities. *Science* **295**, 1009-1014

37.   Post, M. J. (2014) Cultured beef: medical technology to produce food. *J Sci Food Agric* **94**, 1039-1041

38.   Unsworth, B. R., and Lelkes, P. I. (1998) Growing tissues in microgravity. *Nat Med* **4**, 901-907

39.   Pietsch, J., Gass, S., Nebuloni, S., Echegoyen, D., Riwaldt, S., Baake, C., Bauer, J., Corydon, T. J., Egli, M., Infanger, M., and Grimm, D. (2017) Three-dimensional growth of human endothelial cells in an automated cell culture experiment container during the SpaceX CRS-8 ISS space mission - The SPHEROIDS project. *Biomaterials* **124**, 126-156

40.   Ma, X., Wehland, M., Schulz, H., Saar, K., Hubner, N., Infanger, M., Bauer, J., and Grimm, D. (2013) Genomic approach to identify factors that drive the formation of three-dimensional structures by EA.hy926 endothelial cells. *Plos one* **8**, e64402

41.   Grimm, D., Bauer, J., Ulbrich, C., Westphal, K., Wehland, M., Infanger, M., Aleshcheva, G., Pietsch, J., Ghardi, M., Beck, M., El-Saghire, H., de Saint-Georges, L., and Baatout, S. (2010) Different responsiveness of endothelial cells to vascular endothelial growth factor and basic fibroblast growth factor added to culture media under gravity and simulated microgravity. *Tissue Eng Part A* **16**, 1559-1573

42.   Ulbrich, C., Westphal, K., Pietsch, J., Winkler, H. D., Leder, A., Bauer, J., Kossmehl, P., Grosse, J., Schoenberger, J., Infanger, M., Egli, M., and Grimm, D. (2010) Characterization of human chondrocytes exposed to simulated microgravity. *Cell Physiol Biochem* **25**, 551-560

43.   Ma, X., Pietsch, J., Wehland, M., Schulz, H., Saar, K., Hubner, N., Bauer, J., Braun, M., Schwarzwalder, A., Segerer, J., Birlem, M., Horn, A., Hemmersbach, R., Wasser, K., Grosse, J., Infanger, M., and Grimm, D. (2014) Differential gene expression profile and altered cytokine secretion of thyroid cancer cells in space. *FASEB J.* **28**, 813-835

44.   Kopp, S., Warnke, E., Wehland, M., Aleshcheva, G., Magnusson, N. E., Hemmersbach, R., Corydon, T. J., Bauer, J., Infanger, M., and Grimm, D. (2015) Mechanisms of three-dimensional growth of thyroid cells during long-term simulated microgravity. *Sci Rep* **5**, 16691

45.   Ferlay, J., Soerjomataram, I., Dikshit, R., Eser, S., Mathers, C., Rebelo, M., Parkin, D. M., Forman, D., and Bray, F. (2015) Cancer incidence and mortality worldwide: sources, methods and major patterns in GLOBOCAN 2012. *Int J Cancer* **136**, E359-386

46.   WHO. (2017) Cancer. *World Health Organization*

47.   Omur, O., and Baran, Y. (2014) An update on molecular biology of thyroid cancers. *Crit Rev Oncol Hematol* **90**, 233-252

48.   Dai, X., Li, T., Bai, Z., Yang, Y., Liu, X., Zhan, J., and Shi, B. (2015) Breast cancer intrinsic subtype classification, clinical use and future trends. *Am J Cancer Res* **5**, 2929-2943

49.   Wehland, M., Bauer, J., Infanger, M., and Grimm, D. (2012) Target-based anti-angiogenic therapy in breast cancer. *Curr Pharm Des* **18**, 4244-4257

50.   Grosse, J., Wehland, M., Pietsch, J., Ma, X., Ulbrich, C., Schulz, H., Saar, K., Hubner, N., Hauslage, J., Hemmersbach, R., Braun, M., van Loon, J., Vagt, N., Infanger, M., Eilles, C., Egli, M., Richter, P., Baltz, T., Einspanier, R., Sharbati, S., and Grimm, D. (2012) Short-term weightlessness produced by parabolic flight maneuvers altered gene expression patterns in human endothelial cells. *FASEB J* **26**, 639-655

51.   Riwaldt, S., Pietsch, J., Sickmann, A., Bauer, J., Braun, M., Segerer, J., Schwarzwalder, A., Aleshcheva, G., Corydon, T. J., Infanger, M., and Grimm, D. (2015) Identification of proteins involved in inhibition of spheroid formation under microgravity. *Proteomics* **15**, 2945-2952

52.   Riwaldt, S., Bauer, J., Pietsch, J., Braun, M., Segerer, J., Schwarzwalder, A., Corydon, T. J., Infanger, M., and Grimm, D. (2015) The Importance of Caveolin-1 as Key-Regulator of Three-Dimensional Growth in Thyroid Cancer Cells Cultured under Real and Simulated Microgravity Conditions. *Int J Mol Sci* **16**, 28296-28310

53.   Bolat, F., Gumurdulu, D., Erkanli, S., Kayaselcuk, F., Zeren, H., Ali Vardar, M., and Kuscu, E. (2008) Maspin overexpression correlates with increased expression of vascular endothelial growth factors A, C, and D in human ovarian carcinoma. *Pathol Res Pract* **204**, 379-387

54.   Butler, S. M., Abrassart, J. M., Hubbell, M. C., Adeoye, O., Semotiuk, A., Williams, J. M., Mata-Greenwood, E., Khorram, O., and Pearce, W. J. (2011) Contributions of VEGF to age-dependent transmural gradients in contractile protein expression in ovine carotid arteries. *Am J Physiol Cell Physiol* **301**, C653-666

55.   Saleh, A., Stathopoulou, M. G., Dade, S., Ndiaye, N. C., Azimi-Nezhad, M., Murray, H., Masson, C., Lamont, J., Fitzgerald, P., and Visvikis-Siest, S. (2015) Angiogenesis related genes NOS3, CD14, MMP3 and IL4R are associated to VEGF gene expression and circulating levels in healthy adults. *BMC Med Genet* **16**, 90

56.   Hiratsuka, S., Nakamura, K., Iwai, S., Murakami, M., Itoh, T., Kijima, H., Shipley, J. M., Senior, R. M., and Shibuya, M. (2002) MMP9 induction by vascular endothelial growth factor receptor-1 is involved in lung-specific metastasis. *Cancer Cell* **2**, 289-300

57.   Yamauchi, K., Nishimura, Y., Shigematsu, S., Takeuchi, Y., Nakamura, J., Aizawa, T., and Hashizume, K. (2004) Vascular endothelial cell growth factor attenuates actions of transforming growth factor-beta in human endothelial cells. *J Biol Chem* **279**, 55104-55108

58.   Charoen, K. M., Fallica, B., Colson, Y. L., Zaman, M. H., and Grinstaff, M. W. (2014) Embedded multicellular spheroids as a biomimetic 3D cancer model for evaluating drug and drug-device combinations. *Biomaterials* **35**, 2264-2271

59. Pisanu, M. E., Noto, A., De Vitis, C., Masiello, M. G., Coluccia, P., Proietti, S., Giovagnoli, M. R., Ricci, A., Giarnieri, E., Cucina, A., Ciliberto, G., Bizzarri, M., and Mancini, R. (2014) Lung cancer stem cell lose their stemness default state after exposure to microgravity. *Biomed Res Int* **2014**, 470253

60. Ferrara, N., Hillan, K. J., Gerber, H. P., and Novotny, W. (2004) Discovery and development of bevacizumab, an anti-VEGF antibody for treating cancer. *Nat Rev Drug Discov* **3**, 391-400

61. Grosse, J., Wehland, M., Pietsch, J., Schulz, H., Saar, K., Hubner, N., Eilles, C., Bauer, J., Abou-El-Ardat, K., Baatout, S., Ma, X., Infanger, M., Hemmersbach, R., and Grimm, D. (2012) Gravity-sensitive signaling drives 3-dimensional formation of multicellular thyroid cancer spheroids. *FASEB J* **26**, 5124-5140

62. Bauer, J., Kopp, S., Schlagberger, E. M., Grosse, J., Sahana, J., Riwaldt, S., Wehland, M., Luetzenberg, R., Infanger, M., and Grimm, D. (2017) Proteome Analysis of Human Follicular Thyroid Cancer Cells Exposed to the Random Positioning Machine. *Int J Mol Sci* **18**

7 Figure Index

8 Acknowledgment

9 Eidesstattliche Erklärung

Ich erkläre, dass ich die an der Medizinischen Fakultät der Otto-von-Guericke-Universität zur Promotion eingereichte Dissertation mit dem Titel:

"Effects of real and simulated microgravity on human cancer cells"

in der Klinik für Plastische, Ästhetische und Handchirurgie ohne Hilfe durchgeführt und bei der Abfassung der Dissertation außer den genannten Hilfsmitteln keine weiteren benutzt habe.

Bei der Abfassung der Dissertation sind Rechte Dritter nicht verletzt worden.

Ich habe diese Dissertation bisher an keiner in- oder ausländischen Hochschule zur Promotion eingereicht. Ich übertrage der Medizinischen Fakultät das Recht, weitere Kopien meiner Dissertation herzustellen und zu vertreiben.

Magdeburg, den

Sascha Kopp

10 Curriculum Vitae

Sascha Kopp

Email: sascha.kopp@med.ovgu.de

Hands-on Experience

Currently	Research assistant; Plastic, Esthetic und Hand Surgery, Otto-von-Guericke-University Magdeburg
Currently	PhD Student; Plastic, Esthetic und Hand Surgery, Otto-von-Guericke-University Magdeburg
Since 09/2017	Tutor of a master student. Project: Chondrocyte Tissue Engineering
Since 07/2017	Tutor of a PhD student. Project: BREASTEX
Since 06/2017	Organization and execution of the TEXUS 54 Mission scheduled for April 2018. BREASTEX: Life cell imaging of cytoskeletal parts during a sounding rocket flight.
Since 06/2017	Organization and execution of the CELLBOX2 Mission. Flown on the 15.12.2017. Thyroid cancer cells on the International Space Station.
Since 06/2017	Organization of the ESA SPHEROIDS Project. Ground controls for: endothelial cells cultured on the ISS
02/2017	Exchange student at University Aarhus, Denmark, in the group of Prof. Daniela Grimm, Institute for Biomedicine: PRODEX-project (Sutures under unloading conditions).
04.09. – 18.09.2016	Organization and execution of the 29. DLR parabolic flight campaign: Breast cancer cells during short-term microgravity
04/2016 - 06/2016	Exchange student at University Aarhus, Denmark, in the group of Prof. Thomas J. Corydon, Institute for Biomedicine: Stable transfection of breast cancer cells.
02/2016	Organization and execution of the TEXUS 53 Mission, Kiruna, Sweden: Thyroid cancer cells exposed to a sounding rocket flight.
04/2015	Organization and execution of the TEXUS 52 Mission, Kiruna, Sweden: Live cell imaging of cytoskeletal changes in responds to microgravity.
10/2014	Guest scientist during a parabolic flight campaign in Bordeaux, France, being part of the group of Prof. Daniela Grimm, University Aarhus: Chondrocytes in Microgravity.

09/2012 - 10/2012	Scientific temporary stuff at the German Aerospace Center (DLR), Institute for Spacemedicine, Biomedical Support Center
10/2010 - 04/2012	Scientific temporary stuff at the German Aerospace Center (DLR), Institute for Spacemedicine, Biomedical Support Center
11/2011	Owner of the Astrium Spacelab Prize. Category: Microgravity Research

Education

Currently	PhD student rerum medicinalium at the University Clinic Magdeburg, Otto-von- Guericke University, Germany
	Titel: The Effect of Real and Simulated Microgravity on human cancer cells.
04/2012 – 12/2014	Master of Science in Biologie at the Rheinisch-Westfälischen Technischen Hochschule Aachen (RWTH), Germany
	Master These: Impact of microgravity on human thyroid cells
10/2007 - 04/2011	Bachelor of Science in Applied Biology at the Hochschule Bonn-Rhein-Sieg
	Bachelor These: Impact of Gravity on the Actin Filament System of the Macrophage Cell Line RAW 264.7

Publications

2013

1. Eiermann P, **Kopp S**, Hauslage J, Hemmersbach R, Gerzer R, Ivanova K (2013) Adaptation of a 2-D clinostat for simulated microgravity experiments with adherent cells. Microgravity Sci. Technol. doi: 10.1007/s12217-013-9341-1

2015

2. Wuest SL, Richard S, **Kopp S**, Grimm D, Egli M (2015) Simulated microgravity: critical review on the use of random positioning machines for mammalian cell culture. Biomed Res Int. 2015:971474. doi: 10.1155/2015/971474.

3. Svejgaard B, Wehland M, Ma X, **Kopp S**, Sahana J, Warnke E, Aleshcheva G, Hemmersbach R, Hauslage J, Grosse J, Bauer J, Corydon TJ, Islam T, Infanger M, Grimm D (2015) Common effects on cancer cells exerted by a Random Positioning Machine and a 2D clinostat. PLoS One 10(8):e0135157. doi: 10.1371/journal.pone.0135157. eCollection 2015

4. Warnke E, **Kopp S**, Wehland M, Hemmersbach R, Bauer J, Infanger M, Grimm D (2015) Thyroid cells exposed to simulated microgravity conditions – comparison of the fast rotating clinostat and the Random Positioning Machine. Microgravity Sci. Technol. doi: 10.1007/s12217-015-9456-7

5. **Kopp S**, Warnke E, Wehland M, Aleshcheva G, Magnusson NE, Hemmersbach R, Corydon TJ, Bauer J, Infanger M, Grimm D (2015) Mechanisms of three-dimensional growth of thyroid cells during long-term simulated microgravity. Sci Rep. 5:16691. doi: 10.1038/srep16691.

2016

6. Corydon TJ, **Kopp S**, Wehland M, Braun M, Schütte A, Mayer T, Hülsing T, Oltmann H, Schmitz B, Hemmersbach R, Grimm D (2016) Alterations of the cytoskeleton in human cells in space proved by life-cell imaging. Sci Rep. 6:20043. doi: 10.1038/srep20043.

7. Riwaldt S, Bauer J, Wehland M, Slumstrup L, **Kopp S**, Warnke E, Dittrich A, Magnusson NE, Pietsch J, Corydon TJ, Infanger M, Grimm D (2016) Pathways regulating spheroid formation of human follicular thyroid cancer cells under simulated microgravity conditions: a genetic approach. Int J Mol Sci. 17(4). pii: E528. doi: 10.3390/ijms17040528.

8. **Kopp S**, Wehland M, Grimm D (2016) Einfluss von Schwerelosigkeit auf Krebszellen: Effekte der Mikrogravitation auf Schilddrüsenkrebszellen. GIT Lab Journal 4:16 pp 50

9. **Kopp S**, Slumstrup L, Corydon TJ, Sahana J, Aleshcheva G, Islam T, Magnusson NE, Wehland M, Bauer J, Infanger M, Grimm D (2016) Identifications of novel mechanisms in breast cancer cells involving duct-like multicellular spheroid formation after exposure to the Random Positioning Machine. Sci Rep. 6:26887. doi: 10.1038/srep26887.

10. Laursen R, Wehland M, **Kopp S**, Pietsch J, Infanger M, Grosse J, Grimm D (2016) Effects and role of multikinase inhibitors in thyroid cancer. Curr Pharm Des. 22(39):5915-5926.

11. Frandsen S, **Kopp S**, Wehland M, Pietsch J, Infanger M, Grimm D (2016) Latest results for anti-angiogenic drugs in cancer treatment. Curr Pharm Des. 22(39):5927-5942.

12. Corydon TJ, Mann V, Slumstrup L, **Kopp S**, Sahana J, Askou AL, Magnusson NE, Echegoyen D, Bek T, Sundaresan A, Riwaldt S, Bauer J, Infanger M, Grimm D (2016) Reduced expression of cytoskeletal and extracellular matrix genes in human adult retinal pigment epithelium cells exposed to simulated microgravity. Cell Physiol Biochem. 40(1-2):1-17.

2017

13. Bauer J, **Kopp S**, Schlagberger EM, Grosse J, Sahana J, Riwaldt S, Wehland M, Luetzenberg R, Infanger M, Grimm D (2017) Proteome analysis of human follicular thyroid cancer cells exposed to the Random Positioning Machine. Int J Mol Sci. 18(3). pii: E546. doi: 10.3390/ijms18030546.

14. Warnke E, Pietsch J, **Kopp S**, Bauer J, Sahana J, Wehland M, Krüger M, Hemmersbach R, Infanger M, Lützenberg R, Grimm D (2017) Cytokine Release and Focal Adhesion Proteins in Normal Thyroid Cells Cultured on the Random Positioning Machine. Cell Physiol Biochem. 43(1):257-270. doi: 10.1159/000480368.

15. Riwaldt S, Monici M, Graver Petersen A, Birk Jensen U, Evert K, Pantalone D, Utpatel K, Evert M, Wehland M, Krüger M, **Kopp S**, Frandsen S, Corydon T, Sahana J, Bauer J, Lützenberg R, Infanger M, Grimm D (2017) Preparation of A Spaceflight: Apoptosis Search in Sutured Wound Healing Models. Int J Mol Sci. 18(12). pii: E2604. doi: 10.3390/ijms18122604.

16. Krüger M, Wehland M, **Kopp S**, Corydon TJ, Infanger M, Grimm D (2017) Life-Cell Imaging of F-Actin Changes induced by 6 min of Microgravity on a TEXUS Sounding Rocket Flight.

Conference: 23rd ESA Symposium on European Rocket and Balloon Programmes and Related Research, At Visby, Sweden

17.   Grimm D, Corydon TJ, **Kopp S**, Krüger M, Infanger M, Wehland M (2017) Human Cells in Space. Conference: 23rd ESA Symposium on European Rocket and Balloon Programmes and Related Research, At Visby, Sweden

2018

18.   **Kopp S**, Sahana J, Islam T, Bauer J, Corydon TJ, Schulz H, Saar K, Hübner N, Slumstrup L,Riwaldt S, Wehland M, Infanger M, Lützenberg R, Grimm D (2018) The role of NF-κB in spheroid formation of human breast cancer cells cultured on the Random Positioning Machine. Sci Rep. 8:921. doi: 10.1038/s41598-017-18556-8

Conferences and Presentations

07.04.2016	International presentation: Space Medicine. Institute for Biomedizine, University Aarhus, Denmark
05.10.2016	DLR Status Seminar, Bonn. Presentation: Results of the TEXUS 53 Mission
09.12.2016	16. Gravimeeting, Erlangen. Presentation: Impact of simulated microgravity on human breast cancer cells.
11.06.-15.06.2017	23rd ESA Symposium on European Rocket and Balloon Programs and Related Research. Presentation: Results of the TEXUS 53 Mission

Grants

11.06.-16.06.2017	SELGRA Travel Grant for the 23rd ESA PAC Symposium in Visby, Sweden
11.06.-16.06.2017	DAAD Travel Grant (offered but resigned) for the 23rd ESA PAC Symposium in Visby, Sweden
2017	AU (Aarhus University), guest student, 3 month stay in Denmark
2016	AUFF Travel Grant for guest scientists, 3 month stay in Denmark
01.04.-30.09.2014	ERASMUS Travel Grant for studies abroad, Master Thesis in Aarhus, Denmark

----

Magdeburg, den

Sascha Kopp

11 Appendix

11.1 Publication #1

Corydon TJ, **Kopp S**, Wehland M, Braun M, Schütte A, Mayer T, Hülsing T, Oltmann H, Schmitz B, Hemmersbach R, Grimm D. Alterations of the cytoskeleton in human cells in space proved by life-cell imaging. Sci Rep. 2016 Jan 28;6:20043. doi: 10.1038/srep20043.

SCIENTIFIC REPORTS

OPEN

Alterations of the cytoskeleton in human cells in space proved by life-cell imaging

Thomas J. Corydon[1], Sascha Kopp[2], Markus Wehland[2], Markus Braun[3,4], Andreas Schütte[5], Tobias Mayer[6], Thomas Hülsing[5], Hergen Oltmann[5], Burkhard Schmitz[5], Ruth Hemmersbach[7] & Daniela Grimm[1]

Microgravity induces changes in the cytoskeleton. This might have an impact on cells and organs of humans in space. Unfortunately, studies of cytoskeletal changes in microgravity reported so far are obligatorily based on the analysis of fixed cells exposed to microgravity during a parabolic flight campaign (PFC). This study focuses on the development of a compact fluorescence microscope (FLUMIAS) for fast live-cell imaging under real microgravity. It demonstrates the application of the instrument for on-board analysis of cytoskeletal changes in FTC-133 cancer cells expressing the Lifeact-GFP marker protein for the visualization of F-actin during the 24th DLR PFC and TEXUS 52 rocket mission. Although vibration is an inevitable part of parabolic flight maneuvers, we successfully for the first time report life-cell cytoskeleton imaging during microgravity, and gene expression analysis after the 31st parabola showing a clear up-regulation of cytoskeletal genes. Notably, during the rocket flight the FLUMIAS microscope reveals significant alterations of the cytoskeleton related to microgravity. Our findings clearly demonstrate the applicability of the FLUMIAS microscope for life-cell imaging during microgravity, rendering it an important technological advance in live-cell imaging when dissecting protein localization.

Although studies on adherently growing human cells exposed to short-term real microgravity during parabolic flight maneuvers prior to fixation and subsequent analysis on Earth have provided some evidence of cytoskeleton alterations[1–5], in-flight live-cell imaging has not been performed. To overcome this obstacle, we have developed a spinning-disc Fluorescence Microscopy Analysis System (FLUMIAS) and investigated cytoskeletal changes during Parabolic Flight Campaigns (PFCs) on-board the Airbus A300 ZERO-G and during the TEXUS 52 sounding rocket mission in stable transfected human follicular thyroid carcinoma cells (FTC-133) expressing the Lifeact-GFP fusion protein for the visualization of F-actin.

Long-term spaceflights have an enormous impact on human health[6]. Several health problems have been reported, such as muscle atrophy, bone loss, cardiovascular problems, among others[6]. The immune system is also altered by the microgravity environment, resulting in immunosuppression in space[6]. A large proportion of the immune cells are compromised and the secretion of cytokines is changed[7]. Changes in the vimentin cytoskeleton were induced in Jurkat cells – a T-lymphoid cell line – by real microgravity (in a Maxus rocket flight)[8]. Another study showed that J-111 monocytes exposed to low gravity conditions exhibited reduced fluorescence intensity of F-actin fibres[9].

A variety of cellular alterations have been observed after short-term and long-term culture of cells under conditions of simulated and real microgravity[10–15]. Adherently growing human cancer cells and benign cells, which grow normally under static 1*g*, can be induced to grow three-dimensionally when they are cultured under microgravity conditions. They change their protein content and secretion, as well as displaying differential gene expression[12]. Our understanding of the fundamental role of gravity in cancer cell growth and function is a new paradigm

[1]Department of Biomedicine, Aarhus University, 8000 Aarhus C, Denmark. [2]Clinic for Plastic, Aesthetic and Hand Surgery, Otto-von-Guericke University, 39120 Magdeburg, Germany. [3]Deutsches Zentrum für Luft- und Raumfahrt (DLR), Raumfahrtmanagement Bonn-Oberkassel, Bonn, 53227 Germany. [4]Institute for Molecular Physiology and Biotechnology of Plants (IMBIO), Gravitational Biology Group, University of Bonn, 53115 Bonn, Germany. [5]Airbus Defense and Space, Airbus DS GmbH, 28199 Bremen, Germany. [6]FEI Munich GmbH, 82166 Gräfeling, Germany. [7]DLR German Aerospace Center, Department of Gravitational Biology, 51147, Köln, Germany. Correspondence and requests for materials should be addressed to T.J.C. (email: corydon@biomed.au.dk)

in cell biology[10,11]. Notably, changes in the cytoskeleton have been observed in different types of cells such as chondrocytes, lymphocytes, glial cells, breast cancer cells, endothelial cells, and thyroid cancer cells[1,3,5,16–20]. These experiments performed in microgravity showed changes in morphology, cytoskeleton and function. Studies on microtubules in altered gravity conditions have shown that they also are gravity-sensitive[18,21–23].

We aim to extend our knowledge in understanding the biology of cancer by using microgravity as a new method, which may be useful to detect interesting proteins, which may become a future target. Hence, to investigate changes in the cytoskeleton of cancer cells during microgravity conditions the compact spinning-disc FLUMIAS device for live-cell imaging under real microgravity was developed and used for on-board analysis in FTC-133 cancer cells expressing the Lifeact-GFP marker protein. It allowed us the visualization of F-actin during a Deutsches Zentrum für Luft- und Raumfahrt (DLR) PFC and the DLR TEXUS 52 sounding rocket mission. The aircraft and also the TEXUS sounding rocket fly parabolic trajectories that produce a period of free fall (microgravity). The term microgravity in general refers to the still existing residual accelerations. For parabolic flights (PF) the free fall phase persists for 22 seconds in which the experiments will experience microgravity in the range of $\sim 10^{-2} g$[1,3–5,15,24]. For the TEXUS 52 rocket flight the payload is in free fall for a period of up to 390 seconds with a high quality of microgravity ($<10^{-4} g$). Hypergravity and vibrations are inexorable events of PF and spaceflights appearing prior and after the free fall phase which need to be taken into consideration, when evaluating the impact of microgravity[1].

Results

Development of the FLUMIAS microscope.
Two versions of the FLUMIAS microscope module have been built (Fig. 1) and used on the 24th DLR PFC and the DLR TEXUS 52 sounding rocket mission (Supplementary Figure S1A,B). The first one as an engineering model (EM) was used for functional verification and mechanical qualification of FLUMIAS. Furthermore, it is suitable for PFCs and ground support tasks (Supplementary Figure S1C). The second one is the actual TEXUS 52 flight model (FM) (Supplementary Figure S1D). Both versions are identical with respect to the microscope core components and differ only in the way the experiment service subsystem has been implemented. The heart of the FLUMIAS experiment module is the confocal laser spinning disc fluorescence microscope which allows for the parallel scanning of thousands (1200/FOV) of sample points resulting in fast image creation. This set-up was chosen in order to obtain thin slices by eliminating the contribution of out-of-focus light in each image plane, rather than actual physical sectioning. Referred to as optical sectioning, the resulting image planes provide a high level of contrast with improved signal-to-noise ratio, which is equally important for real-time cell monitoring during operation, especially on PFCs, and subsequent data analysis.

The FLUMIAS confocal laser spinning disc fluorescence microscope was developed by FEI Munich GmbH, Germany (Fig. 1). Figure 1A shows the key components of the confocal laser spinning disc fluorescence microscope. The FEI iMIC was a good fit to the space requirements and was used as the main microscope body. Due to the restricted available space, the alignment of the components had to be adjusted and some components had to be re-designed to be more compact so that they could fit into the rocket. To withstand the vibrations and high accelerations during the ascent of the sounding rocket, the number of moveable parts (such as the filter slider and the nosepiece) was reduced to a minimum. The cells were seeded onto an Ibidi-slide (see Methods), which was installed inside the late access and fixation unit (designed and built by Airbus DS, Supplementary Figure S1E). The late access and fixation unit could be separately mounted to the FLUMIAS experiment module. Hence, it was possible to hand over the cells shortly (around two hours) before lift-off. The unit is temperature-controlled and allowed the chemical fixation of the cells under investigation at any time point during the flight. Due to guiding elements, a positional stability of about $10\,\mu m$ in the x- and y-directions for the demounting-/mounting-process was achieved. The late access and fixation unit was mounted on top of the X/Y-stage, allowing movement in the x- and y-direction (around 24 mm travel range in both axes). This travel range allowed the observation of three out of the six channels of the Ibidi slide during the flight. The X/Y-stage is directly attached to the octagonal base of the microscope body, the iMIC. The iMIC contained the microscope objective (Carl Zeiss, Plan-Apochromat 40x/0.95 Corr), which was mounted on a voice coil focus drive for movements in z-direction. The spinning disc unit (called Andromeda) is connected to the iMIC and to the camera and besides the spinning disc contained several optical elements necessary for beam shaping of the incoming laser light. The laser light originated from the laser line combiner (Omicron-Laserage Laserprodukte) and was coupled into the spinning disc unit via an optical multimode fiber. In the current configuration four different excitation wavelengths could be chosen out of three diode lasers (405 nm/120 mW, 488 nm/200 mW and 642 nm/140 mW) and one diode-pumped solid state (DPSS) laser (561 nm/150 mW). While the diode lasers could be easily switched on and off very fast, the DPSS laser could only be indirectly switched using an acousto-optical modulator (AOM), which needed an individual controller. The initialization and interaction of all components is managed by the imaging control unit (ICU), which also supplied power to the iMIC and the X/Y-stage.

As a supporting structure and for power supply, cooling and control of the microscope, an experiment service subsystem (Airbus DS) was built for the FLUMIAS TEXUS 52 FM, which is depicted in Fig. 1B. The experiment service subsystem can be roughly separated in two parts. The first part below the base plate contained the battery and the electronics (DC/DC converter, experiment timer, etc.). This part experienced vacuum during the flight. The second part above the base plate was shielded with a dome structure (Fig. 1C) against vacuum and besides the supporting structure contained a water-cooling circuit and a PC with microscope control software (an adapted release of the software package L.A. by FEI Munich GmbH) and storage for the high-resolution images. Before flight the FLUMIAS module was integrated into the dome structure (Fig. 1C) and stacked with other experiment modules to form the TEXUS 52 payload (Supplementary Figure S1F). To regulate the module temperature inside the dome structure, the camera and the cold plate were connected to the water-cooling circuit. The ICU, being the
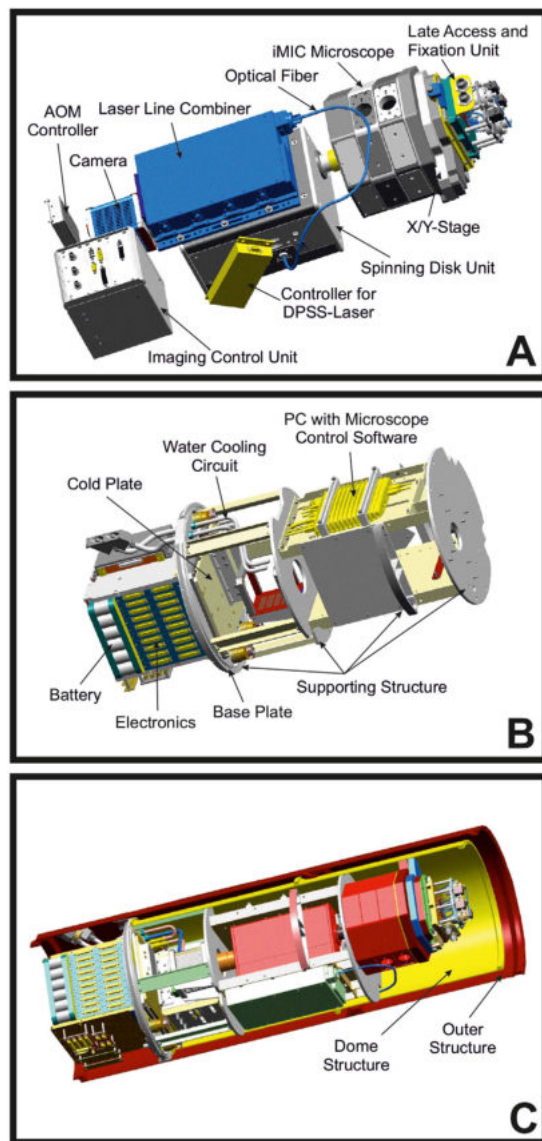
Figure 1. The FLUMIAS experiment module. (**A**) Main components of the inverted confocal laser spinning disc fluorescence microscope with late access and fixation unit. (**B**) Experiment service subsystem for the FLUMIAS TEXUS 52 FM. (**C**) The FLUMIAS experiment module with dome structure integrated into the outer structure.

main heat source, was directly mounted onto the cold plate. During lift-off the cooling circuit was automatically disconnected.

A sketch depicting the working principle of a confocal laser spinning disc fluorescence microscope is shown in Fig. 2. The laser light (excitation light) enters the spinning disc unit through a small hole in the corner cube and is reflected by a dichroic mirror onto the spinning disc. In the first run only a small amount of light passes the pinholes, but the majority of light is reflected by the concave micro-mirrors back to the dichroic mirror. After taking the path from the dichroic mirror to the corner cube and the dichroic mirror, the light again reaches the spinning disc but this time most of the light passes the pinholes due to the effect of the micro-mirrors and is focused onto the sample. Based on the confocality only fluorescent light originating from the focal plane in the sample can pass the pinholes of the spinning disc and reach the camera chip, after transmission by the dichroic mirror (the emission wavelength is distinctly larger than the excitation wavelength).

The confocal laser spinning disc fluorescence microscope offers a high axial resolution (around $1.5\,\mu m$) compared to normal light microscopes by efficiently suppressing the fluorescent light, which does not originate from the focal plane. The central part of the confocal fluorescence microscope is the spinning disc, which contains many pinholes (approximately 1200) and around each pinhole micro mirrors are etched into the substrate (see Fig. 2). The pinholes have a fixed diameter of a few tenths of micrometers and are arranged in a spiral pattern. Due to this special arrangement all pixels of the camera chip are exposed to fluorescence light and accordingly a complete new frame is created whenever the disc is rotated through about 30 degrees (12 frames per 360° rotation).
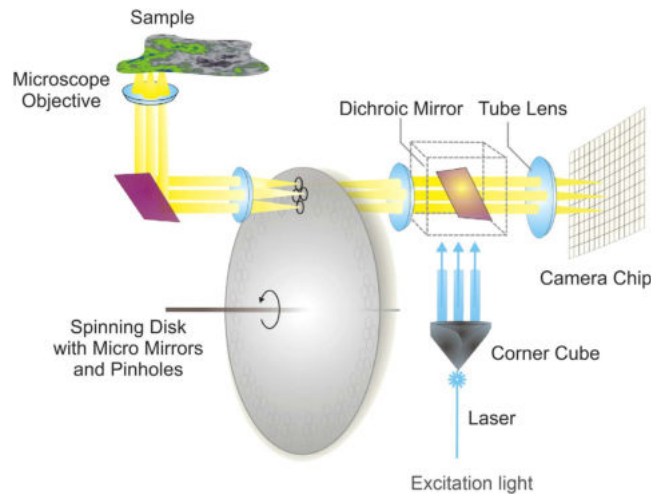
Figure 2. Sketch of the working principle of a confocal laser spinning disc fluorescence microscope. A laser beam is coupled through a multimode fiber into the spinning disk system. The beam is focused through a hole in the corner cube and sent collimated towards the disk with pinholes. Micro mirrors around the pinholes reflect a beam bundle back into the corner cube. Each sub-beam is retro-reflected and focused through the pinholes. The light passes the objective and is focused on the sample plane, where it generates fluorescence in the sample. The fluorescence emission is focused though the pinholes and transmits the dichroic mirror towards the camera chip.

As the spinning disc is rotating with a speed of 5000 rpm, it is theoretically possible to record 1000 frames per second. However, for standard biological samples the exposure time is typically above 50 ms, hence the resulting image is averaged over several frames.

Live-cell imaging of the cytoskeleton in FTC-133 cells. To extend our knowledge about changes in the cytoskeleton of poorly differentiated follicular thyroid cancer cells during microgravity conditions, live-cell imaging of the cytoskeleton was performed in FTC-133 cells. Importantly, these cells had been investigated in space twice previously[4,14,25] and they are very robust, when cultured under microgravity especially during launch[4,14,25]. Interestingly, the cells have developed a less-aggressive phenotype during one of the space missions[4], so exploring these changes induced by microgravity may lead to the identification of new targets for cancer therapy. Furthermore, they were investigated on PFCs[4] and have been thoroughly analyzed in simulated microgravity[12,25,26] making FTC-133 cells to one of the best-characterized cell types, cultured under altered gravity conditions. In addition, they can be easily transfected. The cells were stably transfected with a pcDNA3.1(+)-based vector, entitled pLAGICT, expressing Lifeact-GFP for the visualization of F-actin (Fig. 3A). The vector also encodes mCherry-Tubulin fusion proteins enabling parallel analysis of both actin and tubulin counterparts of the cytoskeleton. However, due to the experimental setup only live-cell imaging of Lifeact-GFP was performed during microgravity. Following transfection with pLAGICT and G418 selection, resistant FTC-133 clones (Fig. 3B) were isolated and inspected by fluorescent microscopy. A clone (designated Lifeact-GFP) with bright Lifeact-GFP labeling of F-actin was chosen and further expanded (Fig. 3C).

The FLUMIAS microscope is functional in microgravity during parabolic flights maneuvers. During a parabolic flight, 31 consecutive parabolas were performed. One parabola contains three phases (pull up, free fall, and pull out). A parabola starts from the horizontal flight level followed by a 45° ascent for 20 seconds in which experiments and the passengers experience hypergravity in the range of 1.5–1.8 g. Following a reduction in the thrust, the aircraft follows the trajectory of a parabola initiating the 22-second-long free fall (or microgravity) phase. Finally, the engines are powered up again, and a second phase of 1.8 g for 20 seconds terminates the parabola. Due to turbulence acting on the aircraft as well as the manual operation of the aircraft, the microgravity is in the range of $\sim 10^{-2} g$[1,3–5,15,24]. Prior to each flight an Ibidi-slide (Fig. 3D) with FTC-133 cells expressing Lifeact-GFP seeded into it was installed inside the late access and fixation unit (Supplementary Figure S1E) and brought to the aircraft. The live-cell imaging results obtained on-board the Airbus A300 ZERO-G indicated that disturbances of actin bundles and "holes" within the cytoplasm, appeared immediately during the μg phase of parabola 1 in cells expressing Lifeact-GFP when the cells were cultivated adherently on slides (compare Fig. 4A,B). This process seemed to develop during the following parabola (Fig. 4C). Conversely, no "holes" were observed in the cytoplasm of the cells expressing Lifeact-GFP before parabola 1 (Fig. 4A). Moreover, the analysis indicated the disappearance of microvilli or filopodia-, and lamellipodia-like structures during the parabolic flight (Fig. 4A–C). Taking into account that the "holes" are considered to indicate points of cell cytoplasm discontinuity, the results clearly indicate that the cytoskeleton of low-differentiated follicular thyroid cancer cells is not resistant to a fast and short removal of the influence of gravity for 20 seconds, and importantly, that the cytoskeletal changes occur rapidly after entrance into the μg-phase of parabola 1. The finding that the cytoskeletal alterations occur after only 1 parabola is supported by our previous findings[3,5]. However, by using the FLUMIAS-based live-imaging approach during PFCs, we are now able to dissect the point of action to be in the μg-phase. No
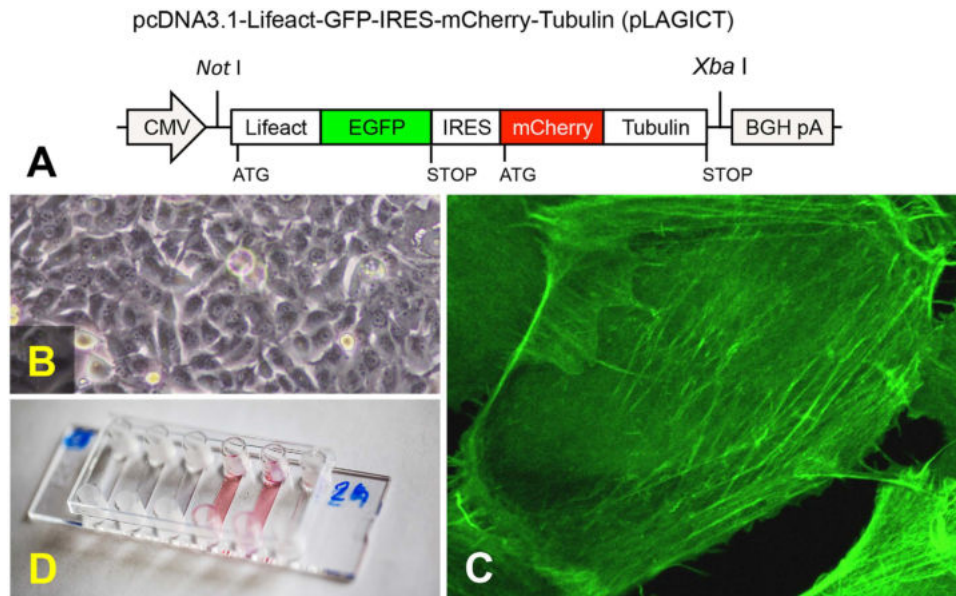
Figure 3. Generation of FTC-133 cells expressing Lifeact-GFP for FLUMIAS-based life-cell imaging.
(**A**) Schematic presentation of the versatile pLAGICT plasmid containing the Lifeact-eGFP-IRES-mCherry-Tubulin (LAGICT) expression cassette for visualization of F-actin and α-tubulin. A CMV promoter drives the expression of the LAGICT cassette and efficient transcriptional termination is provided by the bovine growth hormone (BGH) polyadenylation site of the pcDNA3.1(+) vector. For selection purposes the vector contains the neomycin gene driven by a SV40 promoter. (**B**) Bright field image of FTC-133 cells. (**C**) Example of Lifeact-GFP-visualization of F-actin in FTC-133 cells stable transfected with pLAGICT. (**D**) The μ-slide VI 0.4 ibiTreat slide assembled with medium containing flexible tubes prior to insertion into the late access and fixation unit.

apoptotic or dead cells as judged by visual inspection of the cells at the end of each of the individual experiments were identified in the 1*g*-controls on the ground or in the cells exposed to the parabolic flight profile.

To test whether the observed changes in the cytoskeleton during the parabolic flight maneuvers may reflect transcriptional alterations, *ACTB*, *EZR*, *RDX* and *MSN* gene expressions after 31 parabolas were measured. *ACTB* expression was not altered during the parabolic flight, but a 2-fold increase was observed during hyper-*g* in non-transfected cells (Fig. 4D). The expression of *ACTB* was found to be increased 3.5-fold in cells expressing Lifeact-GFP exposed to parabolic flight maneuvers compared to 1*g* control cells (Fig. 4E). No changes in the expression of *ACTB* were detected during vibration and hyper-*g* in cells expressing Lifeact-GFP (Fig. 4E). This observation might either be related to the integration site(s) of the expression pLAGICT cassette or to the fact that the cells expressing Lifeact-GFP were exposed to a selection procedure.

The proteins ezrin, radixin and moesin (ERM) are known to crosslink the plasma membrane and the actin cytoskeleton[27]. By this procedure, they provide both structural links to strengthen the cell cortex and control signal transduction pathways. Hence, the ERM proteins are involved in membrane dynamics, adhesion, cell survival, cell motility and morphogenesis[27]. Despite the overall similarity in function and structure, individual functions of the three proteins appear to be specialized[27]. Notably, there is evidence that ERM proteins are involved in the regulation of tumor progression and metastasis. Ezrin functions as a protein-tyrosine kinase substrate in microvilli[28] and is frequently overexpressed in metastatic tumor cells[29]. The ezrin gene was up-regulated in established anaplastic thyroid carcinoma cells[30]. Radixin functions as a membrane-cytoskeletal crosslinker in actin-rich cell surface structures[27] and it is reported that the expression level of radixin is found to be significantly unregulated in colon tumor tissues[31]. Moesin is phosphorylated at the site of entry of mitosis and is involved in several important steps throughout cell division[32]. Inactivation of moesin disrupts spindle organization. It acts as a potential marker in breast and pancreatic cancer, and the expression level of moesin is linked to tumor development of oral squamous cell carcinoma[33].

In general little is known about ERM proteins and thyroid cancer. We recently had shown that the secretion of ezrin by FTC-133 cells is increased after 10 days in space[4]. Here we detected an increase of *EZR* mRNA after only 31 parabolas, indicating an early signaling process (Fig. 4F). This *EZR* mRNA increase may also be induced by hyper-*g*. This finding could be confirmed with the ML-1 cell line, in which *EZR*, *RDX* and *MSN* mRNAs were also increased by hyper-*g*[34]. In endothelial cells *EZR* mRNA was up-regulated after 31 flown parabolas, a finding corresponding well to the results found for FTC-133 cells.

Overall, no significant changes in the expression of the *EZR*, *RDX* and *MSN* genes in cells expressing Lifeact-GFP compared to the ground control cells were detected (Fig. 4G,I,K), except that during the PFC *EZR* expression was reduced by approximately 40% (Fig. 4G). In the FTC-133 cells we found that *EZR* expression was increased approximately 2-fold during both PFC and hyper-*g* compared to 1*g* (Fig. 4F). Similarly, the *RDX* expression was increased 3.5-fold during hyper-*g* (Fig. 4H). *MSN* expression was also increased during hyper-*g*, whereas *MSN* expression appeared to be reduced by 20% during vibration compared to 1*g* (Fig. 4J).
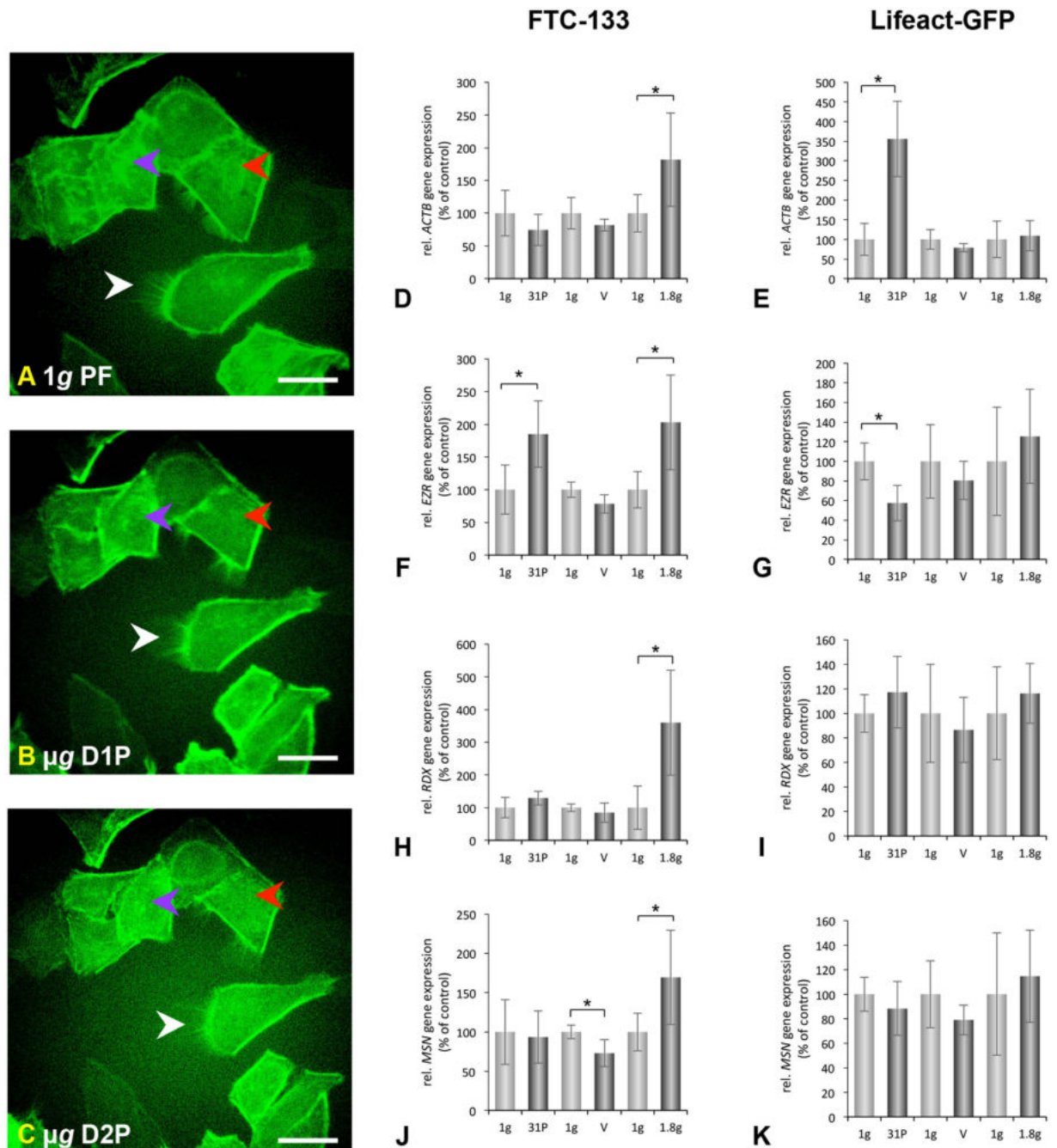
Figure 4. Inflight analyses of cytoskeletal changes during the PFC. (A–C) Imaging of F-actin visualized by Lifeact-GFP using the FLUMIAS EM. **(D–K)** Gene expression analysis assessed by RT qPCR to investigate changes in the cytoskeleton. FTC-133 cells expressing Lifeact-GFP were cultivated in μ-slides for life-cell imaging. The position of cells displaying Lifeact-GFP fluorescence signals was selected and life-cell imaging of these selected cells was performed both pre-flight **(A)** as well as during the microgravity phase of the 1 parabola (D1P) **(B)** and the second parabola (D2P) **(C)**. Scale bars $= 20\,\mu$m. Purple arrowheads indicate cytoskeleton alterations in the form of "holes" in the cytoplasm. Red arrowheads indicate disturbance of F-actin bundles. White arrowheads indicate disappearance of microvilli or filopodia-, and lamellipodia-like structures. For gene expression analysis non-transfected FTC-133 cells and FTC-133 cells expressing Lifeact-GFP were cultivated in T175 cell culture flasks. To rule out the effect of vibration and hyper-g, which are obligatory events occurring both before and after each parabola, cell cultures were independently subjected to either vibration experiments using a Vibraplex device or hyper-g experiments using a short-arm human centrifuge with corresponding ground controls ($1\,g$) as described in Methods. **(D,E)** Gene expression of *ACTB* in FTC-133 and cells expressing Lifeact-GFP, respectively after 31 parabolas (31P), vibration (V), and hyper-g ($1.8\,g$) with corresponding ground controls ($1\,g$). **(F,G)** Gene expression of *EZR* in FTC-133 and cells expressing Lifeact-GFP, respectively after 31 parabolas (31P), vibration (V), and hyper-g ($1.8\,g$) with corresponding ground controls ($1\,g$). **(H,I)** Gene expression of *RDX* in FTC-133 and Lifeact-GFP, respectively after 31 parabolas (31P), vibration (V), and hyper-g ($1.8\,g$) with corresponding ground controls ($1\,g$). **(J,K)** Gene expression of *MSN* in FTC-133 and

Lifeact-GFP, respectively after 31 parabolas (31P), vibration (V), and hyper-*g* (1.8 *g*) with corresponding ground controls (1 *g*). All results are shown as mean ± standard deviation (SD) of n = 8 (PFC), n = 12 (hyper-*g*) and n = 5 (vibration) independent samples, with significance indicated by *P < 0.05 vs. 1 *g*.

Moreover, we focused on four proteins regulating cellular signaling processes: Copine 1, plastin 2, sept11 (septin-11) and LIMA. Copine 1 can bind several intracellular proteins with diverse biological functions[35], its role in regulating biological processes remains unclear. In mammalian cell lines, copines 1, 2, 3, 6 and 7 can move to the plasma membrane following increases in intracellular Ca^{2+} triggered by ionomycin treatment of cells in medium containing 1.8 mm calcium. Copine 1 is a calcium-dependent membrane-binding protein regulating signaling at the cell membranes[36]. The FTC-133 cell line is *CPNE1*-positive and we could demonstrate for the first time in Fig. 5A,B that real microgravity increases *CPNE1* mRNA after the 31st parabola in Lifeact-GFP transfected cells, whereas hyper-*g* and vibration had no effect on this gene.

We recently had detected lymphocyte cytosolic protein 1 (LCP-1 or plastin 2) by proteome analysis in FTC-133 poorly differentiated follicular thyroid cancer cells[37] and demonstrated that LCP-1 protein was down-regulated in FTC-133 cells cultured in simulated microgravity on the Random Positioning Machine (RPM) for 3 days[38]. LCP-1 is an actin-binding protein and had been earlier identified as an ovarian cancer tumor biomarker[39]. During a PFC we detected a slight increase in *LCP1* gene expression after 31 parabolas and also an increase in hyper-*g* samples. Vibration had no effect on the expression of *LCP1* (Fig. 5C).

Recently, we had investigated ML-1 thyroid cancer cells on a PFC[5]. We found that *LIMA1* mRNAs were slightly, not significantly up-regulated under microgravity, but up-regulated in hyper-*g* after 31 parabolas and unchanged by vibrations. Interestingly, no significant changes were observed when investigating the FTC-133 cell line, but an increase in *LIMA1* mRNA in hyper-*g* samples was detectable (Fig. 5E,F). The LIMA1 protein is a cytoskeletal-associated protein involved in the regulation of actin dynamics and cell motility. It is known to suppress actin depolymerization and to stabilize F-actin fibers[40]. This results in the establishment of the adhesion belt[40]. The up-regulation of *LIMA1* mRNA under hyper-*g* indicates a mechanism of the thyroid cancer cells to stabilize the actin cytoskeleton.

SEPT11 (septin-11) is a GTP-binding protein organized in filaments and was detected in FTC-133 thyroid cancer cells[37]. It is involved in cytokinesis and in microtubule/actin cytoskeleton organization[41]. In transfected cells real microgravity significantly reduced the gene expression of *SEPT11* after 31 parabolas, whereas conditions of hyper-*g* significantly elevated its expression and vibration did not change *SEPT11* (Fig. 5G,H).

Microgravity during a sounding rocket flight changes the cytoskeleton. After examining the functionality of the FLUMIAS EM during a PFC, we next investigated the effect of microgravity during a sounding rocket flight. An advantage of such an experiment compared to a PFC is the considerably longer duration of microgravity (approximately 6 minutes) as well as only one period of hypergravity and vibration preceding the microgravity phase of the rocket flight parabola. This experiment was performed on-board the TEXUS 52 rocket using the FLUMIAS FM. A video of the sounding rocket flight mission is shown in Supplementary Video S2. Even though this version of the microscope is equipped with multiple lasers enabling parallel imaging of Lifeact-GFP and mCherry-Tubulin, we chose to only use the 488 nm diode laser for detection of GFP-Lifeact in order to obtain as much information as possible regarding the actin counterpart of the cytoskeleton immediately after the beginning of microgravity and during the 6 minutes of the microgravity phase. Approximately 60 seconds after lift-off of TEXUS-52, live-images from the FLUMAIS FM were received by telemetry allowing a final adjustment of the x, y and z coordinates selected before launch. Live-cell imaging was then performed in five separate rounds of approximately 25 seconds duration resulting in data collection corresponding to four Z-stacks of 28 layers separated by 300 nm. As presented in Fig. 6, a palette of different actin structures was observed. The pre-flight 1*g*-image revealed the actin cytoskeleton of three cells as visualized by Lifeact-GFP expression (Fig. 6A). As expected, well-structured filament-bundles were observed in the cells and stress fibers as well as filopodia- and lamellipodia-like structures were barely visible. Notably, following entrance into microgravity the actin-based cytoskeleton rapidly underwent dramatic changes (Fig. 6B). These changes included the disturbance of F-actin bundles, the appearance of filopodia- and lamellipodia-like structures and cellular detachment. To obtain information of the dynamics of these changes, a live-cell imaging video was assembled from corresponding sections. The video was created from the z-stacks over the total observation time of approximately 125 seconds (see Supplementary Video S1). In support of the data presented in Fig. 6A,B, the changes, especially the formation of filopodia- and lamellipodia-like structures, occurred rapidly after entrance into the microgravity phase. The appearance of filopodia- and lamellipodia-like structures was most likely a combined result of microgravity and vibration. The structures observed in the 1*g*-ground control cells (Fig. 6C) most likely represent microvilli, which then disappear during hypergravity (Fig. 6D). In addition, stress fibers can then be observed in the hypergravity sample, while microvilli and filopodia- as well as lamellipodia-like structures disappeared (Fig. 6D). In response to 2h-vibrations stress granules appeared as presented in Fig. 6E. Stress fibers could also be observed in response to vibrations (Fig. 6E).

Discussion

The aim of this study was to investigate the influence of real microgravity on the cytoskeleton on human thyroid cancer cells. For this purpose, we developed a compact fluorescence microscope (FLUMIAS) for fast live-cell imaging under real microgravity. To our knowledge, this is the first report of such a live-cell imaging analysis in space on a TEXUS rocket flight or onboard a parabolic flight aircraft. We used the poorly differentiated thyroid cancer cell line FTC-133 as our cell model system, which was already studied two-times in space (Sino-German
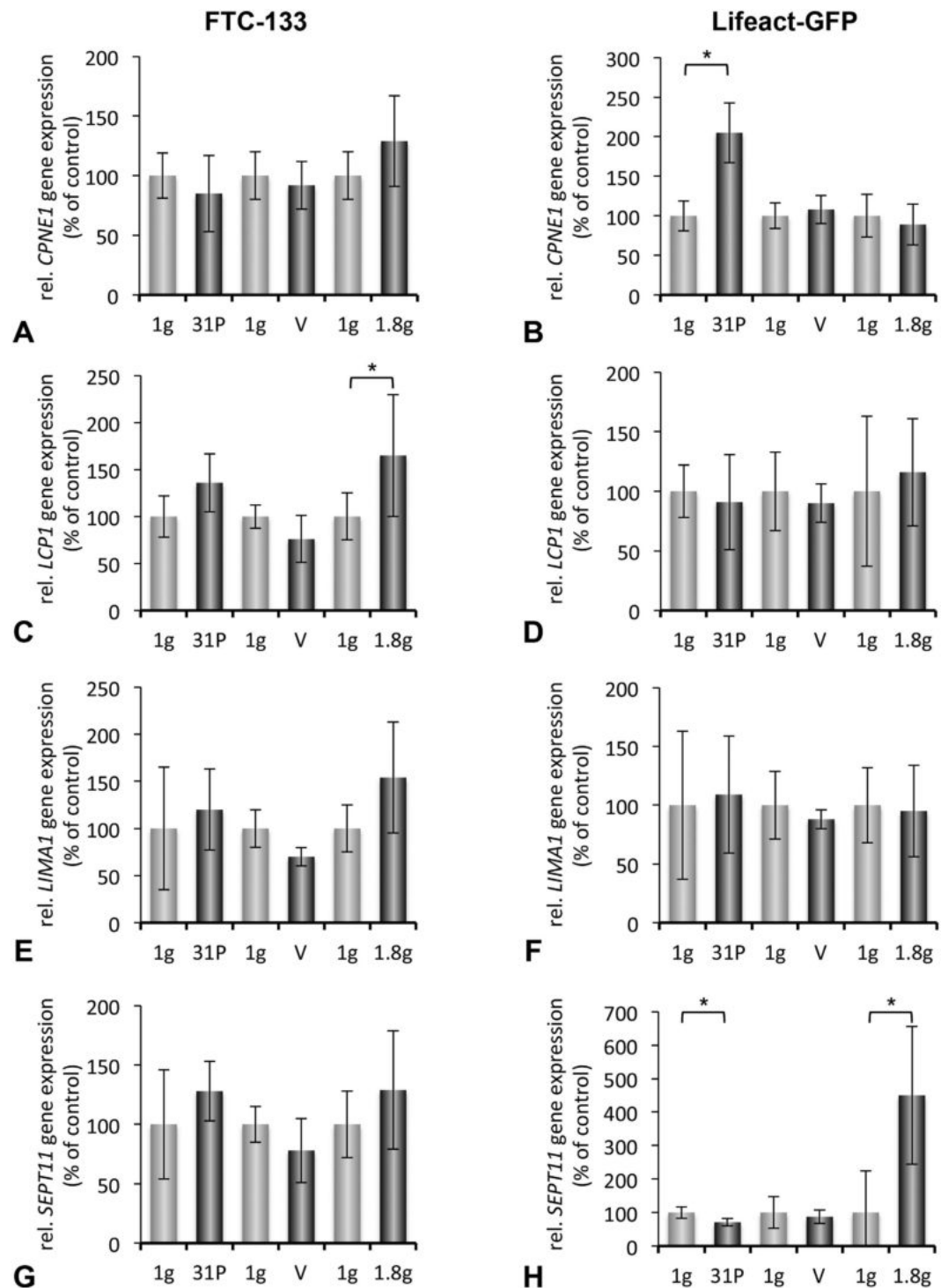
Figure 5. Gene expression analysis evaluated by RT qPCR to investigate the changes of proteins regulating cellular signaling processes. Non-transfected FTC-133 cells and FTC-133 cells expressing Lifeact-GFP were cultivated in T175 cell culture flasks and brought to the aircraft approximately one hour prior take off. To rule out the effect of vibration and hyper-*g*, vibration experiments or hyper-*g* experiments with corresponding ground controls (1*g*) were performed as described in Methods. (**A,B**) Gene expression of *CPNE1* in FTC-133 and cells expressing Lifeact-GFP, respectively after 31 parabolas (31P), vibration (V), and hyper-*g* (1.8*g*) with corresponding ground controls (1*g*). (**C,D**) Gene expression of *LCP1* in FTC-133 and cells expressing Lifeact-GFP, respectively after 31 parabolas (31P), vibration (V), and hyper-*g* (1.8*g*) with corresponding ground controls (1*g*). (**E,F**) Gene expression of *LIMA1* in FTC-133 and Lifeact-GFP, respectively after 31 parabolas (31P), vibration (V), and hyper-*g* (1.8*g*) with corresponding ground controls (1*g*). (**G,H**) Gene expression of *SEPT11* in FTC-133 and Lifeact-GFP, respectively after 31 parabolas (31P), vibration (V), and hyper-*g* (1.8*g*) with corresponding ground controls (1*g*). All results are shown as mean ± standard deviation (SD) n = 8 (PFC), n = 12 (hyper-*g*) and n = 5 (vibration) independent samples, with significance indicated by *P < 0.05 vs. 1*g*.

Figure 6. Inflight analyses of F-actin cytoskeleton changes during the TEXUS 52 mission using the FLUMIAS FM. Live-cell imaging of F-actin visualized by Lifeact-GFP in FTC-133 cells experiencing (**A,B**) microgravity during the TEXUS 52 rocket flight, (**C**) normal gravity (1 g), (**D**) hypergravity (1.8 g), or (**E**) vibration. Two hours before lift-off a μ-slides containing Lifeact-GFP expressing FTC-133 cells was mounted in the late access and fixation unit and transferred to the rocked as described in Methods. The position of three cells display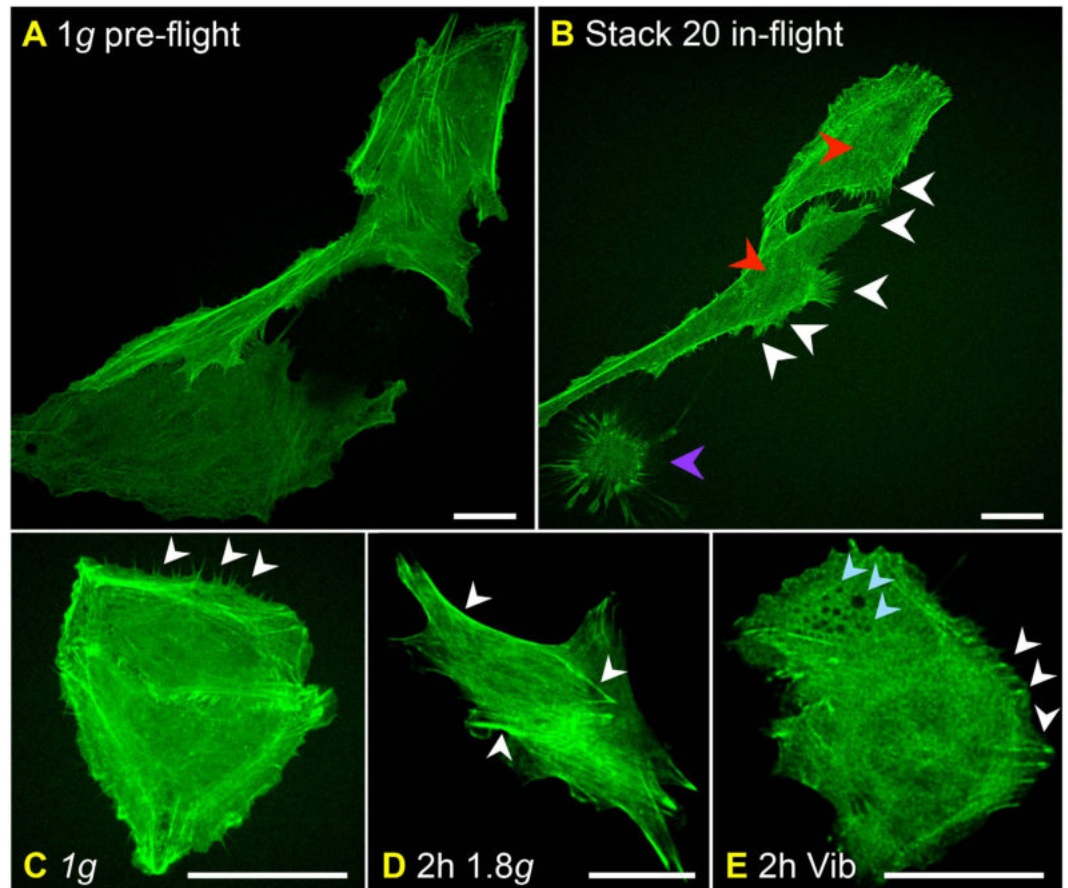ing Lifeact-GFP fluorescence signals was selected and live-cell imaging of these cells was performed both before lift-off (**A**) and during the 6-min-long microgravity phase of the flight (**B**). As controls live-cell imaging was performed on cells experiencing 1 g, two hours of hyper-g and two hours of vibration. (**A**) 1 g pre-flight. (**B**) Stack 20 in-flight of the same cells shown in (**A**). (**C**) 1 g control. (**D**) 2 hours of hyper-g (1.8 g). (**E**) 2 hours of vibration (Vib). Scale bars = 20 μm. Red arrowheads indicate disturbance of F-actin bundles. In (**B**) white arrowheads indicate appearance of filopodia-, and lamellipodia-like structures. In (**C**) white arrowheads indicate microvilli. In (**D**) and (**E**) white arrowheads indicate stress fibers. Purple arrowhead denotes cellular detachment. Light blue arrowheads indicate cytoskeleton alterations in forms of stress granules in the cytoplasm.

Shenzhou-8/SIMBOX space mission in 2011 and NanoRacks-Cellbox-1 ISS experiment in 2014). For this purpose, we cultivated FTC-133 cells for the TEXUS 52 experiment in Kiruna, Swedish Space Center, ESRANGE, Sweden. In addition, we also cultivated the cells under altered gravity conditions on a short-arm human centrifuge and a Vibraplex device (both constructed by DLR, Cologne, Germany) and exposed them to short-term real microgravity on parabolic flights.

A long-term spaceflight has enormous impact on the health of humans in space. Several health problems can occur such as heart problems, bone loss, muscle atrophy, disturbances of the immune system, and more[6,42]. Since many years we know that microgravity induces a variety of changes in cells and plants cultured under real and simulated microgravity conditions[2]. Researchers demonstrated changes in growth behavior, differentiation, proliferation, cell adhesion, migration as well as increases in programmed cell death and changes in the cytoskeleton as well as elevated amounts of extracellular matrix proteins in many different cell types cultured under microgravity conditions[11,18,19,43–51].

Simulated microgravity (or functional weightlessness) is based on the assumption that sensing no weight and neutralization of sedimentation would have effects comparable to those of weightlessness[52] (0 g), a condition which is never completely reached. Therefore, the term "microgravity" is used to indicate the very weak residual acceleration forces. On ground, different facilities have been developed aiming to achieve functional weightlessness (simulated microgravity), such as RPMs or fast-rotating clinostats. Even though RPMs and clinostats have been shown to imitate microgravity responses consistently for several, but not all, experimental conditions, they

generally seem to underestimate the effects observed in real microgravity during spaceflights[53]. Therefore, the development of a fluorescence microscope for live-cell imaging studies on different types of cells suitable to perform analyses during parabolic flight missions, on rocket flights and on the International Space Station in space is a necessary step to prove the earlier findings on living cells.

Until now live-cell imaging was not possible in space. This is the first study investigating the cytoskeleton in living thyroid cancer cells. In the past and also currently, researchers had to work with samples treated with paraformaldehyde (PFA) or other fixatives to perform fluorescence staining of the cytoskeleton in different cell types, when they conducted their experiments under conditions of real microgravity. The F-actin network can be visualized by rhodamine-phalloidin staining. Potential pitfalls of PFA fixations and immunolabeling artifacts including severe damage of the cellular cytoskeleton and a shrinking cell volume do often receive little attention arguing that immunostaining experiments in dead, permeabilized cells should be accompanied with live-cell imaging when dissecting protein localization[54]. Taking the data from the PFC and the TEXUS mission together, we found that changes in the cytoskeleton occur rapidly after entrance into microgravity, which confirms the results obtained on fixed samples. In both cases we detected a disturbance of F-actin bundles, which was not observed during 1.8 g or vibration. Another important finding observed during microgravity was the formation of filopodia- and lamellipodia-like structures, which were not observed during hypergravity. Contrary, formation of stress fibers occurred in the 1.8 g experiments, while microvilli, which were observed in 1 g- samples, and filopodia- as well as lamellipodia-like structures disappeared. The cytoskeletal alterations in form of "holes" in the cytoplasm observed during the parabolic flight maneuvers, presumably representing stress granules, were not evident during the TEXUS flight. However, as stress granules are seen in the cells exposed only to vibration, these changes are most likely linked to the vibration events occurring during each parabola. Notably, stress fibers are present in the samples, experiencing vibration.

The disappearance of filopodia-, and lamellipodia-like structures, as observed in Fig. 4A–C might be explained by the fact that they disappear during the two 1.8 g phases of each parabola as they are not observed during the 1.8 g experiment. The expression data show that *ACTB* is significantly up-regulated in cells expressing Lifeact-GFP during PFC. This up-regulation is most likely a consequence of µg, since expression of *ACTB* is not altered during vibration and hyper-g. Conversely, *ACTB* expression is not altered in FTC-133 during the PFC. However, a 2-fold up-regulation is observed during hyper-g.

Viable cells *in vitro* use a tension-dependent form of architecture (tensegrity) for the organization and stabilization of the cytoskeleton[55]. The tensegrity model describes how cells might control their shape and mechanics through use of an architectural mechanism. Even though a growing body of evidence suggests that this model accounts for a number of features of living cells including control of shape and physical connections between the chromosomes[55,56], it remains controversial and has a number of limitations[57]. All cytoskeletal filament systems are involved in this special stress (altered gravity) response[55]. Cytoskeletal disruption is an important factor known to increase programmed cell death[58] in a variety of cells, but not in all cells. Human chondrocytes cultured on the RPM showed cytoskeletal alterations, but no increase in apoptosis[16,59]. Programmed cell death was found in thyroid cancer cells[45] and in adherent EC cultivated on the RPM as well as in Jurkat cells and lymphocytes cultured in space[18,43]. This is in agreement with our finding of one dying FTC-133 cell during the rocket flight (Fig. 6B). These data support the hypothesis that the cytoskeletal and ERM proteins seem to be the first proteins influenced by microgravity because their networks of interaction are disturbed in a few seconds when the gravity vector is annulled. Therefore, they cannot longer function in a proper manner. The result is a rapid influence on gene regulation, initiating a cascade of protein changes. Thus, exact knowledge of the proteome in different cell types, together with the gene array technique, is useful to clarify which signaling pathways are involved in cancer or other diseases occurring in space[4,25].

The ERM protein group, consisting of the three closely related proteins ezrin, radixin and moesin, is known to crosslink actin with the cellular plasma membranes. We had detected an accumulation of F-actin at the outer membranes of different cell types so that we focused on changes in these proteins in space and after the PFC. The expression of ERM genes, with the exception of *EZR*, was not altered in cells expressing Lifeact-GFP during the PFC, vibration or hyper-g. Increased expression of *EZR* in FTC-133 during the PFC may be caused by hyper-g as a similar increase of *EZR* is observed under 1.8 g conditions. The increase of *ACTB* in FTC-133 during hyper-g was also reflected in an increased expression of *RDX* and *MSN*.

Our observations demonstrate that the cells sense gravitational unloading rapidly after the onset of microgravity, which consequently leads to immediate formation of filopodia-, and lamellipodia-like structures. Since these actin-dependent filaments are involved in cellular processes like adhesion and migration, it makes sense for the cells to make use of such molecular architecture elements[60]. Our experiments also provide data indicating alteration in expression of ERM genes. These proteins strongly localize to microvilli and it has recently been shown that over-activation of ERM proteins leads to tightening of the cortex-membrane linkage as reported by Fritzsche *et al.*[61]. In response to over-expression of ezrin and F-actin, an orchestrated sequence of different actin structures may thus be envisioned for the cells until they experience severe issues characteristic for stress granules[62].

In conclusion, the FLUMIAS microscope has elegantly proven its applicability for live-cell imaging during both PFC and TEXUS 52 flights and by using this platform, in combination with gene expression analysis, we have documented significant alterations of the cytoskeleton, occurring rapidly after entrance to microgravity. We believe that the concept of using the FLUMIAS live-cell imaging system in microgravity might provide important knowledge in our understanding of the fundamental role of gravity in cell biology including cancer cell growth and function. We also believe that the FLUMIAS microscope is an important technological advance in live-cell imaging when dissecting protein localization.

Methods

The FLUMIAS spinning disc microscope. The FLUMIAS confocal laser spinning disc fluorescence microscope was developed by the company FEI Munich GmbH, Germany (Fig. 1, see text for details). A sketch depicting the working principle of a confocal laser spinning disc fluorescence microscope is shown in Fig. 2. The biological samples are seeded to an Ibidi-slide (ibidi GmbH, μ-slide VI 0.4 ibiTreat slide) (Fig. 3D), which is installed inside the late access and fixation unit (designed and built by Airbus DS) (Supplementary Figure S1E). The FLUMIAS microscope is equipped with a 40x objective (Carl Zeiss Microscopy GmbH, Plan-Apochromat 40x/0.95 Corr), a spinning disc unit (called Andromeda) and a camera (Hamamatsu Photonics Deutschland GmbH, Orca flash 4.0). The laser light originates from the laser line combiner (Omicron-Laserage Laser products GmbH, LightHUB-4). As a supporting structure and for power supply, cooling and control of the microscope Airbus DS built an experiment service subsystem for the FLUMIAS TEXUS 52 FM.

Parabolic flight. The parabolic flight experiments were carried out on-board the Airbus A300 ZERO-G, operated by the Bordeaux-Merignac-based company Novespace (France) (Supplementary Figure S1A). The parabolic maneuvers each consisted of 31 consecutive parabolas during the flight[1]. The procedure was described earlier in detail[1,3–5,24].

Cell culture procedure for the PFC. The cell culture procedure for the 24th and 25th DLR parabolic flight campaigns was published earlier[1,4]. The human follicular thyroid carcinoma cell line FTC-133 was purchased from the Health Protection Agency Culture Collections (HPACC). The cells were cultivated in RPMI 1640 (Life Technologies) medium supplemented with 10% FCS (Biochrom AG) and 1% penicillin/streptomycin (Life Technologies) and cultured under standard cell culture conditions at 37 °C and 5% CO_2. In brief, the cells were cultivated in 16 T175 cell culture flasks (175 cm^2; Sarstedt). During this time, the cells were covered by 15 ml (T175 flasks) of complete medium. Half of the flasks (n = 8) with appropriate medium were used as 1 *g* ground control cells, cultured, and fixed in the laboratory, and the other half were, in parallel, taken to the aircraft for the parabolic flight (n = 8). Syringes containing the appropriate fixative (RNA*later*) were connected to both types of flasks for the parabolic flight via a flexible tube and 3-way valve[1]. One hour before each flight, the cell culture flasks and slides were transported to the aircraft and placed into the 37 °C preheated incubator on an experimental rack. After the flight the samples were immediately brought to the cell culture laboratory at Novespace, Bordeaux-Merignac, France.

TEXUS 52 sounding rocket flight mission. The rocket flight experiment was performed on-board a sounding rocket as part of the DLR TEXUS (Technologische EXperimente Unter Schwerlosigkeit) 52 mission launched from Esrange, Swedish Space Center (SSC), in Kiruna in Northern Sweden (see Supplementary Figure S1B and Supplementary Video S2). The rocket type was a Brazilian two-stage solid propellant VSB 30 rocket (Supplementary Figure S1F). The duration of the flight was approximately 15 minutes and the parabolic flight brought the sounding rocket to an altitude of 261 km. Following launch, the rocket enters microgravity after 75 seconds of flight and the payload is then exposed to $<10^{-4}\,g$ for a period up to 390 seconds. At this stage the rocket re-enters the atmosphere and following parachute-mediated deceleration the payload is recovered after landing on the Earth.

Construction of a versatile construct to visualise F-actin and α-tubulin. To construct pcDNA3.1-Lifeact-eGFP-IRES-mCherry-Tubulin, briefly, pLAGICT, a DNA sequence construct harboring a *Not*I restriction site, the Lifeact sequence, encoding a 17 amino acid long F-actin marker[63] followed by a seven amino acid long linker (GDPPVAT) in frame with Lifeact, the cDNA sequence encoding eGFP, an internal ribosome entry site (IRES) sequence, the cDNA sequence encoding mCherry, a 7 amino acid long linker (SGLRSRA) in frame with mCherry, and the cDNA sequence encoding α-tubulin, followed by a *Xba*I restriction site was ordered from Genscript (Fig. 3A). The Lifeact-eGFP-IRES-mCherry-Tubulin sequence, provided in a pUC57 plasmid, was excised by digestion with *Not*I/*Xba*I (New England Biolabs), purified by gel extraction and ligated into the *Not*I/*Xba*I restriction sites of pcDNA3.1(+) (Invitrogen). Following transformation in ultracompetent *Escherichia coli* strain XL2-Blue (Stratagene) and overnight growth on LB/agar plates supplemented with ampicillin, colonies of interest were cultured overnight in 2 ml LB supplemented with ampicillin and plasmid DNA was purified from the remaining pellet by QIAprep spin column (Qiagen). Following digestion with *Not*I/*Xba*I plasmid DNA preparations harboring inserts of the expected size (~3.5 kb) were submitted to sequencing.

Generation of Lifeact-GFP expressing FTC-133 cells and cell culture procedure. To generate stable transfected cells FTC-133 cells were seeded in T75 flasks 75 cm^2 (Sarstedt). The next day the cells were transfected with pLAGICT as previously described[64]. In brief, a total of 11.25 μg plasmid DNA and 33.75 μl X-tremeGENE 9 transfection (Roche) reagent in a total volume of 750 μl serum free medium was used according to the manufacturer's instructions. Twenty-four hours post transfection, cells were seeded into P15 dishes (Greiner). Six to twelve hours later the medium was replaced with medium containing Neomycine (G418) 1.5 mg/ml (VWR). Approximately one week after the initiation of the selection procedure non-transfected cells were dead and several positive clones were harvested after an additional week of selection. Expression of Lifeact-GFP was validated by fluorescent microscopy.

For the PFC, the cells were cultivated either in T175 cell culture flasks (Sarstedt) until subconfluent monolayers were obtained or in μ-slide VI 0.4 ibiTreat slides (Ibidi) (Fig. 3D). One slide (each flight day) was taken to the aircraft for live-cell imaging with the FLUMIAS microscope, and another slide was investigated by fluorescence microscopy on ground (1 *g*) in the laboratory. Approximately one hour prior each of the three flights, a μ-slide (Fig. 3D) was mounted in the late access and fixation unit of the microscope (Supplementary Figure S1E) and

brought to the aircraft together with the cell culture flasks. The late access and fixation unit containing the slide was loaded into the pre-heated FLUMIAS EM placed in a protective dome-shaped rack (Supplementary Figure S1C). The cell culture flasks were placed in the incubator, likewise pre-heated, on an experimental rack[1].

Cells used for the TEXUS 52 mission were seeded into six μ-slides 28 hours prior to lift-off (Fig. 3D). Two hours before lift-off one μ-slide was selected and mounted in the late access and fixation unit and brought to the rocket, where it was loaded into the pre-heated FLUMIAS FM placed in a protective dome-shaped rack (Supplementary Figure S1D). The remaining μ-slides were used as ground control cells, hyper-g (1.8 g) control cells, and vibration (Vib) control cells, respectively (see below).

Hypergravity experiments. Experiments in hyper-g were conducted on the short-arm human centrifuge (DLR (German Aerospace Agency), Cologne, Germany) as described recently[1]. In brief, two portable incubators were placed in a swing-out device on the centrifuge to ensure that the cells were exposed to a correct vertical acceleration. The cells were exposed to a continuous hyper-g phase of 1.8 g for 2 h corresponding to the time period of 31 parabolas (31P). In parallel, the static 1 g controls were cultured in the laboratory. For real-time qPCR analysis n = 12 static 1 g controls and n = 12 1.8 g hyper-g-samples were collected. For imaging of cells exposed to hyper-g a μ-slide was placed in a Heraeus Omnifuge 2.0 RS centrifuge using a swing-out rotor and centrifuged at a continuous hyper-g phase of 1.8 g for 2 h. Imaging on the FLUMIAS FM was performed immediately after centrifugation.

Vibration experiments. T25 cell culture flasks containing 80–90% confluent monolayers were attached to a Vibraplex platform in an incubator at 37 °C with 5% CO_2 and treated as previously described[5]. On the Vibraplex device the cells were exposed to vibrations comparable to those occurring during parabolic flights[65]. Frequencies ranging from 0.2 to 14 Hz were applied, corresponding to the three phases of a parabola, over 2 h, which corresponds to the total time period of 31 parabolas during a parabolic maneuver. For real-time qPCR analysis n = 5 static 1 g controls and n = 5 vibration samples were collected. For imaging of cells exposed to vibration the μ-slide was placed on a Vibraplex platform in an incubator at 37 °C and exposed to vibrations as described above. Imaging on the FLUMIAS FM was performed immediately after vibration.

RNA isolation and real-time qPCR analysis. qPCR was used to determine the expression levels of the genes of interest. The medium or the mixture of medium and RNA*later* was removed and replaced by 5–10 ml fresh RNAlater. Following storage at 4 °C the cells were scraped off by using cell scrapers (Sarstedt), transferred to 50 ml tubes, and pelleted by centrifugation (2500 g for 10 minutes at 4 °C). Total RNA was isolated according to the manufacturer's instructions using the RNeasy Mini Kit (Qiagen). The quality and concentration of RNA were assessed spectrophotometrically by means of a NanoDrop instrument (Thermo Scientific). In all cases purified RNA had an A260/280 ration of >1.7.

cDNA obtained with the First-strand cDNA synthesis Kit (Fermentas) by applying 1 μg of total RNA in a 20 μl reverse transcription reaction was used for qPCR analysis in order to determine the expression levels of genes of interest. Primer Express software (Applied Biosystems) was applied to design appropriate primers with a Tm of ~60 °C (Supplementary Table S1). The assays were performed on a StepOnePlus Real-Time PCR System using the Power SYBR Green PCR Master Mix (both Applied Biosystems). The total reaction volume was 25 μl including 1 μl of template cDNA with a final primer concentration of 500 nM. PCR conditions were as follows: 10 minutes at 95 °C, 40 cycles of 30 seconds at 95 °C and 1 minute at 60 °C. The run was followed by a melting curve analysis step. If all amplicons showed a Tm similar to the one predicted by the Primer Express software, the PCR reactions were considered specific. Every sample was measured in triplicate, and relative quantification was obtained by means of the comparative C_T ($\Delta\Delta C_T$) method. 18S rRNA was used as a housekeeping gene to normalize the expression data.

Statistics.
All statistical analyses were performed using SPSS 16.0 software (SPSS, Inc., Chicago, IL, USA). Data are presented as the mean ± SD. Statistical differences between two groups were evaluated using Mann-Whitney-U. $P < 0.05$ was considered statistically significant.

References

1. Aleshcheva, G. *et al.* Moderate alterations of the cytoskeleton in human chondrocytes after short-term microgravity produced by parabolic flight maneuvers could be prevented by up-regulation of BMP-2 and SOX-9. *FASEB J* 2303–2314 (2015).
2. Grimm, D., Wise, P., Lebert, M., Richter, P. & Baatout, S. How and why does the proteome respond to microgravity? *Expert Rev Proteomics* **8,** 13–27 (2011).
3. Grosse, J. *et al.* Short-term weightlessness produced by parabolic flight maneuvers altered gene expression patterns in human endothelial cells. *FASEB J* **26,** 639–655 (2012).
4. Ma, X. *et al.* Differential gene expression profile and altered cytokine secretion of thyroid cancer cells in space. *FASEB J* **28,** 813–835 (2014).
5. Ulbrich, C. *et al.* Differential gene regulation under altered gravity conditions in follicular thyroid cancer cells: relationship between the extracellular matrix and the cytoskeleton. *Cell Physiol Biochem* **28,** 185–198 (2011).
6. White, R. J. & Averner, M. Humans in space. *Nature* **409,** 1115–1118 (2001).
7. Crucian, B., Stowe, R., Quiriarte, H., Pierson, D. & Sams, C. Monocyte phenotype and cytokine production profiles are dysregulated by short-duration spaceflight. *Aviat Space Environ Med* **82,** 857–862 (2011).
8. Sciola, L., Cogoli-Greuter, M., Cogoli, A., Spano, A. & Pippia, P. Influence of microgravity on mitogen binding and cytoskeleton in Jurkat cells. *Adv Space Res* **24,** 801–805 (1999).
9. Meloni, M. A. *et al.* Space flight affects motility and cytoskeletal structures in human monocyte cell line J-111. *Cytoskeleton (Hoboken)* **68,** 125–137 (2011).
10. Becker, J. L. & Souza, G. R. Using space-based investigations to inform cancer research on Earth. *Nat Rev Cancer* **13,** 315–327 (2013).

11. Grimm, D. *et al.* Growing tissues in real and simulated microgravity: new methods for tissue engineering. *Tissue Eng Part B Rev* **20,** 555–566 (2014).

12. Grosse, J. *et al.* Gravity-sensitive signaling drives 3-dimensional formation of multicellular thyroid cancer spheroids. *FASEB J* **26,** 5124–5140 (2012).

13. Nasir, A. *et al.* The influence of microgravity on Euglena gracilis as studied on Shenzhou 8. *Plant Biol (Stuttg)* **16** Suppl 1, 113–119 (2014).

14. Pietsch, J. *et al.* Spheroid formation of human thyroid cancer cells in an automated culturing system during the Shenzhou-8 Space mission. *Biomaterials* **34,** 7694–7705 (2013).

15. Wehland, M. *et al.* Differential gene expression of human chondrocytes cultured under short-term altered gravity conditions during parabolic flight maneuvers. *Cell Commun Signal* **13,** 18 (2015).

16. Aleshcheva, G. *et al.* Changes in morphology, gene expression and protein content in chondrocytes cultured on a random positioning machine. *PLoS One* **8,** e79057 (2013).

17. Infanger, M. *et al.* Modeled gravitational unloading induced downregulation of endothelin-1 in human endothelial cells. *J Cell Biochem* **101,** 1439–1455 (2007).

18. Lewis, M. L. *et al.* Spaceflight alters microtubules and increases apoptosis in human lymphocytes (Jurkat). *FASEB J* **12,** 1007–1018 (1998).

19. Uva, B. M. *et al.* Microgravity-induced apoptosis in cultured glial cells. *Eur J Histochem* **46,** 209–214 (2002).

20. Vassy, J. *et al.* The effect of weightlessness on cytoskeleton architecture and proliferation of human breast cancer cell line MCF-7. *FASEB J* **15,** 1104–1106 (2001).

21. Crawford-Young, S. J. Effects of microgravity on cell cytoskeleton and embryogenesis. *Int J Dev Biol* **50,** 183–191 (2006).

22. Hughes-Fulford, M. Function of the cytoskeleton in gravisensing during spaceflight. *Adv Space Res* **32,** 1585–1593 (2003).

23. Pietsch, J. *et al.* A proteomic approach to analysing spheroid formation of two human thyroid cell lines cultured on a random positioning machine. *Proteomics* **11,** 2095–2104 (2011).

24. Wehland, M. *et al.* The impact of altered gravity and vibration on endothelial cells during a parabolic flight. *Cell Physiol Biochem* **31,** 432–451 (2013).

25. Riwaldt, S. *et al.* Identification of proteins involved in inhibition of spheroid formation under microgravity. *Proteomics* **15,** 2945–2952 (2015).

26. Warnke, E. *et al.* Spheroid formation of human thyroid cancer cells under simulated microgravity: a possible role of CTGF and CAV1. *Cell Commun Signal* **12,** 32 (2014).

27. Fehon, R. G., McClatchey, A. I. & Bretscher, A. Organizing the cell cortex: the role of ERM proteins. *Nat Rev Mol Cell Biol* **11,** 276–287 (2010).

28. Vaheri, A. *et al.* The ezrin protein family: membrane-cytoskeleton interactions and disease associations. *Curr Opin Cell Biol* **9,** 659–666 (1997).

29. Akisawa, N., Nishimori, I., Iwamura, T., Onishi, S. & Hollingsworth, M. A. High levels of ezrin expressed by human pancreatic adenocarcinoma cell lines with high metastatic potential. *Biochem Biophys Res Commun* **258,** 395–400 (1999).

30. Zou, M. *et al.* Microarray analysis of metastasis-associated gene expression profiling in a murine model of thyroid carcinoma pulmonary metastasis: identification of S100A4 (Mts1) gene overexpression as a poor prognostic marker for thyroid carcinoma. *J Clin Endocrinol Metab* **89,** 6146–6154 (2004).

31. Kanaan, Z., Qadan, M., Eichenberger, M. R. & Galandiuk, S. The actin-cytoskeleton pathway and its potential role in inflammatory bowel disease-associated human colorectal cancer. *Genet Test Mol Biomarkers* **14,** 347–353 (2010).

32. Roubinet, C. *et al.* Molecular networks linked by Moesin drive remodeling of the cell cortex during mitosis. *J Cell Biol* **195,** 99–112 (2011).

33. Kobayashi, H. *et al.* Clinical significance of cellular distribution of moesin in patients with oral squamous cell carcinoma. *Clin Cancer Res* **10,** 572–580 (2004).

34. Ma, X. *et al.* Interleukin-6 expression under gravitational stress due to vibration and hypergravity in follicular thyroid cancer cells. *PLoS One* **8,** e68140 (2013).

35. Tomsig, J. L., Snyder, S. L. & Creutz, C. E. Identification of targets for calcium signaling through the copine family of proteins. Characterization of a coiled-coil copine-binding motif. *J Biol Chem* **278,** 10048–10054 (2003).

36. Perestenko, P. V. *et al.* Copines-1, -2, -3, -6 and -7 show different calcium-dependent intracellular membrane translocation and targeting. *FEBS J* **277,** 5174–5189 (2010).

37. Pietsch, J. *et al.* Application of free-flow IEF to identify protein candidates changing under microgravity conditions. *Proteomics* **10,** 904–913 (2010).

38. Grimm, D. *et al.* The impact of microgravity-based proteomics research. *Expert Rev Proteomics* **11,** 465–476 (2014).

39. Kang, S. *et al.* Molecular proteomics imaging of tumor interfaces by mass spectrometry. *J Proteome Res* **9,** 1157–1164 (2010).

40. Abe, K. & Takeichi, M. EPLIN mediates linkage of the cadherin catenin complex to F-actin and stabilizes the circumferential actin belt. *Proc Natl Acad Sci USA* **105,** 13–19 (2008).

41. Froidevaux-Klipfel, L. *et al.* Modulation of septin and molecular motor recruitment in the microtubule environment of the Taxol-resistant human breast cancer cell line MDA-MB-231. *Proteomics* **11,** 3877–3886 (2011).

42. Pietsch, J. *et al.* The effects of weightlessness on the human organism and mammalian cells. *Curr Mol Med* **11,** 350–364 (2011).

43. Battista, N. *et al.* 5-Lipoxygenase-dependent apoptosis of human lymphocytes in the International Space Station: data from the ROALD experiment. *FASEB J* **26,** 1791–1798 (2012).

44. Grenon, S. M., Jeanne, M., Aguado-Zuniga, J., Conte, M. S. & Hughes-Fulford, M. Effects of gravitational mechanical unloading in endothelial cells: association between caveolins, inflammation and adhesion molecules. *Sci Rep* **3,** 1494 (2013).

45. Grimm, D. *et al.* Simulated microgravity alters differentiation and increases apoptosis in human follicular thyroid carcinoma cells. *FASEB J* **16,** 604–606 (2002).

46. Lewis, M. L. *et al.* cDNA microarray reveals altered cytoskeletal gene expression in space-flown leukemic T lymphocytes (Jurkat). *FASEB J* **15,** 1783–1785 (2001).

47. Maccarrone, M. *et al.* Creating conditions similar to those that occur during exposure of cells to microgravity induces apoptosis in human lymphocytes by 5-lipoxygenase-mediated mitochondrial uncoupling and cytochrome c release. *J Leukoc Biol* **73,** 472–481 (2003).

48. Martinez, E. M., Yoshida, M. C., Candelario, T. L. & Hughes-Fulford, M. Spaceflight and simulated microgravity cause a significant reduction of key gene expression in early T-cell activation. *Am J Physiol Regul Integr Comp Physiol* **308,** R480–488 (2015).

49. Versari, S., Longinotti, G., Barenghi, L., Maier, J. A. & Bradamante, S. The challenging environment on board the International Space Station affects endothelial cell function by triggering oxidative stress through thioredoxin interacting protein overexpression: the ESA-SPHINX experiment. *FASEB J* **27,** 4466–4475 (2013).

50. Kopp, S. *et al.* Mechanisms of three-dimensional growth of thyroid cells during long-term simulated microgravity. *Sci Rep* **5,** 16691 (2015).

51. Svejgaard, B. *et al.* Common effects on cancer cells exerted by a Random Positioning Machine and a 2D clinostat. *PLoS One* **10,** e0135157 (2015).

52. Hejnowicz, Z., Sondag, C., Alt, W. & Sievers, A. Temporal course of graviperception in intermittently stimulated cress roots. *Plant Cell Environ* **21,** 1293–1300 (1998).

53. Wuest, S. L., Richard, S., Kopp, S., Grimm, D. & Egli, M. Simulated microgravity: critical review on the use of random positioning machines for mammalian cell culture. *Biomed Res Int* **2015,** 971474 (2015).
54. Schnell, U., Dijk, F., Sjollema, K. A. & Giepmans, B. N. Immunolabeling artifacts and the need for live-cell imaging. *Nat Methods* **9,** 152–158 (2012).
55. Ingber, D. How cells (might) sense microgravity. *FASEB J* **13** Suppl, S3–15 (1999).
56. Ingber, D. E., Wang, N. & Stamenovic, D. Tensegrity, cellular biophysics, and the mechanics of living systems. *Rep Prog Phys* **77,** 046603 (2014).
57. Volokh, K. Y. On tensegrity in cell mechanics. *Mol Cell Biomech* **8,** 195–214 (2011).
58. Lewis, M. L. The cytoskeleton, apoptosis, and gene expression in T lymphocytes and other mammalian cells exposed to altered gravity. *Adv Space Biol Med* **8,** 77–128 (2002).
59. Ulbrich, C. *et al.* Characterization of human chondrocytes exposed to simulated microgravity. *Cell Physiol Biochem* **25,** 551–560 (2010).
60. Mattila, P. K. & Lappalainen, P. Filopodia: molecular architecture and cellular functions. *Nat Rev Mol Cell Biol* **9,** 446–454 (2008).
61. Fritzsche, M., Thorogate, R. & Charras, G. Quantitative analysis of ezrin turnover dynamics in the actin cortex. *Biophys J* **106,** 343–353 (2014).
62. Decker, C. J. & Parker, R. P-bodies and stress granules: possible roles in the control of translation and mRNA degradation. *Cold Spring Harb Perspect Biol* **4,** a012286 (2012).
63. Riedl, J. *et al.* Lifeact: a versatile marker to visualize F-actin. *Nat Methods* **5,** 605–607 (2008).
64. Askou, A. L. *et al.* Multigenic lentiviral vectors for combined and tissue-specific expression of miRNA- and protein-based antiangiogenic factors. *Mol Ther Methods Clin Dev* **2,** 14064 (2015).
65. Schmidt, W. Quickly changing acceleration forces (QCAFs) vibration analysis on the A300 ZERO-G. *Microgravity Sci Technol* **15,** 42–48 (2004).

Acknowledgements

Author Contributions

T.J.C., M.W., M.B. and D.G. designed work; T.J.C., M.W., R.H. and S.K. performed experiments; T.J.C., M.W., S.K. and D.G. analyzed the data; A.S., T.M., T.H., H.O. and B.S. provided analytic tools, T.J.C., T.H., H.O. and D.G. supervised work and wrote manuscript.

Additional Information

Supplementary information accompanies this paper at http://www.nature.com/srep

Competing financial interests: The authors declare no competing financial interests.

How to cite this article: Corydon, T. J. *et al.* Alterations of the cytoskeleton in human cells in space proved by life-cell imaging. *Sci. Rep.* **6**, 20043; doi: 10.1038/srep20043 (2016).

11.2 Publication #2

Riwaldt S, Bauer J, Wehland M, Slumstrup L, **Kopp S**, Warnke E, Dittrich A, Magnusson NE, Pietsch J, Corydon TJ, Infanger M, Grimm D. Pathways Regulating Spheroid Formation of Human Follicular Thyroid Cancer Cells under Simulated Microgravity Conditions: A Genetic Approach. Int J Mol Sci. 2016 Apr 8;17(4):528. doi: 10.3390/ijms17040528.

Article

Pathways Regulating Spheroid Formation of Human Follicular Thyroid Cancer Cells under Simulated Microgravity Conditions: A Genetic Approach

Stefan Riwaldt [1], Johann Bauer [2,*], Markus Wehland [1], Lasse Slumstrup [3], Sascha Kopp [1], Elisabeth Warnke [1], Anita Dittrich [3], Nils E. Magnusson [4], Jessica Pietsch [1], Thomas J. Corydon [3], Manfred Infanger [1] and Daniela Grimm [1,3]

[1] Plastic, Aesthetic and Hand Surgery, Otto-von-Guericke University Clinic, Leipziger Str. 44, 39120 Magdeburg, Germany; stefan.riwaldt@med.ovgu.de (S.R.); markus.wehland@med.ovgu.de (M.W.); sascha.kopp@med.ovgu.de (S.K.); elisabeth.warnke@med.ovgu.de (E.W.); jessica.pietsch@med.ovgu.de (J.P.); manfred.infanger@med.ovgu.de (M.I.); dgg@biomed.au.dk (D.G.)

[2] Max Planck Institute for Biochemistry, Am Klopferspitz 18, 82152 Martinsried, Germany

[3] Institute of Biomedicine, Aarhus University, Wilhelm Meyers Allé 4, 8000 Aarhus C, Denmark; slumstrup@biomed.au.dk (L.S.); adit88@gmail.com (A.D.); corydon@biomed.au.dk (T.J.C.)

[4] Medical Research Laboratory, Department of Clinical Medicine, Faculty of Health, Aarhus University, 8000 Aarhus C, Denmark; nm@clin.au.dk

* Correspondence: jbauer@biochem.mpg.de; Tel.: +49-89-8578-3803

Abstract: Microgravity induces three-dimensional (3D) growth in numerous cell types. Despite substantial efforts to clarify the underlying mechanisms for spheroid formation, the precise molecular pathways are still not known. The principal aim of this paper is to compare static 1*g*-control cells with spheroid forming (MCS) and spheroid non-forming (AD) thyroid cancer cells cultured in the same flask under simulated microgravity conditions. We investigated the morphology and gene expression patterns in human follicular thyroid cancer cells (UCLA RO82-W-1 cell line) after a 24 h-exposure on the Random Positioning Machine (RPM) and focused on 3D growth signaling processes. After 24 h, spheroid formation was observed in RPM-cultures together with alterations in the F-actin cytoskeleton. qPCR indicated more changes in gene expression in MCS than in AD cells. Of the 24 genes analyzed *VEGFA*, *VEGFD*, *MSN*, and *MMP3* were upregulated in MCS compared to 1*g*-controls, whereas *ACTB*, *ACTA2*, *KRT8*, *TUBB*, *EZR*, *RDX*, *PRKCA*, *CAV1*, *MMP9*, *PAI1*, *CTGF*, *MCP1* were downregulated. A pathway analysis revealed that the upregulated genes code for proteins, which promote 3D growth (angiogenesis) and prevent excessive accumulation of extracellular proteins, while genes coding for structural proteins are downregulated. Pathways regulating the strength/rigidity of cytoskeletal proteins, the amount of extracellular proteins, and 3D growth may be involved in MCS formation.

Keywords: thyroid cancer; simulated microgravity; random positioning machine; pathway studio; caveolin-1; vascular endothelial growth factor; matrix metalloproteinases; growth

1. Introduction

Altered gravity conditions, such as real or simulated microgravity (μ*g*), offer new and unique approaches to cell biology in general and tissue engineering in particular. Research in Space and experiments using ground-based facilities, such as the fast rotating clinostat (FRC), the random positioning machine (RPM) or rotating wall vessel (RWV) have revealed microgravity-dependent alterations of extracellular matrix proteins and the cytoskeleton, changes in apoptosis, proliferation, and differentiation as well as differences in the growth behavior of human cells [1–4]. Moreover,

microgravity has been shown to promote the scaffold-free growth of 3D multicellular constructs from a monolayer culture of a variety of different cell types, with striking resemblance to actual *in vivo* tissue in several cases [5–7].

During the last few years, we have focused on the behavior of malignant thyroid cells [8] under conditions of altered gravity and vibration [9]. We have exposed different healthy and malignant human thyroid cell lines to both real (on parabolic flight campaigns and on the SimBox/Shenzhou-8 Space Mission) and simulated (RPM) μ*g* for different time periods [2–4,8,10–14]. These studies showed that healthy and malignant human thyroid cell lines share the capability to form 3D multicellular spheroids (MCS) after exposure to annulled gravity conditions for various time periods [10–12]. In general, the cell lines exhibited a similar behavior overall with some differences in detail concerning gene and protein expression as well as the speed of aggregation [2]. The MCS are of great interest for cancer research, because they provide the possibility to study cancer cells *in vitro*. They provide a 3D structure with a known cellular composition. In this state, the cells interact with each other in a 3D way like they do *in vivo*, but differently to being grown within monolayers. In addition, the spheroids′ cells show a much higher invasive potential than monolayer cells [15]. Therefore, by investigating formation and growth of MCS, it might be possible to learn about the formation of metastases and thus to find new, so far neglected targets for cancer therapy/suppression.

Based on the findings of our previous studies, the aim of this study was to further analyze candidate genes and proteins in MCS of human UCLA RO82-W-1 grown on a RPM after 24 h and identify pathways involved in MCS formation by employing both molecular biological (quantitative real-time PCR) as well as *in silico* (Partek analyses) methods.

2. Results and Discussion

2.1. Spheroid Formation

Phase contrast microscopy revealed that the static control UCLA RO82-W-1 cells grew as a normal monolayer, when the cell culture flasks were placed next to the RPM in the incubator (Figure 1a). However, after a 24 h-exposure of UCLA RO82-W-1 follicular thyroid cancer cells to the RPM, two types of growth were observed: irrespectively of the culture dish used, one part of the cells grew as 3D aggregates, the other part as a two-dimensional monolayer (Figure 1b,c).
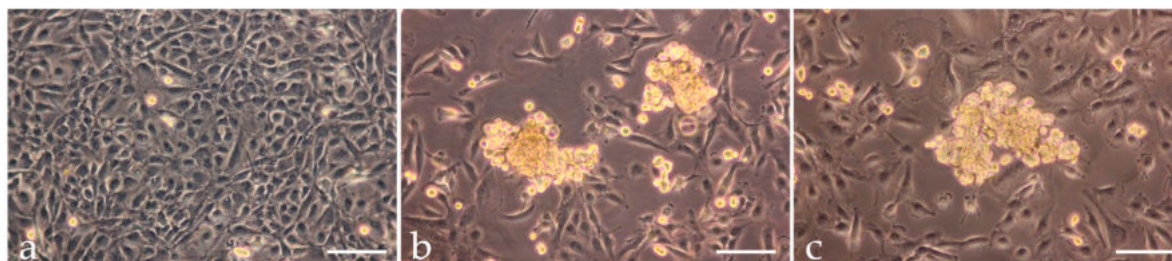
Figure 1. Phase contrast microscopic pictures of UCLA RO82-W-1 1*g*-control cells (**a**), and RO82-W-1 cells cultivated on the Random Positioning Machine (RPM) in slides flasks; (**b**) and T25 cell culture flasks; (**c**) for 24 h. Control cells remained adherent and formed a (sub)confluent monolayer (**a**). In both RPM-samples, some cells remained adherent, while others detached forming 3D spheroids of similar size, thus constituting two distinct cell populations (**b,c**). Scale bars = 100 μm.

This process is well known and has been detected in populations of various types of cells including endothelial cells, chondrocytes, and thyrocytes [6]. It occurs by culturing normal and malignant cells and seems to be due to the effects of microgravity but not to healthy or malignant states of the cells [6,8,14]. Follicle formation can also be induced when the cells are cultured on agarose-coated dishes with a special follicle induction medium [16] or by using the liquid-overlay technique [12]. From these studies, we concluded that a set of proteins interacting properly with each other, drive a cell

into a 3D kind of growth. This set is not specific for thyroid cells and does not comprise all proteins changeable under microgravity. For example, thyroid hormones and thyroglobulin are reduced as well as TSH receptors are changed when thyroid cells are cultured under microgravity conditions, while spheroid formation occurs even in their absence [3,17].

Moreover, in the adherent part of the RPM-exposed UCLA RO82-W-1 cell stress fibers are visible as well as lamellipodia, filopodia, and microvilli (Figure 2b), which cannot be detected in the corresponding 1*g*-control cells (Figure 2a). This is also in accordance with earlier studies performed on human cells exposed to microgravity, which demonstrated that the cytoskeletal proteins are a preferred target affected by conditions of real and simulated microgravity, irrespectively of whether a cell remains adherent or forms MCS [12,13,18,19].
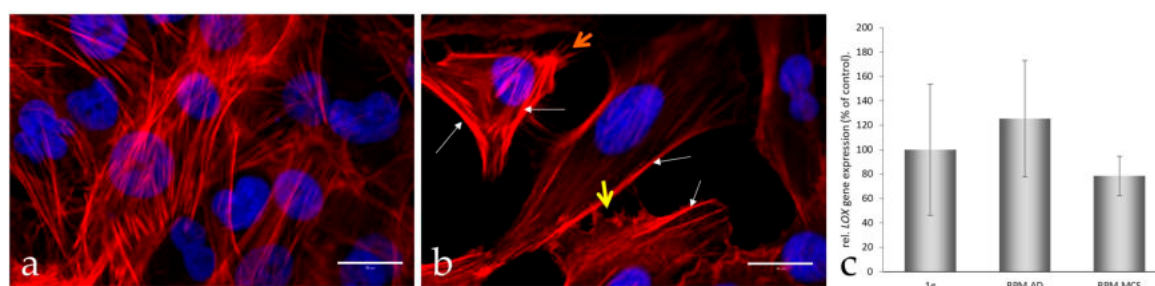

Figure 2. Actin cytoskeleton network visualization and *LOX* gene expression analysis. Rhodamine-phalloidin staining of UCLA RO82-W-1 cells exposed to 1*g* (**a**) and altered gravity on the RPM; (**b**) for 24 h. White arrows designate stress fibers accumulating at the cell borders, the yellow arrow shows lamellipodia and filopodia, the orange one microvilli. Quantitative rtPCR analyses of the *LOX* gene expression in 1*g*-control cells, RPM-adherent cells (AD) and RPM-multicellular spheroids (MCS) cells after a 24 h-culture (**c**). Scale bars = 20 μm (**a** and **b** in bottom right corner).

2.2. Impact of Simulated Microgravity on the Activation of Genes Coding for Selected Proteins

In order to find reasons for the transition of the cells from a two- to a three-dimensional kind of growth, we selected 24 genes (Table 1), which attracted attention in our earlier proteomic and genomic studies on spheroid formation of various types of cells [6,18,20]. The genes to be analyzed were selected from a number of preceding publications, where we found that cytoskeletal proteins change, that an overgrowth of extracellular proteins can prevent spheroid formation, that membrane proteins influence this process, and that nuclear proteins are activated [2,4,10,21]. These genes are coding for proteins belonging to three groups: (i) proteins establishing and regulating cell structures (Figure 3a–g); (ii) extracellular proteins regulating the cell behavior (Figures 2c, 4 and 5); and (iii) proteins involved in angiogenesis and signaling processes (Figures 3h, 4 and 5). A Pathway Studio analysis revealed that aside from *TUBB*, the expression of the genes is mutually controlled within the frame of a network (Figure 6). The proteins coded by these genes consisted of five membrane proteins, nine soluble factors, and nine extracellular proteins. They also form a network of regulation, which stretches across the membranes (Figure 7).

Table 1. Primer used for quantitative real-time PCR.

Gene	F-Primer	Sequence	R-Primer	Sequence
18S rRNA	18S-F	GGAGCCTGCGGCTTAATTT	18S-R	CAACTAAGAACGGCCATGCA
ACTA2	ACTA2-F	GAGCGTGGCTATTCCTTCGT	ACTA2-R	TTCAAAGTCCAGAGCTACATAACACAGT
ACTB	ACTB-F	TGCCGACAGGATGCAGAAG	ACTB-R	GCCGATCCACACGGAGTACT
AKT1	AKT1-F	CTTCTATGGCGCTGAGATTGTG	AKT1-R	CAGCATGAGGTTCTCCAGCT
CAV1	CAV1-F	CCTCCTCACAGTTTTCATCCA	CAV1-R	TGTAGATGTTGCCCTGTTCC
CAV2	CAV2-F	GATCCCCACCGGCTCAAC	CAV2-R	CACCGGCTCTGCGATCA
CTGF	CTGF-F	ACAAGGGCCTCTTCTGTGACTT	CTGF-F	GGTACACCGTACCACCGAAGAT
EZR	EZR-F	GCAATCCAGCCAAATACAACTG	EZR-R	CCACATAGTGGAGGCCAAAGTAC
FLK1	FLK1-F	TCTTCTGGCTACTTCTTGTCATCATC	FLK1-R	GATGGACAAGTAGCCTGTCTTCAGT
KRT8	KRT8-F	GATCTCTGAGATGAACCGGAACA	KRT8-R	GCTCGGCATCTGCAATGG
LOX	LOX-F	TGGGAATGGCACAGTTGTCA	LOX-R	AGCCACTCTCCTCTGGGTGTT
MCP1	MCP1-F	GCTATAGAAGAATCACCAGCAGCAA	MCP1-R	TGGAATCCTGAACCCACTTCTG
MMP3	MMP3-F	ACAAAGGATACAACAGGGACCAA	MMP3-R	TAGAGTGGGTACATCAAAGCTTCAGT
MMP9	MMP9-F	CCTGGAGACCTGAGAACCAATC	MMP9-R	TTCGACTCTCCACGCATCTCT
MSN	MSN-F	GAAATTTGTCATCAAGCCCATTG	MSN-R	CCATGCACAAGGCCAAGAT
PAI1	PAI1-F	AGGCTGACTTCACGAGTCTTTCA	PAI1-R	CACTCTCGTTCACCTCGATCTTC
PRKCA	PRKCA-F	TGGGTCACTGCTCTATGGACTTATC	PRKCA-R	CGCCCCCTCTTCTCAGTGT
RDX	RDX-F	GAAAATGCCGAAACCAATCAA	RDX-R	GTATTGGGCTGAATGGCAAATT
RHOA	RHOA-F	CGTTAGTCCACGGTCTGGTC	RHOA-R	GCCATTGCTCAGGCAACGAA
TGFB1	TGFB1-F	CACCCGCGTGCTAATGGT	TGFB1-R	AGAGCAACACGGGTTCAGGTA
TGFBR1	TGFBR1-F	CGCACTGTCATTCACCATCG	TGFBR1-R	CACGGAACCACGAACGTTC
TUBB	TUBB-F	CTGGACCGCATCTCTGTGTACTAC	TUBB-R	GACCTGAGCGAACAGAGTCCAT
VCAM	VCAM-F	CATGGAATTCGAACCCAAACA	VCAM-R	GGCTGACCAAGACGGTTGTATC
VEGFA	VEGFA-F	GCGCTGATAGACATCCATGAAC	VEGFA-R	CTACCTCCACCATGCCAAGTG
VEGFD	VEGFD-F	TGCAGGAGGAAAATCCACTTG	VEGFD-R	CTCGCAACGATCTTCGTCAA

ACTA2: α-actin-2; *ACTB*: Actin β; *AKT1*: Nuclear factor NF-κ-B activator 1; *CAV1*: Caveolin 1; *CAV2*: Caveolin 2; *CTGF*: Connective tissue growth factor; *EZR*: Ezrin; *FLK1*: Vascular endothelial growth factor receptor 2; *KRT8*: Cytokeratin-8; *LOX*: Oxidized low-density lipoprotein receptor 1; *MCP1*: Monocyte chemotactic protein 1; *MMP3*: Matrix metalloproteinase-3; *MMP9*: Matrix metalloproteinase-9; *MSN*: Moesin; *PAI1*: Plasminogen activator inhibitor 1; *PRKCA*: Protein kinase C alpha type; *RDX*: Radixin; *RHOA*: Ras homolog gene family, member A; *TGFB1*: Transforming growth factor β-1; *TGFBR1*: TGF-β receptor type-1; *TUBB*: Tubulin β, *VCAM*: Vascular cell adhesion protein 1; *VEGFA*: Vascular endothelial growth factor A; *VEGFD*: Vascular endothelial growth factor D; F: Forward; R: Reverse. All sequences are given in 5′–3′ direction.

In order to examine the impact of an up- or downregulation of a given gene on the other members of the network, we determined the expression of the selected genes in cells exposed to the RPM or cultured under normal 1*g*-conditions. For this purpose, the mRNA expression of the genes was determined by qPCR after they had been cultured on (AD or MCS cells) or next (1*g*-controls) to the RPM for 24 h.

The actin cytoskeleton is involved in adhesion molecule clustering. Therefore, we investigated first the effects exerted by simulated microgravity on the mRNA expression of *VCAM* and cytoskeletal proteins. The gene expression of *ACTB* and *ACTA2* was reduced in MCS and AD cells (Figure 3a,e) compared with 1*g*-controls. In addition, the gene expression of *KRT8* and *TUBB* was downregulated in MCS (Figure 3b,f). Furthermore, the EZR mRNA was clearly decreased in RPM AD samples and further downregulated in MCS compared with 1*g*-samples (Figure 3c). RPM-exposure reduced the *RDX* gene expression significantly in both groups—AD and MCS (Figure 3d), whereas *MSN* decreased in AD, but was elevated in MCS (Figure 3g). There was a tendency of *VCAM* upregulation in AD cells and of a downregulation in MCS (Figure 3h). Taking together the results shown in Figure 3 clearly shows that the expression of the examined genes related to the cytoskeleton was downregulated during spheroid formation early within 24 h
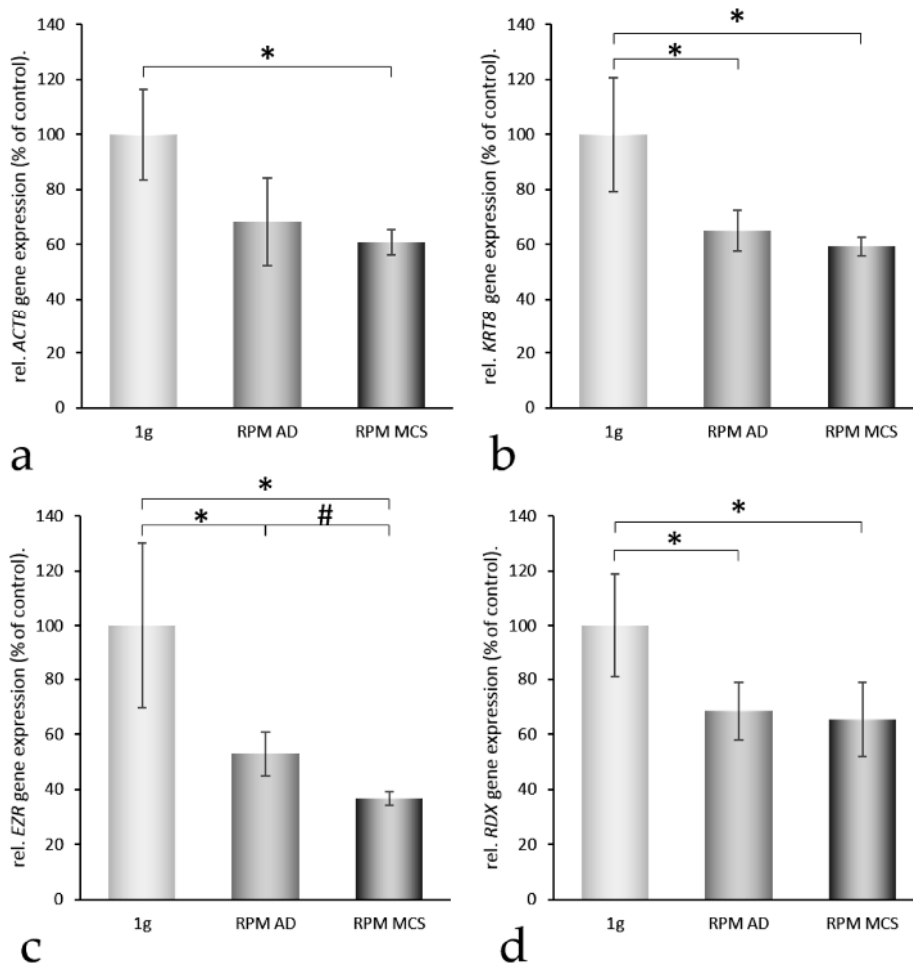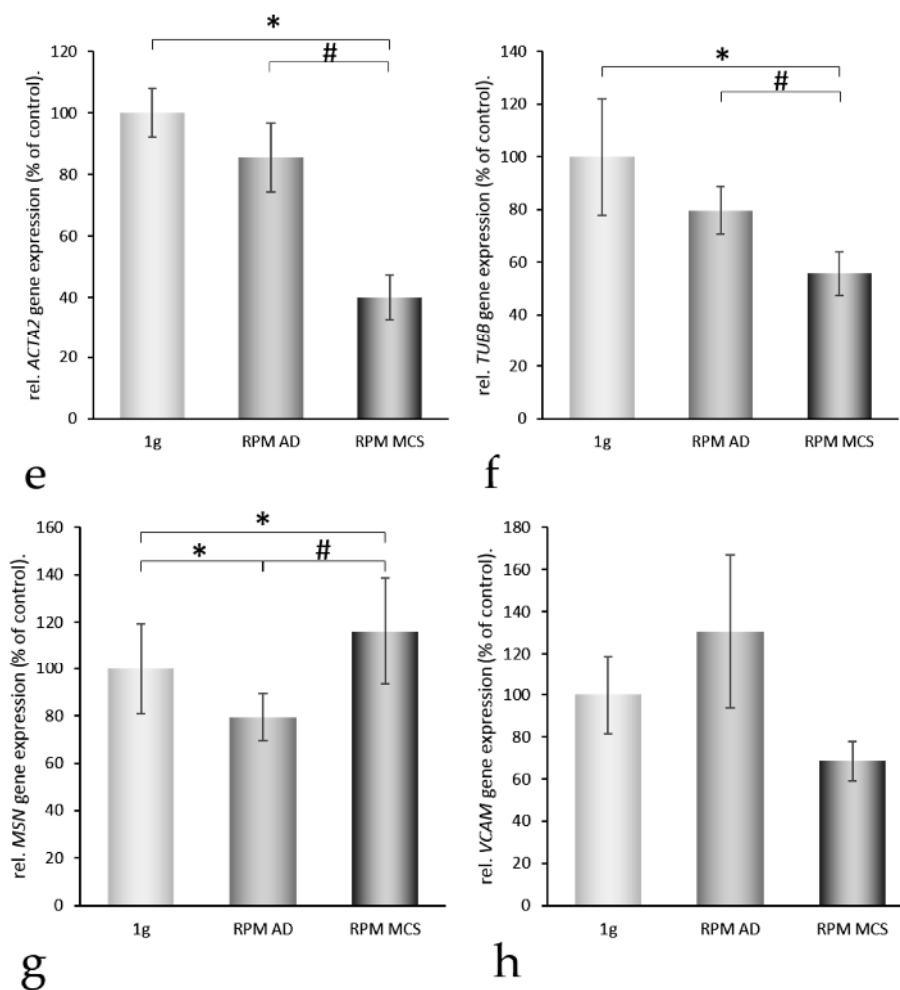

Figure 3. *Cont.*

Figure 3. Quantitative real-time PCR of genes of cytoskeletal proteins (Genes of interest I): After 24 h, 1*g*-control, RPM-adherent (AD) and RPM-multicellular spheroids (MCS) were analyzed for their *ACTB* (**a**); *KRT8* (**b**); *EZR* (**c**); *RDX* (**d**); *ACTA2* (**e**); *TUBB* (**f**); *MSN* (**g**); and *VCAM* (**h**) gene expression levels. * = $p < 0.05$ *vs.* 1*g*; # = $p < 0.05$ *vs.* RPM AD.

2.3. Three-Dimensional Growth Signaling Pathways

Nothing is known about the role of typical angiogenic factors in the early phases of MCS formation. Here we detected a 2.5-fold increase in the *VEGFA* gene expression in MCS samples (Figure 4a) and a 5-fold increase in VEGF protein released in the supernatant (Figure 4e). We could also find an upregulated gene expression of *VEGFD* in MCS samples of UCLA RO82-W-1 cells (Figure 4b). The *VEGFR2* (*FLK1*) mRNA appeared to be slightly although not significantly downregulated in RPM-samples after 24 h (Figure 4f). The *AKT1* gene expression remained unchanged (Figure 4c). Focusing on the protein kinase C (PKC) pathway, which is involved in cell proliferation and is affected during spheroid formation [10], we could measure a clear reduction of *PRKCA* mRNA after RPM-exposure in AD and MCS samples compared with corresponding static 1*g*-controls (Figure 4g). As a representative member of growth factors influencing cell proliferation we investigated possible changes in the connective tissue growth factor (*CTGF*) gene expression. After a 24 h-RPM-exposure, *CTGF* mRNA was downregulated (Figure 4d). Monocyte Chemoattractant Protein-1 (MCP-1) had been identified to play an important role in 3D formation under conditions of weightlessness [21]. The *MCP1* gene expression was downregulated in MCS (Figure 4h), but remained unchanged in AD cells. Hence Figure 4 shows that two of the angiogenic-related genes (*VEGFA*, *VEGFD*) after RPM-exposure of the cells were upregulated.

Figure 4. Quantitative real-time PCR of genes of interest II and *VEGF* secretion. After 24 h, 1*g*-control, RPM-adherent (AD) and RPM-multicellular spheroids (MCS) were analyzed for their *VEGFA* (**a**); *VEGFD* (**b**); *AKT1* (**c**); *CTGF* (**d**); *FLK1* (**f**); *PRKCA* (**g**); and *MCP1* (**h**) gene expression levels. In addition, *VEGF* secretion into the culture medium was determined (**e**) * = $p < 0.05$ *vs.* 1*g*; # = $p < 0.05$ *vs.* RPM AD.

We previously have shown that genes and proteins involved in the regulation of FTC-133 thyroid cancer cell proliferation and metastasis, such as VEGFA and VEGFD were similarly regulated under long-term RPM and spaceflight conditions (10 days microgravity) [4]. After 10 days in Space, we detected a reduced *VEGFA* mRNA in RPM AD cells and MCS cultures, as well as spaceflight AD cells and MCS cultures [4]. Interestingly, the *VEGFD* mRNA was increased in the RPM and in Space cultures of the Shenzhou-8 Space Mission [4], which is comparable to the 24 h-result in UCLA RO82-W-1 RPM samples.

2.4. Factors Regulating the Amount of Extracellular Proteins

We described recently that the quantities of extracellular matrix (ECM) proteins play a decisive role in spheroid formation [22]. An increased ECM together with enhanced amounts of Caveolin-1, which scaffolds several proteins like PKC or KDR within the membrane [21,22] can cause a firm anchoring of the cells within the ECM and inhibits spheroid formation [22].

Therefore, we also studied gene alterations of the matrix metalloproteinases MMP3 and MMP9. They are known to play a role in regulating the amount of extracellular matrix proteins [23,24]. Both, *MMP3* and *MMP9* mRNAs were significantly elevated in AD cells (Figure 5a,e). *MMP3* was further enhanced in MCS compared with 1*g*-controls, whereas *MMP9* was blunted in MCS samples (Figure 5a,e). Caveolin-1 and -2 were both expressed by UCLA RO82-W-1 cells. The *CAV1* mRNA was downregulated in AD and MCS (Figure 5b). A similar result was obtained for *CAV2* (Figure 5f). Both *TGFB1* and *TGFBR1* gene expression remained unaltered (Figure 5c,g).
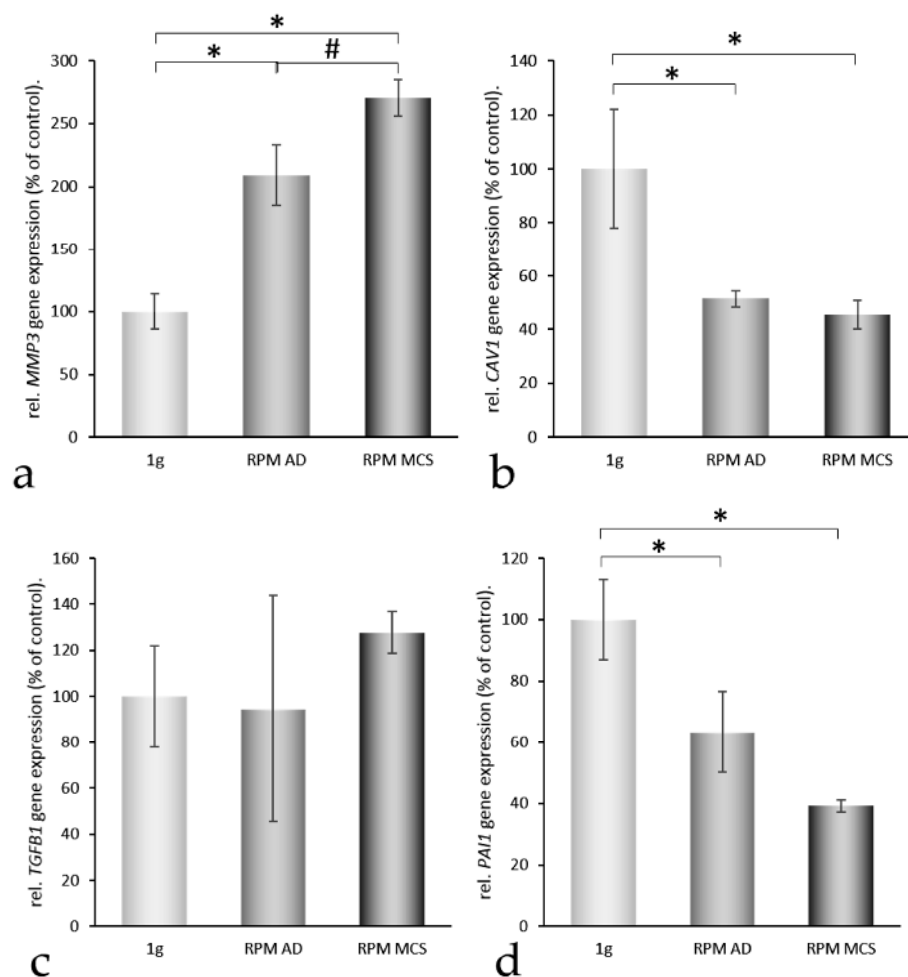
Figure 5. *Cont.*

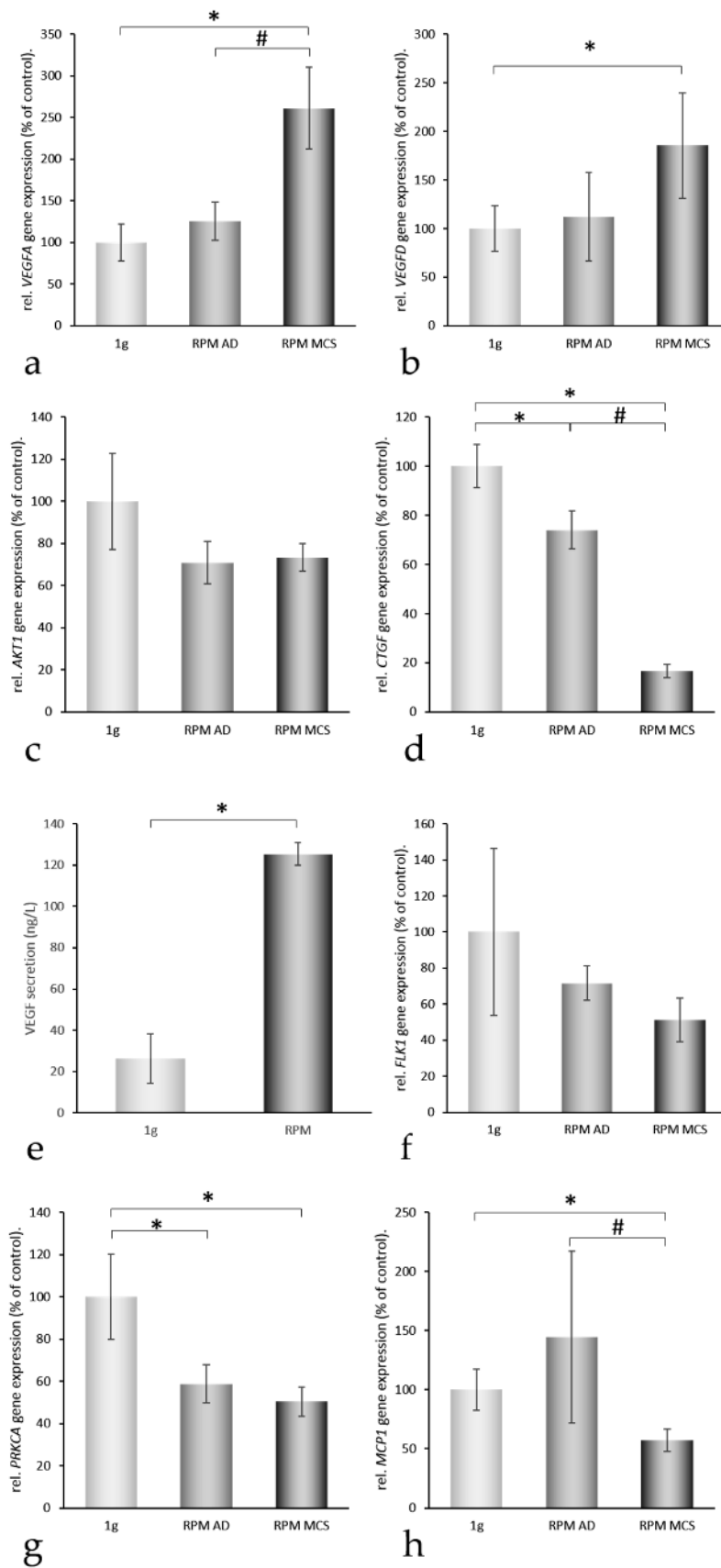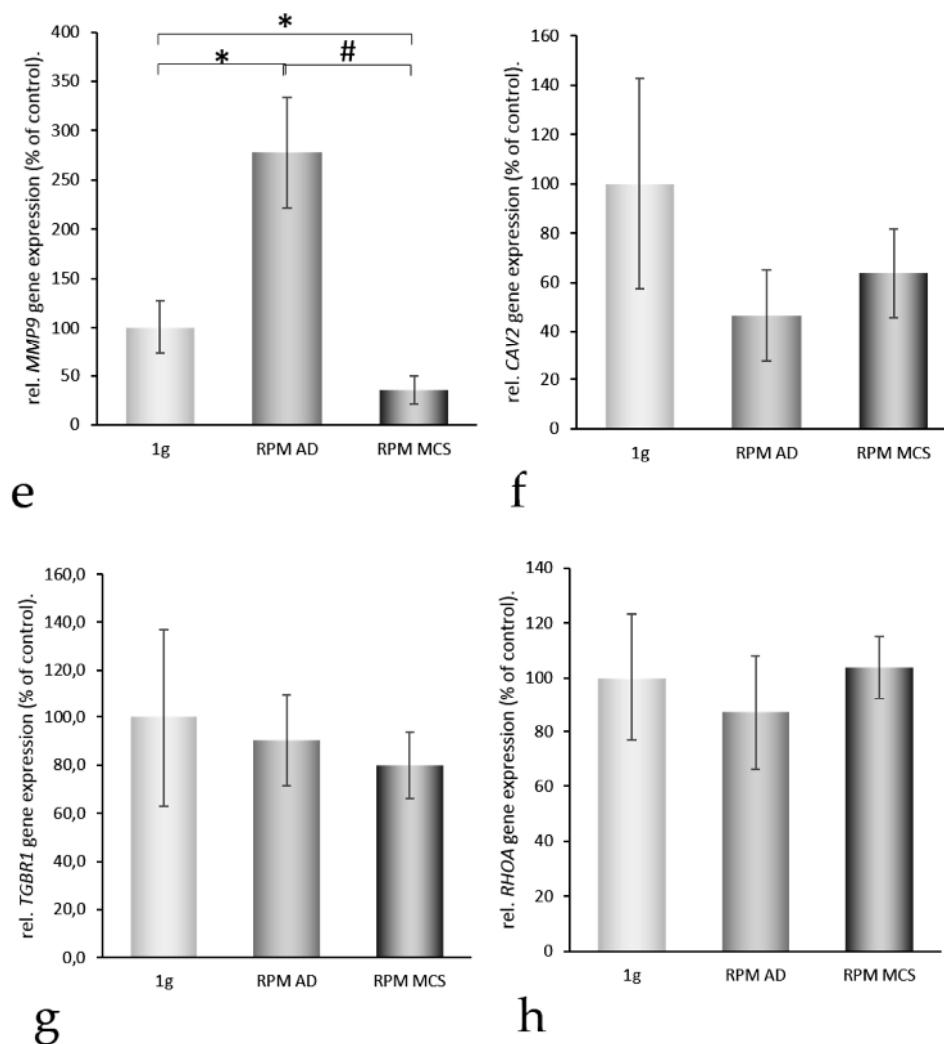**Figure 5.** Quantitative real-time PCR of genes of interest III. After 24 h, 1g-control, RPM-adherent (AD) and RPM-multicellular spheroids (MCS) were analyzed for their MMP3 (**a**); CAV1 (**b**); TBFB1 (**c**); PAI1 (**d**); MMP9 (**e**); CAV2 (**f**); TGFBR1 (**g**) and RHOA (**h**) gene expression levels. * = $p < 0.05$ *vs.* 1*g*; # = $p < 0.05$ *vs.* RPM AD.

Recent pathway analyses demonstrated that enhanced concentrations of plasminogen might inhibit spheroid formation [21,22]. We measured the plasminogen activator inhibitor-1 (*PAI1*) gene expression. *PAI1* was significantly downregulated in AD and MCS samples (Figure 5d), which may favor the degradation of extracellular plasminogen [25]. In addition, the *RHOA* mRNA was not altered after a 24 h-RPM-exposure (Figure 5h).

2.5. In Silico Search for Mutual Gene Regulation

Figures 3–5 indicated that cells remaining adherent during the early 24 h of incubation kept 16 of the 24 genes investigated within the frame of not-significant variation, downregulated seven, and upregulated one. In contrast, cells growing three-dimensionally exerted three upregulated genes, downregulated 11, and kept only 10 within the frame of not-significant variation. In order to find reasons how the changes of the genes mentioned above may contribute to a transition from a two- to three-dimensional growth behavior of UCLA RO82-W-1 follicular thyroid cancer cells, we wanted to find relationships between the networks shown in Figures 6 and 7 and the gene expression changes indicated in Figures 3–5. The most significant upregulation was indicated for the *VEGFA* and *VEGFD*

genes only in MCS cells (Figure 4a,b). A simultaneous upregulation of both genes had already been observed in de-differentiated human ovarian carcinomas [26]. Regarding *VEGFA*, not only the gene was upregulated, but also the quantities of VEGFA proteins released in the supernatant were enhanced (Figure 4e). This indicates that both AD cells and MCS cells grew on the RPM under enhanced concentrations of external VEGFA. However, only those cells, showing an upregulated *VEGFA* mRNA in combination with an elevated *VEGFD* mRNA after the first 24 h of RPM-exposure, formed spheroids (Figure 1).
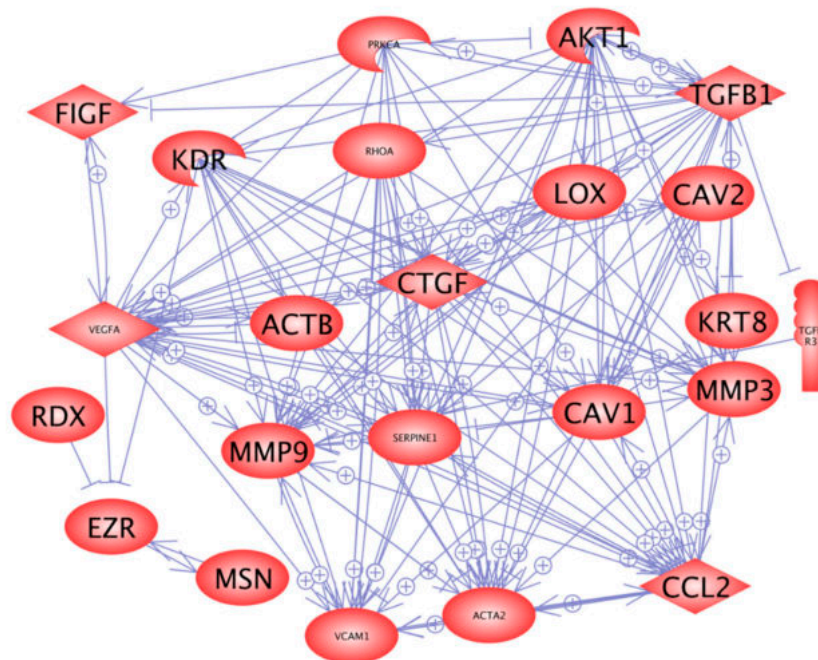
Figure 6. Mutual regulation network at gene expression level. *FIGF*-vascular endothelial growth factor D; *KDR*-kinase insert domain receptor; *SERPINE1*-plasminogen-activator inhibitor-1.
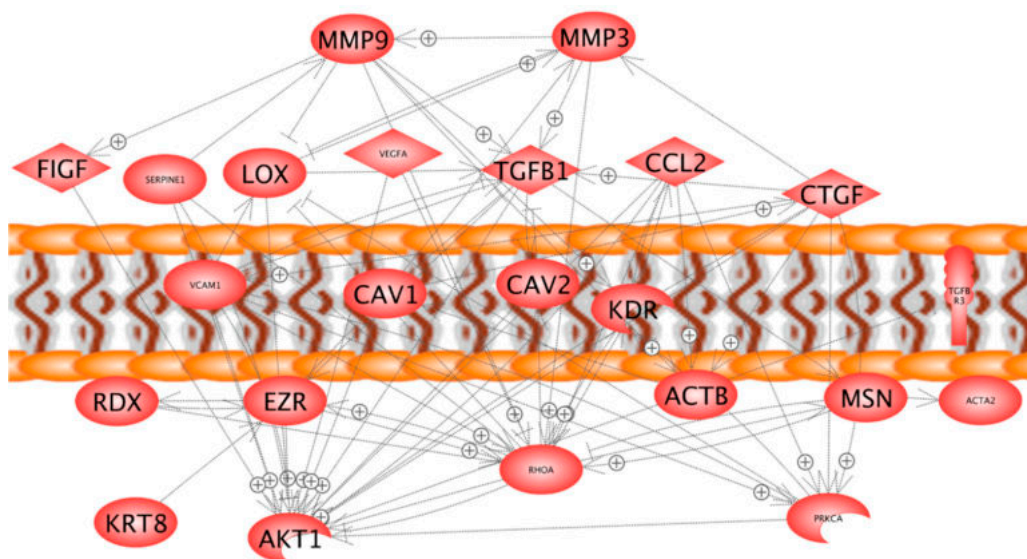
Figure 7. Mutual regulation network at protein level and cellular localization of identified proteins.

In our system, *i.e.*, in the presence of enhanced external VEGFA protein, the MCS-cells with enhanced simultaneous *VEGFA* and *VEGFD* mRNA expression showed a significant downregulation of

the α/β-actin expression, while the AD cells kept their actin expression rates similar to the 1*g*-control cells. It has already been described that VEGF downregulates α/β-actin expression in retinal endothelial cells or in arterial smooth muscle cells after addition of external VEGFA [27,28]. The mechanism is unknown, but could include miR-205 and *EZR* mRNA production, as described by Li *et al.* [29].

The *MMP3* expression is upregulated in AD cells and even more in MCS cells (Figure 5a). This corresponds to the observation of Saleh *et al.* who showed that the *MMP3* gene expression in peripheral blood mononuclear cells is depending on their own expression of the *VEGF* gene as well as on plasma VEGF concentration [30]. In addition, *MMP9* is upregulated (Figure 5e). *VEGF* is known to upregulate the expression of MMP9 in lung macrophages as long as a VEGFR-1 receptor is present on the surface [31]. The *MMP9* expression may also be upregulated by MCP1 [32]. Its expression is elevated in AD cells, but lowered in MCS cells (Figure 5e).

Furthermore, the *PAI-1* (Figure 5d) gene expression was downregulated in the presence of the enhanced VEGF, while *TGFB1* (Figure 5c) gene expression remained unchanged. A similar VEGF effect was described for endothelial cells [33]. We recently found that plasminogen accumulation contributes to inhibition of spheroid formation [22]. Hence, an attenuation of the inhibition of plasminogen activators due to downregulation of *PAI-1* could help to form spheroids [34].

Although it has been demonstrated in a number of studies that VEGF upregulates the FLK1 [34], we observed a slight but insignificant downregulation of the mRNA of *FLK1* (Figure 4f). This might be explained by a decreased amount of *CAV1*, which scaffolds FLK1 [21,35] or by the presence of various VEGF-A isoforms. For example, the VEGF-A121 was found to have little effect on KDR expression [36]. Similarly, the *VCAM* expression depends on the isoforms of the VEGF surrounding the cells [37].

Furthermore, the *LOX* (monoamine oxidase lysyl oxidase) expression was not significantly changed under the conditions of elevated *VEGF* in microgravity (Figure 2c), although in ARPE-19 cells a VEGF-dependent increase of enzyme activity as well as the mRNA expression of *LOX* was found [38]. Interestingly, a slight but insignificant increase of *LOX* mRNA was found in AD cells, while *LOX* was simultaneously decreased in MCS cells (Figure 2c). This is in accordance to our earlier hypothesis that a removal of LOX favors spheroid formation [39]. It is known that LOX is involved in several steps of metastasis and it might be an interesting protein to be investigated in co-culture experiments with endothelial cells in the future.

It is described in the literature that VEGF upregulates *CCL-2* as well as the *CTGF* gene expression [40,41]. In AD cells we found that *CTGF* was slightly downregulated, but *MCP1* is upregulated insignificantly though. In MCS cells both types of genes were further downregulated. This result suggests that AD and MCS respond differently to VEGF.

This study was designed to investigate the underlying mechanisms for 3D growth on the RPM. The study revealed that during exposure to microgravity the UCLA RO82-W-1 cell population splits in adherent and three-dimensionally growing cells. This observation fits to results obtained by others as well as by our group. For example, when cultured on the RPM murine osteoblasts and human breast cancer cells split into two populations with different phenotypes, respectively [42,43]. We previously described malignant FTC-133 thyroid cancer cells, healthy chondrocytes, or endothelial cells growing in one culture flask simultaneously in a two- or a three-dimensional manner [2,3,6,8,44].

Interestingly, only seven of the 24 genes investigated showed significantly different gene expression levels in AD and MCS cells. This finding suggests that neighboring cells of one culture change distinct genes in different ways. Attempts were made to explain the split of cell population into different sub-populations, stressing the phenomenon of bifurcation [43,45–47]. The authors of this hypothesis suggest that the cells, when exposed to microgravity, come into a state in which very small secondary effects, such as gene variations observed in single cell transcriptomes of a seemingly homogenous population, may trigger the development of single cells into different directions [48]. In our earlier experiments, flow cytometry measurements repeatedly indicated considerable variations of the number of distinct antigens at the cell surfaces. Cell electrophoretic studies showed that the overall surface charge density varies from cell to cell in a way that two distinct cell populations emerge [49,50].

In addition, we found that the glycolytic enzyme alpha-enolase was differently expressed in different cells of a population [51]. Therefore, the task remains to examine the accumulation of extracellular proteins, whose overexpression prevent spheroid formation in a whole culture, in regard to individual cells and to study whether different accumulation of the proteins described recently could prevent spheroid formation on an individual cell basis [22]. This way, we will learn whether MCS cells stem from those cells being driven out from the monolayer by microgravity but not by normal gravity, because of their lower accumulation of extracellular matrix proteins than that of their neighbors.

In accordance with earlier investigations performed on human follicular thyroid cells exposed to microgravity, these experiments also suggest that the cytoskeletal proteins and their organizers ezrin, radixin, and moesin [52] are a preferred target affected by conditions of real and simulated microgravity [13,19]. Together they organize and maintain the cell cortex as well as the interface between the extracellular environment/cell membrane, the cytoskeleton, and cytoplasm. They achieve this by interactions with both membrane and filamentous actin or by linking receptors to further signaling components. Moreover, they are involved in the regulation of several signaling pathways [53]. Besides moesin, the genes of all analyzed cytoskeletal proteins were downregulated. As one can assume that both adherent and MCS cells are exposed to similar mechanical forces, it seems reasonable that mechanical forces are not the only factors, affecting the cytoskeleton. However, mechanical forces could be more effective in changing the cell's phenotype, if the quantity of actin or ezrin is reduced [54–56].

α and β actins as well as ezrin, which are cytoskeletal key factors, might be downregulated by VEGF. The most interesting result was that *VEGFA* and *VEGFD* were significantly upregulated only in MCS cells. We do not know the causes of the VEGF upregulation, as all the factors shown in Figure 6 ((+) sign on arrow) to favor upregulation of *VEGF* remained in RPM-exposed cells either similar (*AKT-1*, *TGFB1*, *RHOA*) or were significantly downregulated (*PAI-1*, *MCP-1*) as compared to the 1*g*-controls. Interestingly, *CTGF* was downregulated in AD cells by 25% and in MCS cells by 85%. A downregulation of *CTGF* may enhance the bioavailability of VEGF within the spheroids, because CTGF binding can neutralize VEGF activity [57]. VEGF regulates vascularization in wound healing by challenging outgrowth of endothelial cells [58], but also has a great influence on cancer development and metastasis [59]. It is known that an increase in *VEGFA* indicates neoangiogenesis, low-differentiation and progression in cancer [59,60]. In addition, VEGF production is modified, when cells grow under microgravity [61]. We had recently demonstrated that microgravity-exposure of FTC-133 thyroid cancer cells for 10 days in Space and on the RPM induced a downregulation of VEGFA, but an upregulation of VEGFD [4]. VEGFA and VEGFD exert differently strong effects on their target cells and by competing for the equal receptor-binding site VEGFD may fine-tune the VEGFA activities [62]. Hence, both VEGFs seem to play different roles in wound healing, tumor progression and microgravity-induced reactions. In 2012 Nersita *et al.* [63] reported a low level of VEGFD in metastatic thyroid carcinomas, which may indicate that VEGFA effects are not regulated anymore [63].

It was demonstrated in human endothelial cells (EA.hy926 cell line) that these cells also produced more than normal amounts of VEGF and FLK-1 by themselves [44]. VEGF was increased after a 4 h-RPM-exposure and was further elevated after 12 h [44]. In addition, an RPM-exposure of the EAhy926 endothelial cells early induced FLK-1 protein (within 4 h). This increase was further elevated after a 12 h-RPM-exposure [44]. Interestingly, the external application of 10ng/mL VEGF to the culture medium reduced the amount of synthesized VEGF protein [44]. Furthermore, EAhy926 cells incubated for seven days either under 1*g*-conditions or under s-μg revealed a clear increase in the VEGF expression of RPM-exposed cells compared with 1*g*-controls [61]. In this long-term experiment, it could be demonstrated that external VEGF (10 ng/mL) did not induce a further elevation of VEGF [61]. Gravitational unloading alone stimulated the endothelial cells to synthesize VEGF early. The EA.hy926 cell line is a human umbilical vein cell line, established by fusing primary human umbilical vein cells with a thioguanine-resistant clone of A549 lung carcinoma cells by exposure to polyethylene glycol [64]. Cancer cells are able to fuse spontaneously with endothelial cells to form hybrid cells, facilitating the cells traversing the endothelial barrier to form metastases [65]. These characteristics will help to

increase our knowledge in the processes of angiogenesis or metastasis with the aim of finding future drug targets for cancer therapy. In future studies, it is a matter of interest to investigate the impact of conditioned medium of microgravity-related cancer cells on endothelial cells or by a co-culture assay.

MMP3 had shown to be upregulated under microgravity. The *MMP3* gene product can have several functions. First, it may be located within the nucleus of cells like chondrocytes and activate transcription enhancers, which may e.g., in chondrocytes activate the transcription of *CTGF* genes [66]. This pathway seems not to be active in our system, because the *CTGF* gene is downregulated at enhanced transcription of *MMP3* (Figures 4 and 5). It is more probable that MMP3 degrades the VEGFR or digests products of the extracellular matrix [67]. In a recent spaceflight experiment, we found that an elevated protein accumulation in the extracellular space could detain 3D formation, while profilin-1 was phosphorylated in Space [22]. Hence, elevated MMP3 may favor the degradation of proteins surrounding the cells and in this way support spheroid formation.

CTGF is involved in the spheroid formation of FTC-133 thyroid cancer cells in Space [11]. The *CTGF* mRNA expression was enhanced by annulling gravity in space-flown samples, suggesting a key role of this growth factor in continuing 3D growth type [11]. A reduced *CTGF* mRNA expression in 3D aggregates compared to adherent cells was observed on the two devices [68]. *In vitro*, CTGF has been shown to stimulate ECM production, chemotaxis, proliferation, and integrin expression and has been implicated in various biological processes, such as cell proliferation, migration, angiogenesis, and tumorigenesis [69]. It has also been shown that *CTGF* expression level was elevated in primary papillary thyroid carcinoma samples and was correlated with clinical features, such as metastasis, tumor size, or the clinical stage [70]. After 24 h on the RPM, *CTGF* was downregulated in UCLA RO82-W-1 cells. Therefore, the importance of *CTGF* in spheroid formation of thyroid cancer cells has to be further investigated in the future.

In vitro, the protein kinase C-α (PRKCA) is involved in the control of human medullar thyroid carcinoma cell proliferation and survival by modulating apoptosis [71]. *PRKCA* gene expression was downregulated by vibration in human thyroid cells. In this experiment, it was also downregulated. A factor triggering this downregulation could not be seen in our experiments. However, it is known that PRKCA initiates upregulation of *CAV1* or *CTGF* [72,73]. Therefore, one might conclude that *PRKCA* expressed as found in our experiments may not be capable to enforce upregulation of *CAV1* or *CTGF* genes [21]. It appears worthwhile to study the PRKCA effects on *CAV1* expression because of the capability of CAV1 to inhibit the cellular sheering out of a monolayer in cancer cells [21].

3. Experimental Section

3.1. Cells

The UCLA RO82-W-1 cell line was used in this study and purchased from Sigma-Aldrich Chemie (Munich, Germany). The cell line was derived from the metastases of a follicular carcinoma in a female patient. The primary tumor released thyroglobulin (>10,000 ng/mL), but the uptake of I^{131} was less than 2%. Immunoperoxidase staining revealed thyroglobulin-positivity within the cells. The cell line was tumorigenous in nude mice [74]. The cells were cultured in RPMI-1640 medium containing 100 μM sodium pyruvate and 2 mM· L-glutamine, supplemented with 10% fetal calf serum (FCS), 100 U/mL penicillin and 100 μg/mL streptomycin (all Invitrogen, Eggenstein, Germany).

3.2. Random Positioning Machine

30 T25 culture flasks were seeded with 1×10^6 UCLA RO82-W-1 cells each and incubated over night at 37 °C and 5% CO_2 in an incubator to ensure attachment of the cells to the bottom of the culture flask. The next day, the flasks were completely filled with medium carefully avoiding air bubbles. 15 T25 were fixed on the RPM, as close as possible to the center of the platform, which was then rotated at a speed of 60 °/s in real random mode. The RPM was positioned in a commercially available

incubator set at 37 °C and supplied with 5% CO_2. 15 T25 culture flasks for 1*g*-ground control cultures grown in parallel in identical equipment were kept statically in the same incubator as the RPM.

3.3. F-Actin Staining

UCLA RO82-W-1 cells were seeded into slide flasks (BD, Heidelberg, Germany) and placed in an incubator (37 °C, 5% CO_2) overnight, until they attached to the slides. The next day, the slide flasks were completely filled with medium avoiding air bubbles, sealed with parafilm, and placed on the RPM for 24 h. F-actin was visualized by means of rhodamine-phalloidin staining (Molecular Probes®, Eugene, OR, USA). The method was described earlier in detail [75,76].

3.4. RNA Isolation

Directly after the experiments, the cells were fixed with RNA*later* (Thermo Fisher Scientific, Roskilde, Denmark). For harvesting of the cells, RNA*later* was replaced by PBS (Invitrogen, Darmstadt, Germany). The method was published recently in detail [75,77].

3.5. Quantitative Real Time PCR

We employed the real-time quantitative RT PCR to quantify expression levels of the genes of interest. Appropriate primers with a Tm of about 60 °C were designed with the Primer Express® (Version 2.0.0, Applied Biosystems, Foster City, CA, USA) software. The primers were synthesized by TIB Molbiol (Berlin, Germany) and listed in Table 1. The method was published recently in detail [75,77].

3.6. Pathway Studio Analysis

Pathway Studio v11 was purchased from Elsevier Research Solutions, Amsterdam, The Netherlands. This program was used online [78]. To start an analysis, the SwissProt numbers of the proteins of interest were entered.

3.7. Statistics

All statistical analyses were performed using SPSS 21.0 (SPSS, Inc., Chicago, IL, USA, 2012). The data was analyzed with the Mann–Whitney *U* test. To account for multiple comparisons, a Kruskal–Wallis Test was performed beforehand, and Bonferroni corrections were applied. The data was expressed as means ± standard deviation (SD). Differences were considered significant at $p < 0.05$.

4. Conclusions

This is the first study, using pathway analyses programs to investigate the molecular mechanisms responsible for 3D growth of follicular thyroid cancer cells grown under conditions of simulated microgravity for 24 h on the RPM. Earlier studies have shown, that human and rat benign thyroid cells as well as cancer cells *in vitro* and *in vivo* respond to microgravity conditions and induce a variety of changes in these cells [3,8,17,79–86]. This response might give important hints for cancer research on Earth [87].

The appearance of the two distinct cell populations, adherent cells and MCS, fits very well to the phenomenon of the bifurcation point. It remains unclear if initially a shift in the phenotype leads to a change in gene expression or if the differential gene expression leads to the shift in the phenotype, but it is very certain that both can influence each other. We still do not know, which one of the differentially expressed genes is the very first step triggered by the removal of gravity. However, we recognized, that in the cells with an upregulated *VEGFA* and *VEGFD* mRNA, spheroid formation could be favored, because upregulated *MMP-3* mRNA and simultaneously downregulated *PAI1* mRNA favor the degradation of the extracellular proteins and reduction of actin and ezrin proteins. These changes

may facilitate a transition of the phenotypes, while the *PRKCA* mRNA expression is too low to enforce upregulation of *CAV-1* and *MCP1*.

Author Contributions: Daniela Grimm, Manfred Infanger, Stefan Riwaldt, and Johann Bauer conceived and designed the experiments. Stefan Riwaldt, Lasse Slumstrup, Sascha Kopp, Anita Dittrich, Nils E. Magnusson, and Daniela Grimm performed the experiments. Daniela Grimm, Marcus Wehland, Johann Bauer, and Thomas J. Corydon analyzed the data. Stefan Riwaldt, Daniela Grimm, Marcus Wehland, Jessica Pietsch, Elisabeth Warnke, Thomas J. Corydon, and Johann Bauer wrote the paper.

Conflicts of Interest: The authors declare no conflict of interest.

Abbreviation

ACTA2	Actin aortic smooth muscle (P62736)
ACTB	Actin cytoplasmic 1 (P60709)
AD	Adherent
AKT1	RAC-α serine/threonine-protein kinase (P31749)
CAV1	Caveolin-1 (Q03135)
CAV2	Caveolin-2 (P51636)
CCL2	C–C motif chemokine 2 (P13500)
CTGF	Connective tissue growth factor (P29279)
EZR	Ezrin (P15311)
FIGF or VEGFD	Vascular endothelial growth factor D (O43915)
FLK1 or KDR	Vascular endothelial growth factor receptor 2 (P35968)
KRT8	Keratin type II cytoskeletal 8 (P05787)
LOX	Protein-lysine 6-oxidase (P28300)
MCS	Multicellular spheroids
MCTS	Multicellular tumor spheroid
MMP-3	Matrix metalloproteinase-3 or Stromelysin-1 (P08254)
MMP-9	Matrix metalloproteinase-9 (P14780)
MSN	Moesin (P26038)
PRKCA	Protein kinase C alpha type (P17252)
qPCR	Quantitative real-time PCR
RDX	Radixin (P35241)
RHOA	protein: Ras homolog gene family, member A; gene: Transforming protein RhoA (P61586)
RPM	Random Positioning Machine
RWV	Rotating Wall Vessel
SERPINE1	Plasminigen activator inhibitor 1 (P05121)
TGFB1	Transforming growth factor β-1 (P01137)
TGFBR1	Transforming growth factor beta receptor type 1 (P36897)
TGFBR3	Transforming growth factor beta receptor type 3 (Q03167)
TUBB	Tubulin β (P07437)
VCAM1	Vascular cellular adhesion protein 1 (P19320)
VEGFA	Vascular endothelial growth factor A (P15692)

References

1. Pietsch, J.; Kussian, R.; Sickmann, A.; Bauer, J.; Weber, G.; Nissum, M.; Westphal, K.; Egli, M.; Grosse, J.; Schonberger, J.; *et al.* Application of free-flow ief to identify protein candidates changing under microgravity conditions. *Proteomics* **2010**, *10*, 904–913. [CrossRef] [PubMed]
2. Pietsch, J.; Sickmann, A.; Weber, G.; Bauer, J.; Egli, M.; Wildgruber, R.; Infanger, M.; Grimm, D. A proteomic approach to analysing spheroid formation of two human thyroid cell lines cultured on a random positioning machine. *Proteomics* **2011**, *11*, 2095–2104. [CrossRef] [PubMed]

3.　Grimm, D.; Bauer, J.; Kossmehl, P.; Shakibaei, M.; Schoberger, J.; Pickenhahn, H.; Schulze-Tanzil, G.; Vetter, R.; Eilles, C.; Paul, M.; *et al.* Simulated microgravity alters differentiation and increases apoptosis in human follicular thyroid carcinoma cells. *FASEB J.* **2002**, *16*, 604–606. [CrossRef] [PubMed]

4.　Ma, X.; Pietsch, J.; Wehland, M.; Schulz, H.; Saar, K.; Hubner, N.; Bauer, J.; Braun, M.; Schwarzwalder, A.; Segerer, J.; *et al.* Differential gene expression profile and altered cytokine secretion of thyroid cancer cells in space. *FASEB J.* **2014**, *28*, 813–835. [CrossRef] [PubMed]

5.　Grimm, D.; Infanger, M.; Westphal, K.; Ulbrich, C.; Pietsch, J.; Kossmehl, P.; Vadrucci, S.; Baatout, S.; Flick, B.; Paul, M.; *et al.* A delayed type of three-dimensional growth of human endothelial cells under simulated weightlessness. *Tissue Eng. A* **2009**, *15*, 2267–2275. [CrossRef] [PubMed]

6.　Grimm, D.; Wehland, M.; Pietsch, J.; Aleshcheva, G.; Wise, P.; van Loon, J.; Ulbrich, C.; Magnusson, N.E.; Infanger, M.; Bauer, J. Growing tissues in real and simulated microgravity: New methods for tissue engineering. *Tissue Eng. B* **2014**, *20*, 555–566. [CrossRef] [PubMed]

7.　Ma, X.; Wehland, M.; Schulz, H.; Saar, K.; Hubner, N.; Infanger, M.; Bauer, J.; Grimm, D. Genomic approach to identify factors that drive the formation of three-dimensional structures by EA.hy926 endothelial cells. *PLoS ONE* **2013**, *8*, e64402. [CrossRef] [PubMed]

8.　Kopp, S.; Warnke, E.; Wehland, M.; Aleshcheva, G.; Magnusson, N.E.; Hemmersbach, R.; Corydon, T.J.; Bauer, J.; Infanger, M.; Grimm, D. Mechanisms of three-dimensional growth of thyroid cells during long-term simulated microgravity. *Sci. Rep.* **2015**, *5*. [CrossRef] [PubMed]

9.　Ma, X.; Wehland, M.; Aleshcheva, G.; Hauslage, J.; Waßer, K.; Hemmersbach, R.; Infanger, M.; Bauer, J.; Grimm, D. Interleukin-6 expression under gravitational stress due to vibration and hypergravity in follicular thyroid cancer cells. *PLoS ONE* **2013**, *8*, e68140. [CrossRef] [PubMed]

10.　Grosse, J.; Wehland, M.; Pietsch, J.; Schulz, H.; Saar, K.; Hubner, N.; Eilles, C.; Bauer, J.; Abou-El-Ardat, K.; Baatout, S.; *et al.* Gravity-sensitive signaling drives 3-dimensional formation of multicellular thyroid cancer spheroids. *FASEB J.* **2012**, *26*, 5124–5140. [CrossRef] [PubMed]

11.　Pietsch, J.; Ma, X.; Wehland, M.; Aleshcheva, G.; Schwarzwälder, A.; Segerer, J.; Birlem, M.; Horn, A.; Bauer, J.; Infanger, M.; *et al.* Spheroid formation of human thyroid cancer cells in an automated culturing system during the shenzhou-8 space mission. *Biomaterials* **2013**, *34*, 7694–7705. [PubMed]

12.　Svejgaard, B.; Wehland, M.; Ma, X.; Kopp, S.; Sahana, J.; Warnke, E.; Aleshcheva, G.; Hemmersbach, R.; Hauslage, J.; Grosse, J.; *et al.* Common effects on cancer cells exerted by a random positioning machine and a 2d clinostat. *PLoS ONE* **2015**, *10*, e0135157. [CrossRef] [PubMed]

13.　Ulbrich, C.; Pietsch, J.; Grosse, J.; Wehland, M.; Schulz, H.; Saar, K.; Hübner, N.; Hauslage, J.; Hemmersbach, R.; Braun, M.; *et al.* Differential gene regulation under altered gravity conditions in follicular thyroid cancer cells: Relationship between the extracellular matrix and the cytoskeleton. *Cell. Physiol. Biochem.* **2011**, *28*, 185–198. [CrossRef] [PubMed]

14.　Warnke, E.; Kopp, S.; Wehland, M.; Hemmersbach, R.; Bauer, J.; Pietsch, J.; Infanger, M.; Grimm, D. Thyroid cells exposed to simutalted microgravity conditions—Comparison of the fast roating clinostat and the random position maschine. *Microgravity Sci. Technol.* **2015**. [CrossRef]

15.　Faute, M.A.D.; Laurent, L.; Ploton, D.; Poupon, M.-F.; Jardillier, J.-C.; Bobichon, H. Distinctive alterations of invasiveness, drug resistance and cell-cell organization in 3D-cultures of MCF-7, a human breast cancer cell line, and its multidrug resistant variant. *Clin. Exp. Metastasis* **2002**, *19*, 161–168. [CrossRef]

16.　Kogai, T.; Curcio, F.; Hyman, S.; Cornford, E.M.; Brent, G.A.; Hershman, J.M. Induction of follicle formation in long-term cultured normal human thyroid cells treated with thyrotropin stimulates iodide uptake but not sodium/iodide symporter messenger rna and protein expression. *J. Endocrinol.* **2000**, *167*, 125–135. [CrossRef] [PubMed]

17.　Albi, E.; Ambesi-Impiombato, F.S.; Peverini, M.; Damaskopoulou, E.; Fontanini, E.; Lazzarini, R.; Curcio, F.; Perrella, G. Thyrotropin receptor and membrane interactions in FRTL-5 thyroid cell strain in microgravity. *Astrobiology* **2011**, *11*, 57–64. [CrossRef] [PubMed]

18.　Grimm, D.; Pietsch, J.; Wehland, M.; Richter, P.; Strauch, S.M.; Lebert, M.; Magnusson, N.E.; Wise, P.; Bauer, J. The impact of microgravity-based proteomics research. *Expert Rev. Proteom.* **2014**, *11*, 465–476. [CrossRef] [PubMed]

19.　Grimm, D.; Wise, P.; Lebert, M.; Richter, P.; Baatout, S. How and why does the proteome respond to microgravity? *Expert Rev. Proteom.* **2011**, *8*, 13–27. [CrossRef] [PubMed]

20. Pietsch, J.; Bauer, J.; Egli, M.; Infanger, M.; Wise, P.; Ulbrich, C.; Grimm, D. The effects of weightlessness on the human organism and mammalian cells. *Curr. Mol. Med.* **2011**, *11*, 350–364. [CrossRef] [PubMed]

21. Riwaldt, S.; Bauer, J.; Pietsch, J.; Braun, M.; Segerer, J.; Schwarzwälder, A.; Corydon, T.; Infanger, M.; Grimm, D. The importance of caveolin-1 as key-regulator of three-dimensional growth in thyroid cancer cells cultured under real and simulated microgravity conditions. *Int. J. Mol. Sci.* **2015**, *16*, 28296–28310. [CrossRef] [PubMed]

22. Riwaldt, S.; Pietsch, J.; Sickmann, A.; Bauer, J.; Braun, M.; Segerer, J.; Schwarzwälder, A.; Aleshcheva, G.; Corydon, T.J.; Infanger, M.; *et al.* Identification of proteins involved in inhibition of spheroid formation under microgravity. *Proteomics* **2015**, *15*, 2945–2952. [CrossRef] [PubMed]

23. Kanbe, N.; Tanaka, A.; Kanbe, M.; Itakura, A.; Kurosawa, M.; Matsuda, H. Human mast cells produce matrix metalloproteinase 9. *Eur J. Immunol.* **1999**, *29*, 2645–2649. [CrossRef]

24. Kim, E.M.; Hwang, O. Role of matrix metalloproteinase-3 in neurodegeneration. *J. Neurochem.* **2011**, *116*, 22–32. [CrossRef] [PubMed]

25. Plow, E.F.; Herren, T.; Redlitz, A.; Miles, L.A.; Hoover-Plow, J.L. The cell biology of the plasminogen system. *FASEB J.* **1995**, *9*, 939–945. [PubMed]

26. Bolat, F.; Gumurdulu, D.; Erkanli, S.; Kayaselcuk, F.; Zeren, H.; Ali Vardar, M.; Kuscu, E. Maspin overexpression correlates with increased expression of vascular endothelial growth factors A, C, and D in human ovarian carcinoma. *Pathol.-Res. Pract.* **2008**, *204*, 379–387. [CrossRef] [PubMed]

27. Butler, S.M.; Abrassart, J.M.; Hubbell, M.C.; Adeoye, O.; Semotiuk, A.; Williams, J.M.; Mata-Greenwood, E.; Khorram, O.; Pearce, W.J. Contributions of VEGF to age-dependent transmural gradients in contractile protein expression in ovine carotid arteries. *Am. J. Physiol. Cell Physiol.* **2011**, *301*, C653–C666. [CrossRef] [PubMed]

28. Wisniewska-Kruk, J.; Hoeben, K.A.; Vogels, I.M.C.; Gaillard, P.J.; Van Noorden, C.J.F.; Schlingemann, R.O.; Klaassen, I. A novel co-culture model of the blood-retinal barrier based on primary retinal endothelial cells, pericytes and astrocytes. *Exp. Eye Res.* **2012**, *96*, 181–190. [CrossRef] [PubMed]

29. Li, J.; Li, L.; Li, Z.; Gong, G.; Chen, P.; Liu, H.; Wang, J.; Liu, Y.; Wu, X. The role of miR-205 in the VEGF-mediated promotion of human ovarian cancer cell invasion. *Gynecol. Oncol.* **2015**, *137*, 125–133. [CrossRef] [PubMed]

30. Saleh, A.; Stathopoulou, M.G.; Dade, S.; Ndiaye, N.C.; Azimi-Nezhad, M.; Murray, H.; Masson, C.; Lamont, J.; Fitzgerald, P.; Visvikis-Siest, S. Angiogenesis related genes *NOS3*, *CD14*, *MMP3* and *IL4R* are associated to *VEGF* gene expression and circulating levels in healthy adults. *BMC Med. Genet.* **2015**, *16*. [CrossRef] [PubMed]

31. Hiratsuka, S.; Nakamura, K.; Iwai, S.; Murakami, M.; Itoh, T.; Kijima, H.; Shipley, J.M.; Senior, R.M.; Shibuya, M. MMP9 induction by vascular endothelial growth factor receptor-1 is involved in lung-specific metastasis. *Cancer Cell* **2002**, *2*, 289–300. [CrossRef]

32. Tang, C.-H.; Tsai, C.-C. CCL2 increases MMP-9 expression and cell motility in human chondrosarcoma cells via the Ras/Raf/MEK/ERK/NF-κB signaling pathway. *Biochem. Pharmacol.* **2012**, *83*, 335–344. [CrossRef] [PubMed]

33. Yamauchi, K.; Nishimura, Y.; Shigematsu, S.; Takeuchi, Y.; Nakamura, J.; Aizawa, T.; Hashizume, K. Vascular endothelial cell growth factor attenuates actions of transforming growth factor-β in human endothelial cells. *J. Biol. Chem.* **2004**, *279*, 55104–55108. [CrossRef] [PubMed]

34. Liekens, S.; de Clercq, E.; Neyts, J. Angiogenesis: Regulators and clinical applications. *Biochem. Pharmacol.* **2001**, *61*, 253–270. [CrossRef]

35. Hata, Y.; Rook, S.L.; Aiello, L.P. Basic fibroblast growth factor induces expression of VEGF receptor KDR through a protein kinase C and p44/p42 mitogen-activated protein kinase-dependent pathway. *Diabetes* **1999**, *48*, 1145–1155. [CrossRef] [PubMed]

36. Cipriani, P.; di Benedetto, P.; Capece, D.; Zazzeroni, F.; Liakouli, V.; Ruscitti, P.; Pantano, I.; Berardicurti, O.; Carubbi, F.; Alesse, E.; *et al.* Impaired Cav-1 expression in SSc mesenchymal cells upregulates VEGF signaling: A link between vascular involvement and fibrosis. *Fibrogen. Tissue Repair* **2014**, *7*. [CrossRef] [PubMed]

37. Fearnley, G.W.; Odell, A.F.; Latham, A.M.; Mughal, N.A.; Bruns, A.F.; Burgoyne, N.J.; Homer-Vanniasinkam, S.; Zachary, I.C.; Hollstein, M.C.; Wheatcroft, S.B.; *et al.* VEGF-A isoforms differentially regulate ATF-2-dependent *VCAM-1* gene expression and endothelial-leukocyte interactions. *Mol. Biol. Cell* **2014**, *25*, 2509–2521. [CrossRef] [PubMed]

38. Coral, K.; Madhavan, J.; Pukhraj, R.; Angayarkanni, N. High glucose induced differential expression of lysyl oxidase and its isoform in ARPE-19 cells. *Curr. Eye Res.* **2013**, *38*, 194–203. [CrossRef] [PubMed]

39. Bauer, J.; Wehland, M.; Pietsch, J.; Sickmann, A.; Weber, G.; Grimm, D. Annotated gene and proteome data support recognition of interconnections between the results of different experiments in space research. *Microgravity Sci. Technol.* **2015**. [CrossRef]

40. Blom, I.E.; Goldschmeding, R.; Leask, A. Gene regulation of connective tissue growth factor: New targets for antifibrotic therapy? *Matrix Biol.* **2002**, *21*, 473–482. [CrossRef]

41. Marumo, T.; Schini-Kerth, V.B.; Busse, R. Vascular endothelial growth factor activates nuclear factor-κB and induces monocyte chemoattractant protein-1 in bovine retinal endothelial cells. *Diabetes* **1999**, *48*, 1131–1137. [CrossRef] [PubMed]

42. Masiello, M.G.; Cucina, A.; Proietti, S.; Palombo, A.; Coluccia, P.; D'Anselmi, F.; Dinicola, S.; Pasqualato, A.; Morini, V.; Bizzarri, M. Phenotypic switch induced by simulated microgravity on MDA-MB-231 breast cancer cells. *BioMed Res. Int.* **2014**, *2014*. [CrossRef] [PubMed]

43. Testa, F.; Palombo, A.; Dinicola, S.; D'Anselmi, F.; Proietti, S.; Pasqualato, A.; Masiello, M.G.; Coluccia, P.; Cucina, A.; Bizzarri, M. Fractal analysis of shape changes in murine osteoblasts cultured under simulated microgravity. *Rend. Fis. Acc. Lincei* **2014**, *25*, 39–47. [CrossRef]

44. Infanger, M.; Kossmehl, P.; Shakibaei, M.; Baatout, S.; Witzing, A.; Grosse, J.; Bauer, J.; Cogoli, A.; Faramarzi, S.; Derradji, H.; *et al.* Induction of three-dimensional assembly and increase in apoptosis of human endothelial cells by simulated microgravity: Impact of vascular endothelial growth factor. *Apoptosis* **2006**, *11*, 749–764. [CrossRef] [PubMed]

45. Kondepudi, D.K.; Storm, P.B. Gravity detection through bifurcation. *Adv. Space Res.* **1992**, *12*, 7–14. [CrossRef]

46. Mesland, D.A. Possible actions of gravity on the cellular machinery. *Adv. Space Res.* **1992**, *12*, 15–25. [CrossRef]

47. Tabony, J. Morphological bifurcations involving reaction-diffusion processes during microtubule formation. *Science* **1994**, *264*, 245–248. [CrossRef] [PubMed]

48. Junker, J.P.; van Oudenaarden, A. Every cell is special: Genome-wide studies add a new dimension to single-cell biology. *Cell* **2014**, *157*, 8–11. [CrossRef] [PubMed]

49. Schonberger, J.; Bauer, J.; Spruss, T.; Weber, G.; Chahoud, I.; Eilles, C.; Grimm, D. Establishment and characterization of the follicular thyroid carcinoma cell line ML-1. *J. Mol. Med.* **2000**, *78*, 102–110. [CrossRef] [PubMed]

50. Weber, G.; Grimm, D.; Bauer, J. Application of binary buffer systems to free flow cell electrophoresis. *Electrophoresis* **2000**, *21*, 325–328. [CrossRef]

51. Pietsch, J.; Sickmann, A.; Weber, G.; Bauer, J.; Egli, M.; Wildgruber, R.; Infanger, M.; Grimm, D. Metabolic enzyme diversity in different human thyroid cell lines and their sensitivity to gravitational forces. *Proteomics* **2012**, *12*, 2539–2546. [CrossRef] [PubMed]

52. Tsukita, S.; Yonemura, S. Cortical actin organization: Lessons from ERM (ezrin/radixin/moesin) proteins. *J. Biol. Chem.* **1999**, *274*, 34507–34510. [CrossRef] [PubMed]

53. Corydon, T.J.; Kopp, S.; Wehland, M.; Braun, M.; Schutte, A.; Mayer, T.; Hulsing, T.; Oltmann, H.; Schmitz, B.; Hemmersbach, R.; *et al.* Alterations of the cytoskeleton in human cells in space proved by life-cell imaging. *Sci. Rep.* **2016**, *6*. [CrossRef] [PubMed]

54. Haynes, J.; Srivastava, J.; Madson, N.; Wittmann, T.; Barber, D.L. Dynamic actin remodeling during epithelial-mesenchymal transition depends on increased moesin expression. *Mol. Biol. Cell* **2011**, *22*, 4750–4764. [CrossRef] [PubMed]

55. Neisch, A.L.; Fehon, R.G. Ezrin, radixin and moesin: Key regulators of membrane–cortex interactions and signaling. *Curr. Opin. Cell Biol.* **2011**, *23*, 377–382. [CrossRef] [PubMed]

56. Yang, H.-S.; Hinds, P.W. Increased ezrin expression and activation by CDK5 coincident with acquisition of the senescent phenotype. *Mol. Cell* **2003**, *11*, 1163–1176. [CrossRef]

57. Inoki, I. Connective tissue growth factor binds vascular endothelial growth factor (VEGF) and inhibits VEGF-induced angiogenesis. *FASEB J.* **2001**, *16*, 219–221. [CrossRef] [PubMed]

58. Bao, P.; Kodra, A.; Tomic-Canic, M.; Golinko, M.S.; Ehrlich, H.P.; Brem, H. The role of vascular endothelial growth factor in wound healing. *J. Surg. Res.* **2009**, *153*, 347–358. [CrossRef] [PubMed]

59. Grimm, D.; Bauer, J.; Schoenberger, J. Blockade of neoangiogenesis, a new and promising technique to control the growth of malignant tumors and their metastases. *Curr. Vasc. Pharmacol.* **2009**, *7*, 347–357. [CrossRef] [PubMed]

60. Bass, M.B.; Sherman, S.I.; Schlumberger, M.J.; Davis, M.T.; Kivman, L.; Khoo, H.-M.; Notari, K.H.; Peach, M.; Hei, Y.-J.; Patterson, S.D. Biomarkers as predictors of response to treatment with motesanib in patients with progressive advanced thyroid cancer. *J. Clin. Endocrinol. Metab.* **2010**, *95*, 5018–5027. [CrossRef] [PubMed]

61. Grimm, D.; Bauer, J.; Ulbrich, C.; Westphal, K.; Wehland, M.; Infanger, M.; Aleshcheva, G.; Pietsch, J.; Ghardi, M.; Beck, M.; *et al.* Different responsiveness of endothelial cells to vascular endothelial growth factor and basic fibroblast growth factor added to culture media under gravity and simulated microgravity. *Tissue Eng. A* **2010**, *16*, 1559–1573. [CrossRef] [PubMed]

62. George, M.L.; Tutton, M.G.; Janssen, F.; Arnaout, A.; Abulafi, A.M.; Eccles, S.A.; Swift, R.I. VEGF-A, VEGF-C, and VEGF-D in colorectal cancer progression. *Neoplasia* **2001**, *3*, 420–427. [CrossRef] [PubMed]

63. Nersita, R.; Matrone, A.; Klain, M.; Scavuzzo, F.; Vitolo, G.; Abbondanza, C.; Carlino, M.V.; Giacco, V.; Amato, G.; Carella, C. Decreased serum vascular endothelial growth factor-D levels in metastatic patients with differentiated thyroid carcinoma. *Clin. Endocrinol.* **2011**, *76*, 142–146. [CrossRef] [PubMed]

64. Edgell, C.J.; McDonald, C.C.; Graham, J.B. Permanent cell line expressing human factor VIII-related antigen established by hybridization. *Proc. Natl. Acad. Sci. USA* **1983**, *80*, 3734–3737. [CrossRef] [PubMed]

65. Lu, Z.J.; Ren, Y.Q.; Wang, G.P.; Song, Q.; Li, M.; Jiang, S.S.; Ning, T.; Guan, Y.S.; Yang, J.L.; Luo, F. Biological behaviors and proteomics analysis of hybrid cell line Eahy926 and its parent cell line A549. *J. Exp. Clin. Cancer Res.* **2009**, *28*. [CrossRef] [PubMed]

66. Mannello, F.; Medda, V. Nuclear localization of matrix metalloproteinases. *Prog. Histochem. Cytochem.* **2012**, *47*, 27–58. [CrossRef] [PubMed]

67. Werle, M.J.; VanSaun, M. Activity dependent removal of agrin from synaptic basal lamina by matrix metalloproteinase 3. *J. Neurocytol.* **2003**, *32*, 905–913. [CrossRef] [PubMed]

68. Warnke, E.; Pietsch, J.; Wehland, M.; Bauer, J.; Infanger, M.; Gorog, M.; Hemmersbach, R.; Braun, M.; Ma, X.; Sahana, J.; *et al.* Spheroid formation of human thyroid cancer cells under simulated microgravity: A possible role of ctgf and cav1. *Cell Commun. Signal.* **2014**, *12*. [CrossRef] [PubMed]

69. Chu, C.-Y.; Chang, C.-C.; Prakash, E.; Kuo, M.-L. Connective tissue growth factor (CTGF) and cancer progression. *J. Biomed. Sci.* **2008**, *15*, 675–685. [CrossRef] [PubMed]

70. Cui, L.; Zhang, Q.; Mao, Z.; Chen, J.; Wang, X.; Qu, J.; Zhang, J.; Jin, D. CTGF is overexpressed in papillary thyroid carcinoma and promotes the growth of papillary thyroid cancer cells. *Tumor Biol.* **2011**, *32*, 721–728. [CrossRef] [PubMed]

71. Molè, D.; Gentilin, E.; Gagliano, T.; Tagliati, F.; Bondanelli, M.; Pelizzo, M.R.; Rossi, M.; Filieri, C.; Pansini, G.; degli Uberti, E.C.; *et al.* Protein kinase C: A putative new target for the control of human medullary thyroid carcinoma cell proliferation *in vitro*. *Endocrinology* **2012**, *153*, 2088–2098. [CrossRef] [PubMed]

72. He, Z.; Way, K.J.; Arikawa, E.; Chou, E.; Opland, D.M.; Clermont, A.; Isshiki, K.; Ma, R.C.W.; Scott, J.A.; Schoen, F.J.; *et al.* Differential regulation of angiotensin II-induced expression of connective tissue growth factor by protein kinase C isoforms in the myocardium. *J. Biol. Chem.* **2005**, *280*, 15719–15726. [CrossRef] [PubMed]

73. Tourkina, E.; Gooz, P.; Pannu, J.; Bonner, M.; Scholz, D.; Hacker, S.; Silver, R.M.; Trojanowska, M.; Hoffman, S. Opposing effects of protein kinase C and protein kinase C on collagen expression by human lung fibroblasts are mediated via MEK/ERK and caveolin-1 signaling. *J. Biol. Chem.* **2005**, *280*, 13879–13887. [CrossRef] [PubMed]

74. Estour, B.; Herle, A.J.; Juillard, G.J.F.; Totanes, T.L.; Sparkes, R.S.; Giuliano, A.E.; Klandorf, H. Characterization of a human follicular thyroid carcinoma cell line (UCLA RO 82 W-1). *Virchows Arch. B Cell Pathol. Mol. Pathol.* **1989**, *57*, 167–174. [CrossRef]

75. Aleshcheva, G.; Sahana, J.; Ma, X.; Hauslage, J.; Hemmersbach, R.; Egli, M.; Infanger, M.; Bauer, J.; Grimm, D. Changes in morphology, gene expression and protein content in chondrocytes cultured on a random positioning machine. *PLoS ONE* **2013**, *8*, e79057. [CrossRef] [PubMed]

76. Aleshcheva, G.; Wehland, M.; Sahana, J.; Bauer, J.; Corydon, T.J.; Hemmersbach, R.; Frett, T.; Egli, M.; Infanger, M.; Grosse, J.; *et al.* Moderate alterations of the cytoskeleton in human chondrocytes after short-term microgravity produced by parabolic flight maneuvers could be prevented by upregulation of BMP-2 and SOX-9. *FASEB J.* **2015**, *29*, 2303–2314. [CrossRef] [PubMed]

77. Wehland, M.; Aleshcheva, G.; Schulz, H.; Saar, K.; Hubner, N.; Hemmersbach, R.; Braun, M.; Ma, X.; Frett, T.; Warnke, E.; *et al.* Differential gene expression of human chondrocytes cultured under short-term altered gravity conditions during parabolic flight maneuvers. *Cell Commun. Signal.* **2015**, *13*. [CrossRef] [PubMed]

78. Thomas, S.; Bonchev, D. A survey of current software for network analysis in molecular biology. *Hum. Genom.* **2010**, *4*, 353–360. [CrossRef]

79. Meli, A.; Perrella, G.; Curcio, F.; Hemmersbach, R.; Neubert, J.; Impiombato, F.A. Response to thyrotropin of normal thyroid follicular cell strain FRTL5 in hypergravity. *Biochimie* **1999**, *81*, 281–285. [CrossRef]

80. Meli, A.; Perrella, G.; Curcio, F.; Impiombato, F.A. Response to hypergravity of normal *in vitro* cultured follicular cells from thyroid. *Acta Astronaut.* **1998**, *42*, 465–472. [CrossRef]

81. Albi, E.; Curcio, F.; Spelat, R.; Lazzarini, A.; Lazzarini, R.; Cataldi, S.; Loreti, E.; Ferri, I.; Ambesi-Impiombato, F.S. Loss of parafollicular cells during gravitational changes (microgravity, hypergravity) and the secret effect of pleiotrophin. *PLoS ONE* **2012**, *7*, e48518. [CrossRef] [PubMed]

82. Albi, E.; Curcio, F.; Spelat, R.; Lazzarini, A.; Lazzarini, R.; Loreti, E.; Ferri, I.; Ambesi-Impiombato, F.S. Observing the mouse thyroid sphingomyelin under space conditions: A case study from the mds mission in comparison with hypergravity conditions. *Astrobiology* **2012**, *12*, 1035–1041. [CrossRef] [PubMed]

83. Martin, A.; Zhou, A.; Gordon, R.E.; Henderson, S.C.; Schwartz, A.E.; Friedman, E.W.; Davies, T.F. Thyroid organoid formation in simulated microgravity: Influence of keratinocyte growth factor. *Thyroid* **2000**, *10*, 481–487. [PubMed]

84. Masini, M.A.; Albi, E.; Barmo, C.; Bonfiglio, T.; Bruni, L.; Canesi, L.; Cataldi, S.; Curcio, F.; D'Amora, M.; Ferri, I.; *et al.* The impact of long-term exposure to space environment on adult mammalian organisms: A study on mouse thyroid and testis. *PLoS ONE* **2012**, *7*, e35418. [CrossRef] [PubMed]

85. Albi, E.; Curcio, F.; Lazzarini, A.; Floridi, A.; Cataldi, S.; Lazzarini, R.; Loreti, E.; Ferri, I.; Ambesi-Impiombato, F.S. How microgravity changes galectin-3 in thyroid follicles. *Biomed Res. Int.* **2014**, *2014*, 652863. [CrossRef] [PubMed]

86. Albi, E.; Curcio, F.; Lazzarini, A.; Floridi, A.; Cataldi, S.; Lazzarini, R.; Loreti, E.; Ferri, I.; Ambesi-Impiombato, F.S. A firmer understanding of the effect of hypergravity on thyroid tissue: Cholesterol and thyrotropin receptor. *PLoS ONE* **2014**, *9*, e98250. [CrossRef] [PubMed]

87. Becker, J.L.; Souza, G.R. Using space-based investigations to inform cancer research on earth. *Nat. Rev. Cancer* **2013**, *13*, 315–327. [CrossRef] [PubMed]

11.3   Publication #3

Kopp S, Slumstrup L, Corydon TJ, Sahana J, Aleshcheva G, Islam T, Magnusson NE, Wehland M, Bauer J, Infanger M, Grimm D. Identifications of novel mechanisms in breast cancer cells involving duct-like multicellular spheroid formation after exposure to the Random Positioning Machine. Sci Rep. 2016 May 27;6:26887. doi: 10.1038/srep26887.

SCIENTIFIC REP⚙RTS

Identifications of novel mechanisms in breast cancer cells involving duct-like multicellular spheroid formation after exposure to the Random Positioning Machine

Sascha Kopp[1], Lasse Slumstrup[2], Thomas J. Corydon[2], Jayashree Sahana[2], Ganna Aleshcheva[1], Tawhidul Islam[2], Nils E. Magnusson[3], Markus Wehland[1], Johann Bauer[4], Manfred Infanger[1] & Daniela Grimm[1,2]

Many cell types form three-dimensional aggregates (MCS; multicellular spheroids), when they are cultured under microgravity. MCS often resemble the organ, from which the cells have been derived. In this study we investigated human MCF-7 breast cancer cells after a 2 h-, 4 h-, 16 h-, 24 h- and 5d-exposure to a Random Positioning Machine (RPM) simulating microgravity. At 24 h few small compact MCS were detectable, whereas after 5d many MCS were floating in the supernatant above the cells, remaining adherently (AD). The MCS resembled the ducts formed *in vivo* by human epithelial breast cells. In order to clarify the underlying mechanisms, we harvested MCS and AD cells separately from each RPM-culture and measured the expression of 29 selected genes with a known involvement in MCS formation. qPCR analyses indicated that cytoskeletal genes were unaltered in short-term samples. *IL8*, *VEGFA*, and *FLT1* were upregulated in 2 h/4 h AD-cultures. The *ACTB*, *TUBB*, *EZR*, *RDX*, *FN1*, *VEGFA*, *FLK1 Casp9*, *Casp3*, *PRKCA* mRNAs were downregulated in 5d-MCS-samples. *ESR1* was upregulated in AD, and *PGR1* in both phenotypes after 5d. A pathway analysis revealed that the corresponding gene products are involved in organization and regulation of the cell shape, in cell tip formation and membrane to membrane docking.

Breast cancer is the second most common cancer worldwide with 1.7 million cases in 2012[1]. Advances in prevention, early diagnosis, surgical treatment and postsurgical therapies enhanced the possibility of a complete cure[2]. Known molecular targets (e.g. VEGF, VEGFR, HER2/neu) for approved drugs (e.g. tyrosine kinase inhibitors like sorafenib), or approved therapeutic antibodies (e.g. bevacizumab, ramucirumab, trastuzumab) are proteins, which are predominantly expressed in breast cancer cells and are simultaneously involved in promoting cell growth or apoptosis[3,4]. However, it is difficult at the current state of technology to apply the optimal cocktail of drugs to hit all cancer cells of any given patient. Under these circumstances, it is absolutely necessary to find new proteins, which can serve as targets to develop drugs against this cancer type.

In earlier studies we proved repeatedly that exposing various cell types like thyroid cells, endothelial cells and chondrocytes to simulated microgravity (s-μg) results in a scaffold-free production of three-dimensional (3D) aggregates so-called multicellular spheroids (MCS)[5–10]. The MCS very often resemble the tissue, from which the cells have been derived. In case of cancer cells, the *in vivo* structure of tumors appears more closely represented by MCS than by monolayer cell cultures[11–13]. A proteomics investigation on thyroid cancer cells had shown that FTC-133 cells express surface proteins binding fibronectin which induces 3D cohesion[5].

[1]Clinic for Plastic, Aesthetic and Hand Surgery, Otto-von Guericke-University, D-39120 Magdeburg, Germany. [2]Department of Biomedicine, Aarhus University, DK-8000 Aarhus C, Denmark. [3]Medical Research Laboratory, Department of Clinical Medicine, Aarhus University, DK-8000 Aarhus C, Denmark. [4]Max-Planck-Institute of Biochemistry, D-82152 Martinsried, Germany. Correspondence and requests for materials should be addressed to D.G. (email: dgg@biomed.au.dk)

Vassy and coworkers were the first scientists who investigated MCF-7 human breast cancer cells exposed to microgravity. When these cells came back from a Photon capsule mission, their cytoskeleton was changed[14]. Later Qian et al.[15] demonstrated that culturing MCF-7 cells on a clinostat affected several cell features including cancer cell migration and adhesion[15]. Moreover, Li et al. found that MCF-7 cells are sensitive to simulated microgravity in regard to integrin expression and microtubule formation[16]. Furthermore, Zheng et al. reported a protective role of the estrogen receptor on MCF-7 cells exposed to simulated microgravity[17].

Masiello et al. demonstrated 3D aggregates and adherently growing MDA-MB-231 breast cancer cells after a 24 h- and 72 h-RPM-exposure[18]. These morhological differences were accompanied by changes in biological processes such as proliferation and apoptosis as well as signaling pathways[18].

In this study, we used the method of annulling gravity by a Random Positioning Machine (RPM) to find alterations of the MCF-7 breast cancer cell growth behavior in concert with changes in the expression of selected genes, playing a role in angiogenesis and tumor metastasis[7], because the RPM not only prevents cell sedimentation, but also ensures a favorable environment for cell cultures, as the movements of the platforms enable sufficient oxygen, nutrient and waste transport[19,20]. We cultured the MCF-7 cell line on the RPM for 2 h, 4 h, 16 h, 24 h, and 5d respectively to focus on short-term and long-term effects of simulated microgravity on breast cancer cells. The cell line was derived from a pleural effusion of a patient with metastatic mammary carcinoma. It is described to build up 3D-dome structures upon absolute confluence, which however remain attached to the bottom. In addition, the cells retained breast cell common features like estrogen receptor and progesterone receptor[21].

After exposing the MCF-7 breast cancer cells to the RPM, cells which remained adherently to the bottom of the culture dish (AD) and cells included in 3D aggregates were harvested separately. This different growth behavior was also found in endothelial cells and thyroid cells[6,7,13,22]. Morphology and gene expression patterns of AD and MCS cells were analyzed in comparison to each other and to cells grown in a normal laboratory incubator as 1 g (gravity)-controls. The principal aim of this study was to identify the underlying mechanisms of spheroid formation, when human breast cancer cells were cultured under conditions of simulated microgravity on the RPM. Using pathway analysis programs the interactions of genes and proteins were studied in detail.

Results

MCF-7 tumor cells form 3D aggregates by RPM-exposure.
Short-term study. Phase contrast microscopy revealed epithelial-like MCF-7 cells growing in monolayers under normal static 1 g-conditions (Fig. 1A,C,E,G). MCF-7 cells are small and have a polygonal shape. MCF-7 cells exposed to the RPM for 2 h, 4 h, and 16 h showed no three-dimensional growth and only an adherent phenotype (Fig. 1B,D,F), whereas after a 24 h-RPM-exposure small compact round three-dimensional (3D) multicellular spheroids (MCS) were found floating in the supernatant (Fig. 1H). Two phenotypes were now detectable – adherently growing MCF-7 cells (AD) and 3D MCS.

Long-term study. After culturing MCF-7 cells on the RPM for 5 days (d) respectively, the cellular morphology of the 1 g-cultures was not altered (Fig. 1I). After culturing MCF-7 cells for 5d on the RPM, two distinct cell morphologies were clearly detectable. One AD cell population and another 3D growing population which had detached from the bottom and built solid (Fig. 1J, yellow arrow) and hollow, loose (Fig. 1J, white arrow) 3D MCS.

These 3D aggregates were further investigated by histochemistry using hematoxylin-eosin (HE) and Periodic Acid-Schiff (PAS) staining. Figure 2A shows normal HE-stained MCF-7 breast cancer cells. Figure 2B–D show the typical glandular structure of MCS with a clear lumen. The breast cancer cells reveal an apical-basal cell polarity. Whereas mechanisms of cell polarity are quite complex, the Par3(Bazooka)-Par6-aPKC protein complex plays an important role in the establishment and maintenance of apical-basal cell polarity[23]. The Par3(Bazooka)-Par6-aPKC protein complex localizes to the apical membrane domain and promotes the apical-membrane-domain identity. Here we determined the gene expression of the players of the complex and found a down-regulation of *PRKCI* mRNA in 5d-MCS-samples compared to AD and 1 g-samples (Fig. 2E). The *PARD3*, *PARD6A* and *RhoA* mRNAs were not significantly changed (Fig. 2F–H).

Changes of the cytoskeleton and associated proteins.
In order to detect further changes of the cell shape and the cytoskeleton, the cells had been fixed and stained for F-actin (visualized by means of rhodamine-phalloidin staining) and 4′,6-diamidino-2-phenylindole (DAPI) staining after cultivation for 2 h, 4 h, 16 h and 24 h as well as for 5d on the RPM or under static 1 g-conditions (Fig. 3).

Short-term study. The cells appeared to be more evenly distributed under conditions of 1 g than after RPM-exposure. The cell membrane structure was changed after a 2 h-RPM-exposure (Fig. 3B). A membrane blebbing (white arrows) was detectable in 2 h-RPM-samples, whereas no blebbing was found in corresponding static 1 g-controls (Fig. 3A). Stress fibers were detectable after 4 h (yellow arrow) in the cell periphery in cells exposed to the RPM in concert with a decreased membrane blebbing, but no changes were visible in control cells. The stress fibers decreased with the duration of the experiment and were less prominent 16 h and 24 h. However, the bundles of actin filaments were thin and did not show a long-range orientation. After 24 h culturing on the RPM, cytoskeletal holes were visible (Fig. 3H, white arrow).

Long-term study. 5d 1 g-control cells showed a normal microfilament system with visible actin fibers, evenly distributed in the cells (Fig. 3I). In contrast, RPM-exposed adherent cells presented an accumulation of F-actin at the cell boundaries (Fig. 3J). Some cells displayed pronounced holes (Fig. 3J, white arrow) and stress fibers (Fig. 3J, yellow arrow), while their nuclei were intact. The MCS after 5d-exposure revealed solid aggregates of living cells
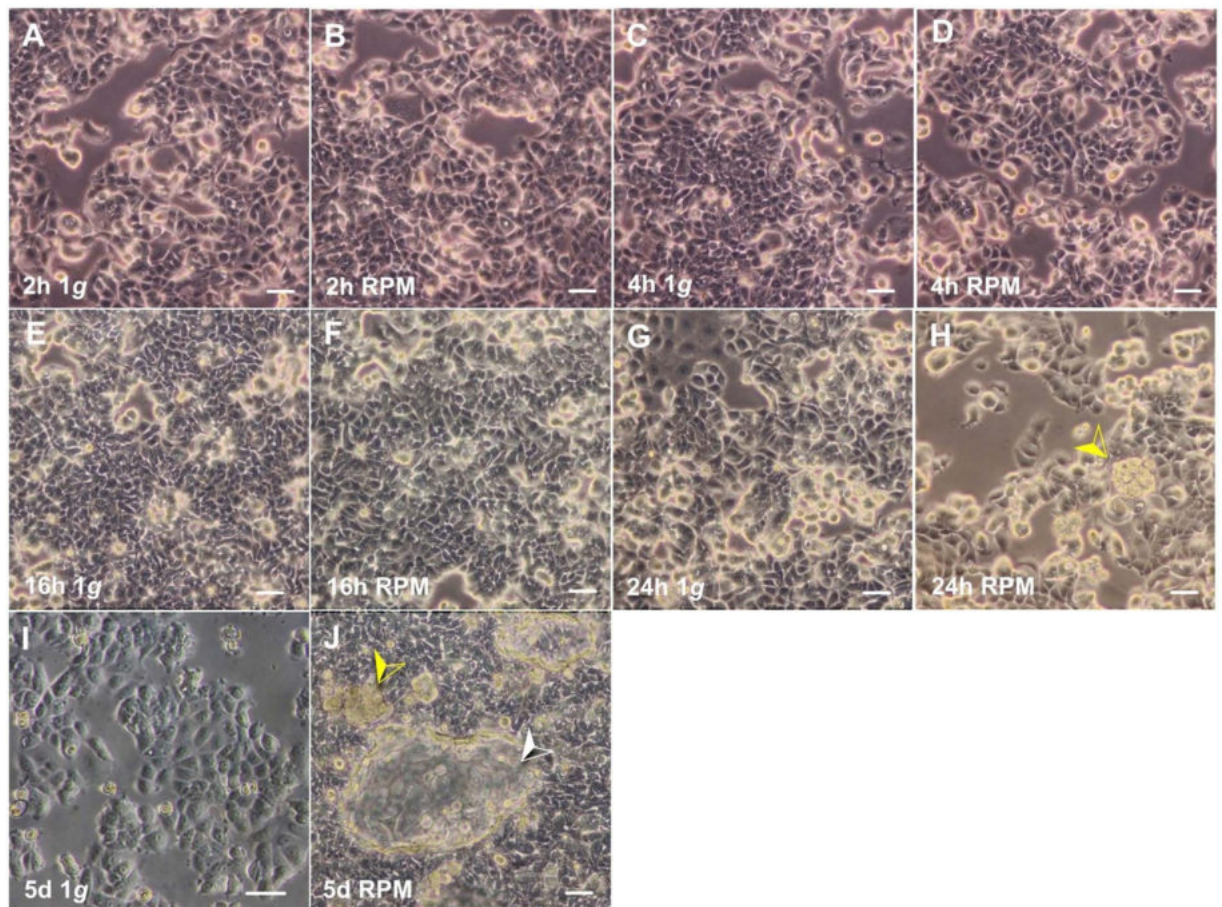
Figure 1. Morphologic examination of the cells. Phase-contrast microscopy of MCF-7 breast cancer cells cultured under normal static 1 g-conditions for 2 h (**A**), 4 h (**C**), 16 h (**E**), 24 h (**G**), 5d (**I**) and on the RPM for 2 h (**B**), 4 h (**D**), 16 h (**F**), 24 h (**H**) and 5d (**J**). Control samples of 5d (**I**) formed no MCS. Samples cultured for 5d on the RPM (**J**) revealed cells that stayed adherently as a monolayer, and solid MCS (yellow arrow) as well as hollow MCS (white arrow). Scale bar: 50 μm.

with an accumulation of F-actin towards the cell boundaries, but no distinct polymerization direction (Fig. 3K) and MCS with a small lumen (Fig. 3, white arrow L).

Investigation of the underlying mechanisms of the phenotypical changes of the cells. In order to find the mechanisms for the transition of the cells from a 2D to a 3D kind of growth behavior, we selected 29 genes (Table 1), which code for proteins known to be involved either in regulation and maintaining cell structures and shapes or in cell migration or in apoptosis[5–10,24] or were specific for female epithelial cells[17,21]. A pathway analysis revealed that aside from β-tubulin (*TUBB*), the expression of the other 28 genes is mutually controlled within the frame of a network (Fig. 4). The proteins coded by these genes consisted of 6 extracellular proteins, 6 membrane proteins, 15 cytoplasmic proteins and 2 nuclear proteins. They also form a network of regulation which stretches from the outside, across the membranes towards the nucleus (Fig. 5). In order to see which influence an up- or down-regulation of a given gene could have on the rest of the network, we analysed the interaction of the selected genes and determined how their up- and down-regulation is linked. Figure 4 gives an overview on the status of regulation of the 29 genes determined by the PCR after 5d of culturing on the RPM and shown in Figs 2 and 6–9. Blue background indicates down-regulation, red background shows up-regulation. The yellow background refers to non-regulated genes. The lower part of each icon indicates the gene status in MCS cells, whereas the upper part indicates the status of the gene in the AD cells. The green arrows indicate activating and the red one inhibiting effects. The picture clearly indicates that the cytokine interleukin-8 (*IL-8 or* CXCL8) gene influences the most of the neighboring genes and thus, may play a central role within this complicated network of regulation. It is followed by *FN1, VEGFA, ICAM1* and *Casp3* genes as we have seen in earlier studies on cells exposed to the RPM[13]. Of these genes *IL-8* and *Casp3* were only downregulated in MCS, whereas *VEGFA* and *FN1* mRNAs were reduced in both populations.

Simulated microgravity on the RPM changes the gene expression and protein production of cytoskeletal and of cytoskeleton-binding proteins. *Short-term study.* Genes associated with the cytoskeleton such as β-actin (*ACTB*), β-tubulin (*TUBB*), cytokeratin-8 (*KRT8*), ezrin (*EZR*), and radixin
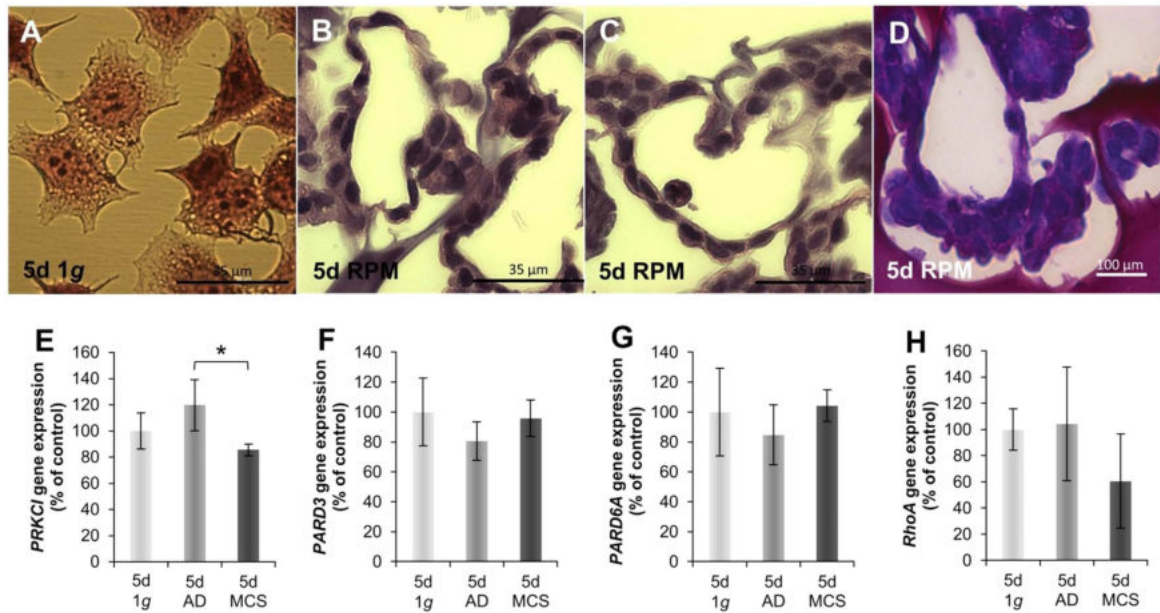
Figure 2. Structural investigations of the MCS. (**A**–**C**) HE staining: (**A**) 5d, 1g-control cells; (**B,C**) examples of 3D MCS with glandular structures. Scale bar: 35 μm (**D**) PAS-stained MCS with apical-basal polarity of the cancer cells. Scale bar 100 μm (**E**) *PRKCI* gene-expression; (**F**) *PARD3* gene-expression; (**G**) *PARD6A* gene expression and (**H**) *RhoA* gene expression. *p < 0.05.

(*RDX*) mRNAs were not significantly changed after short-term incubation (2 h, 4 h, 16 h and 24 h) on the RPM (Fig. 6A–E). The moesin (*MSN*) mRNA was reduced at early time points, but was up-regulated after 24 h (Fig. 6F).

Long-term study. As compared to 1g-control cells, the gene expression of *ACTB* after a 5d-cultivation on the RPM revealed no changes in AD cells, while a significant down-regulation in MCS was measured compared to AD and 1g-samples (Fig. 6A). Taking a look at the corresponding proteins by Western blot analysis revealed that the β-actin protein content was increased in both phenotypes of 5d-RPM-samples compared to 1g-controls (Fig. 6G).

The *TUBB* gene expression presented a comparable picture to β-actin. After 5d no changes were visible for AD cells. However, MCS after 5d showed a significant down-regulation compared to 1g-controls (Fig. 6B). Western blot analyses revealed no changes in the protein content of RPM-exposed samples compared to their corresponding controls (Fig. 6H).

The *KRT8* gene expression was slightly elevated in 5d-AD-samples, but significantly down-regulated in MCS compared to AD samples and not significantly changed compared to 1g-controls (Fig. 6C). In addition, the amount of pan-cytokeratin protein was enhanced after a 5d- culture on the RPM in both phenotypes in comparison to 1g-controls (Fig. 6I). The *EZR* gene expression of AD samples was not significantly changed compared to the 1g-control group (Fig. 6D), but MCS samples exhibited a decrease in *EZR* mRNA. No change was found in the protein after 5d, respectively (Fig. 6J). The *RDX* gene expression in MCS after 5d was significantly down-regulated (Fig. 6E). In addition, the protein content was decreased in AD cells after a 5d-exposure of MCF-7 cells on the RPM as compared to MCS and 1g-controls (Fig. 6K). The *MSN* gene expression after 5d was significantly down-regulated in AD and MCS cells compared to the 1g-controls (Fig. 6F).

Cultivation of MCF-7 cells on the RPM induces changes in the extracellular matrix. *Short-term study.* In this study we investigated the expression of extracellular matrix (ECM) proteins. The laminin α 3 (*LAMA3*) gene expression was unaltered in cells exposed for 2 h, 4 h and 16 h to the RPM. In addition, the *LAMA3* mRNA was significantly elevated in MCS compared to 1g- and AD-samples after 24 h (Fig. 7A). The fibronectin (*FN1*) mRNA is decreased after a 2 h-RPM-exposure compared to 1g-samples, but remained unalterd at the other short-term time points (Fig. 7B).

Levels of integrin-β$_1$ (*IGTB1*) transcripts of AD cells were slightly elevated compared to 1g-samples after 2 h, then significantly up-regulated after 4 h, and then unaltered after a 16 h-RPM-exposure (Fig. 7C). After 24 h, the *ITGB1* mRNA was down-regulated in MCS compared to AD and 1g (Fig. 7C).

The ECM protein collagen type 4 (*COL4A5*) mRNA was not significantly altered under all conditions (Fig. 7D). The gene expression of intercellular adhesion molecule 1 (*ICAM1*) was significantly down-regulated in both RPM-cultures after a 24 h-RPM exposure (Fig. 7E).

The neutrophil gelatinase-associated lipocalin (NGAL) secretion was significantly decreased after 4 h and 24 h of incubation on the RPM compared to 1g (Fig. 7K). The release of NGAL was below the detection level of the technique after 2 h of incubation of the MCF-7 cells on the RPM.
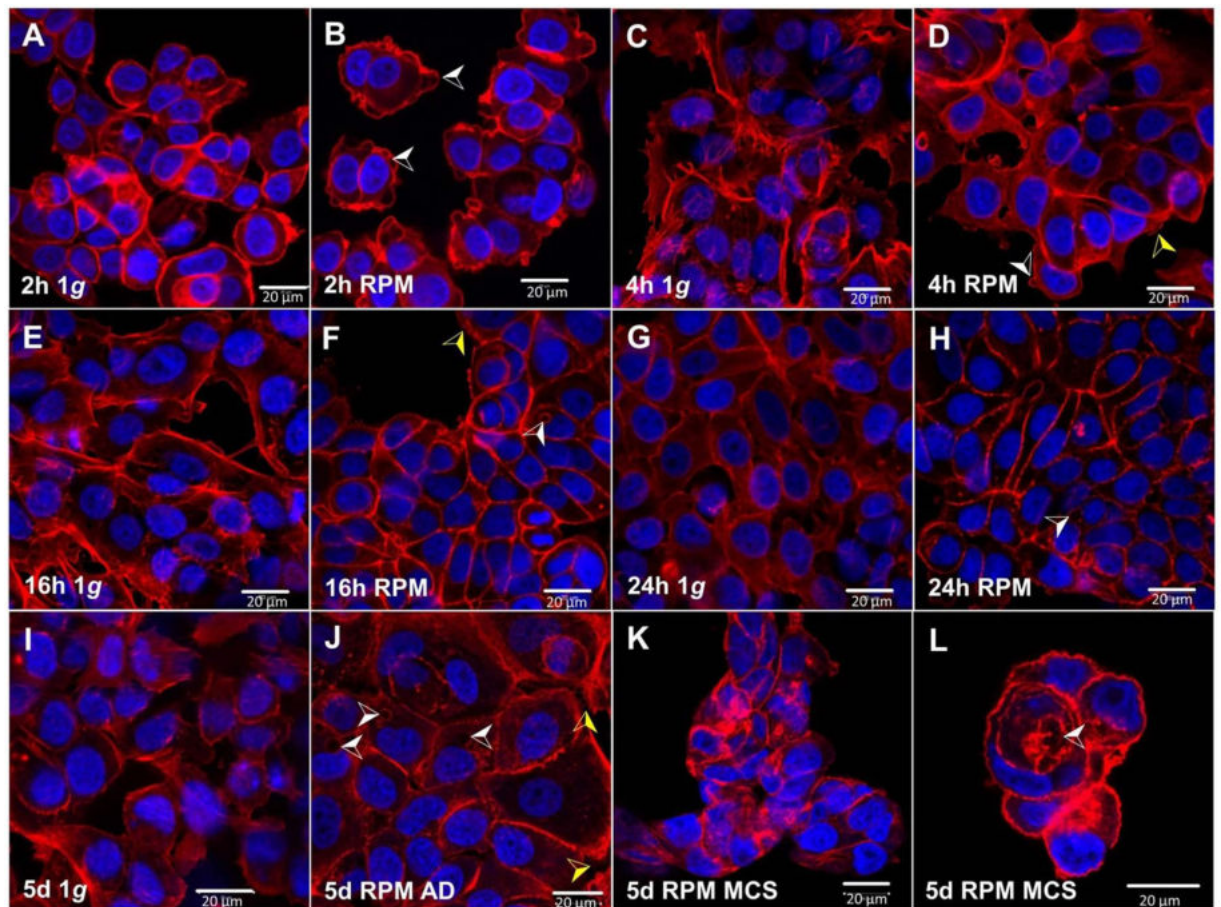
Figure 3. F-actin cytoskeleton. Confocal laser scanning microscopy of rhodamine-phalloidin stained MCF-7 cells after a 2h-, 4h-, 16h-, 24h- and 5d-RPM-exposure and corresponding 1g-control cells. (**A**) 2h 1g; (**B**) 2h RPM-culture, white arrow indicated membrane blebbing; (**C**) 4h 1g; (**D**) 4h RPM-culture, the white arrow indicated membrane bleebing, the yellow arrow shows stress fibers; (**E**) 16h 1g; (**F**) 16h RPM-culture, the yellow arrow shows stress fibers, the white arrow presents cytoskeletal holes; (**G**) 24h 1g; (**H**) 24h RPM-culture, the white arrow indicates cytoskeletal holes; (**I**) 5d, 1g; (**J**) 5d RPM AD cells, the white arrow indicates holes, the yellow arrows show stress fibers; (**K,L**) 5d RPM MCS, the white arrow indicates a glandular structure. Scale bar: 20 μm; blue staining: DAPI highlights the nucleus; red staining: rhodamine-phalloidin to visualize the F-actin.

Long-term study. The *LAMA3* mRNA was decreased in AD compared to MCS and 1g-samples after a 5d-RPM-exposure (Fig. 7A). The amount of laminin protein was elevated in AD cells and significantly reduced to the 1g-level in MCS (Fig. 7H). The *FN1* expression was significantly down-regulated after a 5d-RPM-exposure in AD cells and in MCS (Fig. 7B). In contrast, the amount of fibronectin protein was decreased in AD cells after 5d. However, MCS showed an normalization of the protein synthesis like 1g-samples (Fig. 7I).

Concerning the gene expression of *ITGB1*, there was a slight down-regulation visible after 5d and a further decrease in MCS cells compared to 1g-samples (Fig. 7C). Determination of the protein content showed that MCS cells exhibited a significant decrease in β_1-integrin protein compared to AD samples (Fig. 7J). The gene expression of the extracellular matrix protein *Col4A5* was not significantly changed after a 5d-RPM exposure (Fig. 7D). In addition, the *ICAM1* gene expression was not altered after 5d (Fig. 7E). Moreover, the *Ngal* gene expression was not remarkably changed after a 5d-RPM-exposure (Fig. 7F). In addition, the release of NGAL protein into the supernatant was significantly decreased in RPM-exposed samples compared to the 1g-controls after 5d (Fig. 7K). Furthermore, *CD44* was not significantly changed after 5 days. AD cells presented a tendency to elevate the expression (Fig. 7G).

Vascular endothelial growth factor signalling pathway molecules are altered by simulated microgravity.

Short-term study. Both genes, vascular endothelial growth factor A (*VEGFA*) and its receptor vascular endothelial growth factor receptor 1 or fms related tyrosine kinase 1 (*FLT1*) were significantly up-regulated after a 2h-incubation on the RPM (Fig. 8A,B), while the vascular endothelial growth factor receptor 2 or fetal liver kinase 1 (*FLK1*) mRNA was unchanged at all short-term time points (Fig. 8C). The *VEGFA* and *FLT1* mRNAs were still significantly up-regulated after a 4h-RPM-exposure. Interestingly later after 16h we detected a down-regulated *VEGFA* mRNA in AD samples and after 24h in both AD and MCS samples (Fig. 8A).

Gene	Primer Name	Sequence
18S rRNA	18S-F	GGAGCCTGCGGCTTAATTT
	18S-R	CAACTAAGAACGGCCATGCA
ACTB	ACTB-F	TGCCGACAGGATGCAGAAG
	ACTB-R	GCCGATCCACACGGAGTACT
Casp3	Casp3-F	AACTGCTCCTTTTGCTGTGATCT
	Casp3-R	GCAGCAAACCTCAGGGAAAC
Casp9	Casp9-F	CTCCAACATCGACTGTGAGAAGTT
	Casp9-R	GCGCCAGCTCCAGCAA
CD44	hCD44-F	ACCCTCCCCTCATTCACCAT
	hCD44-R	GTTGTACTACTAGGAGTTGCCTGGATT
Col4A5	Col4A5-F	GGTACCTGTAACTACTATGCCAACTCCTA
	Col4A5-R	CGGCTAATTCGTGTCCTCAAG
ERK1	ERK1-F	ACCTGCGACCTTAAGATTTGTGA
	ERK1-R	AGCCACATACTCCGTCAGGAA
ERK2	ERK2-F	TTCCAACCTGCTGCTCAACA
	ERK2-R	TCTGTCAGGAACCCTGTGTGAT
ESR	ESR1-F	TTCAAGAGAAGTATTCAAGGACATAACG
	ESR1-R	TCGTATCCCACCTTTCATCATTC
EZR	EZR-F	GCAATCCAGCCAAATACAACTG
	EZR-R	CCACATAGTGGAGGCCAAAGTAC
FLK1	hFLK1-F	TCTTCTGGCTACTTCTTGTCATCATC
	hFLK1-R	GATGGACAAGTAGCCTGTCTTCAGT
FLT1	FLT1-F	CCCTCGCCGGAAGTTGTAT
	FLT1-R	GATAATTAACGAGTAGCCACGAGTCAA
FN1	FN-F	AGATCTACCTGTACACCTTGAATGACA
	FN-R	CATGATACCAGCAAGGAATTGG
ICAM1	ICAM1-F	CGGCTGACGTGTGCAGTAAT
	ICAM1-R	CTTCTGAGACCTCTGGCTTCGT
IL8	IL8-F	TGGCAGCCTTCCTGATTTCT
	IL8-R	GGGTGGAAAGGTTTGGAGTATG
ITGB1	ITGB1-F	GAAAACAGCGCATATCTGGAAATT
	ITGB1-R	CAGCCAATCAGTGATCCACAA
KRT8	KRT8-F	GATCTCTGAGATGAACCGGAACA
	KRT8-R	GCTCGGCATCTGCAATGG
LAMA3	LAMA3-F	AAAGCAAGAAGTCAGTCCAGC
	LAMA3-R	TCCCATGAAGACCATCTCGG
MSN	MSN-F	GAAATTTGTCATCAAGCCCATTG
	MSN-R	CCATGCACAAGGCCAAGAT
NGAL	NGAL-F	AGGGAGTACTTCAAGATCACCCTCTA
	NGAL-R	AGAGATTTGGAGAAGCGGATGA
PARD3	PARD3-F	TACAGTGGGATTGAGGGGCT
	PARD3-R	GCTGGTATTTACCTGACTCACC
PARD6A	PARD6A-F	ATACGGATGCTCATGGCGAC
	PARD6A-R	GTCAGCTTCTGCCCGCTTCT
PKB	AKT1-F	CTTCTATGGCGCTGAGATTGTG
	AKT1-R	CAGCATGAGGTTCTCCAGCTT
PKC	PKC-F	CATTCAACAGCTGGGCAAGTT
	PKC-R	GTAGATGATGCCCTGATTGTGAAG
PGR	PGR-F	GTGGGAGCTGTAAGGTCTTCTTTAAGA
	PGR-R	TGACAGCACTTTCTAAGGCGACA
PRKCI	PRKCI-F	GTGTAAGGAAGGATTACGGCCA
	PRKCI-R	GCCCACCAGTCAACACTGAA
RDX	RDX-F	GAAAATGCCGAAACCAATCAA
	RDX-R	GTATTGGGCTGAATGGCAAATT
RhoA	RhoA-F	CGTTAGTCCACGGTCTGGTC
	RhoA-R	GCCATTGCTCAGGCAACGAA
Continued		

Gene	Primer Name	Sequence
TUBB	TUBB-F	CTGGACCGCATCTCTGTGTACTAC
	TUBB-R	GACCTGAGCGAACAGAGTCCAT
VEGFA	VEGFA-F	GCGCTGATAGACATCCATGAAC
	VEGFA-R	CTACCTCCACCATGCCAAGTG

Table 1. Primers used for qRT-PCR.
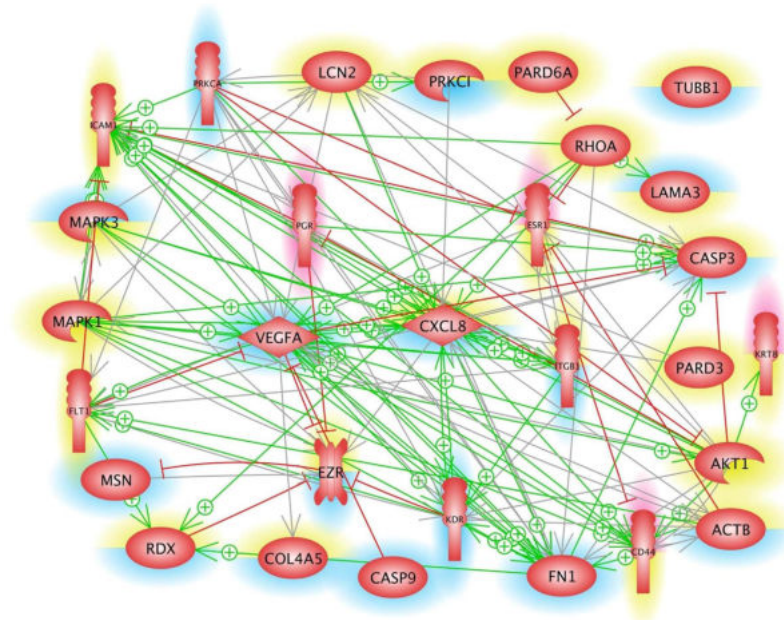
Figure 4. Mutual interaction of selected genes at gene expression level. 29 selected genes, whose up- or downregulation were analysed by qRT-PCR after 5d of culturing on the RPM and shown in Figs 2 and 6–9. Blue background indicates down-regulation, red background shows up-regulation. The yellow background refers to non-regulated genes. The lower part of each icon indicates the gene status in MCS cells, whereas the upper part indicates the status of the gene in the AD cells. The green arrows indicate activating and the red one inhibiting effects. The interaction network was built up using Elsevier Pathway Studio v.11.

Figure 5. Mutual interaction and localization of proteins coded by the 29 selected genes. The green arrows indicate activating and the red one inhibiting effects. The interaction network was built up using Elsevier Pathway Studio v.11.
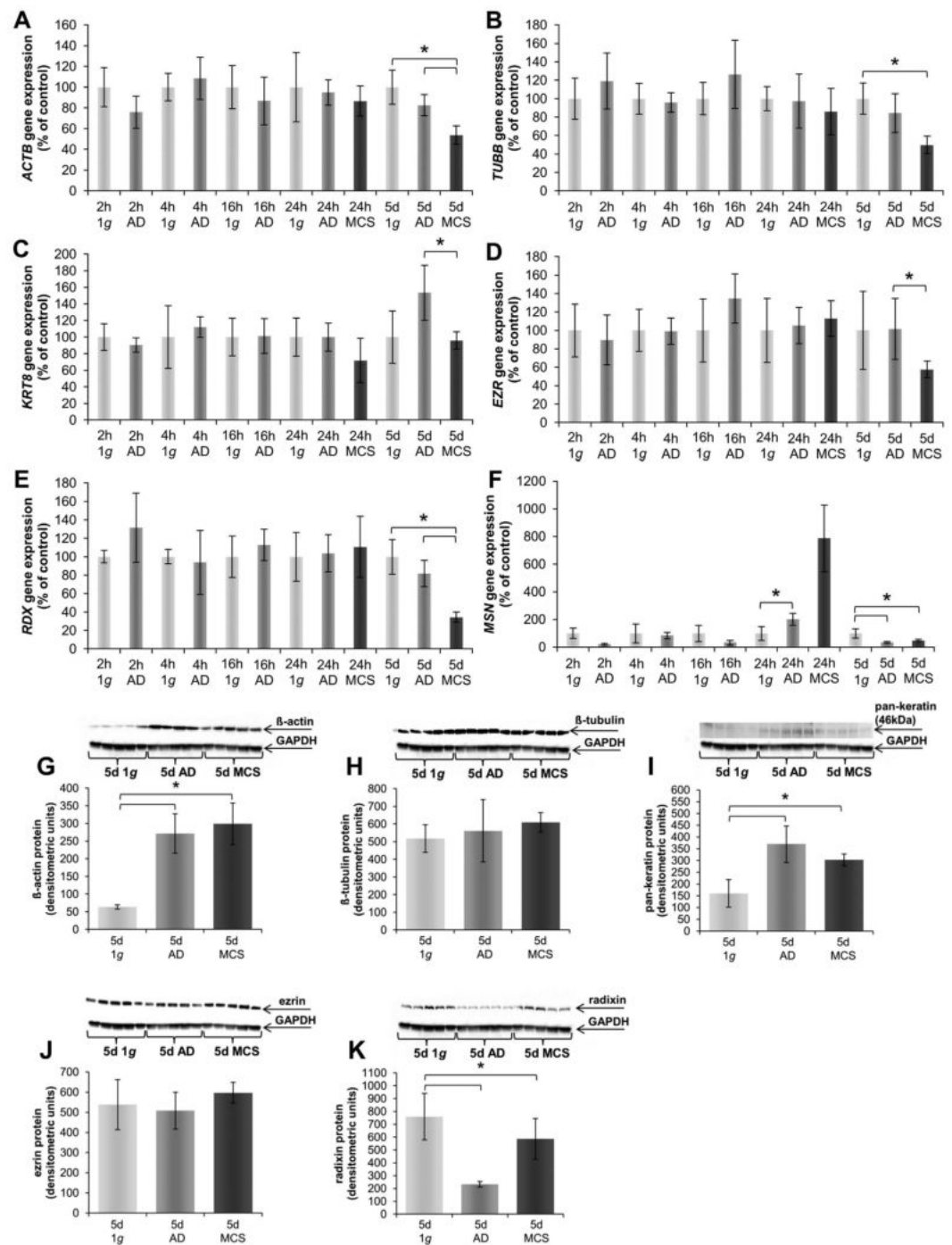
Figure 6. Quantitative alterations of gene expression and protein content of cytoskeletal and associated proteins: Genes. *ACTB* (**A**) 2 h, 4 h, 16 h, 24 h and 5 d RPM-experiments. *TUBB* (**B**) 2 h, 4 h, 16 h, 24 h and 5 d RPM-experiments. *KRT8* (**C**) 2 h, 4 h, 16 h, 24 h and 5 d RPM- experiments. *E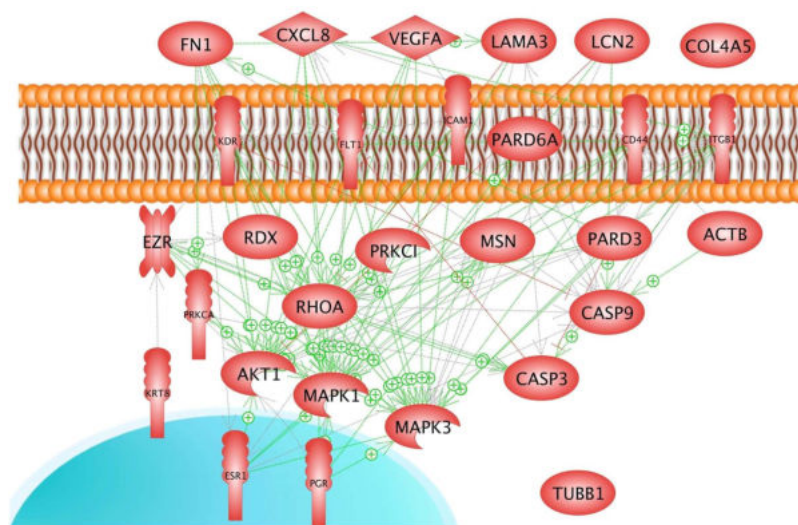ZR* (**D**) 2 h, 4 h, 16 h, 24 h and 5 d RPM-experiments. *RDX* (**E**) 2 h, 4 h, 16 h, 24 h and 5 d RPM-experiments. *MSN* (**F**) 2 h, 4 h, 16 h, 24 h and 5 d RPM-experiments. **Proteins of 5d-experiments:** 5d β-actin (**G**); 5d β-tubulin (**H**); 5d cytokeratin (**I**); 5d Ezrin (**J**) 5d Radixin (**K**); *p < 0.05.

The amount of secreted VEGF protein was measured in the cell culture supernatants of 1 *g*- and RPM-experiments by time resolved immunofluorometric assays (TRIFMA). The results showed that the amount of VEGF protein was significantly decreased in RPM-cultures compared to 1 *g*-controls after a 4 h-RPM-exposure (Fig. 8J). There was no difference between 1 *g*- and RPM-cultures after 24 h. However, comparing the VEGF levels in s-μ*g* after 4 h and 24 h against each other, a significant lower level after 24 h could be observed.
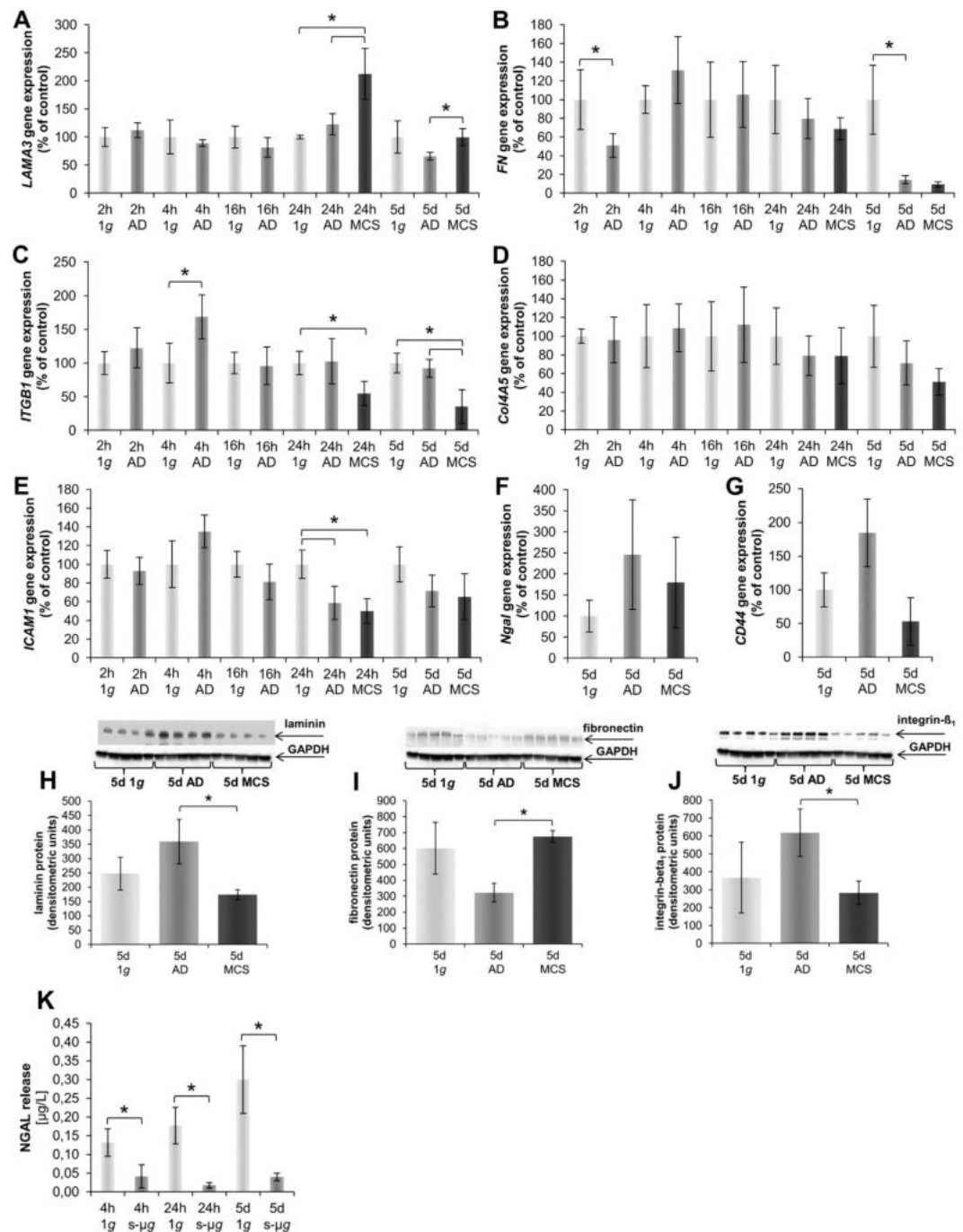
Figure 7. Quantitative alterations of gene expression and protein content of extracellular matrix and associated proteins: Genes. *LAMA3* (**A**) 2 h, 4 h, 16 h, 24 h and 5d RPM-experiments. *FN1* (**B**) 2 h, 4 h, 16 h, 24 h and 5d RPM-experiments. *ITGB1* (**C**) 2 h, 4 h, 16 h, 24 h and 5d RPM-experiments. *Col4A5* (**D**) 2 h, 4 h, 16 h, 24 h and 5d RPM-experiments. *ICAM1* (**E**) 2 h, 4 h, 16 h, 24 h and 5d RPM-experiments. *Ngal* (**F**) 5d RPM-experiment. *CD44* (**G**) 5d RPM-experiment. **Proteins:** 5d laminin (**H**); 5d fibronectin (**I**); 5d integrin-β-1 (**J**). NGAL release (**K**) 4 h, 24 h and 5d. $*p < 0.05$.

Long-term study. The gene expression of *VEGFA* was significantly down-regulated after 5d of culturing MCF-7 cells on the RPM (Fig. 8A). This is in concert with the VEGF protein release in the supernatant as measured by TRIFMA. The release of VEGF protein was significantly lower in RPM-samples compared to corresponding static 1 *g*-controls (Fig. 8J). The Western blot analysis revealed no significant change in AD cells, but a slight elevation of VEGF protein in MCS compared to 1 *g*-cultures (Fig. 8K).

The gene *FLK1* was significantly down-regulated after 5d in both cell populations (Fig. 8C). In contrast to *FLK1*, the *FLT1* mRNA was not altered in cells cultured on the RPM at this time point (Fig. 8B).
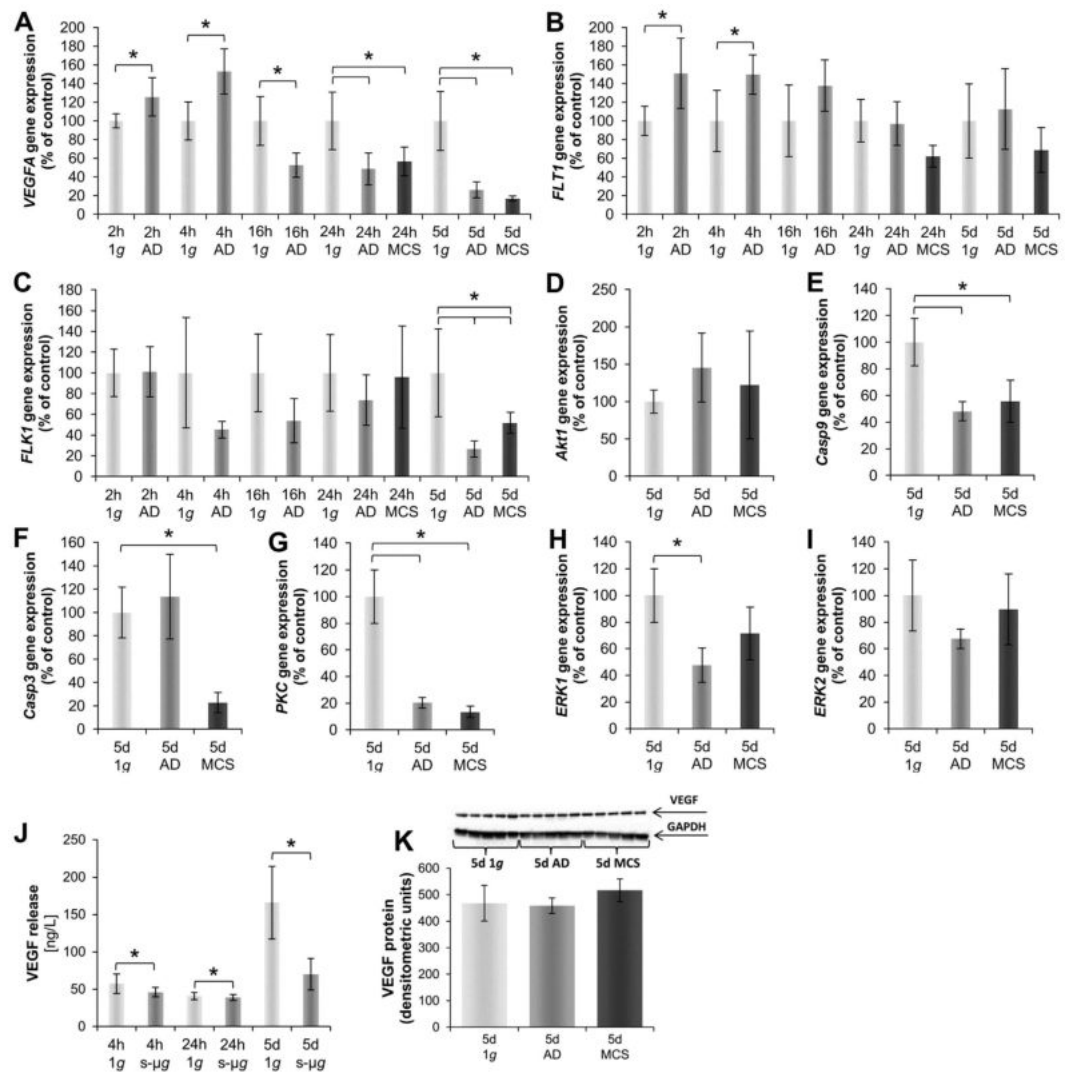
Figure 8. Quantitative alterations of gene expression and protein content of VEGF signalling pathway molecules: Genes. *VEGFA* (**A**) 2 h, 4 h, 16 h, 24 h and 5d RPM-experiments. *FLT1* (**B**) 2 h, 4 h, 16 h, 24 h and 5d RPM-experiments. *FLK1* (**C**) 2 h, 4 h, 16 h, 24 h and 5d RPM- experiments. *Akt1* (**D**) 5d. *Casp9* (**E**) 5d. *Casp3* (**F**) 5d. *PKC* (**G**) 5d. *ERK1* (**H**) 5d. *ERK2* (**I**) 5d. **Proteins:** VEGF release in the supernatant (**J**) 4 h, 24 h and 5d; 5d VEGF protein content (**K**). *p < 0.05.

The threonine-protein kinase (*akt1* or *PKB*) gene coding for a signaling cascade molecule was unaltered after 5d of cultivation on the RPM (Fig. 8D).

The caspase-9 (*Casp9*) gene expression was significantly down-regulated in MCF-7 cells after RPM-exposure compared to 1 *g*-controls (Fig. 8E). In contrast to caspase-9, the caspase-3 (*Casp3*) gene expression was signifi-cantly down-regulated only in MCS after 5d (Fig. 8F). The gene expression of protein kinase C (*PKC* or *PRKCA*) was significantly down-regulated in both cell populations after 5d compared to their corresponding 1 *g*-controls (Fig. 8G).

The extracellular-signal regulated kinase (*Erk*)-1 (Fig. 8H) and *Erk-2* (Fig. 8I) presented a similar behavior after RPM-exposure. After 5d only the AD cell populations exhibited a significantly down-regulated expression of *Erk-1*, the other groups showed a slight decrease compared to 1 *g*-controls (Fig. 8H,I).

RPM-exposure induces expression changes of interleukin-8, estrogen- and progesterone receptors.
The cytokine interleukin-8 (*IL8*) gene expression was not altered in AD, but slightly decreased in MCS cells on the RPM after 5d (Fig. 9A). After 2 h and 4 h a clear up-regulation of the *IL8* gene was detectable in AD RPM-cultures. After 16 h this elevation was attenuated again to the normal 1 *g*-level. In 24 h-samples MCS exhibited an up-regulated *IL8* mRNA compared to AD and 1 *g*-samples (Fig. 9A).

The estrogen receptor (*ESR1*) expression was unchanged in all short-term samples, but was up-regulated after 5 days in AD cells. In MCS the *ESR1* mRNA was unaltered (Fig. 9B). The progesterone receptor (*PGR1*) expres-sion was significantly up-regulated in both AD cells as well as in MCS cells after 5 days (Fig. 9C).
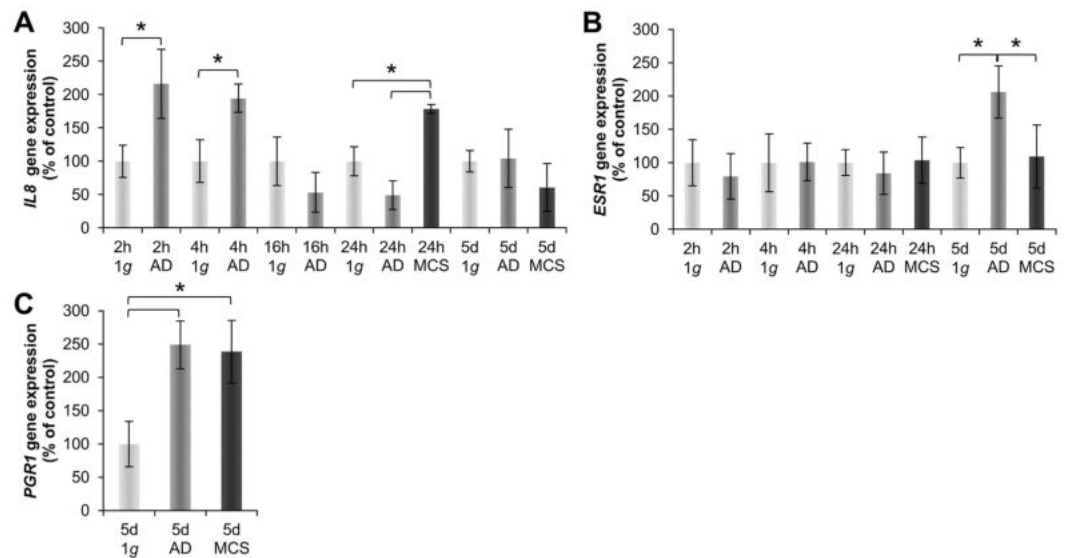
Figure 9. Quantitative alterations of gene expression of cytokines and hormone receptors: Genes. *IL8* (**A**) 2 h, 4 h, 16 h, 24 h and 5d RPM-experiments. *ESR1* (**B**) 2 h, 4 h, 16 h, 24 h and 5d RPM-experiments. *PGR1* (**C**) 5d RPM-experiments. *p < 0.05.

Discussion

In this study we used simulated microgravity conditions created by the RPM for 3D tissue engineering of MCS and investigated the underlying mechanisms for a scaffold-free 3D growth behaviour of human breast cancer cells. Under normal laboratory conditions single cancer cells grow as monolayers. If sophisticated methods of tissue engineering are applied, MCS can be obtained which resemble the original, individual tumor more closely than corresponding cell monolayers[22]. Most interesting are methods of tissue engineering, which do not need scaffolds exerting unfavorable side-effects[24,25]. A suitable method to trigger the formation of MCS is culturing cells under microgravity conditions which is best provided by space missions[9,26]. Space research such as human space exploration and research applying simulated microgravity using ground-based facilities have increased our knowledge in cellular and molecular biology and given us new insights into the behavior of human cells under altered gravity conditions[13,27,28]. Devices simulating microgravity allow performing rather effective scaffold-free tissue engineering experiments in a much cheaper way and with a higher throughput[13,22]. It has been observed that normal and human thyroid cells grew in form of an adherent monolayer and as 3D aggregates[7]. This observation is in concert with results obtained by others as well as by our group. For example, when cultured on the RPM endothelial cells, murine osteoblasts and human breast cancer cells split into two populations with different phenotypes, respectively[18,29,30]. To explain this special behavior the non-equilibrium thermodynamics theory will be discussed. The non-equilibrium thermodynamics or birfurcation theory is describing the direct action of gravity on single cells[31,32].

Biochemical reactions catalyzed by enzymes and controlled by feedback mechanisms in the organism are nonlinear and far away from an equilibrium. Therefore, a cell may answer unexpectedly to changed conditions of the cellular microenvironment. The key elements of a reaction remain constant and they can react with a known phase, frequency or amplitude. This crossroad or bifurcation system is depending on the microenvironment[31,32]. Microgravity can influence the cell to react in a different way compared with cells cultured under static normal 1 g-conditions. A large number of publications of studies performed in simulated and real microgravity in space have shown that different kinds of cells exhibit dramatic changes after microgravity-exposure[22,33].

Since a long time scientists observed changes in a variety of cellular biological processes, such as apoptosis or angiogenesis. The cells showed changes in cell morphology, growth behavior, proliferation, differentiation, cell adhesion, extracellular matrix, among others[34–39].

Furthermore, it is known that microgravity induces alterations in the cytoskeleton[34,38,39]. These cytoskeletal changes occur early as shown by parabolic flight maneuvers[40,41]. In addition, alterations in the actin cytoskeleton have been detected in space-flown xenopus embryonic muscle cells which exhibited marked changes in the distribution and organization of actin filaments[42]. These alterations of the actin cytoskeleton and microtubules are accompanied by changes of the shape of the cells[42–44]. This could already be seen after a 2 h-RPM exposure (Fig. 3). F-actin staining showed that AD cells on the RPM exhibited a membrane blebbing and at later time points stress fibers. After 24 h and 5d AD cells exhibited holes in the actin cytoskeleton. The cytoskeleton is sensing changes in gravity, and thus it is influencing signalling pathways[44] and gene expression as well as protein synthesis and secretion[26]. Therefore, a variety of signaling processes such as cellular metabolism, proliferation, differentiation are changed when cells are cultured under altered gravity conditions[22,40,45].

Real and simulated microgravity can directly or indirectly influence a cell[27,46]. Human cells are able to react to environmental changes. When, for example, cells are cultured on agarose in 96-well plates normal adherent cells grow in form of multicellular spheroids[47] Under hypoxia or irradiation the cells will become apoptotic[48]. Altered

gravity conditions have shown to influence gene expression, protein synthesis and the release of proteins in the cell supernatant in space[26].

Changes in shape, cytoskeleton disruption, differential gene expression or altered protein synthesis/secretion cannot be only explained by considering changes in microenvironmental biophysical parameters. Gravitation might influence some general properties of the cells and thus acting "directly" as an organizing field parameter[46]. According to the non-equilibrium theory[49] murine osteoblasts and breast cancer cells underwent a transition after a bifurcation point to new phenotypic configurations[18,30]. It is known for several cell types such as thyroid cancer cells, endothelial cells or chondrocytes that real and simulated microgravity induces two forms of growth, such as adherently growing cells and cells growing in form of 3D spheroids[6,8,13,29,50]. It has been demonstrated that some of the endothelial cells grown on the RPM form tubular intima-like structures[24,51]. In this paper the MCF-7 cells grew adherently after RPM-exposure and also in form of 3D aggregates after 24 h and showed gland-like structures after 5d as demonstrated in Fig. 2 by histochemical staining. The cells show an apical-basal polarity. To establish cell polarity, the MCF-7 cells have to interact with the surrounding medium, their neighbor cells and the ECM. Two main events are necessary for the development of 3D glandular structures. First the communication of the cells to the ECM and second the formation of a lumen. This might be possible with the interaction of integrins with laminin, which is like collagen type IV a constituent of the basement membrane. Both are known to efficiently induce the polarization of epithelial cells[52–54] We measured an increase in *LAMA3* gene expression after 24 h in MCS (Fig. 8A) and after 5d an up-regulation of *LAMA3* in MCS compared with AD. This finding indicates that laminin may be involved in producing apical-basal polarity and the development of glandular structures. Collagen type IV was not significantly changed during all selected time points. Future investigations are necessary to study this process in more detail.

In this study, a few compact small aggregates had been detected in 24 h-RPM-cultures. This process starts after 16 h of RPM-exposure. MCF-7 cells appear to be very sensitive to RPM-exposure. A 24 h-period of microgravity is sufficient to induce a multitude of adaptive mechanisms inside the cells[6]. Similar to breast cancer cells (Fig. 1), two cell populations of FTC-133 thyroid cancer cells could be detected in RPM cultures: 2D growing adherent cells and floating 3D spheroids. Both populations exhibited a different growth behavior and signaling. Most interestingly, the adherent cells showed the highest rate of apoptosis and the most prominent gene expression of NF-kB, while the genomic profile of MCS cells appeared closer to that of 1 g-control cells than AD cells[6]. Similar results were found for endothelial cells[24].

A microgravity-dependent inhibition of cancer cell proliferation, migration, and survival was found in MCF-7 cells and poorly differentiated follicular thyroid cancer cells[15,16,39,55]. This effect is cell type-dependent. For example chondrocytes reveal a decrease in apoptosis after simulated microgravity-exposure as well as fetal fibroblasts[56,57]. As already mentioned, MDA-MB-231 breast cancer cells exposed to the RPM also revealed two distinct phenotypes after 24 h[18]. A similar finding was observed in osteoblasts and chondrocytes cultured in microgravity[30,58]. This could be confirmed for MCF-7 breast cancer cells in this study. Moreover, we detected glandular structures which were only detected in long-term cultures. The first phenotype remained adherent to the cell culture flask as shown in Fig. 1. These cells exhibited a similar morphology as the 1 g-control cells. The second phenotype had detached from the bottom and was growing in form of 3D spheroids floating in the supernatant as earlier shown for thyroid cancer cells after RPM- or clinostat-exposure[6,7,10,47]. In this study, we investigated the F-actin cytoskeleton and the expression of genes coding for proteins which might be involved in the perception of gravity and the formation of MCS[6–10,24]. Between 16 h and 24 h MCF-7 cells started to form small round 3D aggregates. We could show for the first time that a part of the MCF-7 cells exhibited duct-like MCS after 5d on the RPM. These structures seemed to resemble a gland-like appearance to be found in mammary glands known as *alveoli* which align in lobules[59]. Before, we had repeatedly observed that cell populations split on the RPM into one subpopulation staying adherent to the bottom of the culture dish and another population, which had detached from the bottom and built up MCS (Figs 1–3)[7,50]. However, only healthy cells like the chondrocytes or the endothelial cells formed structures resembling the original cartilage tissue or the blood vessel intima, respectively[8,51], while culturing de-differentiated human thyroid cancer cells always led to rounded spheres[5,7,9]. The gland-like appearance of MCS formed by MCF-7 cells might be due to a high differentiation status of the MCF-7 cells, which still express estrogen and progesterone receptors[17,21]. Moreover, other studies suggested that simulated microgravity enacts the reversion of the neoplastic phenotype of lung cancer stem cells[60]. This is supported by studies investigating cancer cells in a different tissue environment. This model of tumor reversion has demonstrated a clinical benefit in hematological malignancies. These cells show a shift from a neopalstic toward a normal phenotype[61]. Cell morphology of cells growing as monolayer in 1 g-cultures is different from those observed in tissue and organs. The shape of the cells is influenceing cell growth, cell metabolism as well as gene expression and thus, this might explain the differences in the gene expression of AD and MCS cells[62].

In addition, it was described that either induced by drugs or by fibroblasts, MCF-7 may adopt almost normal biochemical characteristics and form nodules[63,64]. Moreover, a possible microgravity-dependent change in the cellular differentiation of the cells was suggested by the results obtained after dedifferentiated thyroid cancer had been flown on the Shenzhou-8 spaceflight[26].

Although the expression of estrogen receptors is a marker of the high-differentiation status of the MCF-7 cells, their presence may promote breast cancer proliferation under some circumstances[65]. However, the simultaneous presence of the progesteron receptor often attenuates the proliferative action of the estrogen receptor switching a tumor cell to a more differentiated state[66]. We found an up-regulation of the *ESR1* gene expression in AD cells after a 5d-RPM-exposure. The *ESR1* gene remained unchanged during the short-term study. The expression of *PGR1* was up-regulated in both phenotypes of 5d-RPM-samples (Fig. 9). The up-regulation of both hormone receptors is transient like the production of caspase-3 in thyroid cells[67]. An upregulation of *PGR1* genes in MCF-7 MCS and AD cells seem not to influence the fibronectin promoter like in fibroblasts[68]. *FN1* was down-regulated after 5d in AD and MCS, which could be a cause that also kinase insert domain receptor (*KDR*)

gene is down-regulated in AD and MCS, because its gene status is under the positive influence of *FN1* as shown in Fig. 4 and described in the literature[69–73].

Interestingly, according to the Elsevier Pathway Studio analysis *FN1, KDR,* and *ICAM1* genes code for proteins which are members of a signalling pathway that regulates the shape of the cells, while MSN-RDX-proteins and ICAM1-MSN-proteins together with EZR, respectively, participate in triggering tip formation of cells and membrane to membrane docking. Cell shape changes and renewed membrane to membrane docking can clearly be seen in Figs 1, 2 and 3.

It is known that cancer cells actively remodel their ECM and that the cell adhesion molecule fibronectin is important for survival signaling, progression and metastasis in breast cancer cells[74]. Thyroid cancer cells (FTC-133 cell line) express surface proteins that bind fibronectin, strengthening the 3D cell cohesion[5]. The moesin gene is regulated like *FN1* (Figs 6F and 7B). This parallel regulation may be due to miR-200c, which can target *FN1* as well as *MSN*[75]. Ezrin, radixin and moesin belong to the ERM protein family and connect the plasma membrane with the actin cytoskeleton and are therefore of high interest to be part of the external signal transport into the cell[76]. The ERM proteins are strongly associated with ICAM1[77,78]. A suppression of ERM proteins resulted in a destruction of cell-cell and cell-substrate adhesion, while an overexpression enhanced cell adhesion[78]. Hence, the decreased expression of ERM genes after a 5d-exposure might be a reason for the detachment of the cells and the undefined appearance of the MCS.

This transition process is accompanied by a rearrangement of the actin (Fig. 3) as it has been shown earlier in spaceflight-MCF-7-samples[14]. In this study, the 1*g*-control cells presented visible filaments, like it was seen in endothelial cells and thyroid cells. In duct-like MCS the actin filament systems of the MCF-7 cells is more similar to actin filament systems of tubes formed by EAhy cells than to that formed by thyroid cancer cells[29,47]. Actin as well as tubulin and keratin are major parts in the cytoskeleton bearing different functions and are thought to be critical for the perception and forwarding of external chemical and physical signals like the gravity force[44].

Gravity is known to influence directly or indirectly the behavior of cells[46]. It follows nonequilibrium dynamic rules[49]. A nonequilibrium reaction influenced by gravity in living cells is represented by the dynamices of the cytoskeleton, by shape and differentiation of the cells[30]. Epithelial cell migration is regulated by three major signaling nodes, β-catenin, integrin-β_1 and actin[79]. Many of these genes are involved in cell-cell and cell-matrix adhesion through regulation of the actin cytoskeleton and EGFR signaling[79].

MCF-7 cells exposed to the RPM for 2 h, 4 h, 16 h and 24 h exhibited no changes in the gene expression of cytoskeletal genes. In contrast, we found β-actin and β-tubulin genes in MCS to be significantly down-regulated after 5d. Simultaneously, the amount of β-actin protein was elevated in AD and MCS cells after 5d, while equal amounts of tubulin were found in all measurements. In addition, *KRT8*, which is a luminar marker[80], was equally expressed after 5d of cultivation on the RPM as in 1*g*-controls. Densitometric analyses revealed a higher content of keratin 8 (subunit 46 kDa) in AD and MCS after 5d compared to their corresponding 1*g*-controls. Moreover, up-regulation in β-actin gene expression had also been found for human thyroid cells cultured on the RPM for 7 and 14 days[7]. However, a direct mutual influence of these three cytoskeletal proteins could not be seen on the gene nor on the protein level.

Integrins are known to crosslink with ICAM1 and co-localizes with moesin in microvilli in endothelial cells[81]. By this, the small GTPase RhoA is activated which induces the production of stress fibers and the up-regulation of the *rhoA* gene[82]. We found *ITGB1* up-regulated in 4 h-AD-samples. Later *ITGB1* was significantly down-regulated in 24 h-MCS and then non-significantly down-regulated after 5d in RPM-samples as in 1*g*-samples. The densitometric analyses presented a slight decrease in integrin-β_1 protein after 5 days. Integrin-β_1 is a membrane protein, linking to the extracellular matrix with the cytoskeleton and is capable of transmitting signals[83]. Primarily found in focal adhesions it is described to be pivotal to activate signalling pathways which lead to differentiation, angiogenesis, proliferation and cytoskeleton rearrangements among others[81]. Our findings suggest that integrin-β_1 is involved in the detachment of the cells from the culture flask. The ECM is also involved in tissue polarity and architecture. Integrin-β_1 maintains this polarity in the mammary gland[84]. The integrins' extracellular interaction with the ECM and intracellular interactions with the cellular cytoskeleton, are examples of cellular mechano-transducers[85].

It has been shown that an abnormal ECM promotes the formation of a tumor microenvironment and plays a role in tumor angiogenesis. ECM components are involved in vessel formation and ECM fragments deriving from collagen type IV and others can influence angiogenesis. They interact with angiogenesis signaling factors including VEGF to initiate vascular branching[84].

In this study, the expression and release of VEGF after a 4 h-, 24 h- and 5d-RPM-exposure was significantly reduced compared to the corresponding controls. This is in concert to previous experiments using thyroid cancer cells which presented a decrease in VEGF, however, experiments using endothelial cells presented an upregulation of VEGF[10,26,50,86]. Its signaling pathways control survival, proliferation, and migration and actin reorganization among others[87]. Their interruptions may have beneficial effects to cancer patients[88]. VEGFR1 expression was not altered, while VEGFR2 presented a down-regulation in both 5-day-populations. This suggests that the VEGFR2 is the more important VEGF receptor, when MCF-7 cells react to microgravity. Binding of VEGF to VEGFR activates MAPK and Akt1 pathway which are responsible to control proliferation and survival[89]. *Akt1* gene expression was not altered after a 5-day-exposure, however, the downstream signalling molecules caspase-9 and caspase-3 were significantly down-regulated which can hint to a higher survival rate as less protein was produced. This finding indicates a higher survival rate of adherent cells compared to the cells accumulated to MCS. The MAPK/ERK pathway inherits PRKCA and downstream ERK1/ERK2 controlling proliferation among others. *PRKCA* as well as *ERK1* were down-regulated after 5 days on the RPM. Taken together, the VEGF-dependent pathways do not seem to be the dominant driving force, when MCF-7 cells transit from the 2D to 3D kind of growth.

Instead of VEGFA, IL-8 could be a potential key-player, as it is capable of acting on a variety of different cell types while being elevated in some tumour types[47] (Fig. 4). IL-8 expression is associated with a higher invasiveness potential of breast cancer cells *in vitro*, proposing IL-8 as a novel marker of tumor aggressiveness[90].

IL-8 is involved in 3D-aggregate-formation in thyroid cancer cells[47]. In this study, we found the *IL8* gene expression to be elevated after 2 h and 4 h in RPM-exposed adherent cells, then after 24 h up-regulated in MCS, but later unaltered in AD and slightly decreased in MCS after a 5d-exposure. IL-8 has recently been shown to modulate breast cancer invasion and angiogenesis[91]. Further studies will be performed to increase our knowledge of its role in 3D formation.

Also the *RhoA* gene expression does not seem to be involved in the alteration of growth of MCF-7 cells, because its gene was unaltered as compared to the 1 *g*-controls after a 5-RPM-exposure. Further experiments are required to descramble the network of regulation of genes and proteins triggering MCS formation in MCF-7 cells.

Conclusion

The exposure of human cells to simulated microgravity conditions created by an RPM has an enormous influence on their morphology and biology. It seems, that upon cultivation on the RPM the cells transform from monolayer into their *in vivo* typical 3D tissues. The formation of multicellular spheroids of MCF-7 breast cancer cells after RPM-exposure starting between 16 and 24 h is an important finding. After a 5d-RPM-exposure glandular structures are visible. In this process, disconnecting and reconnecting cell-cell connections as well as a strong regulation of the cell shape appear important. It has to be clarified in the future, whether gravity influences human cancer cells directly or indirectly. The non-equilibrium theory may explain how the cytoskeleton is sensitive enough to sense gravity changes, and induces the transfer of the mechano-signal into biochemical pathways[46]. Recently, it was shown that during a rocket flight and a parabolic flight live cell imaging of LifeAct-GFP-transfected thyroid cancer cells revealed significant alterations of the cytoskeleton related to microgravity[92]. Life-cell imaging during microgravity proved early changes in the actin cytoskeleton in real microgravity, which was described earlier on fixed cells.

Future investigations, using additional growth factors for histological and functional investigations, will show, if cultivation of normal breast cells on the RPM can produce functionally active breast tissues. Furthermore, impending studies should further investigate the possiblity of using fibronectin and IL8 as novel future targets in the treatment of breast cancer.

Methods

Cell culture. MCF-7 human breast adenocarcinoma cells were purchased from the American Type Culture Collection (MCF7 (ATCC® HTB-22™)) and cultivated in RPMI 1640 (Life Technologies, Naerum, Denmark) medium supplemented with 10% fetal calf serum (FCS) (Biochrom AG, Berlin, Germany) and 1% penicillin/ streptomycin (Life Technologies) and maintained under standard cell culture conditions at 37 °C and 5% CO_2. One day prior to the RPM experiment, 1×10^6 cells were counted and seeded into T25 cm^2 vented cell culture flasks (Sarstedt, Newton, USA) or 2.5×10^5 cells were seeded into slide flasks (Thermo Scientific, Roskilde, Denmark) for F-actin cytoskeleton investigations. Each flask was completely filled with medium, taking care that no air bubbles remained in the cell culture flasks. The flasks were installed on the centre plate of the RPM and run for 2 h (n = 30), 4 h (n = 30), 16 h (n = 30), 24 h (n = 30) and 5d (n = 30) respectively using the real random mode. 1 *g*-static controls were prepared in parallel (n = 30 each group) and stored next to the device in the same incubator.

After each time point the cells were investigated by phase contrast microscopy and photographed. The supernatant was collected and centrifuged at 4 °C to collect the MCS. After centrifugation the supernatant was collected for cytokine investigation on ice and then frozen at −20 °C. The MCS were collected and stored in liquid nitrogen.

For harvesting the adherent cells, 5 ml of ice-cold phosphate buffered saline (PBS) (Life Technologies) was carefully added to each T25 cm^2 flask and the cells were scraped off with a scraper. The cell suspension was collected and centrifuged at 4 °C. The PBS was discarded and the dry pellet was stored in liquid nitrogen.

Random Positioning Machine (RPM). The RPM (ADS, former Dutch Space, Leiden, Netherlands) was run in a commercially available incubator at 37 °C and 5% CO_2. The method was intensively investigated and published earlier[5,6,10,26]. Mode of choice was the real random mode with random speed and random interval and a maximum speed of 75°/s. 15 T25 cm^2 flasks were fixed to the operating platform, resulting in a maximal distance of 7.5 cm to the rotation axis, and were rotated for the selected time periods respectivly. Static, non-rotated controls were exposed to the same environmental conditions nearby the device.

Phase contrast microscopy. Phase contrast microscopy was performed for visual observation of the morphology of the cells, using a Leica (Microsystems GmbH, Wetzlar, Germany). Pictures had been taken by a Canon EOS 550D (Canon GmbH, Krefeld, Germany).

F-actin cytoskeleton staining. Cells exposed for 2 h, 4 h, 16 h, 24 h and 5d to the RPM in slideflasks were investigated. F-actin was visualized by means of rhodamine-phalloidin staining (Molecular Probes®, Eugene, OR, USA). In addition, the nuclei were stained with 4′,6-diamidino-2-phenylindole (DAPI, Life Technologies). The method was described earlier in detail[47,93].

Hematoxylin-Eosin and Periodic acid–Schiff staining. After a 5d-RPM-culture of MCF-7 cells, the MCS were collected, three times carefully washed in PBS and fixed in 4% paraformaldehyde. The MCS were embedded in paraffin[94] and sectioned with a microtome. The MCS were cut into 3 μm sections. Hematoxylin and eosin stains were used to evaluate the cell morphology and polarity of the breast cancer cells. In addition, the Periodic acid-Schiff (PAS) was applied to investigate the cellular basement membranes of the MCS cells. All sections were visualized by light microscopy using an oil immersion objective with a calibrated magnification of ×400.

Protein	Dilution	Company
β-actin	1:1000	Cell Signaling Technology, Inc., Danvers, MA, USA
β-tubulin	1:100	Sigma Aldrich, St. Louis, MO, USA
Ezrin	1:1000	Cell Signaling Technology, Inc., Danvers, MA, USA
Fibronectin	1:1000	Sigma Aldrich, St. Louis, MO, USA
GAPDH	1:1000	Cell Signaling Technology, Inc., Danvers, MA, USA
Integrin-b_1	1:1000	Cell Signaling Technology, Inc., Danvers, MA, USA
Keratin	1:1000	Cell Signaling Technology, Inc., Danvers, MA, USA
Laminin	1:1000	Sigma Aldrich, St. Louis, MO, USA
Radixin	1:1000	Cell Signaling Technology, Inc., Danvers, MA, USA
VEGF	1:200	Abcam plc, Cambridge, UK

Table 2. Primary antibodies used for Western blot analyses.

NGAL and VEGF measurements. NGAL and VEGF levels were measured using in-house time resolved immunofluorometric assays (TRIFMA) according to previously described methods[7,95]. For all determinations, the supernatant samples were diluted 1:2 and the 96-well plates were read using a VICTOR 2030 (Perkin Elmer, Inc.) Standard curves were used to calculate the concentrations using the standard software implemented in the VICTOR 2030.

RNA and protein isolation and quantitative real-time PCR. RNA isolation and quantitative real-time PCR were performed according to routine protocols[7,25,94]. RNA and protein were isolated using the AllPrep RNA/Protein kit (Qiagen GmbH, Hilden, Germany) following the manufacturer's instructions. The RNA was quantified via the SpectraMax M2 (Molecular Devices, California, USA). Reverse transcription was performed using the First Strand cDNA Synthesis Kit (Thermo Scientific, Waltham, Massachusetts, USA) following manufacturer's instructions. Quantitative real-time PCR was utilized to determine the expression levels of target genes, shown in Table 1, using the SYBR® Select Master Mix (Applied Biosystems, Darmstadt, Germany) and the 7500 Real-Time PCR System (Applied Biosystems). cDNA-selective Primers were designed to span exon-exon boundaries and to have a Tm of 60 °C using Primer Express software (Applied Biosystems), and were synthesized by TIB Molbiol (Berlin, Germany). All samples were measured in triplicate and normalized to the housekeeper 18S rRNA. Comparative CT ($\Delta\Delta$CT) methods were used for relative quantification of transcription levels, with 1 g set as 100%.

Western blot analysis. Gel electrophoresis, trans-blotting, and densitometry were carried out following routine protocols as described previously[94]. 20 μL of lysate containing 2 μg/μL protein was loaded onto SDS-PAGE per sample. A total number of 5 samples were analyzed per cell population for 5 and 10 days respectively. Primary antibodies were applied as described in Table 2. HRP-linked, secondary antibody was used at a dilution of 1:3000 (Cell Signaling Technology, Inc., Danvers, MA, USA). A final analysis was performed in a ChemiDoc XRS+ (Bio Rad, Hercules, CA, USA). To quantify the bands desitometrically, the membranes were analysed using ImageJ software (U.S. National Institutes of Health, Bethesda, MD, USA).

Pathway Studio Analysis. Pathway Studio v11 was purchased from Elsevier Research Solutions, Amsterdam, Netherlands. This program was used online[96]. To start an analysis, the SwissProt numbers of the proteins of interest were entered[97].

Statistical Evaluation. All statistical analyses were performed using SPSS 21.0 (SPSS, Inc., Chicago, IL, USA, 2012). The data was analyzed with the Mann-Whitney U test. To account for multiple comparisons, a Kruskal-Wallis Test was performed beforehand, and Bonferroni corrections were applied. The data was expressed as means ± standard deviation (SD). Differences were considered significant at $p < 0.05$.

References

1. Ferlay, J. *et al.* Cancer incidence and mortality worldwide: sources, methods and major patterns in GLOBOCAN 2012. *Int. J. Cancer* **136,** E359–386, doi: 10.1002/ijc.29210 (2015).
2. Kristensen, T. B. *et al.* Anti-vascular endothelial growth factor therapy in breast cancer. *Int. J. Mol. Sci.* **15,** 23024–23041, doi: 10.3390/ijms151223024 (2014).
3. Grimm, D., Wehland, M., Pietsch, J., Infanger, M. & Bauer, J. Drugs interfering with apoptosis in breast cancer. *Curr. Pharm. Des.* **17,** 272–283, doi: 10.2174/138161211795049723 (2011).
4. Wehland, M., Bauer, J., Infanger, M. & Grimm, D. Target-based anti-angiogenic therapy in breast cancer. *Curr. Pharm. Des.* **18,** 4244–4257, doi: 10.2174/138161212802430468 (2012).
5. Pietsch, J. *et al.* A proteomic approach to analysing spheroid formation of two human thyroid cell lines cultured on a random positioning machine. *Proteomics* **11,** 2095–2104, doi: 10.1002/pmic.201000817 (2011).
6. Grosse, J. *et al.* Gravity-sensitive signaling drives 3-dimensional formation of multicellular thyroid cancer spheroids. *FASEB J.* **26,** 5124–5140, doi: 10.1096/fj.12-215749 (2012).
7. Kopp, S. *et al.* Mechanisms of three-dimensional growth of thyroid cells during long-term simulated microgravity. *Sci. Rep.* **5,** 16691, doi: 10.1038/srep16691 (2015).
8. Aleshcheva, G. *et al.* Scaffold-free tissue formation under real and simulated microgravity conditions. *Basic Clin. Pharmacol. Toxicol.*, doi: 10.1111/bcpt.12561 (2016).

9. Pietsch, J. *et al.* Spheroid formation of human thyroid cancer cells in an automated culturing system during the Shenzhou-8 Space mission. *Biomaterials* **34,** 7694–7705, doi: 10.1016/j.biomaterials.2013.06.054 (2013).

10. Warnke, E. *et al.* Spheroid formation of human thyroid cancer cells under simulated microgravity: a possible role of CTGF and CAV1. *Cell Commun. Signal.* **12,** 32, doi: 10.1186/1478-811X-12-32 (2014).

11. Kunz-Schughart, L. A. Multicellular tumor spheroids: intermediates between monolayer culture and *in vivo* tumor. *Cell Biol. Int.* **23,** 157–161, doi: 10.1006/cbir.1999.0384 (1999).

12. Hirschhaeuser, F. *et al.* Multicellular tumor spheroids: an underestimated tool is catching up again. *J. Biotechnol.* **148,** 3–15, doi: 10.1016/j.jbiotec.2010.01.012 (2010).

13. Grimm, D. *et al.* Growing tissues in real and simulated microgravity: new methods for tissue engineering. *Tissue Eng. Pt. B Rev.* **20,** 555–566, doi: 10.1089/ten.TEB.2013.0704 (2014).

14. Vassy, J. *et al.* The effect of weightlessness on cytoskeleton architecture and proliferation of human breast cancer cell line MCF-7. *FASEB J.* **15,** 1104–1106, doi: 10.1096/fj.00-0527fje (2001).

15. Qian, A. *et al.* Simulated weightlessness alters biological characteristics of human breast cancer cell line MCF-7. *Acta Astronaut.* **63,** 947–958, doi: http://dx.doi.org/10.1016/j.actaastro.2008.01.024 (2008).

16. Li, J. *et al.* Modeled microgravity causes changes in the cytoskeleton and focal adhesions, and decreases in migration in malignant human MCF-7 cells. *Protoplasma* **238,** 23–33, doi: 10.1007/s00709-009-0068-1 (2009).

17. Zheng, H.-X. *et al.* Expression of estrogen receptor α in human breast cancer cells regulates mitochondrial oxidative stress under simulated microgravity. *Adv. Space Res.* **49,** 1432–1440, doi: 10.1016/j.asr.2012.02.020 (2012).

18. Masiello, M. G. *et al.* Phenotypic switch induced by simulated microgravity on MDA-MB-231 breast cancer cells. *Biomed Res. Int.* **2014,** 652434, doi: 10.1155/2014/652434 (2014).

19. Wuest, S. L., Richard, S., Kopp, S., Grimm, D. & Egli, M. Simulated microgravity: critical review on the use of random positioning machines for mammalian cell culture. *Biomed Res. Int.* **2015,** 971474, doi: 10.1155/2015/971474 (2015).

20. Pietsch, J. *et al.* Metabolic enzyme diversity in different human thyroid cell lines and their sensitivity to gravitational forces. *Proteomics* **12,** 2539–2546, doi: 10.1002/pmic.201200070 (2012).

21. Soule, H. D., Vazguez, J., Long, A., Albert, S. & Brennan, M. A human cell line from a pleural effusion derived from a breast carcinoma. *J. Natl. Cancer Inst.* **51,** 1409–1416, doi: 10.1093/jnci/51.5.1409 (1973).

22. Pietsch, J. *et al.* The effects of weightlessness on the human organism and mammalian cells. *Curr. Mol. Med.* **11,** 350–364, doi: 10.2174/156652411795976600 (2011).

23. Suzuki, A. & Ohno, S. The PAR-aPKC system: lessons in polarity. *J. Cell Sci.* **119,** 979–987, doi: 10.1242/jcs.02898 (2006).

24. Ma, X. *et al.* Genomic approach to identify factors that drive the formation of three-dimensional structures by EA.hy926 endothelial cells. *PLoS One* **8,** e64402, doi: 10.1371/journal.pone.0064402 (2013).

25. Calo, E. & Khutoryanskiy, V. V. Biomedical applications of hydrogels: A review of patents and commercial products. *Eur. Polym. J.* **65,** 252–267, doi: 10.1016/j.eurpolymj.2014.11.024 (2015).

26. Ma, X. *et al.* Differential gene expression profile and altered cytokine secretion of thyroid cancer cells in space. *FASEB J.* **28,** 813–835, doi: 10.1096/fj.13-243287 (2014).

27. Bizzarri, M., Monici, M. & van Loon, J. J. How microgravity affects the biology of living systems. *Biomed Res. Int.* **2015,** 863075, doi: 10.1155/2015/863075 (2015).

28. Becker, J. L. & Souza, G. R. Using space-based investigations to inform cancer research on Earth. *Nat. Rev. Cancer* **13,** 315–327, doi: 10.1038/nrc3507 (2013).

29. Grimm, D. *et al.* A delayed type of three-dimensional growth of human endothelial cells under simulated weightlessness. *Tissue Eng. Pt. A* **15,** 2267–2275, doi: 10.1089/ten.tea.2008.0576 (2009).

30. Testa, F. *et al.* Fractal analysis of shape changes in murine osteoblasts cultured under simulated microgravity. *Rend Lincei-Sci Fis.* **25,** S39–S47, doi: 10.1007/s12210-014-0291-3 (2014).

31. Mesland, D. A. Possible actions of gravity on the cellular machinery. *Adv. Space Res.* **12,** 15–25, doi: 10.1016/0273-1177(92)90259-Z (1992).

32. Mesland, D. A. Mechanisms of gravity effects on cells: are there gravity-sensitive windows? *Adv. Space Biol. Med.* **2,** 211–228, doi: 10.1016/S1569-2574(08)60022-2 (1992).

33. Grimm, D., Wise, P., Lebert, M., Richter, P. & Baatout, S. How and why does the proteome respond to microgravity? *Expert Rev. Proteomics* **8,** 13–27, doi: 10.1586/epr.10.105 (2011).

34. Lewis, M. L. *et al.* Spaceflight alters microtubules and increases apoptosis in human lymphocytes (Jurkat). *FASEB J.* **12,** 1007–1018, doi: 0892-6638/98/0012-1007 (1998).

35. Hughes-Fulford, M. & Lewis, M. L. Effects of microgravity on osteoblast growth activation. *Exp. Cell Res.* **224,** 103–109, doi: 10.1006/excr.1996.0116 (1996).

36. Morbidelli, L. *et al.* Simulated hypogravity impairs the angiogenic response of endothelium by up-regulating apoptotic signals. *Biochem. Biophys. Res. Commun.* **334,** 491–499, doi: 10.1016/j.bbrc.2005.06.124 (2005).

37. Cogoli, A., Tschopp, A. & Fuchs-Bislin, P. Cell sensitivity to gravity. *Science* **225,** 228–230, doi: 10.1126/science.6729481 (1984).

38. Uva, B. M. *et al.* Clinorotation-induced weightlessness influences the cytoskeleton of glial cells in culture. *Brain Res.* **934,** 132–139, doi: 10.1016/S0006-8993(02)02415-0 (2002).

39. Grimm, D. *et al.* Simulated microgravity alters differentiation and increases apoptosis in human follicular thyroid carcinoma cells. *FASEB J.* **16,** 604–606, doi: 10.1096/fj.01-0673fje (2002).

40. Ulbrich, C. *et al.* Differential gene regulation under altered gravity conditions in follicular thyroid cancer cells: relationship between the extracellular matrix and the cytoskeleton. *Cell. Physiol. Biochem.* **28,** 185–198, doi: 10.1159/000331730 (2011).

41. Grosse, J. *et al.* Short-term weightlessness produced by parabolic flight maneuvers altered gene expression patterns in human endothelial cells. *FASEB J.* **26,** 639–655, doi: 10.1096/fj.11-194886 (2012).

42. Gruener, R., Roberts, R. & Reitstetter, R. Reduced receptor aggregation and altered cytoskeleton in cultured myocytes after space-flight. *Biol. Sci. Space* **8,** 79–93, doi: http://doi.org/10.2187/bss.8.79 (1994).

43. Lewis, M. L. *et al.* cDNA microarray reveals altered cytoskeletal gene expression in space-flown leukemic T lymphocytes (Jurkat). *FASEB J.* **15,** 1783–1785, doi: 10.1096/fj.00-0820fje (2001).

44. Vorselen, D., Roos, W. H., MacKintosh, F. C., Wuite, G. J. & van Loon, J. J. The role of the cytoskeleton in sensing changes in gravity by nonspecialized cells. *FASEB J.* **28,** 536–547, doi: 10.1096/fj.13-236356 (2014).

45. Boonstra, J. Growth factor-induced signal transduction in adherent mammalian cells is sensitive to gravity. *FASEB J.* **13** Suppl, S35–42, doi: 0892-6638/99/0013-0S35 (1999).

46. Bizzarri, M., Cucina, A., Palombo, A. & Masiello, M. G. Gravity sensing by cells: mechanisms and theoretical grounds. *Rend. Lincei-Sci. Fis.* **25,** S29–S38, doi: 10.1007/s12210-013-0281-x (2014).

47. Svejgaard, B. *et al.* Common Effects on Cancer Cells Exerted by a Random Positioning Machine and a 2D Clinostat. *PLoS One* **10,** e0135157, doi: 10.1371/journal.pone.0135157 (2015).

48. Grosse, J. *et al.* Mechanisms of apoptosis in irradiated and sunitinib-treated follicular thyroid cancer cells. *Apoptosis* **19,** 480–490, doi: 10.1007/s10495-013-0937-0 (2014).

49. Kondepudi, D. K. & Storm, P. B. Gravity detection through bifurcation. *Adv. Space Res.* **12,** 7–14, doi: 10.1016/0273-1177(92)90258-Y (1992).

50. Grimm, D. *et al.* Different responsiveness of endothelial cells to vascular endothelial growth factor and basic fibroblast growth factor added to culture media under gravity and simulated microgravity. *Tissue Eng. Pt. A* **16,** 1559–1573, doi: 10.1089/ten.TEA.2009.0524 (2010).

51. Ma, X. *et al.* Proteomic differences between microvascular endothelial cells and the EA.hy926 cell line forming three-dimensional structures. *Proteomics* **14,** 689–698, doi: 10.1002/pmic.201300453 (2014).

52. Plachot, C. *et al.* Factors necessary to produce basoapical polarity in human glandular epithelium formed in conventional and high-throughput three-dimensional culture: example of the breast epithelium. *BMC Biol.* **7,** 77, doi: 10.1186/1741-7007-7-77 (2009).

53. Debnath, J. *et al.* The role of apoptosis in creating and maintaining luminal space within normal and oncogene-expressing mammary acini. *Cell* **111,** 29–40, doi: http://dx.doi.org/10.1016/S0092-8674(02)01001-2 (2002).

54. Debnath, J. & Brugge, J. S. Modelling glandular epithelial cancers in three-dimensional cultures. *Nat. Rev. Cancer* **5,** 675–688, doi: 10.1038/nrc1695 (2005).

55. Vassy, J. *et al.* Weightlessness acts on human breast cancer cell line MCF-7. *Adv. Space Res.* **32,** 1595–1603, doi: 10.1016/S0273-1177(03)90400-5 (2003).

56. Ulbrich, C. *et al.* Characterization of human chondrocytes exposed to simulated microgravity. *Cell. Physiol. Biochem.* **25,** 551–560, doi: 10.1159/000303059 (2010).

57. Beck, M. *et al.* Simulated microgravity decreases apoptosis in fetal fibroblasts. *Int. J. Mol. Med.* **30,** 309–313, doi: 10.3892/ijmm.2012.1001 (2012).

58. Aleshcheva, G. *et al.* Tissue engineering of cartilage on ground-based facilities. *Microgravity Sci. Technol.* In press, doi: 10.1007/s12217-015-9479-0 (2016).

59. Russo, J., Hu, Y. F., Silva, I. D. & Russo, I. H. Cancer risk related to mammary gland structure and development. *Microsc. Res. Tech.* **52,** 204–223, doi: 10.1002/1097-0029(20010115)52:2<204::AID-JEMT1006>3.0.CO;2-F (2001).

60. Pisanu, M. E. *et al.* Lung cancer stem cell lose their stemness default state after exposure to microgravity. *Biomed Res. Int.* **2014,** 470253, doi: 10.1155/2014/470253 (2014).

61. Kenny, P. A. & Bissell, M. J. Tumor reversion: correction of malignant behavior by microenvironmental cues. *Int. J. Cancer* **107,** 688–695, doi: 10.1002/ijc.11491 (2003).

62. Vidi, P. A., Bissell, M. J. & Lelievre, S. A. Three-dimensional culture of human breast epithelial cells: the how and the why. *Methods Mol. Biol.* **945,** 193–219, doi: 10.1007/978-1-62703-125-7_13 (2013).

63. Nakamura, T. *et al.* E-cadherin-dependent intercellular adhesion enhances chemoresistance. *Int. J. Mol. Med.* **12,** 693–700, doi: 10.3892/ijmm.12.5.693 (2003).

64. Brouty-Boye, D., Mainguene, C., Magnien, V., Israel, L. & Beaupain, R. Fibroblast-mediated differentiation in human breast carcinoma cells (MCF-7) grown as nodules *in vitro*. *Int. J. Cancer* **56,** 731–735, doi: 10.1002/ijc.2910560520 (1994).

65. Kocaturk, B. *et al.* Alternatively spliced tissue factor synergizes with the estrogen receptor pathway in promoting breast cancer progression. *J. Thromb. Haemost.* **13,** 1683–1693, doi: 10.1111/jth.13049 (2015).

66. Mohammed, H. *et al.* Progesterone receptor modulates ERalpha action in breast cancer. *Nature* **523,** 313–317, doi: 10.1038/nature14583 (2015).

67. Infanger, M. *et al.* Simulated weightlessness changes the cytoskeleton and extracellular matrix proteins in papillary thyroid carcinoma cells. *Cell Tissue Res.* **324,** 267–277, doi: 10.1007/s00441-005-0142-8 (2006).

68. Tseng, L., Tang, M., Wang, Z. & Mazella, J. Progesterone receptor (hPR) upregulates the fibronectin promoter activity in human decidual fibroblasts. *DNA Cell Biol.* **22,** 633–640, doi: 10.1089/104454903770238102 (2003).

69. Chen, S. *et al.* Regulation of vascular endothelial growth factor expression by extra domain B segment of fibronectin in endothelial cells. *Invest. Ophthalmol. Vis. Sci.* **53,** 8333–8343, doi: 10.1167/iovs.12-9766 (2012).

70. Sandig, H. *et al.* Fibronectin is a TH1-specific molecule in human subjects. *J. Allergy Clin. Immunol.* **124,** 528–535, 535 e521–525, doi: 10.1016/j.jaci.2009.04.036 (2009).

71. Higashimoto, I., Chihara, J., Kawabata, M., Nakajima, S. & Osame, M. Adhesion to fibronectin regulates expression of intercellular adhesion molecule-1 on eosinophilic cells. *Int. Arch. Allergy Immunol.* **120** Suppl 1, 34–37, doi: 53591 (1999).

72. Orecchia, A. *et al.* Endothelial cell adhesion to soluble vascular endothelial growth factor receptor-1 triggers a cell dynamic and angiogenic phenotype. *FASEB J.* **28,** 692–704, doi: 10.1096/fj.12-225771 (2014).

73. Mainiero, F. *et al.* RAC1/P38 MAPK signaling pathway controls beta1 integrin-induced interleukin-8 production in human natural killer cells. *Immunity* **12,** 7–16, doi: 10.1016/S1074-7613(00)80154-5 (2000).

74. Nam, J. M., Onodera, Y., Bissell, M. J. & Park, C. C. Breast cancer cells in three-dimensional culture display an enhanced radioresponse after coordinate targeting of integrin alpha5beta1 and fibronectin. *Cancer Res.* **70,** 5238–5248, doi: 10.1158/0008-5472.CAN-09-2319 (2010).

75. Howe, E. N., Cochrane, D. R. & Richer, J. K. Targets of miR-200c mediate suppression of cell motility and anoikis resistance. *Breast Cancer Res.* **13,** R45, doi: 10.1186/bcr2867 (2011).

76. Fehon, R. G., McClatchey, A. I. & Bretscher, A. Organizing the cell cortex: the role of ERM proteins. *Nat. Rev. Mol. Cell Biol.* **11,** 276–287, doi: 10.1038/nrm2866 (2010).

77. Tsukita, S. & Yonemura, S. Cortical actin organization: lessons from ERM (ezrin/radixin/moesin) proteins. *J. Biol. Chem.* **274,** 34507–34510, doi: 10.1074/jbc.274.49.34507 (1999).

78. Thompson, P. W., Randi, A. M. & Ridley, A. J. Intercellular adhesion molecule (ICAM)-1, but not ICAM-2, activates RhoA and stimulates c-fos and rhoA transcription in endothelial cells. *J. Immunol.* **169,** 1007–1013, doi: 10.4049/jimmunol.169.2.1007 (2002).

79. Simpson, K. J. *et al.* Identification of genes that regulate epithelial cell migration using an siRNA screening approach. *Nat. Cell Biol.* **10,** 1027–1038, doi: 10.1038/ncb1762 (2008).

80. Vantangoli, M. M., Madnick, S. J., Huse, S. M., Weston, P. & Boekelheide, K. MCF-7 Human Breast Cancer Cells Form Differentiated Microtissues in Scaffold-Free Hydrogels. *PLoS One* **10,** e0135426, doi: 10.1371/journal.pone.0135426 (2015).

81. Hynes, R. O. Integrins: bidirectional, allosteric signaling machines. *Cell* **110,** 673–687, doi: 10.1016/S0092-8674(02)00971-6 (2002).

82. Halon, A., Donizy, P., Surowiak, P. & Matkowski, R. ERM/Rho protein expression in ductal breast cancer: a 15 year follow-up. *Cell. Oncol.* (*Dordr.*) **36,** 181–190, doi: 10.1007/s13402-013-0125-9 (2013).

83. Yeh, Y. C., Lin, H. H. & Tang, M. J. A tale of two collagen receptors, integrin beta1 and discoidin domain receptor 1, in epithelial cell differentiation. *Am. J. Physiol. Cell Physiol.* **303,** C1207–1217, doi: 10.1152/ajpcell.00253.2012 (2012).

84. Lu, P., Weaver, V. M. & Werb, Z. The extracellular matrix: a dynamic niche in cancer progression. *J. Cell Biol.* **196,** 395–406, doi: 10.1083/jcb.201102147 (2012).

85. Dvorak, H. F., Weaver, V. M., Tlsty, T. D. & Bergers, G. Tumor microenvironment and progression. *J. Surg. Oncol.* **103,** 468–474, doi: 10.1002/jso.21709 (2011).

86. Infanger, M. *et al.* Modeled gravitational unloading induced downregulation of endothelin-1 in human endothelial cells. *J. Cell. Biochem.* **101,** 1439–1455, doi: 10.1002/jcb.21261 (2007).

87. Ferrara, N., Gerber, H. P. & LeCouter, J. The biology of VEGF and its receptors. *Nat. Med.* **9,** 669–676, doi: 10.1038/nm0603-669 (2003).

88. Grimm, D., Bauer, J. & Schoenberger, J. Blockade of neoangiogenesis, a new and promising technique to control the growth of malignant tumors and their metastases. *Curr. Vasc. Pharmacol.* **7,** 347–357, doi: http://dx.doi.org/10.2174/157016109788340640 (2009).

89. Kowanetz, M. & Ferrara, N. Vascular endothelial growth factor signaling pathways: therapeutic perspective. *Clin. Cancer Res.* **12,** 5018–5022, doi: 10.1158/1078-0432.CCR-06-1520 (2006).

90. Freund, A. *et al.* IL-8 expression and its possible relationship with estrogen-receptor-negative status of breast cancer cells. *Oncogene* **22,** 256–265, doi: 10.1038/sj.onc.1206113 (2003).

91. Sankpal, N. V., Fleming, T. P. & Gillanders, W. E. EpCAM modulates NF-kappaB signaling and interleukin-8 expression in breast cancer. *Mol. Cancer Res.* **11,** 418–426, doi: 10.1158/1541-7786.MCR-12-0518 (2013).

92. Corydon, T. J. *et al.* Alterations of the cytoskeleton in human cells in space proved by life-cell imaging. *Sci. Rep.* **6,** 20043, doi: 10.1038/srep20043 (2016).

93. Aleshcheva, G. *et al.* Changes in morphology, gene expression and protein content in chondrocytes cultured on a random positioning machine. *PLoS One* **8,** e79057, doi: 10.1371/journal.pone.0079057 (2013).

94. Rothermund, L. *et al.* Early onset of chondroitin sulfate and osteopontin expression in angiotensin II-dependent left ventricular hypertrophy. *Am. J. Hypertens.* **15,** 644–652, doi: 10.1016/S0895-7061(02)02956-4 (2002).

95. Zhang, Y. *et al.* Lipocalin 2 expression and secretion is highly regulated by metabolic stress, cytokines, and nutrients in adipocytes. *PLoS One* **9,** e96997, doi: 10.1371/journal.pone.0096997 (2014).

96. Thomas, S. & Bonchev, D. A survey of current software for network analysis in molecular biology. *Human genomics* **4,** 353–360, doi: 10.1186/1479-7364-4-5-353 (2010).

97. Pietsch, J. *et al.* Interaction of proteins identified in human thyroid cells. *Int. J. Mol. Sci.* **14,** 1164–1178, doi: 10.3390/ijms14011164 (2013).

Acknowledgements

Author Contributions

D.G. and J.B. designed the study. S.K. guided with support of T.I., J.S. and L.S. the RPM experiments as well as the following microscopic and analytical procedures. S.K. and M.W. performed the qPCR measuremnts. N.M. performed the TRIFMAs. S.K., J.B., M.W., T.J.C. and D.G. drafted the manuscript. G.A. helped analyzing the westernblots. D.G., M.I. and T.J.C. supervised the experiments.

Additional Information

How to cite this article: Kopp, S. *et al.* Identifications of novel mechanisms in breast cancer cells involving duct-like multicellular spheroid formation after exposure to the Random Positioning Machine. *Sci. Rep.* **6,** 26887; doi: 10.1038/srep26887 (2016).

11.4 Publication #4

Kopp S, Islam T, Bauer J, Corydon TJ, Schulz H, Saar K, Hübner N, Slumstrup L, Sahana J, Wehland M, Infanger M, Lützenberg R, Grimm D**.** The role of NF-κB in spheroid formation of human breast cancer cells cultured on the Random Positioning Machine. Sci Rep. 2018 Jan 17;8:921. doi:10.1038/s41598-017-18556-8.

SCIENTIFIC REP**O**RTS

The role of NFκB in spheroid formation of human breast cancer cells cultured on the Random Positioning Machine

Sascha Kopp[1], Jayashree Sahana[2], Tawhidul Islam[2], Asbjørn Graver Petersen[2], Johann Bauer[3], Thomas J. Corydon [2,4], Herbert Schulz[5], Kathrin Saar[6], Norbert Huebner[6], Lasse Slumstrup[2], Stefan Riwaldt[2], Markus Wehland[1], Manfred Infanger[1], Ronald Luetzenberg[1] & Daniela Grimm[1,2]

Human MCF-7 breast cancer cells were exposed to a Random Positioning Machine (RPM). After 24 hours (h) the cells grew either adherently within a monolayer (AD) or within multicellular spheroids (MCS). AD and MCS populations were separately harvested, their cellular differences were determined performing qPCR on genes, which were differently expressed in AD and MCS cells. Gene array technology was applied to detect RPM-sensitive genes in MCF-7 cells after 24 h. Furthermore, the capability to form multicellular spheroids *in vitro* was compared with the intracellular distribution of NF-kappaB (NFκB) p65. NFκB was equally distributed in static control cells, but predominantly localized in the cytoplasm in AD cells and nucleus in MCS cells exposed to the RPM. Gene array analyses revealed a more than 2-fold change of only 23 genes including some whose products are affected by oxygen levels or regulate glycolysis. Significant upregulations of the mRNAs of enzymes degrading heme, of *ANXA1*, *ANXA2*, *CTGF*, *CAV2* and *ICAM1*, as well as of *FAS*, *Casp8*, *BAX*, *p53*, *CYC1* and *PARP1* were observed in MCS cells as compared with 1*g*-control and AD cells. An interaction analysis of 47 investigated genes suggested that *HMOX-1* and NFκB variants are activated, when multicellular spheroids are formed.

Exposing cells to devices like the Random Positioning Machine (RPM) triggers them to change their growth behavior together with a number of cellular characteristics[1,2]. This phenomenon has been observed for several types of human cells including thyroid cells, chondrocytes, endothelial cells, human breast cancer MDA-MB-231 cells and others[3–9]. We recently demonstrated that also human Michigan Cancer Foundation-7 (MCF-7) breast cancer cells form three-dimensional (3D) aggregates. Incubated on a RPM, a part of the cells switches from a two-dimensional (2D) growth within a monolayer to a 3D growth within multicellular spheroids (MCS), the other one remains adherent and continues growing within a monolayer (AD)[10]. The occurrence of MCS begins within 24 h on the RPM[10]. After a five-day RPM-exposure, spheroids were floating in the culture supernatant. At that time, the cells of the MCS have changed their gene expression pattern. Among other mRNAs, vascular endothelial growth factor-A (*VEGFA*), vascular endothelial growth factor receptor 2 (*FLK1*), caspase-9 (*Casp9*), caspase-3 (*Casp3*), and protein kinase C alpha (*PRKCA*) mRNAs were downregulated in five-day MCS-samples indicating their involvement in 3D aggregation.

Isochronally with 3D aggregation, microgravity-induced apoptosis was detected in breast cancer cells[6] like it has been observed in other types of cells[11–13]. In addition, FTC-133 thyroid cancer cells exposed to the RPM for 24 h formed spheroids and exhibited simultaneously enhanced levels of apoptosis and of NFκB proteins as compared with 1*g*-control cells[14]. NFκB incorporates a variety of transcriptional regulatory functions and is known to be of great importance in apoptosis[15]. It is inactivated by binding to IκB (inhibitor of NFκB). However,

[1]Clinic for Plastic, Aesthetic and Hand Surgery, Otto-von-Guericke-University Magdeburg, D-39120, Magdeburg, Germany. [2]Department of Biomedicine, Aarhus University, Wilhelm Meyers Allé 4, DK-8000, Aarhus C, Denmark. [3]Max-Planck Institute of Biochemistry, D-82152, Martinsried, Germany. [4]Department of Ophthalmology, Aarhus University Hospital, DK-8000, Aarhus C, Denmark. [5]Cologne Center for Genomics, University of Cologne, D-50931, Cologne, Germany. [6]Max-Delbrück-Center for Molecular Medicine, D-13092, Berlin-Buch, Germany. Correspondence and requests for materials should be addressed to D.G. (email: dgg@biomed.au.dk)

degradation of IκB can result in a translocation of NFκB into the nucleus, where it can activate the transcription of anti-apoptotic genes[16]. In a recent deep proteome analysis the translocation inhibitor IκBKB showed up in AD cells after culturing FTC-133 cells on the RPM, but could not be detected in MCS cells of the same culture flask[17,18]. These observations created the idea that a link between spheroid formation, initiation of apoptosis and NFκB expression may exist[14]. In addition, Becker-Weimann *et al*. postulated a link between NFκB expression and 3D organization of human breast cancer cells[19].

Therefore, the principal aim of this paper was to investigate the early phases of RPM-exposure (24 h) of MCF-7 breast cancer cells and to test whether there is a link between enhancement of apoptosis, changes in NFκB expression and spheroid formation. In a first approach, we exposed MCF-7 breast cancer cells for 24 h to the RPM. Afterwards, we analyzed the intracellular distribution and expression of NFκB by means of gene array analyses as well as quantitative (q)PCR focusing on genes involved in apoptosis and cell adhesion signaling and known to play a role in spheroid formation of human thyroid cells[14]. Furthermore, morphological and molecular biological results were compared. These experiments should increase the knowledge about mechanisms of the self-reliant formation of tissue-comparable cell-aggregates. Finding molecules in various cell types, which mediate a microgravity-dependent cell organization in equal ways, may indicate new targets to improve tissue engineering and cancer treatment. In a further step, we investigated the impact of the poly ADP ribose polymerase (PARP) inhibitor olaparib, the effect of dexamethasone (DEX) and the phosphodiesterase-4 (PDE-4) inhibitor rolipram on spheroid formation.

Results

After MCF-7 human breast adenocarcinoma cells had been cultured on the RPM for 24 h, we detected two different phenotypes: Cells growing adherently within a 2D monolayer (AD) and cells growing in form of 3D aggregates exhibiting no glandular structures after this short-term exposure. The MCS had various sizes (max. 300 μm) and were floating in the supernatant (Fig. 1B). In the corresponding controls incubated under normal 1*g*-conditions only cells growing in 2D monolayers could be seen (Fig. 1A). The cells growing three-dimensionally in form of MCS were viable. This was demonstrated by testing the adhesion of the MCS (Fig. 1C) on slide flasks and by the migration behavior of the cells clearly seen at 4 h of incubation (Fig. 1D). After 24 h a large number of cells are migrating out of the MCS (Fig. 1E). In addition, acridine orange/ethidium bromide staining showed that MCS cells were viable and impermeable to the dye (Fig. 1G; green fluorescence) like the RPM AD cells (Fig. 1G; insert) and the 1*g*-control MCF-7 cells (Fig. 1F). In case of dead or necrotic cells, the cells would have taken up the dye and shown a red fluorescence. This is demonstrated in the insert of Fig. 1F, where red cells are visible when stained living cells are kept without medium under the microscope for another 5 min and photographed afterwards.

Effect of RPM-exposure on NFκB. In order to see, whether the NFκB-p65 location and content of MCF-7 cells is like that of FTC-133 follicular thyroid cancer cells[14] involved in the cellular processes taking place during the first 24 h of RPM-exposure, we performed a NFκB-p65 immunofluorescence staining and Western blot analyses. The antibodies used are listed in Table 1. The Fig. 1H and I reveal MCF-7 cells stained for NFκB-p65. It can be seen that NFκB-p65 is equally distributed in the cytoplasm of cells cultured under static 1*g*-conditions (Fig. 1H). After a 24-hour RPM-exposure NFκB-p65 protein appeared in the nucleus of MCS cells (Fig. 1I; upper insert). Fluorescence brightness shown in the upper and lower inserts of Fig. 1I suggested more NFκB-p65 in the nucleus and cytoplasm of MCS cells than in the cytoplasm of adherent cells exposed to the RPM.

NFκB proteins comprise different variants including NFκB-p50, -p52 and -p65. They are encoded by the gene loci *NFKB1*, *2* and *3*. The various proteins form dimeric transcription factors that regulate the expression of genes influencing a broad range of biological processes[20–22]. NFκB proteins are bound and inhibited by IκB proteins. Both, effectors and inhibitors may be activated by external signals, which trigger expression, phosphorylation and dimerization of various components as well as their translocation from the cytoplasm to nucleus, where it binds to specific DNA sequences (response elements). In order to investigate whether the differences in localization and amount of NFκB-p65 observed in Fig. 1H and I are only due to a re-distribution or are also due to a new synthesis of NFκB-p65 proteins, we performed qPCR of the *NFKB1*, *NFKB2*, *NFKB3*, *NFKBIA*, *NFKBIB*, *NFKBIE and NFKBG* genes (Fig. 2). Figure 2D,F,L indicate a tendency of a non-significant upregulation of *NFKB2*, *NFKB3*, *NFKBIB* genes under simulated microgravity (s-μ*g*) in AD cells and especially in MCS, while Fig. 2A,I,M,N show a significant upregulation of *NFKB1*, *NFKBIA*, *NFKBIE and NFKBG* genes in MCS cells as compared to control cells. In AD cells only the *IKBKG* gene is significantly enhanced in comparison to the control cells. In general, the Western blot analyses performed on the same group as the qPCR, point in a similar direction as the corresponding gene expression pattern along with the corresponding un-phosphorylated proteins (Fig. 2B,G,J). Interestingly, the phosphorylated (p−) variants of the proteins are enhanced mainly in RPM-exposed cells (Fig. 2C,E,H). Hence, a significant phosphorylation of NFκB proteins during MCS formation on the RPM may be considered.

Genes of factors known to be involved in spheroid formation. Because the growth behavior, *NFKB3* gene expression and NFκB p65 protein accumulation were similar in FTC-133 and MCF-7 cells, we investigated the expression of other genes, which are assumed to play a role in the formation of 3D aggregates of human cancer cells[14,23]. The primers used are listed in Table 2. The gene expression status was studied after 24 h by qPCR in 1*g*-control cells, AD and MCS cells comparatively. These qPCR experiments revealed: The gene expression of annexin A1 (*ANXA1*) and annexin A2 (*ANXA2*) were significantly upregulated in MCS compared to 1*g*-control cells, while their expression was unregulated in AD samples (Fig. 3A,B). In addition, caveolin-2 (*CAV2*) and intercellular adhesion molecule 1 (*ICAM1*) mRNAs were both elevated in MCS. The expression was significantly upregulated in MCS compared to the corresponding 1*g*-controls (Fig. 3C,H). In contrast to *CAV2*, the connective tissue growth factor (*CTGF*) gene expression was significantly upregulated in AD as well as in MCS samples (Fig. 3D).
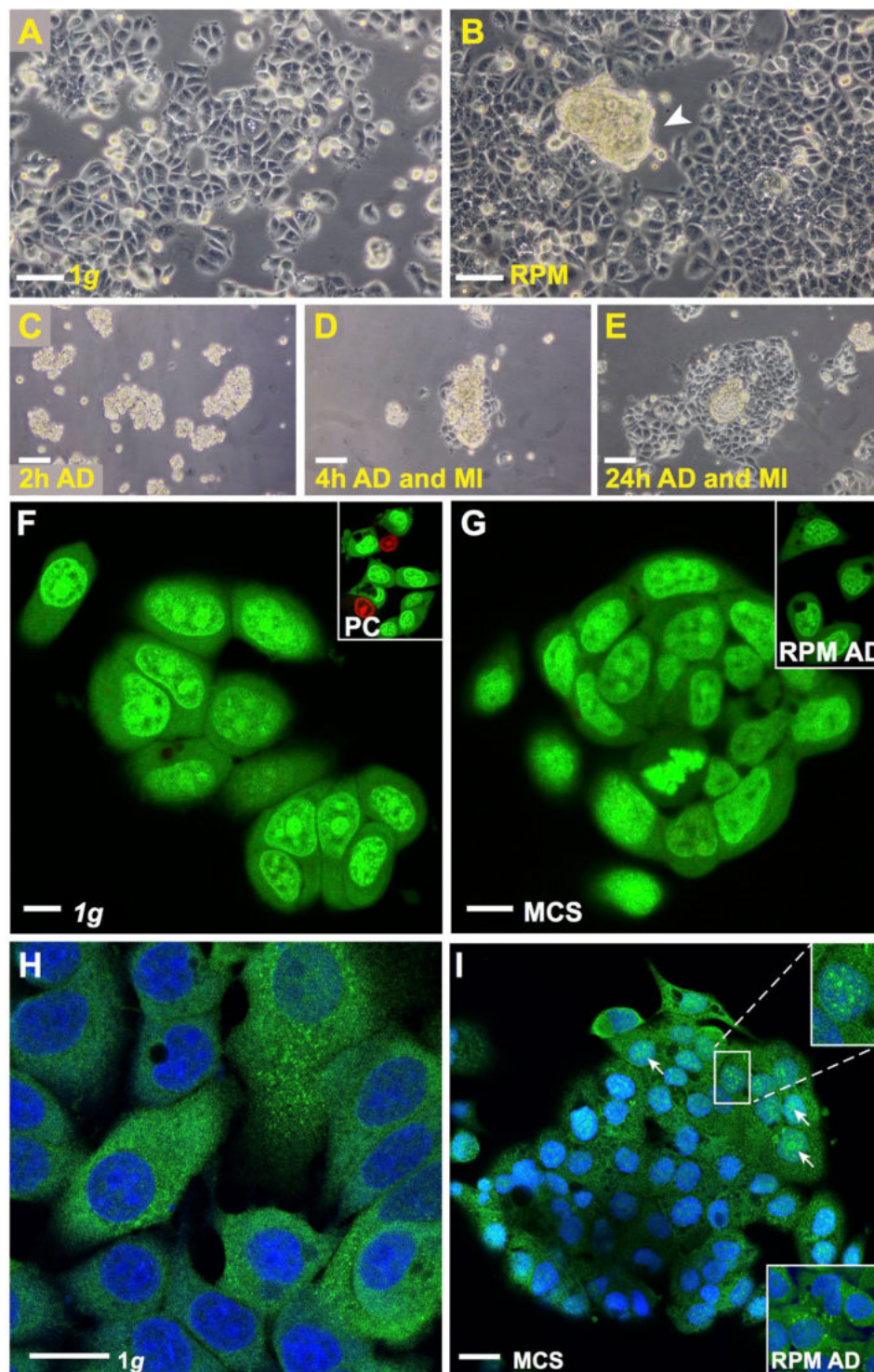
Figure 1. (**A–E**) Phase contrast microscopy: (**A**) Native MCF-7 cells cultured for 24 h under 1*g*-conditions. (**B**) RPM-exposed sample showing two phenotypes (adherently growing MCF-7 cells and MCS). A representative example of a MCS is indicated by the white arrowhead. (**C**) Adhesion of MCS to the bottom of a slide flask after 2 h. (**D**) Migration of MCF-7 cells out of the MCS after 4 h and (**E**) Migration of MCF-7 cells out of the MCS after 24 h. (**F–I**) Confocal laser scanning microscopy: (**F,G**) Acridine orange/ethidium bromide staining revealed a green fluorescence in all cells after 24 h which indicates viability. (**F**) 1*g*-conditions (insert: positive control (PC) of acridine orange/ethidium bromide assay after approximately 5 min incubation). (**G**) viable cells in the MCS (insert: viable RPM-AD cells). (**H**) NFκB immunofluorescence staining of 1*g*-control cells: NFκB is predominantly detectable in the cytoplasm and I: RPM-exposed samples: nuclear (white arrows) and cytoplasmatic NFκB in the MCS. Upper insert: magnification of indicated area. Lower insert: NFκB detection in RPM AD cells, same magnification as in I. Nuclei are counterstained with DAPI. Scale bars in (**A–E**) 100 μm; scale bars in (**F,G**) 10 μm; scale bars in (**H** and **I**): 20 μm. 5 samples of each condition were examined separately.

Antibody	Dilution	Company	Molecular weight	Catalog Number
p-NFκB p50	1/1000	Thermo Fisher	50 kDa	#710460
p-NFκB p52	1/1000	Thermo Fisher	110 kDa	#PA5-17385
Anti-NFκB p105/p50	1/1000	Abcam	50, 100 kDa	#ab32360
Anti-p-NFκB p65	1/1000	Abcam	70 kDa	#ab86299
Anti-IκBα	1/1000	Cell-Signaling	39 kDa	#9242
Anti-p-IκBα	1/1000	Cell-Signaling	40 kDa	#2859
Anti-NFκBp65	1/1000	Cell-Signaling	65 kDa	#C22B4
Anti-Cofilin	1/1000	Abcam	19 kDa	#ab124979

Table 1. Antibodies applied for Western blot Analysis.

Both, tissue inhibitor of metalloproteinases 1 (*TIMP1*) and plasminogen activator inhibitor 1 (*PAI1*) mRNAs were not significantly regulated, however, a tendency of an upregulation in AD and MCS was visible (Fig. 3E,F). Both factors inhibit metalloproteinases including metalloproteinase 9 (MMP9), whose mRNA was not significantly regulated (Fig. 3G).

Additional genes involved in intrinsic and extrinsic pathways of programmed cell death, were selected, because apoptosis was found repeatedly to accompany cell response to removing gravity[1,5,11,14]. *Casp3* and *Casp9* mRNAs were not significantly changed in AD and MCS compared to their corresponding controls (Fig. 4B,D). However, only MCS versus control showed a significant upregulation of caspase-8 (*Casp8*) (Fig. 4C). Furthermore, the cellular tumor antigen p53 (*p53*) gene expression was significantly enhanced in MCS versus control cells (Fig. 4G). The cytochrome c1 (*CYC1*), poly(ADP-ribose)-polymerase 1 (*PARP1*) (Fig. 4H,I) and tumor necrosis factor receptor superfamily member (*FAS*) mRNAs (Fig. 4A) were upregulated in MCS samples compared to the control group. In addition, the apoptosis regulator Bcl-2 (*BCL2*) mRNA remained unregulated in AD and MCS cells (Fig. 4E). In contrast, the apoptosis regulator BAX (*BAX*) gene expression was significantly upregulated in AD and MCS samples compared to the control cells (Fig. 4F). However, many of them exhibited significant regulations in at least one of the three possible permutations of gene expression comparisons between our experimental groups.

Microarray analysis. In order to detect further genes, which change their expression activity, during the first 24 h of culturing MCF-7 cells on the RPM, we performed microarray analyses on 1*g*-control, AD and MCS cells (Fig. 5A). The microarray analysis (Table 3 and Supplemental Table 1) did not show a significant microgravity-dependent change in *NFκB-p65* expression. Moreover, it revealed a rather stable mRNA expression pattern. In total 319 genes (331 probes, 330 probes annotated to 319 genes) transcripts were significantly differentially expressed (5% false discovery rate (FDR) in Analysis of variance (ANOVA)). In the pairwise comparison of control cells, AD and MCS, the expression of 140 significantly differentially expressed genes and open reading frames was changed 1.4-fold (Supplemental Table 1). However, a two- or more-fold change of the mRNA was merely found in 23 genes (Table 3). As a two- or more-fold change is usually considered to indicate biological relevance, we studied these genes in more detail.

19 of the genes were downregulated more than two-fold and 4 genes were upregulated at least two-fold (Table 3). 10 of the down-regulated genes code for proteins linked to oxygen levels or hypoxia[24–30]. The degree of downregulation of the expression of these genes was very similar in AD and MCS cells. But myristoylated alanine-rich C-kinase substrate (*MARCKS*), which codes for an actin interacting protein, is more significantly (5% FDR ANOVA) downregulated in MCS than in AD cells[31]. A more profound difference between AD and MCS cells was seen, when the upregulated genes were analyzed, which code for the cytoskeletal protein gamma-enteric smooth muscle actin (ACTG) and additional three proteins suppressing apoptosis and regulating the concentration of heme, which influences apoptosis[32–34]. All 4 genes indicated were significantly upregulated (>2 fold) only in MCS cells (Table 3).

Because 10 of the 19 genes found significantly downregulated are related to oxygen homeostasis, we applied the Pathway Studio analysis to see whether there is an interaction between them (Figs 6 and 7). Interestingly, we did not see significant interactions of these factors, neither at protein nor at gene level. Interaction at gene and protein level was, however, detected, when all 23 factors shown in Table 3 were analyzed. A cross-linking goes through 7 of the 23 genes (Fig. 5B) which code for 3 extracellular, 1 membrane, 5 nuclear, 2 mitochondrial and 12 cytosolic proteins (see also Fig. 7, Table 3). Hemoxygenase (*HMOX1*) is the most networked gene.

In order to examine, whether the genes determined by qPCR as upregulated in MCS cells interact with the differentially expressed genes detected in the gene array analysis, we subjected the experimental results to the Pathway studio analysis. The candidates comprised 41 items including RELA (NFKB3) and Hemox-1. They completed a complicated network consisting of 31 of the 41 factors at gene (Fig. 6) and protein levels (Fig. 7). Figures 5 and 6 indicate that the genes recognized before to be important in spheroid formation and the genes noticed in gene array analysis very well fit into the networks (see also Table 3). *HMOX1* and *RELA* show strong interaction at a genetic level (Fig. 6), but no mutual influence has so far been detected on the protein level (Fig. 7). In addition, the *ICAM1* gene, which codes for a cell adhesion protein is under the positive influence of upregulated genes such as *FAS*, *PARP1*, *P53*, *CTGF*, and *NFKB1*, but may be suppressed by caspase-3. Besides of *CTGF*, these genes are significantly upregulated only in MCS cells.
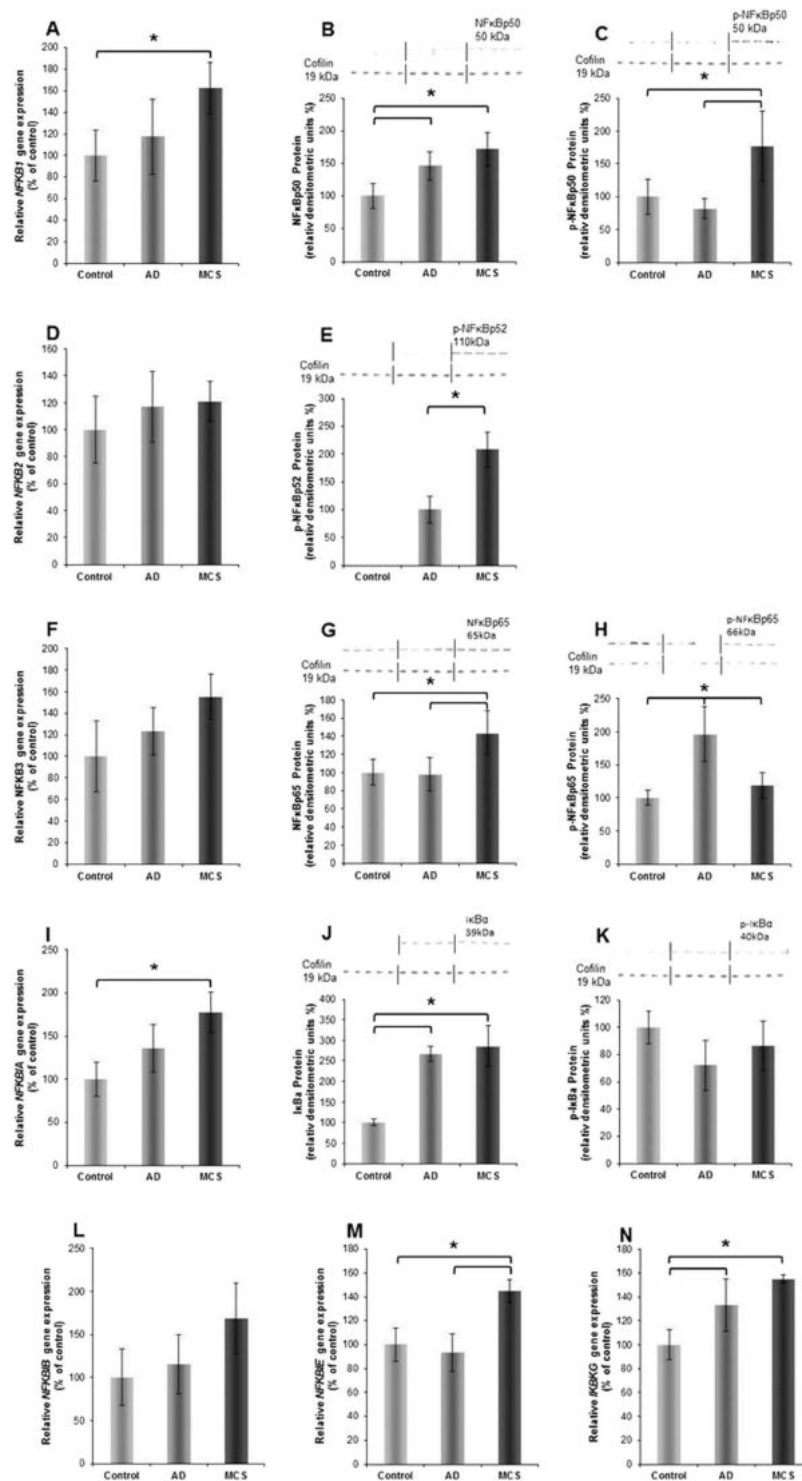
Figure 2. (**A**) *NFKB1* gene expression; (**B**) NFkBp50 Western blot analysis; (**C**) phosphorylated (p)-NFκBp50 Western blot analysis; (**D**) *NFKB2* gene expression; (**E**) p-NFκBp52 Western blot analysis; (**F**) *NFKB3* gene expression; (**G**) NFκBp65 Western blot analysis; (**H**) p-NFkBp65 Western blot analysis; (**I**) *NFKBIA* gene expression; (**J**) IκBα Western blot analysis; (**K**) p- IκBβ Western blot analysis; (**L**) *NFKBIB* gene expression; (**M**) *NFKBIE* gene expression; (**N**) *IKBKG* gene expression. The position (arrow) and molecular size (in kD) of the investigated proteins are indicated on each of the Western blot membrane images. Cofilin 1 was used as loading control. The vertical lines indicate group separation giving n = 5 per group.

Impact of targeting PARP and NFκB on spheroid formation. In order to evaluate the functional effects of PARP and NFκB, we performed inhibition assessments using the drugs olaparib, dexamethasone (DEX) and rolipram. Figure 8 shows the target proteins of the three drugs. According to a STITCH 4 database search

Factor	Primer name	Sequence 5′ - 3′
18 S	*18S-F*	GGAGCCTGCGGCTTAATTT
	18S-R	CAACTAAGAACGGCCATGCA
Annexin A1; *ANXA1*	*ANXA1-F*	GCCAAAGACATAACCTCAGACACAT
	ANXA1-R	GAATCAGCCAAGTCTTCATTCACA
Annexin A2; *ANXA2*	*ANXA2-F*	GGTACAAGAGTTACAGCCCTTATGACA
	ANXA2-R	CATGGAGTCATACAGCCGATCA
Apoptosis Regulator BAX; *BAX*	*BAX-F*	GTCAGCTGCCACTCGGAAA
	BAX-R	AGTAACATGGAGCTGCAGAGGAT
Apoptosis Regulator BCL-2; *BCL2*	*BCL2-F*	TCAGAGACAGCCAGGAGAAATCA
	BCL2-R	CCTGTGGATGACTGAGTACCTGAA
Caspase 3; *CASP3*	*Casp3-F*	CTCCAACATCGACTGTGAGAAGTT
	Casp3-R	GCGCCAGCTCCAGCAA
Caspase 8; *CASP8*	*Casp8-F*	TGCAAAAGCACGGGAGAAAG
	Casp8-R	CTCTTCAAAGGTCGTGGTCAAAG
Caspase 9; *CASP9*	*Casp9-F*	CTCCAACATCGACTGTGAGAAGTT
	Casp9-R	GCGCCAGCTCCAGCAA
Caveolin 2; *CAV2*	*Cav2-F*	GATCCCCACCGGCTCAAC
	Cav2-R	CACCGGCTCTGCGATCA
Connective Tissue Growth Factor; *CTGF*	*CTGF-F*	ACAAGGGCCTCTTCTGTGACTT
	CTGF-R	GGTACACCGTACCACCGAAGAT
Cytochrome C; *CYC*	*Cyc-F*	CACTGCGGGAAGGTCTCTAC
	Cyc-R	GGGGTGCCATCGTCAAACTC
NF-kappa-B transcription complex P105/P50; *NFKB1*	*NFkB1-F*	CTTAGGAGGGAGAGCCCAC
	NFkB1-R	TGAAACATTTGTTCAGGCCTTC
NF-kappa-B transcription complex P100/P52; *NFKB2*	*NFkB2-F*	GTACAAAGATACGCGGACCC
	NFkB2-R	CCAGACCTGGGTTGTAGCA
NF-kappa-B transcription complex P65	*NFkB-F*	CGCTTCTTCACACACTGGATTC
	NFkB-R	ACTGCCGGGATGGCTTCT
NF-kappa-B essential modulator (NEMO); *IKBKG*	*IkBKG-F*	AACTGGGACTTTCTCGGAGC
	IkBKG-R	GGCAAGGGCTGTCAGCAG
NF-kappa-B inhibitor alpha; *NFKBIA*	*NFkBIa-F*	AATGCTCAGGAGCCCTGTAAT
	NFkBIa-R	CTGTTGACATCAGCCCCACA
NF-kappa-B inhibitor beta; *NFKBIB*	*NFkBIb-F*	CCCGGAGGACCTGGGTT
	NFkBIb-R	GCAGTGCCGTGTCCCC
NF-kappa-B inhibitor epsilon; *NFKBIE*	*NFkBIe-F*	TGGGCATCTCATCCACTCTG
	NFkBIe-R	ACAAGGGATTCCTCAGTCAGGT
Tumor necrosis factor receptor superfamily member 6 (Fas); *FAS*	*CD95-F*	AGTCTGGTTCATCCCCATTGAC
	CD95-R	AGGGATTGGAATTGAGGAAGACT
Intercellular adhesion molecule 1; *ICAM1*	*ICAM1-F*	CGGCTGACGTGTGCAGTAAT
	ICAM1-R	CTTCTGAGACCTCTGGCTTCGT
Matrix metalloproteinase-9; *MMP9*	*MMP9-F*	CCTGGAGACCTGAGAACCAATC
	MMP9-R	TTCGACTCTCCACGCATCTCT
Cellular tumor antigen p53; *p53*	*p53-F*	CCTGGATTGGCCAGACTGC
	p53-R	TTTTCAGGAAGTAGTTTCCATAGGT
Plasminogen activator inhibitor 1; *PAI1*	*PAI1-F*	AGGCTGACTTCACGAGTCTTTCA
	PAI1-R	CACTCTCGTTCACCTCGATCTTC
Poly [ADP-ribose] polymerase 1; *PARP1*	*PARP1-F*	CGAGTCGAGTACGCCAAGAG
	PARP1-R	CATCAAACATGGGCGACTGC
Metalloproteinase inhibitor 1; *TIMP1*	*TIMP1-F*	GCCATCGCCGCAGATC
	TIMP1-R	GCTATCAGCCACAGCAACAACA

Table 2. Primers used for quantitative real-time PCR All sequences are given in the 5′–3′ direction.

(chemical-protein interaction networks; http://stitch.embl.de/), it can be assumed that DEX preferentially inhibits NROB1, NR3C1 and NR3C2 (Fig. 8, green bars), but has side effects cross-reacting with a couple of other factors including IL10 and CDK1 (Fig. 8). Similarly, olaparib inhibits PARP1 and PARP2 (Fig. 8, green bars) and has additional effects on other eight proteins (Fig. 8). Rolipram mainly blocks the action of PDE4A, PDE4B and PDE4D (Fig. 8, green bars). To some degree it also interacts with factors like IL6, IL10, APP, and FOS.
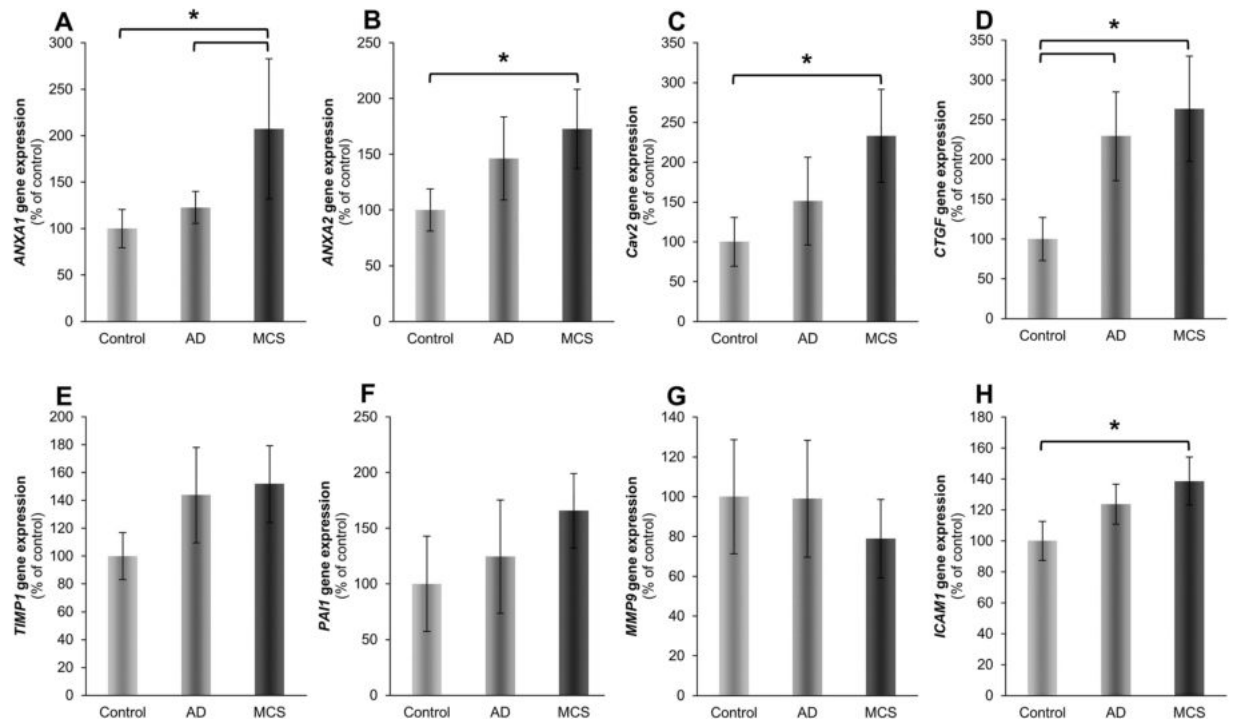
Figure 3. Expression of genes putatively involved in MCS-formation. (**A**) Annexin A1 (*ANXA1*), (**B**) Annexin A2 (*ANXA2*), (**C**) Caveolin-2 (*Cav2*), (**D**) Connective tissue growth factor (*CTGF*), (**E**) Metalloproteinase inhibitor 1 (*TIMP1*), (**F**) Plasminogen activator inhibitor 1 (*PAI1*), (**G**) Matrix metalloproteinase 9 (*MMP9*), (**H**) Intercellular adhesion molecule 1 (*ICAM1*), were analysed after 24 h of RPM-exposure. All values are given as mean ± standard deviation. *p < 0.05 vs. corresponding 1*g*-control. AD: adherent cells, MCS: multicellular spheroids, after RPM-exposure. Number of replicates is 4.

To determine the formation of spheroids when molecules of interest are inhibited, we treated the MCF-7 cells with various concentrations of olaparib (0 M, 2.5 μM, 5 μM and 10 μM), DEX (0 M, 0.01 μM, 0,1 μM, 1 μM) and rolipram (0 M, 1 μM, 10 μM), while exposed to the RPM for 24 h. To exclude toxic effects of the used solvent and/ or the drugs on the MCF-7 cells, we prepared 24 h static 1*g*-experiments with solvent and the mentioned drug concentrations (Supplemental Fig. 1). After a 24 hour-exposure, the cells were stained with acridine orange/ ethidium bromide to examine the cell viability (Supplemental Fig. 1). None of the used concentrations of solvent and drugs had a cytotoxic effect on the cells, as presented by the green staining, while no red staining of the nuclei was detectable (Supplemental Fig. 1). In addition, no increased cell detachment or formation of cell aggregates was noticed due to drug or solvent supplementation.

We exposed the MCF-7 cells to the RPM for 24 h including the drug concentrations mentioned. While treatment with olaparib and rolipram did not show visible effects on the formation of early spheroids (Fig. 9A–F,M–P), the number of visible MCSs seemed to decrease with increasing concentration of DEX (Fig. 9G–L). Acridine orange/ethidium bromide staining revealed viable cells in RPM-AD cells as well as in MCS (Supplemental Fig. 1N, arrow indicates a MCS).

Discussion

Organisms live on Earth under the permanent influence of gravity. Removing this influence results in remodeling of various tissues in humans. For example bone loss and muscle atrophy can be observed in astronauts and cosmonauts after long-term spaceflights[35]. In addition, various changes in different types of human cells were detected. Examples are macrophages producing less reactive oxygen in microgravity compared to 1*g*[36] and human thyroid cancer cells which form 3D cell aggregates, when cultured for a longer time in microgravity[2]. This makes microgravity a valuable environment for studies on a number of cellular characteristics not understood so far[37]. However, long-term removal of gravity achieved by spaceflights is very expensive and seldom performed. With the help of ground-based facilities, which were constructed, to simulate microgravity on Earth, some aspects of annulling gravity can be studied. Such devices, including the RPM, trigger at least a part of the incubated cells to detach from the bottom of a culture flask and to form 3D aggregates like they are observed after spaceflights[1,2]. Even though the RPM produces sheer forces, which are nearly completely absent in real microgravity[38,39], it is generally accepted that the cause of spheroid formation of cells cultured either on a RPM or in space is the absence of cell sedimentation in both conditions[1,2,40], as no other cause could be identified until today.

Also MCF-7 cells form spheroids when exposed to the RPM[10]. In contrast to thyroid cancer cells, which only form spheres, the MCF-7 cells form 3D structures that have central holes after a five-day RPM-exposure, which
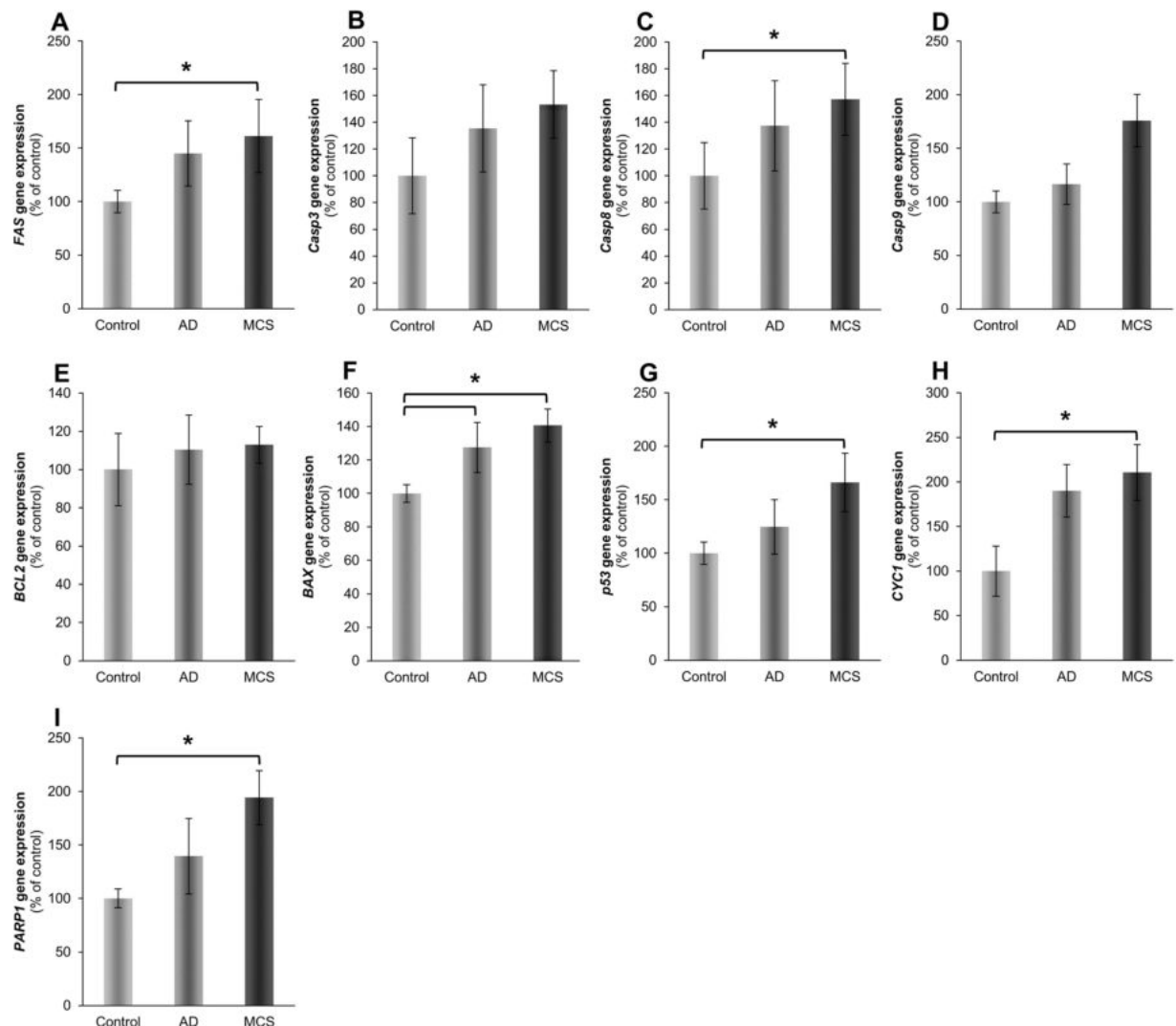
Figure 4. Gene expression of genes whose products are associated with apoptosis pathway. (**A**) Fas, (**B**) Caspase-3 (*Casp3*), (**C**) Caspase-8 (*Casp8*), (**D**) Caspase-9 (*Casp9*), (**E**) Apoptosis regulator Bcl-2 (*BCL2*), (**F**) Apoptosis regulator BAX (*BAX*), (**G**) Cellular tumor antigen p53 (*p53*), (**H**) Cytochrome C 1 (*Cyc1*), (**I**) Poly ADP-ribose polymerase (*PARP1*) were analyzed after 24 h of RPM-exposure. All values are given as mean ± standard deviation. *p < 0.05 vs. corresponding 1*g*-control. AD: adherent cells, MCS: multicellular spheroids, after RPM-exposure. Number of replicates is 4.

remind of duct structures of normal epithelial breast cells[10]. After a 24 h RPM-exposure dense MCS of MCF-7 cells similar to FTC-133 thyroid cancer spheroids or MCS from normal thyroid cells were visible[14,41].

The MCF-7 breast cancer cell line is characterized as estrogen-receptor (ER)-positive, and progesterone receptor (PR)-positive. It belongs to the luminal A molecular subtype[42]. MCF-7 cells show characteristics of differentiated breast epithelium and are positive for epithelial markers and negative for mesenchymal markers like vimentin[42]. MCF-7 cells have demonstrated the ability to form MCS under static 1*g*-conditions using non-adherent Petri dishes[43]. These MCS can mature after long-term culture to lumen-containing spheroids[43].

Normal cells such as endothelial blood vessel cells for example form tubular structures when cultured on a RPM[5]. Human chondrocytes form cartilage pieces when cultured in space and on the Rotating Wall Vessel[44] or when they were exposed to the RPM[45].

These observations point to the possibility that the technique of microgravity-dependent spheroid formation could be exploited for tissue engineering purposes in the future[46], perhaps also in breast reconstruction after surgery. In this study, we investigated the early phase of spheroid formation of MCF-7 cells exposed to simulated microgravity created by a RPM.

MCF-7 cells of a parent population, which grow either as MCS cells or as a monolayer showed similar and different features after a 24 hour-exposure to the RPM. Both states of cellular appearance exhibited an increased expression of *CTGF* and *BAX* and a rather similarly decreased expression of adrenomedullin (*ADM*), aldolase (*ALDOC*), angiopoietin-like 4 (*ANGPTL4*), ankyrin repeat domain 37 (*ANKRD37*), BCL2 interacting protein 3 (*BNIP3*), N-myc downstream regulated 1 (*NDRG1*), whose products are affected by oxygen levels[24–30]. The
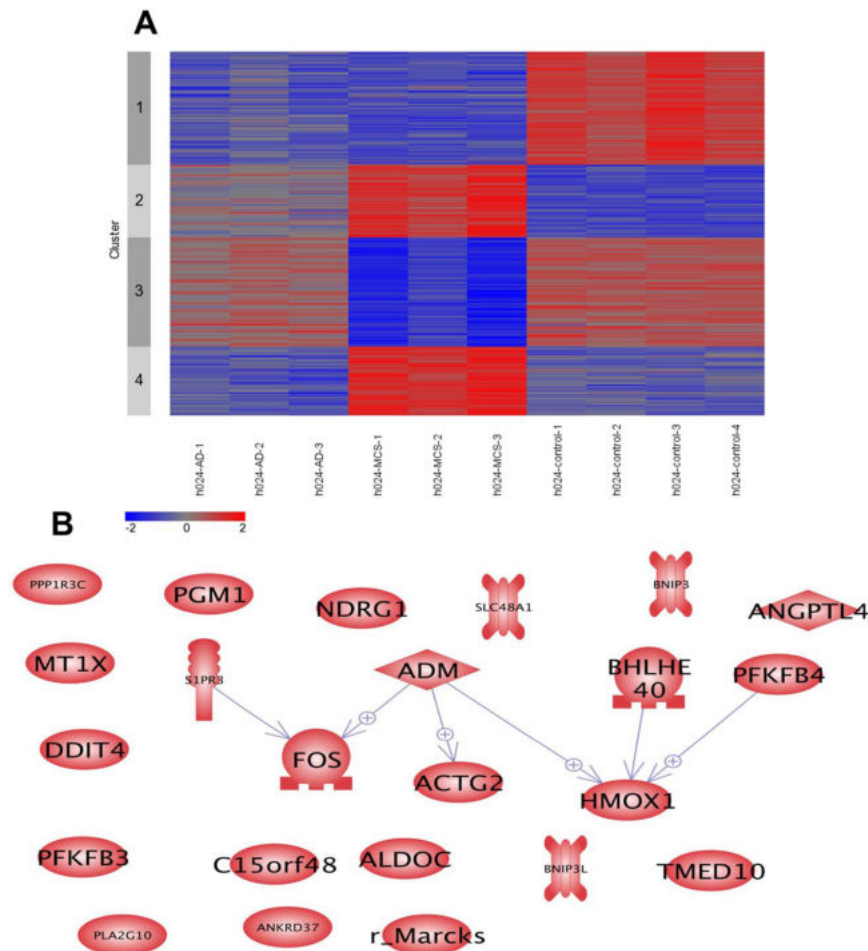
Figure 5. (**A**) K-mean clustering of significant expression differences in the microarray experiment (5% FDR, N = 331 probes). Using k = 4 the first cluster comprises 103 probes downregulated in MCS and AD. The second and forth cluster comprise 66 and 63 probes upregulated in MCS. Cluster 2 genes have an intermediate expression in AD. The 99 probes in cluster three are downregulated in MCS. (**B**) Pathway studio analysis of genes detected by the gene array analysis: The arrows indicate interaction. HMOX1 is most net-worked.

decrease of *ADM*, *ALDOC*, *ANGPTL4*, *ANKRD37*, *BNIP3*, *NDRG1* may be explained by an increase in oxygen concentration within vented culture flasks observed after 24 h of incubation on the RPM[47]. Such an increase may be the reason for the down-regulation of various genes whose products were changed in response to oxygen levels and regulate glycolysis, as the regulation was very similar in adherent and in MCS cells (Supplemental Table 1). In addition, spheroid formation is observed in closed and not-vented incubation chambers during a spaceflight and during clinorotation (clinostat device), which is another method of preventing cell sedimentation on ground[2,40]. This indicates that different oxygen concentrations are not accountable for spheroid formation. Therefore, an enhanced oxygen concentration together with the down-regulation of hypoxia-inducible factor (HIF)-related genes may be an epiphenomenon, when cells are incubated on the RPM in vented culture flasks. As oxygen enhancement cannot be considered to trigger the switch from a 2D to a 3D growth behavior, we focused on genes which have been differently regulated in AD and MCS cells during the early 24 h of incubation.

Differences in gene expression changes were observed in genes of factors playing a role in apoptosis. These genes were clearly elevated in MCS than in AD samples. They comprise *p53*, *CYC1*, *PARP1*, *FAS*, *Casp8* as well as *ANXA1*[48–50]. These elevated apoptotic factors in MCS are accompanied by factors promoting cell survival. One of these genes is sphingosine-1-phosphate receptor 3 (*S1PR3*), the other one is heme oxygenase-1. They are both up-regulated in MCS as detected by microarray and code for proteins favoring cell survival[33,34].

HMOX-1 codes for an enzyme, degrading heme and exhibits together with its degradation products, cyto-protective properties[33]. This enzyme may be localized in various cellular compartments. In caveolae HMOX-1 is inhibited by caveolin-1[51]. In thyroid cells an increased concentration of caveolin-1 prevents spheroid formation[52,53]. Therefore, it may not be excluded that HMOX-1 plays a role in spheroid formation.

According to the literature, both HMOX-1 and NFκB p65 were mutually downregulating their gene expressions[54,55]. In our experimental setting on breast cancer cells grown on the RPM, *HMOX-1* was upregulated, while *NFKB3* remained unregulated. The HMOX-1 upregulation could be due to a positive influence of ADM and PARP-1[56,57]. Despite the *NFKB3* gene expression remained unchanged (Fig. 2F), NFκB p65 protein was

Gene symbol	Fold change AD vs. controls	Fold change MCS vs. controls	Oxygen
ADM	−3.97341	−3.71790	sensitive
ALDOC	−2.72112	−2.93859	sensitive
ANGPTL4	−2.82266	−2.52424	sensitive
ANKRD37	−3.30216	−3.47036	sensitive
BHLHE40	−2.63050	−2.12209	
BNIP3	−2.06507	−1.99325	sensitive
BNIP3L	−2.10573	−2.65328	sensitive
C15ORF48	−1.28973	−2.14925	
DDIT4	−2.36264	−2.80513	sensitive
FOS	−2.23903	−1.62010	
MARCKS	−1.23023	−2.21407	
MT1X	−2.30906	−2.49814	
NDRG1	−2.95903	−2.78486	sensitive
PFKFB3	−2.10202	−3.13231	sensitive
PFKFB4	−3.20572	−2.84829	sensitive
PGM1	−1.77618	−2.05219	
PLA2G10	−1.17541	−2.21319	
PPP1R3C	−1.72085	−2.07604	
TMED10	−1.13444	−2.60338	
SLC48A1	1.31299	2.07465	
S1PR3	1.46902	2.07908	
ACTG2	1.67742	2.17152	
HMOX1	1.23716	2.78409	

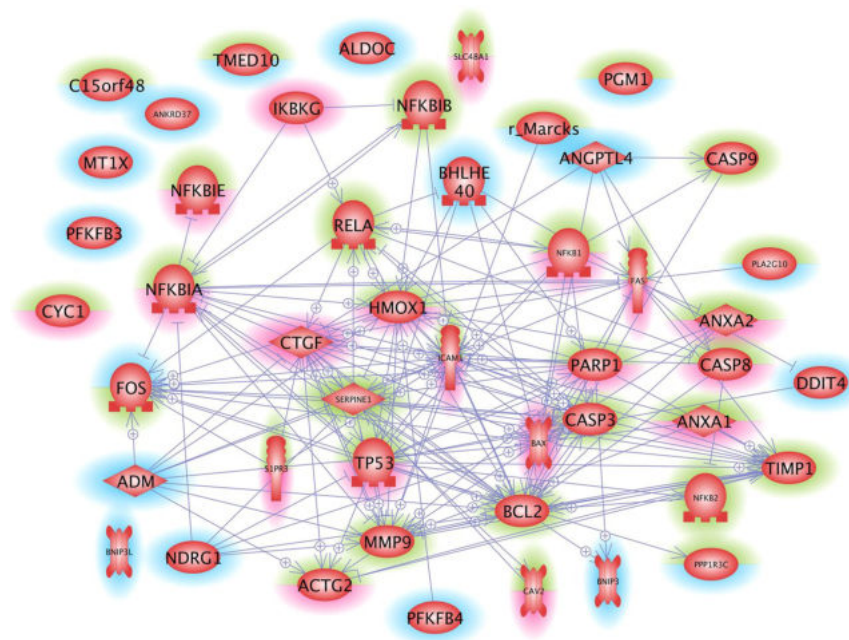**Table 3.** Genes changed two- or more-fold after a 24 h-RPM-exposure.

Figure 6. Pathway studio analysis of genes analyzed in the study by the gene array analysis and qPCR. Arrows indicate influence. Rims around the icon indicate up- (red) and down-regulation (blue). Green means un-regulated. The lower half of a rim indicates regulation in MCS, the upper half indicates regulation in the AD cells.

accumulated in MCS (Fig. 2G) and enriched within the nucleus. This fact points to an enhanced NFκB p65 trans-location activity regulated by NFκBIA and NFκBIB (Figs 6 and 7)[18,58]. Becker-Weimann *et al.*[19] found that NFκB is a key regulator in the formation of organized spheres in breast cancer cells cultured in 3D matrigels. While organized spheres had a low expression of NFκB p65, unorganized spheres presented an upregulation[19]. This is
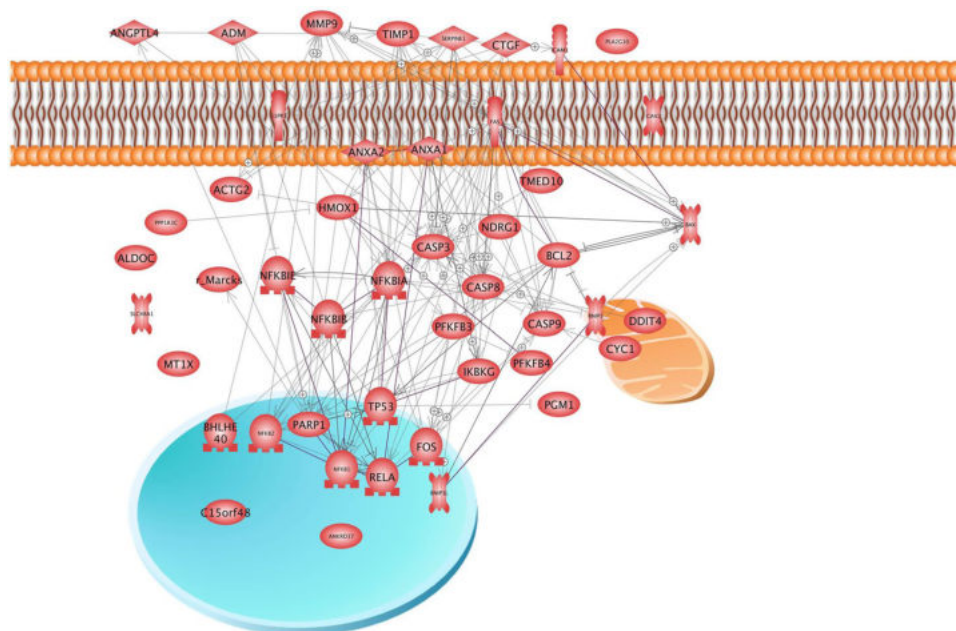
Figure 7. Pathway studio analysis of proteins whose genes were analysed in the study by the gene array analysis and qPCR. Arrows indicate interaction. Mitochondria (yellow), cell membrane (red) and nucleus (blue) are indicated to support localization of the various proteins.
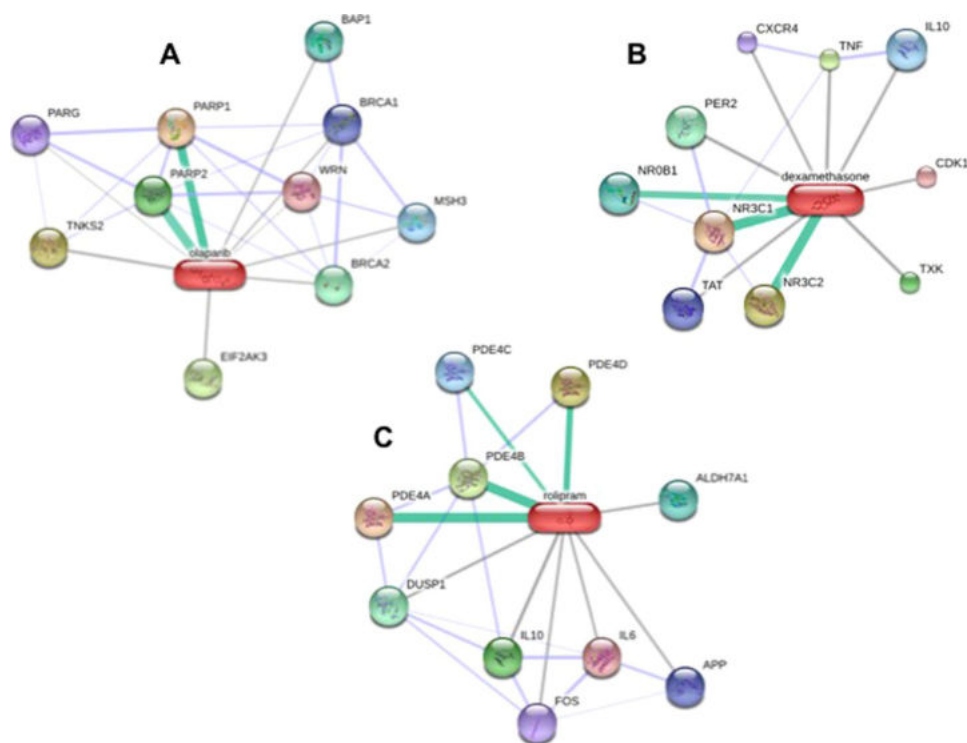

Figure 8. Pharmacological studies. STITCH 4 search for targets of olaparib (**A**), dexamethasone (**B**) and rolipram (**C**). Primary targets are indicated by a green bar between the drug and the protein. Factors affected to a minor degree are shown by grey lines[86].

in concert with our findings that NFκB p65 is enhanced in 24 h adherent and MCS cells as these early spheroids showed a random accumulation of cells (Fig. 1). The random accumulation of MCF7 cells was organized in glandular structures with polarized cells after 5 days of cultivation on the RPM[10]. A deeper investigation of the correlation between cell polarization and NFκB in RPM exposed cells will surely shed further light on the process of
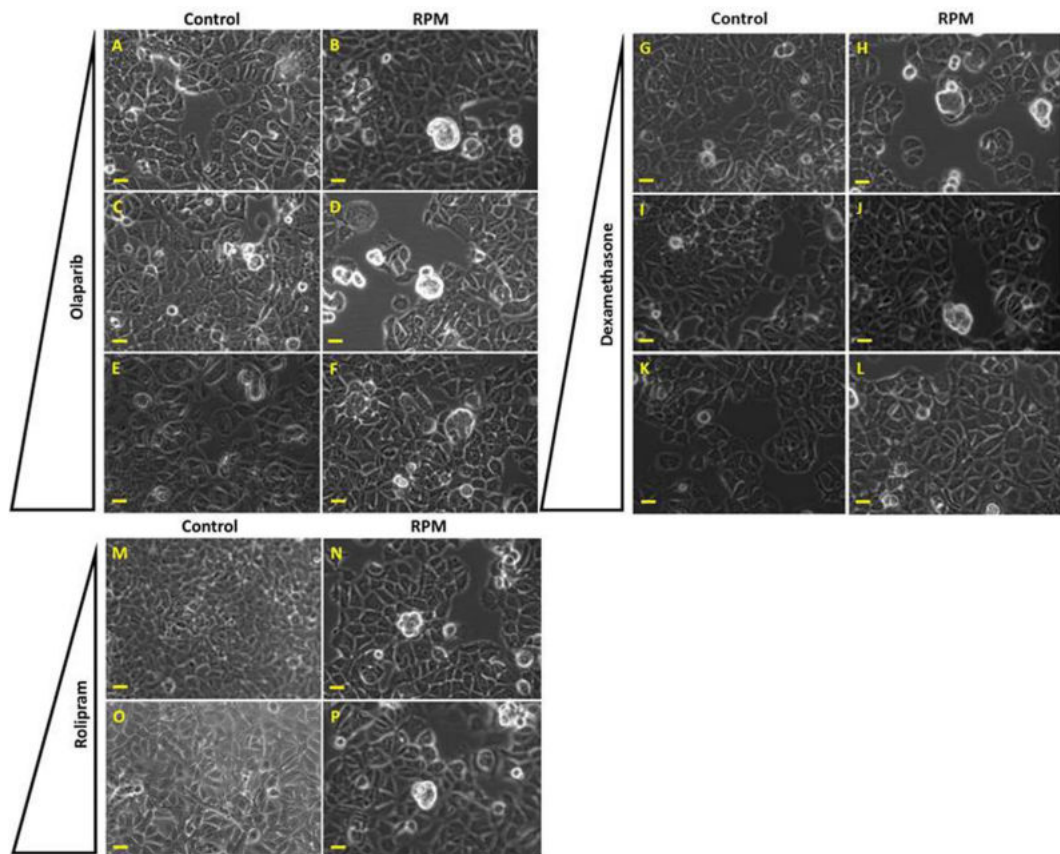
Figure 9. Phase contrast microscopy of drug-treated cells exposed to the RPM. Olaparib-treated cells static control: (**A**) 2.5 μM, (**C**) 5 μM, (**E**) 10 μM. Olaparib-treated cells exposed to the RPM for 24 h: (**B**) 2.5 μM, (**D**) 5 μM, (**F**) 10 μM. DEX-treated cells static control: (**G**) 0.01 μM, (**I**) 0.1 μM, (**K**) 1 μM. DEX-treated cells exposed to the RPM for 24 h: (**H**) 0.01 μM, (**J**) 0.1 μM, (**L**) 1 μM. Rolipram-treated cells static control: M) 1 μM, (**O**) 10 μM. Rolipram-treated cells exposed to the RPM for 24 h: (**N**) 1 μM, (**P**) 10 μM. The pyramid indicates increasing drug concentration. Scale bar: 100 μm.

spheroid formation under microgravity. Furthermore, NFκB p65 translocation triggers the expression of various proteins including *ICAM1*, which in our experiments was upregulated in MCS (Fig. 3H). Hence, NFκB seems to play a central role in spheroid formation, which suggests that manipulation of NFκB activity by biological or pharmacological agents could influence spheroid formation or related processes[59]. The effect of NFκB p65 is directed towards ICAM1 also by PARP1[60]. CTGF, via mitogen-activated protein kinase and NFκB activation, can induce proinflammatory genes in murine tubuloepithelial cells[61]. Interestingly, the *S1PR3* gene was upregulated in the MCS samples (Table 3). A recent paper demonstrated that sphingosine-1-phosphate increases the expansion of cancer stem cells via S1PR3 by a ligand-independent Notch activation in breast cancer[62].

It is known that high levels of PARP-1 were associated with a poor prognosis in early breast cancer. *PARP1* overexpression was detectable in various cancer cell lines and was associated with malignant progression[63]. We found a high *PARP1* expression in the spheroids and targeted it by PARP inhibition. Thus, we investigated the impact of olaparib (a competitive PARP-1/2 inhibitor) on the growth of MCF-7 breast cancer cells exposed to the RPM and to 1*g*-conditions (Fig. 9). MCF-7 cells had been already treated with olaparib in earlier studies and three different doses were tested (2.5, 5 and 10 μM)[64]. Recent data suggested that PARP inhibitors might be useful to treat estrogen receptor-positive and estrogen-dependent tumors[65]. Here we could show that targeting PARP1/2 with olaparib did not alter the 3D aggregation of the MCF-7 cells cultured on the RPM, which indicated that PARP seems not to be the main key factor responsible for 3D spheroids formation in simulated microgravity.

In a second step, we used DEX to modulate the NFκB activity. It has been shown that the application of DEX promoted the NFκB transcriptional activity in MCF-7 cells[66]. Khan *et al.* identified that NFκB was also regulated by glucocorticoids and their receptor in MCF-7 breast cancer cells[66]. Here, we applied DEX to evaluate its impact on spheroid formation. After a 24-hour RPM-exposure we detected that 1 μM might inhibit the spheroid formation. This finding supports the hypothesis that NFκB might be involved in spheroid formation on the RPM. It is known that DEX suppresses the *IL8* gene expression in airway epithelial cells[67]. We had shown earlier that the application of IL-8 protein facilitated the formation of MCS in thyroid cancer cell lines using the liquid-overlay technique[68]. Therefore, DEX might interact with *IL8* to reduce MCS formation in this study, which has to be confirmed in the future.

In addition, we tested a second agent known to target NF-κB. Rolipram is a cyclic adenosine monophosphate (cAMP)-specific phosphodiesterase (PDE-4) inhibitor and earlier used to influence MCF-7 cancer cells[69]. The agent has shown to prevent the NFκB binding activity in human chorionic cells[70]. In this experimental setting, we can report that the drug is not influencing 3D spheroid formation in the first 24 h of RPM-exposure (Fig. 9).

Future studies are necessary to clarify the exact mechanisms involved in the process of 3D aggregation and spheroid formation, such as genetic knockouts or knockins in cell lines[71].

In addition, the genes *CTGF*, *FAS* and *P53*, which were upregulated in MCS and their products, have positive influence on the gene expression of *ICAM1*[72,73]. ICAM1 is a surface protein, mainly detectable in endothelial cells, but also expressed in human breast cancer cells[74]. It may contribute to the cell-cell interaction required for spheroid formation either by direct binding to integrin beta 2[75] or by changing the structure of the cell adhesion complex as it was observed recently on normal thyroid cells[17]. Interestingly, during earlier studies on MCF-7 cells, we detected a downregulation of *ICAM1* in AD and MCS cells after a 24-hour-exposure to the RPM[10]. The reason might be either due to the changed serum supplementation, as growth factor concentration is unpredictable[76], or due to the random walk of the RPM which incorporates different variances of stress[39]. In both cases the onset of apoptosis may vary, which reduces *ICAM1* expression via caspase-3[11,77].

Taken together, our experiments suggest that NFκB family members and *HMOX-1* interact on a gene level, when breast cancer cells transit from a 2D to a 3D growth on the RPM. They are changed in the same direction, when adherent and MCS-cells are compared (Fig. 6). Whether these alterations are accidental parallel events or mutually caused remains to be determined. Whether the up-regulated *ANXA2* or the down-regulated *MARCKS* genes which both code for cytoskeleton interacting proteins or the genes of *CAV2*, *TIMP1*, *PAI1* and *MMP-9*, which either code for membrane proteins or for enzymes regulating the extracellular matrix constitution, contribute to this process remains to be determined in future studies. Interestingly, *CAV2*, *TIMP1*, and *PAI1* show an up-regulation in these experiments, but have exhibited together with *MMP9* a downregulation in earlier experiments on thyroid cells[9].

In addition, our studies deliver new knowledge about how these cells might behave in real microgravity. This data can be used to prepare future spaceflight missions. Hence, using these and earlier results as a basis[10,78,79], we plan to conduct a future NASA and DLR space experiment like the successfully flown Cellbox-1 (NanoRacks-CellBox-Thyroid Cancer: http://www.nasa.gov/mission_pages/station/research/experiments/1648.html [52,53]) onboard the International Space Station in order to increase the current knowledge of the behavior of human breast cancer cells under real microgravity in space with a special focus on early cytoskeletal changes and 3D growth.

Methods

Cell culture.
MCF-7 human breast adenocarcinoma cells (Fig. 1A) were purchased from the American type culture collection (ATCC) (Manassas, VA, USA). Cells were cultivated in RPMI 1640 medium (Life Technologies, Naerum, Denmark) supplemented with 10% fetal calf serum (FCS) (Biochrom, Berlin, Germany) and 1% penicillin/streptomycin (Biochrom) at 37 °C and 5% CO_2. One day prior to the experimental run on the RPM, cells were seeded either in slide flasks (Thermo Fisher Scientific, Roskilde, Denmark) (3×10^5 cells/cm²) for fluorescence staining or in T25 (1×10^6 cells) vented cell culture flasks (Sarstedt, Nümbrecht, Germany) for RNA and protein extraction. Before starting the run, flasks were filled up with medium, taking care that no air bubbles remain. A detailed procedure has been published previously[9,23]. To test the viability of the cells in the multicellular spheroids (MCS), the MCS were collected after 24 h (Fig. 1B) and seeded in slide flasks. The adhesion and migration behavior of the cells of the MCS was examined by phase contrast microscopy after 2 h, 4 h and 24 h (Fig. 1C–E).

Drug treatment.
For targeting molecules of interest, we seeded 10^6 MCF-7 cells in slideflasks. After 24 h the cells were synchronized for 4 h and afterwards treated with the respective chemical agents for 24 h during RPM-exposure or without RPM-exposure. To target PARP we used the PARP 1/2 inhibitor olaparib (Selleckchem, Absource Diagnostics, Munich, Germany). We prepared a stock solution in DMSO. The aliquots were stored at −80 °C until use. Concentrations of 2.5, 5, or 10 μM olaparib in medium were applied[64]. Negative controls were incubated with DMSO only.

For targeting NFκB we applied dexamethasone (DEX) (Sigma-Aldrich, Taufkirchen, Germany). According to Bruxant *et al.*[80] and Khan *et al.*[66] we treated the MCF-7 cells with DEX (0 M, 0,001 μM, 0,1 μM, 1 μM). The MCF-7 cells were treated with DEX dissolved in water for 24 h.

Moreover, we applied the PDE4 inhibitor rolipram. We used the following doses 0 M, 1 μM, and 10 μM[69]. Rolipram was first prepared as a stock solution in ethanol. Control MCF-7 cells were treated with an equivalent volume of the solvent.

Random Positioning Machine.
The desktop RPM (Airbus Defense and Space (ADS), Leiden, The Netherlands) was located in a standard incubator with 37 °C and 5% CO_2. The RPM was operated in real random mode with random direction and interval and a maximum speed of 12.5 revolutions per minute. Sample flasks to be tested were placed onto the middle frame with a maximal distance of 7 cm to the center of rotation allowing a μ*g* quality between 10^{-4} and 10^{-2} *g*, which is reached over time[40,81]. Corresponding static 1*g*-controls, which were completely filled with medium, were placed next to the RPM in the same incubator (n = 15 samples each group/run).

Phase contrast microscopy.
Cells were observed and photographed using an Axiovert 25 Microscope (Carl Zeiss Microscopy, LLC, USA) and a Canon EOS 550D camera (Canon GmbH, Krefeld, Germany)[23].

Sample collection.   After 24 h the cells were investigated and photographed. The MCS were collected by mild centrifugation at 3000 g for 5 min and 4 °C and stored in liquid nitrogen. Harvesting of the adherent cells was performed, by using a cell scraper after carefully adding ice-cold phosphate buffered saline (PBS, Life Technologies). The suspension was collected and centrifuged at 3000 g for 5 min and 4 °C followed by discarding the PBS and storage of the pellet in liquid nitrogen.

Acridine orange/ethidium bromide staining.   Control and RPM-exposed MCF-7 cells of both phenotypes MCS and adherently growing cells were stained with acridine orange/ethidium bromide (Molecular Probes, Darmstadt, Germany) as performed in previous studies[82]. The stained MCF-7 cells were immediately investigated by using a Zeiss LSM 710 confocal laser scanning microscope (Zeiss, Jena, Germany) as previously described[9].

Indirect immunofluorescence staining of NFκB.   Immunofluorescence analysis of NFκB p65 was performed on 80% confluent MCF-7 cells after a 24 hour exposure to the RPM. The cells were fixed with 4% paraformaldehyde for 25 minutes at room temperature (RT), permeabilized with 0.25% Triton™ X-100 for 10 minutes, and blocked with 5% BSA for 1 h at RT. Afterwards, the cells were labelled with NFκB [p65] rabbit polyclonal antibody (Thermo Fisher Scientific) at 2 μg/mL in 1% BSA and incubated overnight at 4 °C, then labelled with Alexa Fluor 488 goat anti-rabbit IgG secondary antibody (Thermo Fisher Scientific) at a dilution of 1:400 for 1 h at RT and washed 3 times. For nuclear staining, we used DAPI (4′,6-diamidin-2-phenylindol) (Sigma-Aldrich, Taufkirchen, Germany) for 5 min and washed the cells twice with DPBS. For evaluation, the slides were mounted with Fluoroshield (Sigma-Aldrich, Taufkirchen, Germany) and analysed with a Zeiss LSM 710 confocal laser scanning microscope[9].

Western Blot Analysis.   Western blot analysis was performed as recently published[17]. The RPM experiment for the Western blot analyses was performed three times. In each of these experiments five different culture flasks were mounted on the RPM. In parallel five 1g-control flasks were cultured next to the RPM. At the end of the experiment cells were harvested and an aliquot from each flask was subjected to Western blot analysis. In RPM-samples we detected two phenotypes (RPM-AD cells and RPM-MCS). Hence, the Western blot contains ten lanes loaded with RPM samples (AD and MCS), and five lanes loaded with 1g-control samples. The Western blot experiment was repeated thrice. The concentration was adjusted to a total protein load of 30 μg per well in Laemmli buffer. Criterion XT 4–12% precast gels (Biorad, Hercules, USA) were loaded and run for 1 h at 150 volts. Transfer to a PVDF membrane was performed at 100 volts and 30 minutes. Membranes were blocked in 0.3% I-Block (Applied Biosystems, Foster City, USA) in TBS-T overnight. The antibodies listed in Table 1 were applied for 2 h at room temperature followed by washing steps. The applied secondary antibody, a Horseradish peroxidase (HRP)-linked antibody was utilized at a dilution of 1:4000 (Cell Signaling Technology, Inc., Danvers, MA, USA) for additional 2 h at room temperature. Membranes were developed using Biorad Clarity Western ECL and imaged with an Image Quant LAS 4000 mini (GE Healthcare Life Science, Freiburg, Germany). Cofilin (CFL1) [EPR6375] (ABCAM, Cambridge, UK) was used as a loading control. The membranes were analyzed using ImageJ software (U.S. National Institutes of Health, Bethesda, MD, USA; http://rsb.info.nih.gov/ij/) for densitometric quantification of the bands[83].

RNA and protein extraction.   The RNA and protein extraction were performed using the AllPrep RNA/Protein kit (Qiagen GmbH, Hilden, Germany) according to the manufacturer's protocol. The concentrations were determined with the spectrophotometer Ultrospec 2100 pro (Amersham Biosciences, Amersham, Great Britain).

Quantitative real-time PCR.   Complementary DNA was produced using the First Strand cDNA Synthesis Kit (Thermo Fisher Scientific) following manufacturer's instructions. qrtPCR was performed using the SYBR® Select Master Mix (Applied Biosystems, Darmstadt, Germany) and the 7500 Real-Time PCR System (Applied Biosystems) to determine the expression levels of target genes, shown in Table 2. Selective primers were designed to span exon-exon boundaries and to have a Tm of 60 °C using Primer Express software (Applied Biosystems), and were synthesized by TIB Molbiol (Berlin, Germany). Samples were measured in triplicate and were normalized to the housekeeper 18 S rRNA. Comparative threshold cycle (ΔΔCT) methods were used for relative quantification of transcription levels, with 1 g set as 100%[84].

Microarray technique.   The 25 Illumina HumanWG-6_V2_0_R3 arrays have been normalized using the BeadStudio Gene Expression Module v3.3.7, and quantile normalization without background correction. After quantile normalization and exclusion of low or not expressed genes (minimum Illumina detection p-value > 0.05) a parametric ANOVA comparing the conditions control, AD and MCS was performed. Probes which undergo 5% FDR[85] were selected as differential expressed. Differentiation of the expression profiles was performed using hierarchical and k-mean clustering. The cluster analysis was done using Partek Genomic Suite 6.3 applying hierarchical average linkage clustering and k-mean clustering with Euclidean distance function on standardized log2 signal values. K was selected by analyses of the hierarchical clustering dendrograms.

Pathway analyses.   To investigate mutual regulation of genes and to visualize localization and interactions between proteins, we entered relevant UniProtKB entry numbers in the Pathway Studio v.11 software (Elsevier Research Solutions, Amsterdam, The Netherlands). Graphs were generated for gene expression and protein regulation and binding. The method was described previously[9,52]. STITCH 4 (Chemical-Protein Interaction Networks, European Molecular Biology Laboratory (EMBL), Heidelberg, Germany) was applied to investigate the interaction of DEX, olaparib and rolipram with their targets. The data is given in Fig. 8.

Statistical evaluation.   Statistical evaluation was performed using SPSS 15.0 (SPSS, Inc., Chicago, IL, USA). The Mann-Whitney-U-Test was used to compare $1g$ and s-μg conditions, as well as AD cells and MCS cells. All data is presented as mean $\pm$ standard deviation (SD) with a significance level of *p < 0.05.

References

1. Grimm, D. *et al*. Simulated microgravity alters differentiation and increases apoptosis in human follicular thyroid carcinoma cells. *FASEB J.* **16**, 604–606, https://doi.org/10.1096/fj.01-0673fje (2002).
2. Pietsch, J. *et al*. Spheroid formation of human thyroid cancer cells in an automated culturing system during the Shenzhou-8 Space mission. *Biomaterials* **34**, 7694–7705, https://doi.org/10.1016/j.biomaterials.2013.06.054 (2013).
3. Pietsch, J. *et al*. A proteomic approach to analysing spheroid formation of two human thyroid cell lines cultured on a random positioning machine. *Proteomics* **11**, 2095–2104, https://doi.org/10.1002/pmic.201000817 (2011).
4. Ulbrich, C. *et al*. Characterization of human chondrocytes exposed to simulated microgravity. *Cell. Physiol. Biochem.* **25**, 551–560, https://doi.org/10.1159/000303059 (2010).
5. Grimm, D. *et al*. Different responsiveness of endothelial cells to vascular endothelial growth factor and basic fibroblast growth factor added to culture media under gravity and simulated microgravity. *Tissue Eng. Part A.* **16**, 1559–1573, https://doi.org/10.1089/ten.TEA.2009.0524 (2010).
6. Masiello, M. G. *et al*. Phenotypic switch induced by simulated microgravity on MDA-MB-231 breast cancer cells. *Biomed. Res. Int.* **2014**, 652434, https://doi.org/10.1155/2014/652434 (2014).
7. Ingram, M. *et al*. Three-dimensional growth patterns of various human tumor cell lines in simulated microgravity of a NASA bioreactor. *In Vitro Cell. Dev. Biol. Anim.* **33**, 459–466, https://doi.org/10.1007/s11626-997-0064-8 (1997).
8. Chang, T. T. & Hughes-Fulford, M. Monolayer and spheroid culture of human liver hepatocellular carcinoma cell line cells demonstrate distinct global gene expression patterns and functional phenotypes. *Tissue Eng. Part A.* **15**, 559–567, https://doi.org/10.1089/ten.tea.2007.0434 (2009).
9. Corydon, T. J. *et al*. Reduced Expression of Cytoskeletal and Extracellular Matrix Genes in Human Adult Retinal Pigment Epithelium Cells Exposed to Simulated Microgravity. *Cell. Physiol. Biochem.* **40**, 1–17, https://doi.org/10.1159/000452520 (2016).
10. Kopp, S. *et al*. Identifications of novel mechanisms in breast cancer cells involving duct-like multicellular spheroid formation after exposure to the Random Positioning Machine. *Sci. Rep.* **6**, 26887, https://doi.org/10.1038/srep26887 (2016).
11. Kossmehl, P. *et al*. Weightlessness induced apoptosis in normal thyroid cells and papillary thyroid carcinoma cells via extrinsic and intrinsic pathways. *Endocrinology* **144**, 4172–4179, https://doi.org/10.1210/en.2002-0171 (2003).
12. Uva, B. M. *et al*. Microgravity-induced apoptosis in cultured glial cells. *Eur. J. Histochem.* **46**, 209–214, https://doi.org/10.4081/1681 (2002).
13. Schatten, H., Lewis, M. L. & Chakrabarti, A. Spaceflight and clinorotation cause cytoskeleton and mitochondria changes and increases in apoptosis in cultured cells. *Acta. Astronaut.* **49**, 399–418, https://doi.org/10.1016/S0094-5765(01)00116-3 (2001).
14. Grosse, J. *et al*. Gravity-sensitive signaling drives 3-dimensional formation of multicellular thyroid cancer spheroids. *FASEB J.* **26**, 5124–5140, https://doi.org/10.1096/fj.12-215749 (2012).
15. Ghobrial, I. M., Witzig, T. E. & Adjei, A. A. Targeting apoptosis pathways in cancer therapy. *CA Cancer J. Clin.* **55**, 178–194, https://doi.org/10.3322/canjclin.55.3.178 (2005).
16. Song, J. K. *et al*. Cell growth inhibition and induction of apoptosis by snake venom toxin in ovarian cancer cell via inactivation of nuclear factor kappaB and signal transducer and activator of transcription 3. *Arch. Pharm. Res.* **35**, 867–876, https://doi.org/10.1007/s12272-012-0512-1 (2012).
17. Bauer, J. *et al*. Proteome Analysis of Human Follicular Thyroid Cancer Cells Exposed to the Random Positioning Machine. *Int. J. Mol. Sci.* **18**, https://doi.org/10.3390/ijms18030546 (2017).
18. Wu, H. *et al*. A negative feedback loop between miR-200b and the nuclear factor-kappaB pathway via IKBKB/IKK-beta in breast cancer cells. *FEBS J.* **283**, 2259–2271, https://doi.org/10.1111/febs.13543 (2016).
19. Becker-Weimann, S. *et al*. NFkB disrupts tissue polarity in 3D by preventing integration of microenvironmental signals. *Oncotarget* **4**, 2010–2020, https://doi.org/10.18632/oncotarget.1451 (2013).
20. Hayden, M. S. & Ghosh, S. Shared principles in NF-kappaB signaling. *Cell* **132**, 344–362, https://doi.org/10.1016/j.cell.2008.01.020 (2008).
21. Perkins, N. D. Post-translational modifications regulating the activity and function of the nuclear factor kappa B pathway. *Oncogene* **25**, 6717–6730, https://doi.org/10.1038/sj.onc.1209937 (2006).
22. Chen, J. & Chen, Z. J. Regulation of NF-kappaB by ubiquitination. *Curr. Opin. Immunol.* **25**, 4–12, https://doi.org/10.1016/j.coi.2012.12.005 (2013).
23. Kopp, S. *et al*. Mechanisms of three-dimensional growth of thyroid cells during long-term simulated microgravity. *Sci. Rep.* **5**, 16691, https://doi.org/10.1038/srep16691 (2015).
24. Benita, Y. *et al*. An integrative genomics approach identifies Hypoxia Inducible Factor-1 (HIF-1)-target genes that form the core response to hypoxia. *Nucleic Acids Res.* **37**, 4587–4602, https://doi.org/10.1093/nar/gkp425 (2009).
25. Zhu, P., Goh, Y. Y., Chin, H. F., Kersten, S. & Tan, N. S. Angiopoietin-like 4: a decade of research. *Biosci. Rep.* **32**, 211–219, https://doi.org/10.1042/BSR20110102 (2012).
26. Bellot, G. *et al*. Hypoxia-induced autophagy is mediated through hypoxia-inducible factor induction of BNIP3 and BNIP3L via their BH3 domains. *Mol. Cell Biol.* **29**, 2570–2581, https://doi.org/10.1128/MCB.00166-09 (2009).
27. Said, H. M. *et al*. Oxygen-dependent regulation of NDRG1 in human glioblastoma cells *in vitro* and *in vivo*. *Oncol. Rep.* **21**, 237–246, https://doi.org/10.3892/or_00000214 (2009).
28. Lv, Y. *et al*. PFKFB3-mediated glycolysis is involved in reactive astrocyte proliferation after oxygen-glucose deprivation/reperfusion and is regulated by Cdh1. *Neurochem. Int.* **91**, 26–33, https://doi.org/10.1016/j.neuint.2015.10.006 (2015).
29. Zhang, H. *et al*. HIF-1alpha activates hypoxia-induced PFKFB4 expression in human bladder cancer cells. *Biochem. Biophys. Res. Commun.* **476**, 146–152, https://doi.org/10.1016/j.bbrc.2016.05.026 (2016).
30. Kim, S. M., Kim, J. Y., Lee, S. & Park, J. H. Adrenomedullin protects against hypoxia/reoxygenation-induced cell death by suppression of reactive oxygen species via thiol redox systems. *FEBS Lett.* **584**, 213–218, https://doi.org/10.1016/j.febslet.2009.11.063 (2010).
31. Aderem, A. Signal transduction and the actin cytoskeleton: the roles of MARCKS and profilin. *Trends Biochem. Sci.* **17**, 438–443, https://doi.org/10.1016/0968-0004(92)90016-3 (1992).
32. Dunn, L. L. *et al*. New insights into intracellular locations and functions of heme oxygenase-1. *Antioxid. Redox Signal.* **20**, 1723–1742, https://doi.org/10.1089/ars.2013.5675 (2014).
33. An, S., Zheng, Y. & Bleu, T. Sphingosine 1-phosphate-induced cell proliferation, survival, and related signaling events mediated by G protein-coupled receptors Edg3 and Edg5. *J. Biol. Chem.* **275**, 288–296, https://doi.org/10.1074/jbc.275.1.288 (2000).
34. Khan, A. A. & Quigley, J. G. Heme and FLVCR-related transporter families SLC48 and SLC49. *Mol. Aspects Med.* **34**, 669–682, https://doi.org/10.1016/j.mam.2012.07.013 (2013).
35. White, R. J. & Averner, M. Humans in space. *Nature* **409**, 1115–1118, https://doi.org/10.1038/35059243 (2001).
36. Adrian, A. *et al*. The oxidative burst reaction in mammalian cells depends on gravity. *Cell Commun. Signal.* **11**, 98, https://doi.org/10.1186/1478-811X-11-98 (2013).

37. Becker, J. L. & Souza, G. R. Using space-based investigations to inform cancer research on Earth. *Nat. Rev. Cancer* **13**, 315–327, https://doi.org/10.1038/nrc3507 (2013).

38. Hauslage, J., Cevik, V. & Hemmersbach, R. Pyrocystis noctiluca represents an excellent bioassay for shear forces induced in ground-based microgravity simulators (clinostat and random positioning machine). *NPJ microgravity* **3**, 12, https://doi.org/10.1038/s41526-017-0016-x (2017).

39. Wuest, S. L., Stern, P., Casartelli, E. & Egli, M. Fluid Dynamics Appearing during Simulated Microgravity Using Random Positioning Machines. *PloS one* **12**, e0170826, https://doi.org/10.1371/journal.pone.0170826 (2017).

40. Warnke, E. *et al*. Spheroid formation of human thyroid cancer cells under simulated microgravity: a possible role of CTGF and CAV1. *Cell Commun. Signal.* **12**, 32, https://doi.org/10.1186/1478-811X-12-32 (2014).

41. Warnke, E. *et al*. Cytokine Release and Focal Adhesion Proteins in Normal Thyroid Cells Cultured on the Random Positioning Machine. *Cell. Physiol. Biochem.* **43**, 257–270, https://doi.org/10.1159/000480368 (2017).

42. Comsa, S., Cimpean, A. M. & Raica, M. The Story of MCF-7 Breast Cancer Cell Line: 40 years of Experience in Research. *Anticancer Res.* **35**, 3147–3154 (2015).

43. do Amaral, J. B., Urabayashi, M. S. & Machado-Santelli, G. M. Cell death and lumen formation in spheroids of MCF-7 cells. *Cell Biol Int* **34**, 267–274, https://doi.org/10.1042/CBI20090024 (2010).

44. Freed, L. E., Langer, R., Martin, I., Pellis, N. R. & Vunjak-Novakovic, G. Tissue engineering of cartilage in space. *Proc. Natl. Acad. Sci. USA* **94**, 13885–13890 (1997).

45. Aleshcheva, G. *et al*. Scaffold-free Tissue Formation Under Real and Simulated Microgravity Conditions. *Basic Clin. Pharmacol. Toxicol.* **119**(Suppl 3), 26–33, https://doi.org/10.1111/bcpt.12561 (2016).

46. Grimm, D. *et al*. Growing tissues in real and simulated microgravity: new methods for tissue engineering. *Tissue Eng. Part B Rev.* **20**, 555–566, https://doi.org/10.1089/ten.TEB.2013.0704 (2014).

47. Pietsch, J. *et al*. Metabolic enzyme diversity in different human thyroid cell lines and their sensitivity to gravitational forces. *Proteomics* **12**, 2539–2546, https://doi.org/10.1002/pmic.201200070 (2012).

48. Zadeh, M. M., Motamed, N., Ranji, N. & Majidi, M. & Falahi, F. Silibinin-Induced Apoptosis and Downregulation of MicroRNA-21 and MicroRNA-155 in MCF-7 Human Breast Cancer Cells. *J. Breast Cancer* **19**, 45–52, https://doi.org/10.4048/jbc.2016.19.1.45 (2016).

49. Parente, L. & Solito, E. Annexin 1: more than an anti-phospholipase protein. *Inflamm. Res.* **53**, 125–132, https://doi.org/10.1007/s00011-003-1235-z (2004).

50. Cregan, S. P., Dawson, V. L. & Slack, R. S. Role of AIF in caspase-dependent and caspase-independent cell death. *Oncogene* **23**, 2785–2796, https://doi.org/10.1038/sj.onc.1207517 (2004).

51. Kim, H. P., Wang, X., Galbiati, F., Ryter, S. W. & Choi, A. M. Caveolae compartmentalization of heme oxygenase-1 in endothelial cells. *FASEB J.* **18**, 1080–1089, https://doi.org/10.1096/fj.03-1391com (2004).

52. Riwaldt, S. *et al*. The Importance of Caveolin-1 as Key-Regulator of Three-Dimensional Growth in Thyroid Cancer Cells Cultured under Real and Simulated Microgravity Conditions. *Int. J. Mol. Sci.* **16**, 28296–28310, https://doi.org/10.3390/ijms161226108 (2015).

53. Riwaldt, S. *et al*. Identification of proteins involved in inhibition of spheroid formation under microgravity. *Proteomics* **15**, 2945–2952, https://doi.org/10.1002/pmic.201500067 (2015).

54. Xie, Y., Wang, Y., Zong, C. & Cheng, J. Transforming growth factor-Beta inhibits heme oxygenase-1 expression in lung fibroblast through nuclear factor-kappa-B-dependent pathway. *Pharmacology* **93**, 185–192, https://doi.org/10.1159/000360638 (2014).

55. Park, S. Y. *et al*. Induction of heme oxygenase-1 expression by cilostazol contributes to its anti-inflammatory effects in J774 murine macrophages. *Immunol. Lett.* **136**, 138–145, https://doi.org/10.1016/j.imlet.2011.01.003 (2011).

56. Qi, Y. F. *et al*. Adrenomedullin induces heme oxygenase-1 gene expression and cGMP formation in rat vascular smooth muscle cells. *Peptides* **26**, 1257–1263, https://doi.org/10.1016/j.peptides.2005.01.012 (2005).

57. Katoh, Y. *et al*. Methionine adenosyltransferase II serves as a transcriptional corepressor of Maf oncoprotein. *Mol. Cell* **41**, 554–566, https://doi.org/10.1016/j.molcel.2011.02.018 (2011).

58. Hideshima, H. *et al*. IKKbeta inhibitor in combination with bortezomib induces cytotoxicity in breast cancer cells. *Int. J. Oncol.* **44**, 1171–1176, https://doi.org/10.3892/ijo.2014.2273 (2014).

59. Tafani, M. *et al*. Modulators of HIF1alpha and NFkB in Cancer Treatment: Is it a Rational Approach for Controlling Malignant Progression? *Front. Pharmacol.* **4**, 13, https://doi.org/10.3389/fphar.2013.00013 (2013).

60. Zerfaoui, M. *et al*. Nuclear translocation of p65 NF-kappaB is sufficient for VCAM-1, but not ICAM-1, expression in TNF-stimulated smooth muscle cells: Differential requirement for PARP-1 expression and interaction. *Cell. Signal.* **20**, 186–194, https://doi.org/10.1016/j.cellsig.2007.10.007 (2008).

61. Sanchez-Lopez, E. *et al*. CTGF promotes inflammatory cell infiltration of the renal interstitium by activating NF-kappaB. *J. Am. Soc. Nephrol.* **20**, 1513–1526, https://doi.org/10.1681/ASN.2008090999 (2009).

62. Hirata, N. *et al*. Sphingosine-1-phosphate promotes expansion of cancer stem cells via S1PR3 by a ligand-independent Notch activation. *Nat Commun* **5**, 4806, https://doi.org/10.1038/ncomms5806 (2014).

63. Zaremba, T. *et al*. Poly(ADP-ribose) polymerase-1 polymorphisms, expression and activity in selected human tumour cell lines. *Br. J. Cancer* **101**, 256–262, https://doi.org/10.1038/sj.bjc.6605166 (2009).

64. Gilardini Montani, M. S. *et al*. ATM-depletion in breast cancer cells confers sensitivity to PARP inhibition. *J. Exp. Clin. Cancer Res.* **32**, 95, https://doi.org/10.1186/1756-9966-32-95 (2013).

65. Kim, H., Tarhuni, A., Abd Elmageed, Z. Y. & Boulares, A. H. Poly(ADP-ribose) polymerase as a novel regulator of 17beta-estradiol-induced cell growth through a control of the estrogen receptor/IGF-1 receptor/PDZK1 axis. *J. Transl. Med.* **13**, 233, https://doi.org/10.1186/s12967-015-0589-7 (2015).

66. Khan, S., Lopez-Dee, Z., Kumar, R. & Ling, J. Activation of NFkB is a novel mechanism of pro-survival activity of glucocorticoids in breast cancer cells. *Cancer Lett.* **337**, 90–95, https://doi.org/10.1016/j.canlet.2013.05.020 (2013).

67. Chang, M. M., Juarez, M., Hyde, D. M. & Wu, R. Mechanism of dexamethasone-mediated interleukin-8 gene suppression in cultured airway epithelial cells. *Am J Physiol Lung Cell Mol Physiol* **280**, L107–115 (2001).

68. Svejgaard, B. *et al*. Common Effects on Cancer Cells Exerted by a Random Positioning Machine and a 2D Clinostat. *PloS one* **10**, e0135157, https://doi.org/10.1371/journal.pone.0135157 (2015).

69. El-Mowafy, A. M. & Alkhalaf, M. Resveratrol activates adenylyl-cyclase in human breast cancer cells: a novel, estrogen receptor-independent cytostatic mechanism. *Carcinogenesis* **24**, 869–873 (2003).

70. Herve, R. *et al*. The PDE4 inhibitor rolipram prevents NF-kappaB binding activity and proinflammatory cytokine release in human chorionic cells. *J. Immunol.* **181**, 2196–2202 (2008).

71. Chira, S. *et al*. CRISPR/Cas9: Transcending the Reality of Genome Editing. *Mol Ther Nucleic Acids* **7**, 211–222, https://doi.org/10.1016/j.omtn.2017.04.001 (2017).

72. Choi, K., Benveniste, E. N. & Choi, C. Induction of intercellular adhesion molecule-1 by Fas ligation: proinflammatory roles of Fas in human astroglioma cells. *Neurosci. Lett.* **352**, 21–24, https://doi.org/10.1016/j.neulet.2003.08.019 (2003).

73. Gorgoulis, V. G. *et al*. p53 activates ICAM-1 (CD54) expression in an NF-kappaB-independent manner. *EMBO J.* **22**, 1567–1578, https://doi.org/10.1093/emboj/cdg157 (2003).

74. Strell, C., Lang, K., Niggemann, B., Zaenker, K. S. & Entschladen, F. Neutrophil granulocytes promote the migratory activity of MDA-MB-468 human breast carcinoma cells via ICAM-1. *Exp. Cell Res.* **316**, 138–148, https://doi.org/10.1016/j.yexcr.2009.09.003 (2010).

75. Chen, L., Vicente-Manzanares, M., Potvin-Trottier, L., Wiseman, P. W. & Horwitz, A. R. The integrin-ligand interaction regulates adhesion and migration through a molecular clutch. *PloS one* **7**, e40202, https://doi.org/10.1371/journal.pone.0040202 (2012).

76. van der Valk, J. *et al.* Optimization of chemically defined cell culture media–replacing fetal bovine serum in mammalian *in vitro* methods. *Toxicol. In Vitro* **24**, 1053–1063, https://doi.org/10.1016/j.tiv.2010.03.016 (2010).

77. Fawcett, H., Mader, J. S., Robichaud, M., Giacomantonio, C. & Hoskin, D. W. Contribution of reactive oxygen species and caspase-3 to apoptosis and attenuated ICAM-1 expression by paclitaxel-treated MDA-MB-435 breast carcinoma cells. *Int. J. Oncol.* **27**, 1717–1726 (2005).

78. Ma, X. *et al.* Genomic approach to identify factors that drive the formation of three-dimensional structures by EA.hy926 endothelial cells. *PloS one* **8**, e64402, https://doi.org/10.1371/journal.pone.0064402 (2013).

79. Pietsch, J. *et al.* Three-dimensional growth of human endothelial cells in an automated cell culture experiment container during the SpaceX CRS-8 ISS space mission - The SPHEROIDS project. *Biomaterials* **124**, 126–156, https://doi.org/10.1016/j.biomaterials.2017.02.005 (2017).

80. Buxant, F., Kindt, N., Laurent, G., Noel, J. C. & Saussez, S. Antiproliferative effect of dexamethasone in the MCF-7 breast cancer cell line. *Mol. Med. Rep.* **12**, 4051–4054, https://doi.org/10.3892/mmr.2015.3920 (2015).

81. van Loon, J. J. W. A. Some history and use of the random positioning machine, RPM, in gravity related research. *Adv. Space Res.* **39**, 1161–1165, https://doi.org/10.1016/j.asr.2007.02.016 (2007).

82. Magnusson, N. E. *et al.* Gene networks modified by sulphonylureas in beta cells: a pathway-based analysis of insulin secretion and cell death. *Basic Clin. Pharmacol. Toxicol.* **111**, 254–261, https://doi.org/10.1111/j.1742-7843.2012.00902.x (2012).

83. Schneider, C. A., Rasband, W. S. & Eliceiri, K. W. NIH Image to ImageJ: 25 years of image analysis. *Nat. Methods* **9**, 671–675, https://doi.org/10.1038/nmeth.2089 (2012).

84. Wehland, M. *et al.* The impact of altered gravity and vibration on endothelial cells during a parabolic flight. *Cell. Physiol. Biochem.* **31**, 432–451, https://doi.org/10.1159/000343380 (2013).

85. Grosse, J. *et al.* Short-term weightlessness produced by parabolic flight maneuvers altered gene expression patterns in human endothelial cells. *FASEB J.* **26**, 639–655, https://doi.org/10.1096/fj.11-194886 (2012).

86. Kuhn, M. *et al.* STITCH 4: integration of protein-chemical interactions with user data. *Nucleic Acids Res.* **42**, D401–407, https://doi.org/10.1093/nar/gkt1207 (2014).

Acknowledgements

Author Contributions

D.G., T.J.C. and S.K. designed the experiment. S.K. and T.I. executed the experiments and collected the material. A.G.P., L.S., J.S. and S.R. performed western blot analyses. S.K. and M.W. performed qrtPCR analyses. J.B. performed the pathway analyses. K.S., N.H. and H.S. performed and analysed the microarray. S.K. performed the olaparib-, DEX- and rolipram-drug tests. D.G., J.B., T.J.C. and S.K. wrote the manuscript. M.I. and R.L. contributed reagents, materials and analysis tools. All authors reviewed the manuscript.

Additional Information

Supplementary information accompanies this paper at https://doi.org/10.1038/s41598-017-18556-8.

Competing Interests: The authors declare that they have no competing interests.

Publisher's note: Springer Nature remains neutral with regard to jurisdictional claims in published maps and institutional affiliations.